MOLECULAR DISSOCIATION IN THE ELECTRON MICROSCOPE

by

Mihir Parikh

ELECTRONICS RESEARCH LABORATORY

College of Engineering
University of California, Berkeley
94720

TABLE OF CONTENTS

TABLE OF CONTENTS, Con't.

Abstract

The ultimate resolution of bio-molecules in an electron microscope (EM), depends not just on the resolving power of the instrument but also on the stability of the molecular specimen under the electron beam. This study is an attempt to understand theoretically the action of fast electrons on small molecules, with the hope that extensions to molecules of interest to the microscopist will be subsequently possible.

The conditions in a high resolution EM permit certain simplifications: Only single scattering from neutral molecules needs to be considered. The small contribution of "knock-on" displacement of atoms leads to the assumption of molecular dissociation occurring via electronic excitation or ionization of a molecule. We assume dissociative ionization occurs via the formation of an activated state. This leads to a separation of the action of the fast electron (creation of an activated molecule) from the slower process of molecular dissociation (fragmentation of the activated state).

The activated state cross section is formulated by considering, at first the interaction of the incident electron with one of the bound molecular electrons. Then possible subsequent interaction with other bound electrons is formulated. The cross section for the ejection of an electron from a one particle system are calculated by the Born and the Binary Encounter theories. Ionization events that include simultaneous excitations of the remaining bound electrons are modelled. The cross sections for all these transitions are formulated to depend only on the 'observable' parameters of the molecule (e.g., ionization and fragmentation

energies, orbital occupancy etc.).

These concepts are used in calculating the ionization and dissociative ionization cross sections of those atoms and small molecules for whom (gas phase) experimental data are available. The results for diatomic molecules show quite a good agreement between experiment and our simple theory. Ionizations and fragmentations of small polyatomic molecules are also considered. The possible decay of the activated state and a variety of decay mechanisms are analyzed; it is found that for gaseous diatomic molecules, the activated state cross sections can be related to the measured dissociative ionization cross sections.

Acknowledgment

This work was initiated by a suggestion from Professor T. E. Everhart. Subsequently he made me aware of its importance and provided the necessary encouragement and stimulus that has now made this report possible. To him I am very thankful. Several critical suggestions from Professor L.M. Falicov have been most helpful. Professor J.C. Wiesner's help with some aspects of computer programming has been quite useful. The suggestion by Professor R.M. Glaeser provided the impetus for an investigation of knock-on damage (Sec. 2.2.a).

I am thankful to my colleagues, R. Bhandari, R. Shankar and W.J. DeVore for many stimulating discussions. Finally, the help of my wife, Neel, has been invaluable. She not only 'allowed' the many late hours and weekends at work but also provided the technical assistance in compiling and key-punching the published experimental data used in Chapter 4. To her I am most thankful.

The skillful typing of Marie Carey and the help of Barbara Kerekes and Paula Bjork have made the mechanics of manuscript preparation almost easy. This research has been supported by NIH Grant GM17523.

CHAPTER 1

INTRODUCTION

In this chapter, we will briefly survey some of the many experimental methods used to monitor degradation of molecular specimens in the electron microscope (EM). In Sec. 1.2, we discuss some generalization that can be made from existing experimental data. Next, the aims of this study are defined; also the philosophy of our method and an outline of the contents of the following chapters are described.

1.1. Experimental methods.

We will restrict ourselves to a brief discussion of five methods used in the study of molecular degradation. They are: (1) Energy loss spectroscopy, (2) Infra-red spectroscopy, (3) Diffraction pattern degradation, (4) Mass loss of specimens and (5) Autoradiography.

The energy loss spectrum is obtained[1] by determining the energy lost by the inelastically scattered transmitted electrons from a thin film specimen. This method involves the use of an electron spectrometer; it separates (depending on the amount of energy lost) the inelastically scattered electrons. Figure 1a shows[2] an energy loss spectrum of a 500 Å film of Adenine. This spectrum is typical of many bio-molecules (and DNA bases in particular). The low energy loss events (< 10 eV) have been related to electronic excitations of the molecule (e.g., $\pi \rightarrow \pi^*$, $\pi \rightarrow \sigma^*$ etc.). The energy loss 'hump' at ~ 20 eV is thought to be due to the condensed nature of the specimen. Part of this spectrum has
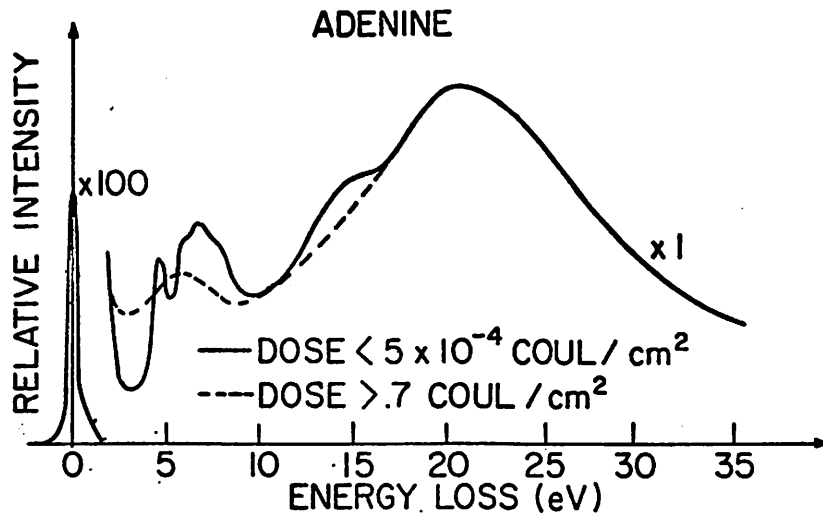
ADENINE

Fig. 1a. Energy loss spectrum for undamaged and electron beam damaged film of Adenine (from Ref. 2).
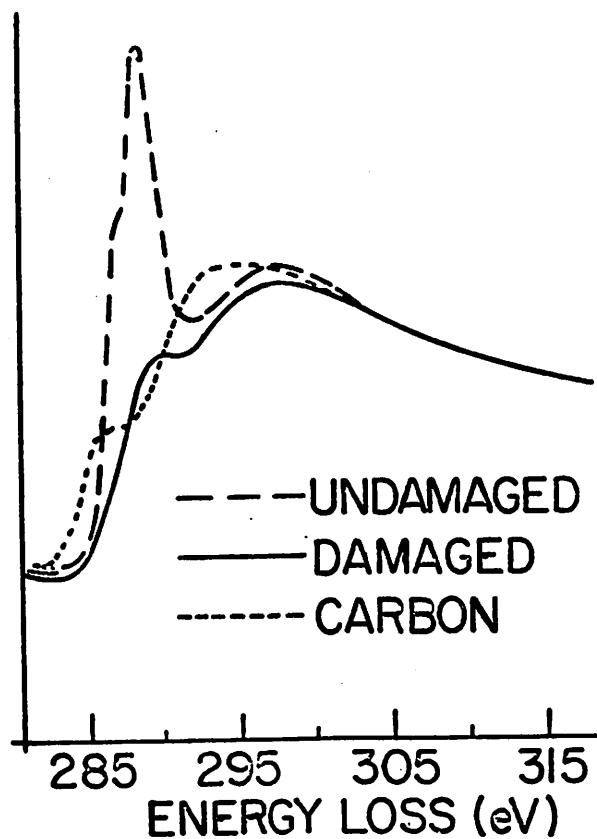
Fig. 1b. Structure at the edge of the Carbon K shell ionization threshold for an undamaged and an electron beam damaged film of Guanine and a film of amorphous Carbon (from Ref. 2).

been related to the observed ultraviolet (UV) spectrum of the molecules. The spectrum of energy loss due to inner shell excitations and ionizations can also be obtained (Fig. 1b). After sufficient exposure to the incident electron beam, the spectrum changes (Figs. 1a and 1b) to reflect the decrease of certain electronic transitions. This change can be related to the disruption of bonds in the molecule. The decrease in the intensity of an energy loss peak is found to be exponentially dependent on the electron beam exposure, hence

$$\sigma_D = \frac{\ell n(I_0/I)}{E_c} .$$

(1)

Here σ_D is considered to be the degradation cross section of the molecule and E_c is the critical exposure (also called the critical "dose", by some authors) for the decrease in the peak height from I_0 to I.

Inspite of the quantitative UV spectrum data that can be obtained, the usefulness (in the determination of the type of bond breakage or the location of the fragmentation site) is quite limited. This is because the UV spectrum provides little of the relevant information compared to the IR (vibrational mode) spectrum. Even if electron spectrometers of much higher resolution (~ 0.05 - 0.1 eV) were available (and the incident electron beam was made monochromatic), the energy loss technique cannot provide sufficient IR signal before destruction of the molecular specimen occurs. This limitation is due to an inherently small probabaility of exciting a vibrational transition in a molecule by the fast inci-

dent electrons in an EM.

Infra-red spectroscopy of molecular specimens can provide[3] information about the absence or presence of a particular type of bond in the molecule. Such information cannot, at present, be obtained with the energy loss technique. Fig. 2 shows the IR spectrum of non-irradiated and irradiated polyethylene. The disappearance of some vibrational modes and appearance of others can lead to an identification of the destruction of one type and formation of another type of bonds. Unfortunately, up to now, the irradiated specimen have to be removed from the microscope (and exposed to the effects of the atmosphere) in order that IR measurements can be taken. The results thus obtained cannot be unambiguously related to the in situ degradation of the molecular specimen in an EM. In the future, use of tunneling spectroscopy[4] (which yields IR and Raman spectra of molecules) may provide in situ determination[5] of molecular degradation in an EM.

The decay in the intensity of a diffraction peak can provide information about the degradation of the crystallinity in a specimen. Quantitative data (expressed in cross section or critical exposure) on the destruction of crystallinity are now being tabulated[6]. Like the energy loss spectra, these measurements are performed in situ. However, the decrease (or disappearance) of a particular diffraction peak cannot be related to the destruction of a particular type of bond. Thus information about changes in molecular structure is not expected from this method.

Loss of mass (or matter) from the specimen occurs after a

linear and branched polyethylene, not irradiated

-CH₂-
-CH₃

(CH₂)ₙ
n≥4

-CH₂-
-CH₃

C≡C-H
C-C-H

C-C-C

C-C

C≡C

linear and branched polyethylene, irradiated
3·10⁻² coul/cm²
75 kv

wavelength (μ)
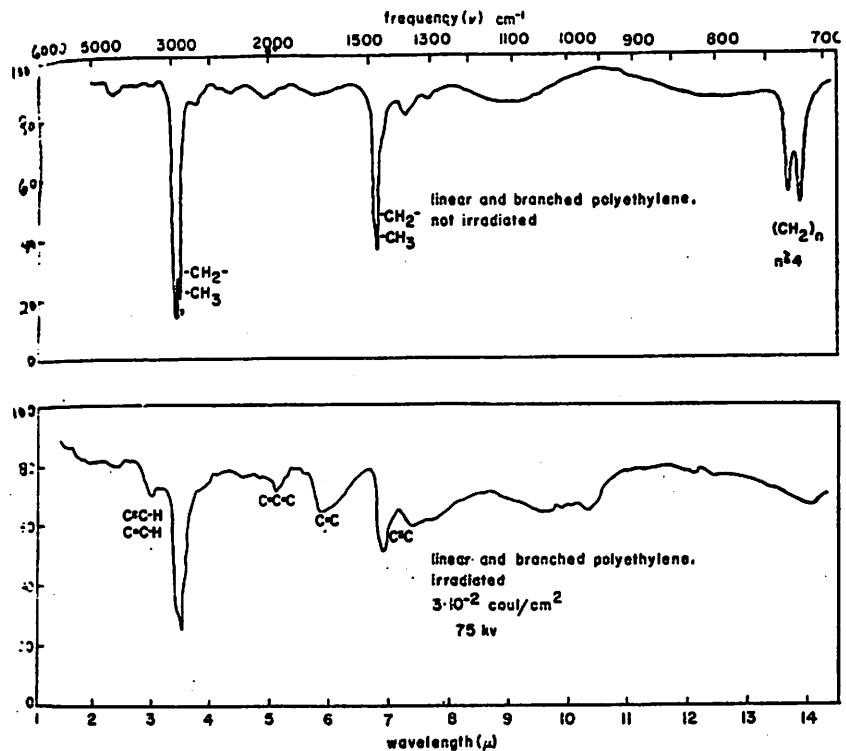
Fig. 2. Infrared absorption spectra of non-irradiated (top) and irradiated (bottom) linear and branched polyethylene (from Ref. 3).

1000

Fading time, seconds

100

10

1

⊸ 80 kV
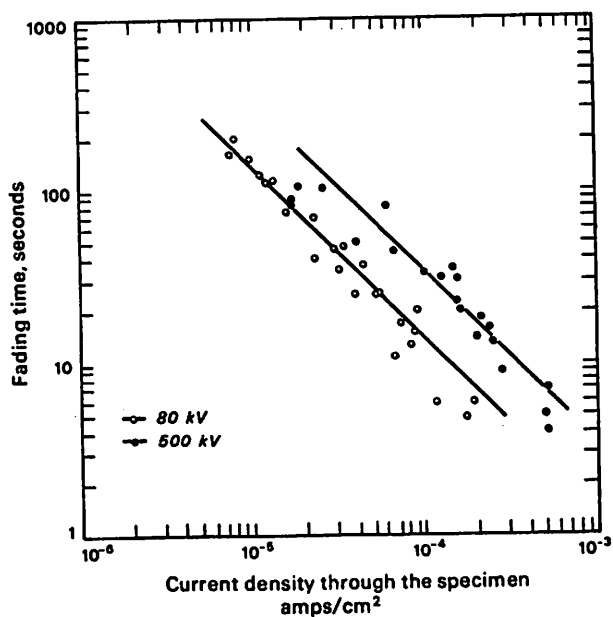⊸ 500 kV

Current density through the specimen
amps/cm²

Fig. 3. Radiation damage of crystalline ℓ-valine (from Ref. 11).

1.5

molecule has fragmented and then some or all of these fragments evaporate into the low vacuum of the EM. Mass loss measurements can be performed, in situ, by densitometric measurements of microscope plates[7] or by collecting scattered electron current[8]. Though this method provides data on the stability of molecules, it cannot provide information on structural changes occuring in the molecule.

Application[9] of autoradiography to determination of mass loss in a molecular specimen in an EM involves doping the molecule with a radioactive isotope (e.g., ^{3}H, ^{32}P). The reduction in the dopant concentration after irradiation gives information about the mass lost by the specimen. However, no information can be obtained about the type or the location of the structural changes in the molecule. Also the experiments cannot be performed in situ, so that there exist[10] uncertainties in measurements and interpretations.

1.2 Observed trends and our approach.

Enough experimental data exists today that some conclusions about the dependences of molecular degradation in a high resolution EM can already be made. First the observed damage seems to depend on the net exposure to the electron beam and not on the exposure-rate. Fig. 3 shows data[11] on diffraction pattern degradation, which illustrates the linear relation between the electron beam current density at the specimen (j_s) and the duration of exposure (τ) necessary to degrade the specimen by a fixed amount. Though the data in Fig. 3 show this linearity over only 3 orders of magnitude in current density, other experiments[12] have shown this linearity over 6 orders of magnitude in current density. The impli-

cation is clearly that the measured degradation is exposure rate independent so that one can write

$$E_c = j_s \cdot \tau \qquad\qquad (2)$$

Of course this was tacitly assumed in the writing of Eqn. (1).

The decrease in the energy loss as well as the diffraction peaks depends exponentially on exposure (Fig. 4). However the diffraction peaks decrease to 1/e of the original value in an exposure about one order of magnitude smaller than that for a similar decrease in the energy loss peaks. Consequently the cross section σ_D for the degradation of a diffraction pattern is an order of magnitude larger than that for the degradation of the energy loss spectrum. Thus even for a particular molecular specimen, the measured 'damage' cross section depends explicitly on the particular type of 'damage' measurement performed. In general, it is found[13] that the cross sections pertaining to diffraction pattern degradation or mass loss measurements are much larger than those for the energy loss spectrum (UV spectrum) degradation.

The dependence of molecular damage is found[14] to be only moderately dependent on the specimen temperature (upto 4.2 K). The exposure necessary to decrease the intensity of a diffracted peak was found to change by less than a factor of five for specimen temperature change from 300 K to ∼ 4 K. However it is discovered that with increasing lower temperatures, an increasing exposure ("latent dose") is necessary before any change in diffracted peak intensity is seen (Fig. 5). If after a certain exposure at low

BEAM DAMAGE - CYTOSINE

△ 7eV Energy Loss Peak
○ 4.75 Å Diffraction Peak
□ 6.52 Å Diffraction Peak

$D_{1/e} = .11 \, C/cm^2$

$D_{1/e} = .009 \, C/cm^2$

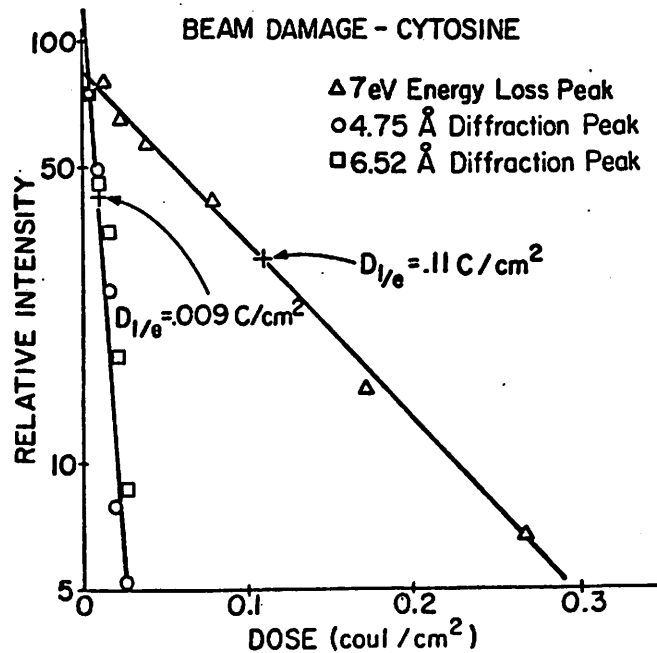RELATIVE INTENSITY

DOSE (coul /cm^2)

Fig. 4. Beam damage of cytosine film, showing exponential decay of intensity (energy loss or diffracted peak) with exposure (from Ref. 2).

Paraffin
100 KeV

Intensity — I_G

4°K

77°K

300°K

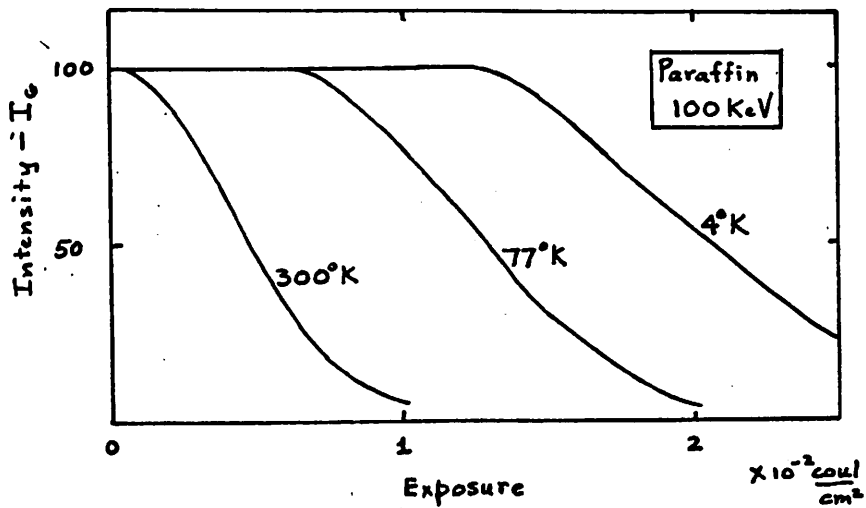Exposure

$\times 10^{-2} \frac{coul}{cm^2}$

Fig. 5. Dependence of the damage (via intensity I_G of a diffracted peak) on specimen temperature (from Ref. 14).

temperature, the specimen temperature is raised, then it is noticed

that concurrently, the intensity of the diffracted peak decreases

to a level that would have been obtained by exposing (the same

amount) the specimen at the higher temperature. Thus it can be

surmised that, at low enough temperatures, some of the fragments

(formed from the incident electron induced dissociations) are in-

hibited from diffusing or evaporating.

As expected, electron beam induced damage of molecules depends

sensitively on the physical structure of the molecule. The damaged

molecule is found to be in a state that is different from amorphous

carbon (This can be inferred from the data in Fig. 1b); however the

actual molecular fragments formed have not yet been established,

even for the simplest of molecules. It is well known[15] that the

highly conjugated aromatic molecules are far more stable under the

electron beam than the saturated aliphatics. Typical values for

critical exposures for these molecules range from ~ 10^{-3} C/cm^2

(~ 0.66 e$^-$/Å^2) for polyethylene to ~ 1 C/cm^2 (~ 660 e$^-$/Å^2) for

phathalocyanine. This sensitivity on molecular structure, though

expected intuitively, is difficult to predict (or even explain)

quantitatively. The influence of a few substituent atoms in

crucial areas of a molecular structure has been shown to change

the sensitivity of the molecule to radiation action. For example,

substitution of fluorine in polyethylene (giving TFE) leads[3] to

a large increase in its sensitivity to the electron beam, while

substitution of chlorine in copper phthalocyanine is believed[16]

to cause a large decrease in its sensitivity. Since all these

measurements have been performed on solid specimens in an EM, it

is not known what the contribution of the solid phase (and thence geometry and substrate) is on the net observed molecular damage. Inclusion of appropriate additives to a molecular film is reported[17] to cause small changes in sensitivity of polymers to radiation action. Thus the observed sensitivity of damage on molecular structure seems to imply that a detailed understanding of the primary interaction of the incident electron with an isolated molecule is imperative to any considerations of inter-molecular interactions.

Finally, we define a set of practical goals and outline an approach taken to achieve them. An idealistic aim might be to develop a theory that predicts the dependence of damage on 1) the inherent properties of an isolated molecule (i.e., geometrical structure, electronic configuration, occupancy etc.) and on 2) the solid phase properties of the molecular film (i.e., inter-molecular parameters, temperature, geometry and composition of substrate etc.). Clearly an endeavour to fulfill such an aim might be overambitious. We define then a more realistic goal of modelling the interaction of electrons with small isolated (gas phase) molecules. The calculations can be compared with available experimental data (cross sections as well as mass spectral fragmentation patterns) and then an attempt to extend these into the solid phase can be made.

Our approach will become evident through an outline of the contents of the following chapters. We begin (Ch. 2) by considering the special conditions in an EM in the modelling of our problem. Some effects provide a simplification in our analysis, others complicate it. Also we develop a general formulation for the calculation

of the exposure necessary to dissociate interacting molecules.
Next (Sec. 2.2), we find that, except for the most resistant highly
conjugated molecules, knock-on displacement of atoms contributes
only a small amount to the observed damage cross sections. Thus
it is assumed that an electronic excitation or ionization leads
to dissociation. A two step activated state concept is introduced
(Sec. 2.2.b) so as to separate the fast ($\leq 10^{-15}$ s) incident
electron induced electronic excitation and ionization (formation
of the activated state) from the slower ($\geq 10^{-13}$ s) process of
the separation of the nuclei (fragmentation of the activated state).
The calculated cross section for the former process on comparison
with observed dissociation cross sections may provide information
about the relative importance of the latter process, at least in
the gaseous phase.

The activated state cross section is formulated by considering,
at first the interaction between the incident electron and one of
the bound electrons; and then extending, phenomenologically, the
two particle scattering concept to interactions with other electrons.
The cross section for the ejection of an electron from a one particle
system can be calculated (Sec. 3.1) by either the Born or the Binary
encounter theories. Next (Sec. 3.2), ionization events that include
simultaneous excitations of the remaining bound electrons are modelled.
The cross section for transitions to direct and rearrangement ioni-
zation states (defined in Sec. 3.2) are formulated to depend only
on the "observable" parameters of the molecule (e.g., ionization and
fragmentation energies, orbital occupancy etc.).

These concepts are applied to the calculations of ionization

and dissociative ionization cross sections of those atoms and

small molecules for whom experimental data (gas phase) is avail-

able. The results (Ch. 4) for diatomic molecules show quite a

good agreement between experiment and our simple theory. Exten-

sions to small polyatomic molecules are attempted. The

decay of the activated state (to a stable state not leading to the

fragmentation of the molecule) is discussed in Ch. 5. Various

possible decay mechanisms are surveyed. Possibility of secondary

dissociations caused by ejected electrons are also considered.

REFERENCES to Chapter 1

1. M. Isaacson, J. Chem. Phys. 56, 1803 (1972).

    D. Johnson, Rad. Res. 49, 63 (1972).

2. A.V. Crewe, M. Isaacson and D. Johnson, Rad. Research (in press).

3. G.F. Bahr, F.B. Johnson and E. Zeitler, Lab. Invest. 14, 1115 (1965).

4. R.C. Jaklevic and J. Lambe, Phys. Rev. Lett. 17, 1139 (1966).

    M.G. Simonsen and R.V. Coleman, Phys. Rev. B 8, 5875 (1973).

5. M. Parikh, Proc. 32nd Annual EMSA Meeting (1974), submitted.

6. R.M. Glaeser, to be published and private communications.

7. E. Zeitler and G.F. Bahr, J. App. Phys. 33, 847 (1962).

8. J. Wall, Proc. 30th Annual EMSA Meeting (1972), p. 186.

9. R.E. Thach and S.S. Thach, Bioph. J. 11, 204 (1971).

10. M.L. Collins, private communications.

11. R.M. Glaeser, J. Ultrastructure Res. 36, 466 (1971).

12. J. Wall, Ph.D. Thesis, The University of Chicago, Dec. 1971.

13. The Chicago group (J.P. Langmore, P. Lin, M. Isaacson, J. Wall etc.), private communications (1973).

14. G. Siegel, Septième Congrès International de Microscopie Electronique, Grenoble (1970), p. 221.

15. L. Reimer, Lab. Invest. 14, 1082 (1965).

16. N. Uyeda et. al., J. App. Phys. 43, 5181 (1972).

17. B. Broyde, Bell System Tech. J., 2095 (Nov. 1970).

CHAPTER 2

MODEL: ASSUMPTIONS AND GOALS

In this chapter, the complex problem of degradation of molecular specimens in the EM will be dissected, so that the various parameters can be isolated and thereby made amenable to calculation and estimation. In Sec. 2.1, we examine the influence of the conditions in a high resolution EM on the observed molecular damage. In Sec. 2.2, the physics of electron scattering from an isolated molecule is examined and the concept of the activated state is developed.

2.1 Considerations of damage in a high resolution EM.

a. Single scattering from neutral molecules.

In this section two approximations relevant to conditions in a high resolution EM are made. First it is assumed that an incident electron is scattered at most once in the typical specimens in an EM. Second one can assume that this scattering occurs from neutral molecules in their ground states.

The first assumption is justified easily under typical conditions of high resolution microscopy. In order to improve resolution by decreasing the probability for multiple scattering and to decrease heating of the specimen by decreasing the energy loss in the specimen, the microscopist chooses the thinnest possible specimens. Typical thicknesses of organic films (or carbon substrates) are of the order of 100 Å, while typical mean free paths for scattering

100 KeV electrons are of the order of 500 Å. Clearly then our restriction to single scattering events is justified. It is worth noting that, if necessary, multiple scattering effects can be taken into account[1] once single scattering cross sections are available.

The second assumption of incident electrons interacting with only neutral de-excited molecules is more difficult to justify. In principle the incident electron can interact with either an ionized or an excited molecule if this molecule does not return back to its ground state before a second electron arrives in the vicinity of the molecule. Thus in order for our assumption to hold, the typical relaxation time of the excited or ionized molecule, τ_r, must be smaller than the average time between successive scatterings by incident electrons of the same molecule, τ_s. In the following paragraphs, we shall justify this assumption for conditions relevant to microscopy.

Typical relaxation times of molecules are determined according to whether they are isolated or interacting with other molecules or entities. Isolated molecules[2] have relaxation times primarily determined by internal conversion, fluorescence and phosphorescence with the time constants in the order of 10^{-13} sec, 10^{-9} sec and 10^{-3} sec or greater respectively. However for a molecule in a condensed phase[3], very rapid relaxation of the excited state and neutralization of the ionized state can occur. The relaxation of the excited molecule can occur by processes, (in addition to those for an isolated molecule) that involve energy transfer to neighboring molecules via electronic (exciton) coupling, vibrational coupling

and ejection and recapture of an electron. The time constants for each of these processes is of the order of 10^{-9} sec or less. An ionized state is usually neutralized by a thermal electron in a time less than 10^{-13} sec. It is then quite probable that a molecule in a condensed medium would not be trapped in a lowest triplet state but would decay back to the ground state by transferring energy to its neighbors. Then the mean relaxation time is not determined by the long lifetimes of phosphorescence in an isolated molecule, but by the lifetimes of energy transfer between molecules. We assume then, that τ_r the relaxation time of a molecule to be of the order of 10^{-8} to 10^{-9} sec.

Now we will determine the average time between successive scatterings of the same molecule, τ_s, for various conditions in the EM. First consider the average time τ_a between successive electrons to arrive at an element of area $A_{e\ell}$. The τ_a is the product of (1) the average time between electron arrival in the area defined by the beam diameter A_b, with beam current at the specimen, i_b, and (2) the ratio of A_b to $A_{e\ell}$. Thus,

$$\tau_a = \frac{e}{i_b} \cdot \frac{A_b}{A_{e\ell}} = \frac{e}{j_s} \frac{1}{A_{e\ell}} \tag{1}$$

where j_s, is the beam current density at the specimen. Typical picture elements in high resolution microscopy have an area of about 25 $\overset{\circ}{A}{}^2$; typical beam currents at the specimen in both a TEM and a STEM are about 10^{-11} amp. However, the TEM illuminates about one μm. square of the specimen (i.e., j_s (TEM) = 10^{-3} amp/cm^2), while the STEM illuminates only the area of the picture element

~ 25 $\overset{\circ}{A}{}^{2}$ (i.e., j_s (STEM) = 4×10^3 amp/cm^2). Consequently τ_a in a STEM is about 1.6×10^{-8} sec, while in a TEM it is 6.4×10^{-2} sec. The average time between scatterings, τ_s, is given by:

$$\tau_s = \tau_a / P_s \qquad (2)$$

where P_s is the probability of scattering from a molecule. Usually P_s is much smaller than one, and can be estimated from the ratio of the film thickness, t, and the scattering mean free path λ_s. The calculated value[4] of λ_s for total scattering of 100 KeV electrons from carbon atoms is 488 $\overset{\circ}{A}$ (the calculation is expected to agree with experiment within a factor of two); while typical thicknesses of carbon films, used in high resolution microscopy, are about 25 $\overset{\circ}{A}$. Thus P_s is of the order 0.05, so that a typical τ_s in a high resolution STEM is of the order of 0.32×10^{-6} sec, while in a TEM it is of the order of 1.3 sec!

The consequence of the above considerations is that in both the STEM and the TEM, the time between scatterings, τ_s, is somewhat larger than the relaxation time, τ_r, and as such our assumption of scattering from neutral de-excited molecules is made plausible. Available experimental data (Sec. 1.2) shows that damage is exposure-<u>rate</u> independent. This macroscopic observation further adds credence to our assumption of the phenomenon on the microscopic scale.

b. Dissociation versus damage.

Damage in the EM involves not just dissociation of the molecules, but also the reaction of the fragments and radicals amongst each

other and with other molecules. Most experiments measure this cumulative effect due to the incident electrons and thus, it is this total action that the theorist has to consider. In this section our goal is restricted to the considerations of the 'primary action' of the incident electron, i.e., to the dissociation of the molecule into fragments, but not to the subsequent reaction of these fragments and molecules. In the following paragraphs, we will discuss the foundations behind this restriction and then consider the conditions in microscopy where this restricted goal might be valid and applicable.

The action of radiation on molecules in condensed media can be separated[5] in three somewhat overlapping temporal stages: (1) The physical stage ($t \leq 10^{-13}$ sec). In this stage the incident electron ionizes or excites the electrons in the molecule or in the condensed medium; also fast energy transfer, via ejection and moderation of electrons and photons can occur. (2) The physico-chemical stage (10^{-13} sec $\leq t \leq 10^{-8}$ sec). During this stage the ions and nuclei move, as in dissociation processes and in processes involving internal conversion and ion-molecule reactions. (3) The chemical stage ($t \geq 10^{-8}$ sec). Here reactions amongst the fragments, radicals, and molecules can occur. Time scales for these reactions, depending on many conditions, can range from 10^{-8} sec to hours and even longer. Thus it is very probably during the chemical stage that fragments (after possible reactions with other fragments or with molecules) form products that may be either stable or be volatile in the vacuum of the EM. The experimentally observed

2.5

'mass-loss' of a specimen (Sec. 1.1), could be caused by such

evaporation of the fragments formed by dissociation.

With the above mentioned discussion in mind, it would be

desirable to have an EM that collected information from a picture

element in a time, $\tau_{e\ell}$, shorter than or comparable to the time,

τ_{ev}, taken by the fragments to evaporate into the vacuum of the

EM. Incidentally, experiments at low specimen temperature[6] show

that radicals formed from dissociation do not evaporate as readily

into the EM vacuum, as they would at higher temperatures. Next,

we will examine conditions in microscopy under which it may be

possible to collect information faster than evaporation can occur.

A typical number of electrons[7], $n_{e\ell}$, needed to image a 25 $\overset{\circ}{A}^2$

picture element is about 5000. Then the average time of information

collection from one picture element $\tau_{e\ell}$ is $\tau_{e\ell} = n_{e\ell} \cdot \tau_a$; for a STEM,

$\tau_{e\ell} \sim 8\times10^{-5}$ sec, while for a TEM, $\tau_{e\ell} \sim 320$ sec. [Of course, the

total time to obtain a picture from one μm square area (same as A_b

in the TEM) in both microscopes is exactly the same, since STEM

images each picture element sequentially while the TEM images all

the picture elements simultaneously.] Now if the evaporation time

of the dissociated fragments from a 25 $\overset{\circ}{A}^2$ element is greater than

10^{-4} sec, then it is possible to collect information in a STEM

from that element before the fragments can evaporate. In a TEM,

this is virtually impossible because fragments are very likely to

evaporate in the 320 sec needed to image a picture element.

It seems than, that our goal of considering only 'initial

damage' i.e., dissociation should be more pertinent to the STEM

than to the TEM. In summary, the approximations that are made

thus far are that in a high resolution EM, we consider only single

scattering of the incident electron from neutral de-excited molecules.

Explicitly, our goal is to estimate the critical exposure, E_c,

necessary to <u>dissociate</u> a certain fraction of the molecules. Note,

that though E_c can not be directly compared to the experimentally meas-

ured exposure (as defined in Sec. 1.1) necessary to damage a certain

fraction of the molecules, one does expect that they are qualitatively

related.

c. Relationship between exposure and dissociation cross sections.

The aim of this section is to derive equations that relate the

incident electron exposure, E_c, to various molecular and inter-

molecular properties. At this stage the primary interest is in

determining the trends in the dependence of E_c on suitably generalized

parameters, rather than on accurate calculation for one particular

molecular specimen. Thus, calculations of these molecular and

inter-molecular parameters will be deferred until subsequent

chapters. For now, arbitrary choices in the magnitudes of the

coupling constants and cross sections will be made to determine

their influence on the behavior and magnitude of E_c.

Consider, at first, a collection of <u>non-interacting</u> molecules

of species α, under the electron beam. We want to determine the

exposure E_c (in units of electrons/unit area) needed to dissociate

a certain fraction of the molecules. Assume an electron beam with

area A_b and current density j_s is incident on n_α molecules per unit

volume, each with molecular dissociation cross section σ_D^α. The number density of molecules that dissociate in time dt is given by:

$$dn_\alpha = - n_\alpha j_s \sigma_D^\alpha dt/e . \qquad (3)$$

If the current density is kept constant during time dt, then $j_s dt/e$ can be abbreviated as dE_c – an incident electron exposure corresponding to the time the beam was incident on the molecules. If the dissociation cross section σ_D^α does not depend on time, Eqn. (3) can be easily integrated. The number density of molecules remaining intact after illuminating the specimen for a time τ is:

$$n_\alpha = n_\alpha^0 \exp(- \sigma_D^\alpha E_c) . \qquad (4)$$

Here n_α^0 is the initial number density of intact molecules and E_c is the critical exposure given by $E_c = j_s \tau/e$. The assumption of time independence of σ_D^α is justified as follows: (1) In the EM, successive incident electrons scatter from neutral de-excited molecules and therefore successive electrons 'see' the same ground state molecular dissociation cross sections, σ_D^α. (2) Experimentally (Sec. 1.2), the critical exposure not the exposure rate determines the damage. Rewriting Eqn. (4) as,

$$E_c = \frac{1}{\sigma_D^\alpha} \ln \frac{n_\alpha^0}{n_\alpha} , \qquad (5)$$

we see the similarity with Eqn. 1.1, which describes the experimentally observed damage. Note also that σ_D^α represents a sum over

the individual cross sections for dissociation, occuring via different processes k (such as dissociative ionization, dissociative attachment etc., that we will discuss below) $\sigma_D^{\alpha,k}$. So that in Eqns. (3)-(5),

$$\sigma_D^{\alpha} = \sum_k \sigma_D^{\alpha,k}.\tag{6}$$

Consider now, a collection of *interacting* molecules under the electron beam. At first, assume that these molecules are randomly distributed and are confined to within the area illuminated by the beam. In microscopy, these assumptions are not always justified and we shall later examine some consequences due to this. The incident electron can cause dissociations of the molecular species α by (1) interacting with a molecule of the species α and causing it to dissociate (direct dissociation) and (2) be exciting or ionizing a molecule, of any species (including α), which subsequently transfers energy to a molecule of species α thereby causing its dissociation (secondary dissociation). The number density of the α-species of molecules, dn_{α}, that dissociate under an electron beam exposure of dE_c is

$$dn_{\alpha} = -n_{\alpha}\sigma_D^{\alpha}dE_c - \sum_{\phi} n_{\phi}\sigma_{SD}^{\alpha\phi}dE_c.\tag{7}$$

Here the second term on the right side of the equation is due to secondary dissociations of molecules of species α (represented by the cross section, $\sigma_{SD}^{\alpha\phi}$) caused by energy transfer from the excited or ionized molecules with density n_{ϕ}, of species ϕ. Note ϕ

2.9

represents the set of all the molecular species present under the beam, including α; thus the secondary dissociations are caused not just by energy transfer between different species of molecules but also between those of the same species. Equations analogous to Eqn. (7) are written for the dissociation of other molecular species, β, γ, etc. belonging in the set ϕ. The set of equations for dn_α, dn_β, dn_γ, etc. are coupled and in general have to be solved simultaneously.

In chapter 5, specific types of energy transfer processes and mechanisms will be considered; for now it will suffice to note that $\sigma_{SD}^{\alpha\gamma}$ can be written in the general form:

$$\sigma_{SD}^{\alpha\gamma} \propto n_\alpha \int c(E) \; \sigma_D^\alpha(E) \; \frac{d\sigma^\gamma}{dE} \; (E,T) dE \qquad (8)$$

Here $d\sigma^\gamma/dE$ is the differential cross section for energy transfer E due to the excitation or ionization of the molecular species γ, by an incident electron of kinetic energy T. The dissociation cross section of the molecular species α due to the energy transfer E is denoted by $\sigma_D^\alpha(E)$, while $c(E)$ represents some constants. The dependance of $\sigma_{SD}^{\alpha\gamma}$ on n_α makes it possible to rewrite the set of equations in (7) as:

$$\frac{dn_\alpha}{dE_c} = - \; n_\alpha \sigma_D^\alpha - n_\alpha^2 \lambda_{SD}^{\alpha\alpha} - n_\alpha \sum_\phi{}' n_\phi \lambda_{SD}^{\alpha\phi}$$

$$\frac{dn_\beta}{dE_c} = - \; n_\beta \sigma_D^\beta - n_\beta^2 \lambda_{SD}^{\beta\beta} - n_\beta \sum_\phi{}' n_\phi \lambda_{SD}^{\beta\phi} \qquad (9)$$

$$\vdots \qquad \vdots \qquad \vdots \qquad \vdots$$

where $\lambda_{SD}^{\alpha\gamma} = \int c(E)\sigma_D^{\alpha}(E) \frac{d\sigma^{\gamma}}{dE}(E,T)dE$ is an inter-molecular coupling

parameter. The physical interpretation of each of the terms in

the Eqns. (9) is quite straight forward. For example, the first

term on the right side of the equation for dn_{γ}/dE_c represents the

decrease in γ-species molecular density due to the direct dissocia-

tion of these molecules. The second term, that due to secondary

dissociations initiated by other molecules of the same species γ.

The third term, that due to secondary dissociations initiated by

molecules of species other than γ. (Note that in the equation for

n_{γ}, the $\sum_{\phi}'$ represents the sum over all the members of ϕ, except the

species γ).

In Appendix 1, these coupled equations are solved for the

cases of a specimen with only one or two molecular species. Ana-

lytical solution for the one species model shows that the surviving

concentration $n(E_c)$, for an exposure of E_c, is not linear in the

initial concentration $n_0 = n(0)$, due to the presence of the non-

linear coupling term $n^2\lambda$. Solutions for certain choices in σ, λ

and n_0 are shown in Fig. 1 of Appendix 1. The two species model

is more interesting. In general, the two coupled equations have

to be solved numerically and the parameters have to be chosen

suitably so that the mathematical solutions have resemblance to

physical reality. Though details of the model and the choices in

parameters and initial concentrations are given in Appendix 1, it

is worth noting that owing to the dependence of $\lambda_{SD}^{\alpha\gamma}$ on $d\sigma^{\gamma}/dE$, it

is modeled that $\lambda_{SD}^{\alpha\gamma}$ is proportional to the dissociation cross

section, σ_D^{γ}. This model relies on the assumption of proportionality

between σ_D^γ and $d\sigma^\gamma/dE$, which can only be justified qualitatively. Nevertheless, within the assumptions of the model, numerical solutions to the coupled equations are obtained. The trends of the molecular species' survival show some interesting dependences on coupling constants. For the case of one molecular species having an initial concentration larger than the other, it is seen (Appendix 1, Table 2) that the survival concentration for a given exposure, depends weakly on the inter-species and similar-species coupling constants (C_{IS} and C_{SS}, respectively; defined in Appendix 1), if the two species have approximately equal direct dissociation cross sections σ_D. If, however, the majority species have a σ_D much larger than minority species' σ_D then the coupling constants, C_{IS} and C_{SS} make a substantial difference in survival of the two species. It is found that increasing C_{IS} decreases the concentration of the surviving minority species, as one expects. However, increasing C_{SS}, decreases the concentration of the surviving majority species and concurrently increases minority species' survival. Trends such as these, if found to exist in more accurate models, could be utilized experimentally in preparing specimens with appropriate inter-molecular coupling constants. Alternatively, experimental data for a specimen prepared under differing conditions (i.e., with for example, different coupling constant) could yield parameters via a correlation between an experimental survival-exposure curve and theory. Finally, it may be possible to formulate an 'effective' dissociation cross section σ_D^{eff}, which approximates the exponential behavior at sufficiently large E_c of the numerical calculations shown in Figure 2 of

Appendix 1.

It has thus far been tacitly assumed that molecules are randomly distributed, so that spatially isotropic coupling constants are justified. Besides enormous mathematical simplicity, no rationalization for this assumption is offered. If spatially anisotropic inter-molecular coupling constants are used, Eqns. (9) would have to be considerably modified. It is not known how, if at all, an experimental measurement of exposure (a spatially averaged quantity) would reveal such anisotropies. Finally, another objection: Experimentally (especially in a STEM), molecules within the beam diameter transfer energy to those outside, possibly causing their dissociation, but the converse does not apply. The model discussed above assumes only mutual interactions and thus only overestimates the damaging effect. Note that the effect of a scanning beam in a STEM cannot 'average out' this non-mutual behavior of molecules close to the beam periphery. This is because the time taken by the beam to move to the adjacent element (and make the interaction mutual) is of the order of the arrival time $\tau_a \sim 10^{-8}$ sec, of the electrons in a STEM, which is much greater than the time required for most fast inter-molecular interactions.

In summary then, it has been shown that within certain simplifying approximations, equations that relate exposure to molecular dissociation, due both to direct incident electron interaction and to inter-molecular interaction, can be developed. Under certain conditions, the model shows that a minority species can have greater survival in the presence of a majority species than

under other conditions. Even though the model is not directly
applicable to experiment, semi-quantitative trends may have some
use in experimental specimen preparation.

2.2 Electron scattering by molecules.

   a. Knock-on displacement of atoms.

The incident electron, in the simplest approximation, can
interact with either the electrons or the atomic nuclei in the
molecule. In the next section the former case will be considered:
here we estimate the relevance of "knock-on" displacement of atoms
from bio-molecules in the medium energy EM. If the energy transfer
from the incident electron to the atomic nucleus is large enough,
then the nucleus (or the atom) will be ejected from the original
site in the molecule. This process is called "knock-on" in the
high voltage (MeV) electron microscopy of non-molecular inorganic
and metallic materials.

The formulation of displacement damage in metals, as reviewed
by Seitz and Koehler[8], is used here with due regard to the binding
energies of atoms in molecules as compared to those in metals.
The maximum energy transfer E_m to the atomic nucleus in a pure
recoil collision is

$$E_m = \frac{2m}{M} \frac{T}{mc^2} (T + 2mc^2),$$ (10)

where m is the rest mass of the electron; T is the electrons'
the kinetic energy and M is the rest mass of the atomic nucleus.
If the energy needed to displace an atom is E_d, the minimum incident
electron energy (or the threshold energy, T_t) for the knock-on

process to occur is obtained by solving Eqn. (10) for T with
$E_m = E_d$; i.e.,

$$T_t = mc^2 \left[\sqrt{1 + M/m \ E_d/_{mc}^2} - 1\right] \tag{11}$$

$$= M/m \ E_d/4 - 1/32 \ (M/m)^2 \cdot E_d^2/mc^2 + \cdots. \tag{11a}$$

Table 1 shows the calculated threshold energies for hydrogen, carbon and iodine for five different values of displacement energies. The threshold energies for hydrogen and carbon are low enough that knock-on displacement is certainly possible in the medium energy EM. However for iodine unless the displacement energy is less than 2 eV the process does not occur in a 100 KeV EM. The displacement energy E_d is, by definition, the minimum kinetic energy that must be imparted to the atomic nucleus by the incident electron so that it separates from the rest of the molecule. Since in knock-on, the energy transfer is only to the atomic nucleus, the molecule is assumed to remain in its initial electronic state; however, its vibrational state changes from v to v'. As the schematic diagram for a hypothetical molecule AB (Figure 1) shows, dissociation can occur only if the transition is to one of the highest vibrational states (v'') of the ground electronic state (X_0) of the molecule. Thus, the incident electron must impart the dissociation energy D(A-B) for that bond. Clearly then, E_d is of the order of D(X-Y) for an X-Y bond. Tabulated[9] experimental measurements of bond dissociation energies indicate that H-C, H-N and H-O have energies between 3 and 5 eV, depending on the particular molecule. The I-H bonds (in HI) and I-C bonds

Table 1:

Incident electron threshold energies (T_t) for "Knock-on" displacement

Element	Displacement Energy, E_d (eV)				
	5.0	4.0	3.0	2.0	1.0
Hydrogen, Z = 1	2.291	1.834	1.376	0.918	0.459
Carbon, Z = 6	26.67	21.44	16.16	10.83	5.444
Iodine, Z = 53	235.1	194.3	151.1	104.9	54.89

Threshold energies are in KeV.
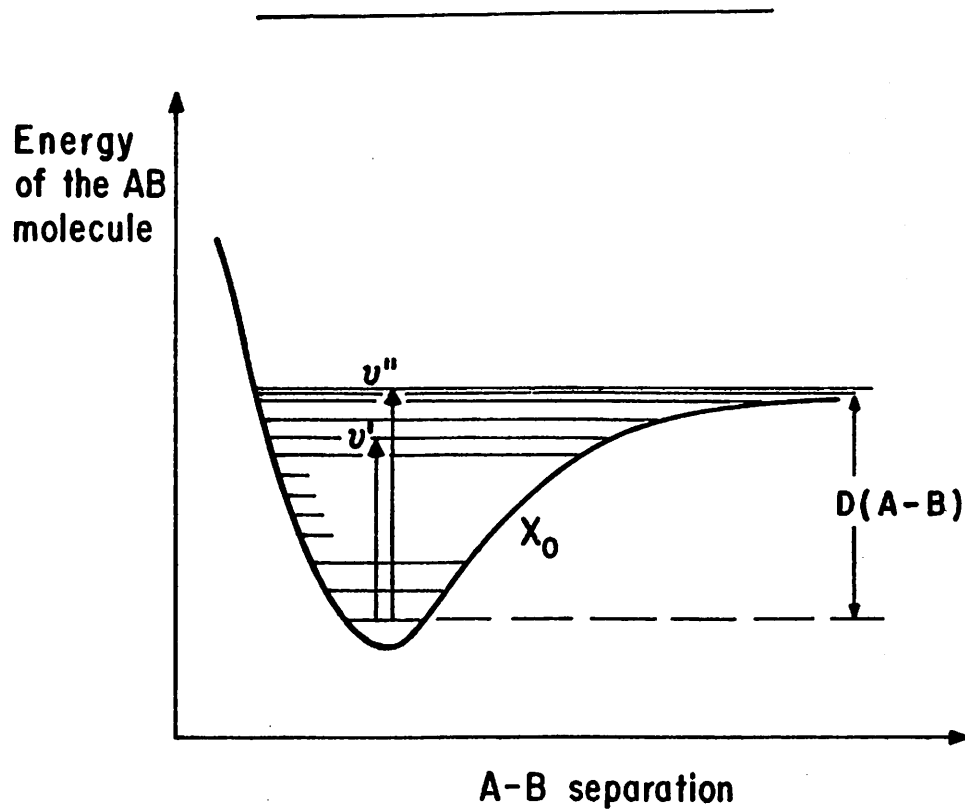
Fig. 1. Schematic diagram showing "knock-on" induced transition to the vibrational state v' cannot lead to dissociation; transition to the state v'' can.

(in CH_3I and C_6H_5I) have energies of about 3 eV and 2.5 eV respectively. Thus in medium energy microscopy, only the low Z elements can suffer from knock-on damage.

The displacement cross section was derived by Seitz and Koehler[8], from an approximation to the relativistic Rutherford equation for scattering of a relativistic electron from the Coulomb potential of an unscreened atomic nucleus. For heavy elements, this approximation is known to fail[10]; but when used for light elements, it should be quite adequate. The Seitz-Koehler equation for displacement cross section is:

$$\sigma_{dp} = \frac{4\pi a_0^2 Z^2 E_R^2}{(mc^2)^2} \left(\frac{1 - \beta^2}{\beta^4}\right) \left[\frac{T_m}{E_d} - 1 - \beta^2 \ln \frac{T_m}{E_d} + \right.$$

$$\left. + \frac{\pi \beta Z}{137} \left(2\sqrt{\frac{T_m}{E_d}} - 2 - \ln \frac{T_m}{E_d}\right)\right]. \tag{12}$$

Note that E_R is the rydberg of energy (= 13.6 eV); a_0 is the bohr radius and β = v/c with v the relativistic velocity of the incident particle. Results of calculations for hydrogen and carbon atoms, for values of E_d = 3 and 5 eV, are shown in Figure 2. Note that in the figure (and here-after) all cross sections are expressed in a unit of πa_0^2 (= 0.8797 × 10^{-16} cm^2). Though the cross section maxima for hydrogen are much greater than those for carbon, the cross sections for carbon decrease more slowly with increasing T, than those of hydrogen. Consequently at 100 KeV, carbon cross sections are more than twice those of hydrogen (and at 1 MeV, almost three times; see Table 2). Thus a general trend of atomic knock-on displacement phenomena is that with increasing
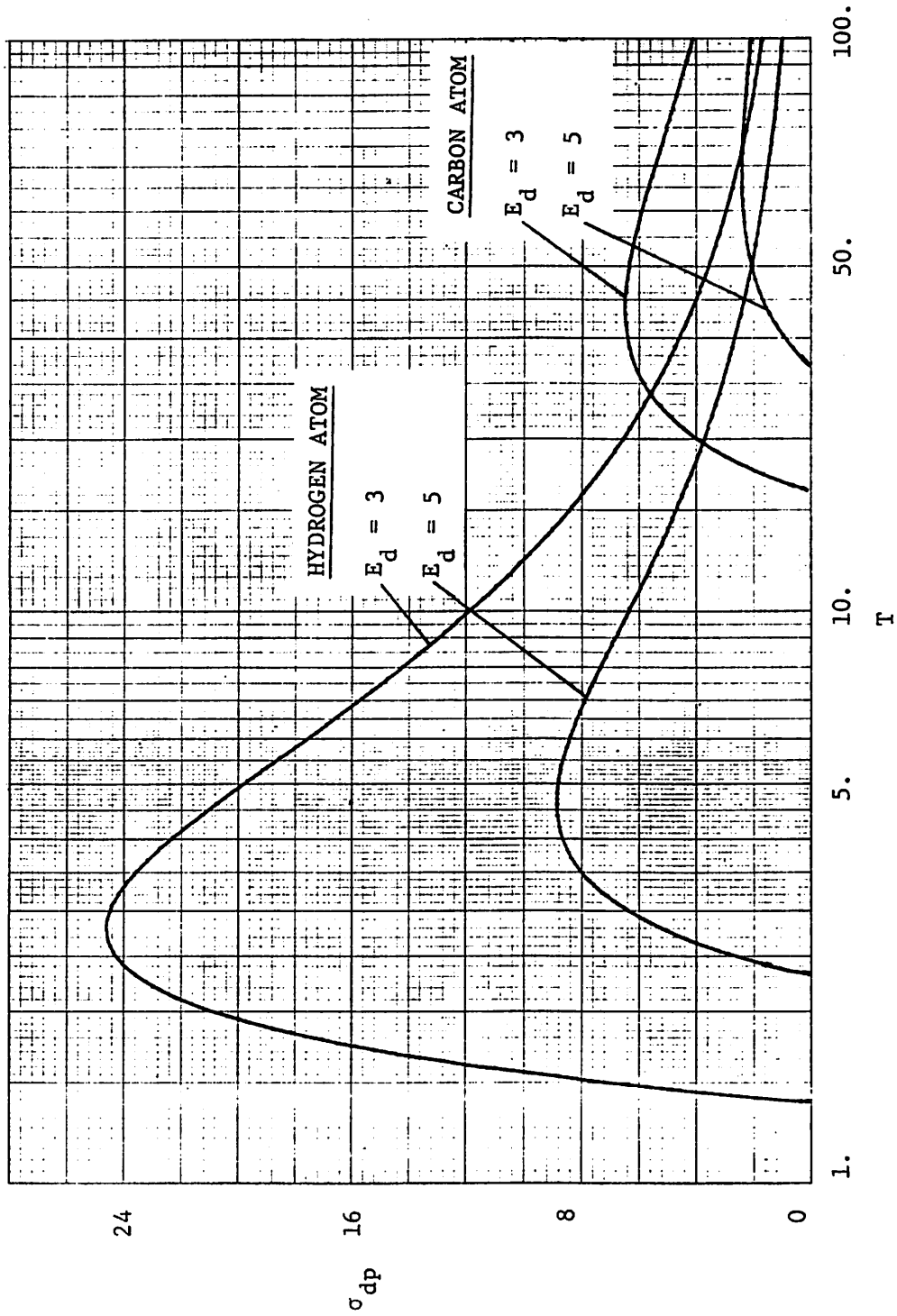
Fig. 2. Knock-on displacement cross section σ_{dp} (in $10^{-6} \cdot \pi a_0^2$) for hydrogen and carbon vs. incident electron energy T (in KeV), for $E_d = 3$ and 5 eV.

Table 2: **Selected values of displacement cross sections at high T**

T \ E_d	Hydrogen (Z = 1)		Carbon (Z = 6)		Iodine (Z = 53)	
	3.0	5.0	3.0	5.0	3.0	5.0
10^5	1.70 (4.03)	1.00 (2.13)	4.11 (5.33)	2.08 (2.35)	0. (0.)	0. (0.
5×10^5	0.699 (2.31)	0.417 (1.27)	1.99 (4.20)	1.14 (2.14)	10.7 (12.3)	4.21 (4.31)
10^6	0.590 (2.24)	0.353 (1.25)	1.74 (4.48)	1.02 (2.38)	12.6 (19.0)	6.54 (8.54)

All energies are in eV; Cross sections are in $10^{-6} \cdot \pi a_0^2$ Values in parenthesis are the "effective" displacement cross sections, $\overline{\nu} \cdot \sigma_{dp}$.

Z of the atoms, the cross sections have knock-on thresholds at higher energies but have lower magnitudes at their maxima. However at higher energies, for equal values of E_d, the higher Z atoms have greater cross sections than atoms with lower Z.

Atoms displaced with large kinetic energies can knock out other atoms from their sites. A cascade of atomic displacements can occur and in the following paragraphs, the importance of this phenomena in the EM will be estimated. The physics of the ejected atom interacting with other atoms is very complicated. We follow the theories outlined in the book by Dienes and Vineyard[11]. It is assumed that inelastic scattering between atoms (mass M) occurs for atomic kinetic energy greater than $E_i \sim 1/8 \frac{M}{m} \cdot I$ where I is the lowest atomic excitation energy. Atoms ejected by electrons with T < 100 KeV have mean kinetic energy $\bar{E}$ ($\sim E_d \cdot E_m/E_m - E_d \cdot \ln(E_m/E_d)$) considerably less than ($\sim$ 2KeV for hydrogen; $\sim$ 12 KeV for carbon), so that only elastic scattering between atoms can be assumed to occur. Even though a particular formulation of the elastic scattering (Rutherford or Hard-Sphere) cannot be justified at these low atomic kinetic energies, fortunately one obtains approximately identical results for the cascade phenomena for all available formulations. It is worth noting that all known theories assume the case of an amorphous specimen, so that E_d is spatially isotropic.

The number of displaced atoms, including the primary displaced atom, produced by a knock-on atom of energy E is given by[11],

$$\nu(E) = E/2E_d \text{ for } E > 2E_d. \tag{13}$$

Physically, this just means that on the average only half of the energy of a moving atom is available for causing further displacements; the other half E_d on the average goes to sub-threshold collisions. Since the primary knock-on's have a distribution of kinetic energy, the $\nu(E)$ has to be averaged over this distribution (for a particular model) and the result, for all known models, can be approximated by,

$$\bar{\nu} = \frac{1}{2}\left(\frac{E_m}{E_m - E_d}\right)\left[1 + \ell n \frac{E_m}{2E_d}\right], \tag{14}$$

for $E_m \geq 2E_d$. Recall E_m is the maximum energy transferred (via a head-on collision) during an elastic encounter and is given by (10). Makin[12], inexplicably, has used (14) without the factors outside the square brackets; this causes, at most, a factor of two difference in $\bar{\nu}$ from that given here. Figure 3 shows the behaviour of $\bar{\nu}$ with T, for H, C and I atoms and reasonable values for E_d. The numbers can be reliably compared with experiment within a factor of two or three. In the medium voltage EM, one can estimate, most pessimistically, that no more than four or five secondary displacements can occur for one primary displacement, even for hydrogen. An "effective" displacement cross section σ_{dp}^{eff} can be defined:

$$\sigma_{dp}^{eff} \equiv \bar{\nu}\, \sigma_{dp} \tag{15}$$

Figures 4a and 4b show the calculated σ_{dp} and σ_{dp}^{eff} for hydrogen and carbon respectively. Careful comparison of σ_{dp}^{eff} for the two atoms shows that (1) the values before and at the maxima are unchanged after the inclusion of the multiplication factor $\bar{\nu}$. And (2) the
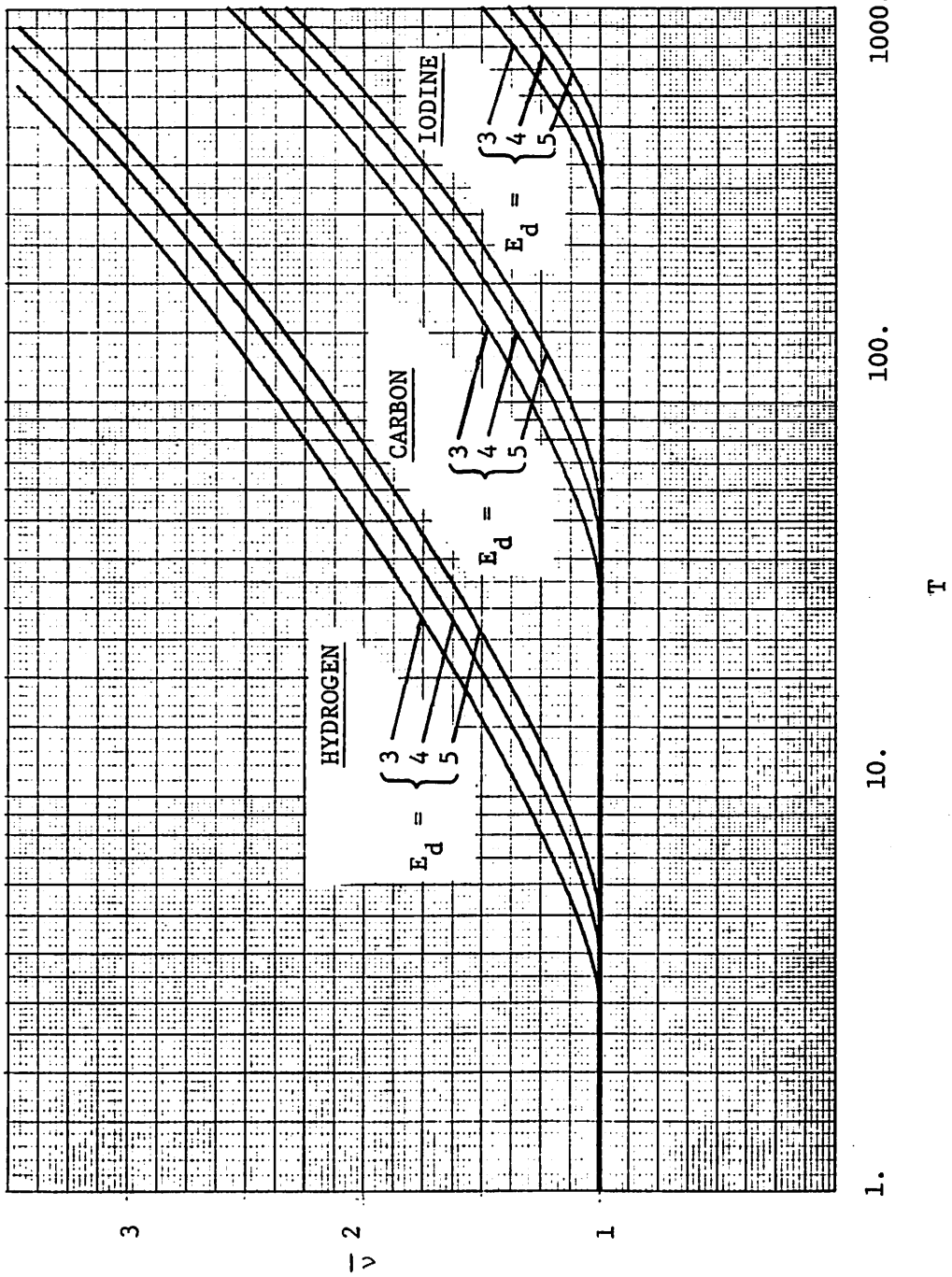
Fig. 3. Average number of displaced atoms $\bar{\nu}$, including the primary knock-on vs. incident electron energy T(in KeV), for hydrogen, carbon and iodine and $E_d = 3$, 4 and 5 eV.
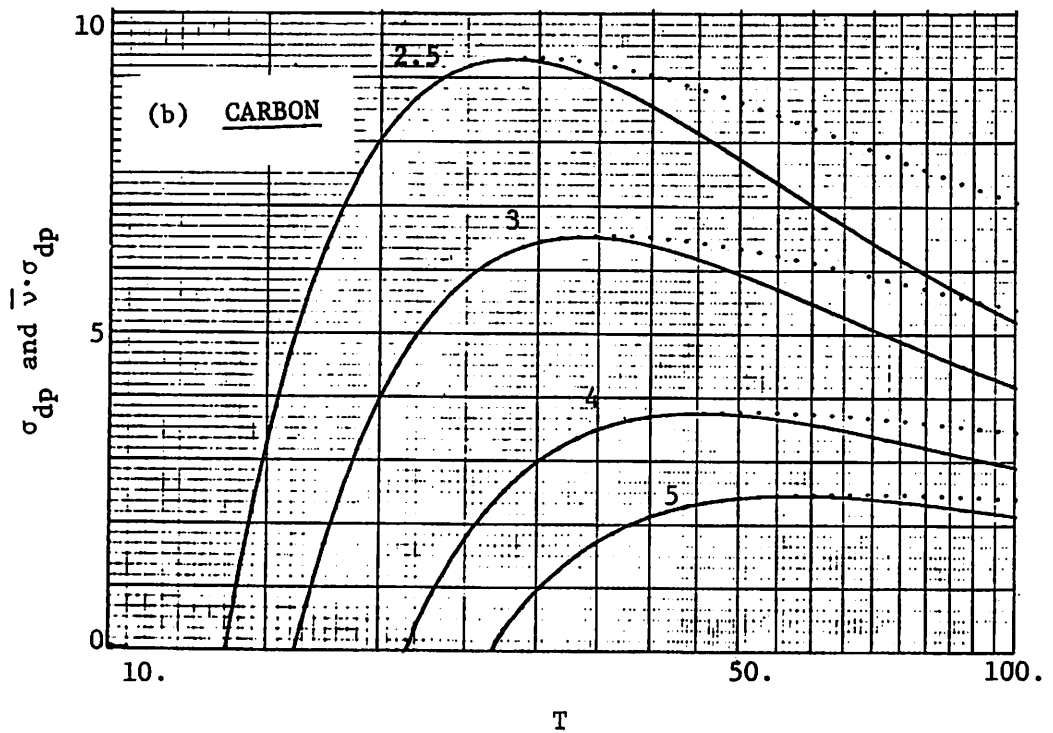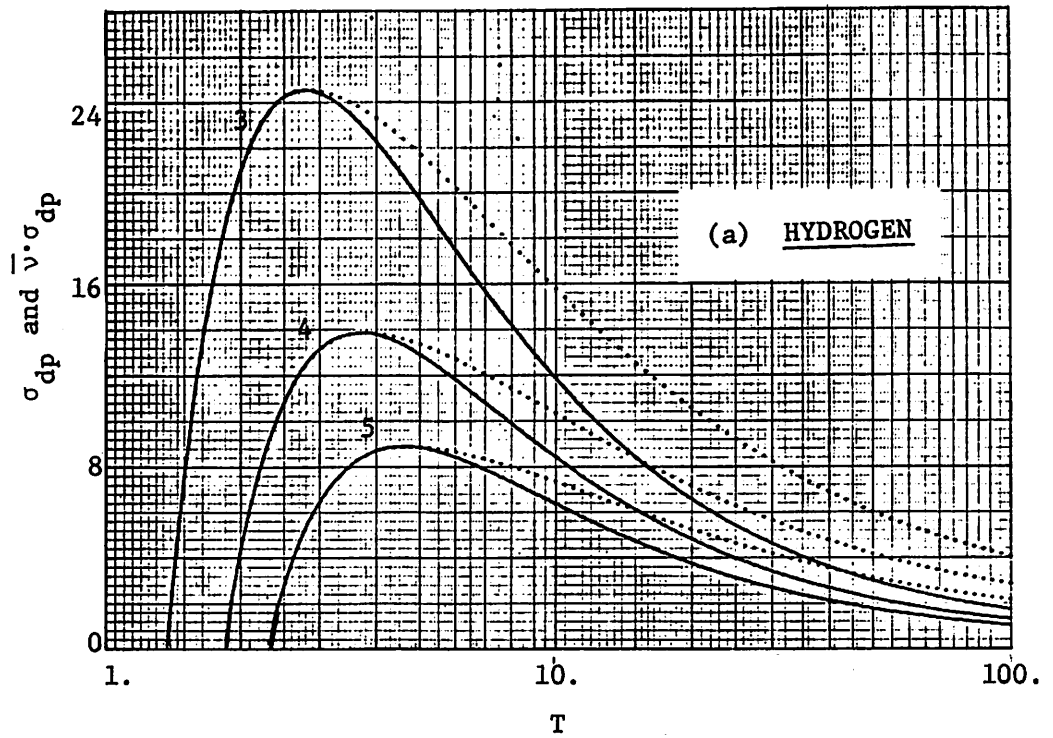
Fig. 4. Displacement cross sections: σ_{dp} (solid-line) and
effective displacement cross sections σ_{dp}^{eff} (dotted line), both
in units of 10^{-6} πa_0^2, vs. incident electron energy T (in KeV)
for (a) hydrogen and (b) carbon and values of E_d (in eV) as
shown.

effective cross section σ_{dp}^{eff} for higher Z atoms is still greater than that for the lower Z atoms, at energies well above the threshold. Consequently, it seems that even after including a reasonable estimate for the cascade of knock-ons through the factor $\bar{v}$, the total knock-on cross sections are probably dominated by atoms with the largest Z, that can be knocked out by the incident electrons.

The importance of knock-on displacements of atoms from bio-molecules in the medium energy EM is difficult to establish. For the case of a molecular solid composed of methane, one needs to only consider the knock-on displacement of the H atoms from each of the four C-H bonds of the molecule. Figure 5 shows results of calculations for the knock-on of the H atom from C-H and N-H bonds, an O atom from C=O bond and a Cl atom from C-Cl bond with the displacement energies E_d chosen from Pauling's text[13]. Using the value of σ_{dp} at 12 KeV, one finds the total cross section for knock-on displacement of an H atom from CH_4 to be $26.6 \times 10^{-6} \pi a_0^2$. The total ionization cross section[14] $\sigma_I(CH_4)$ of gaseous CH_4 at 12 KeV is measured to be $0.14 \pi a_0^2$, the dissociation cross section is certainly a very large fraction of $\sigma_I(CH_4)$, as will be seen in Chapter 4. Thus the knock-on cross section is estimated to be smaller than the dissociation cross section by a factor of the order of 10^3. If this were the case for all molecules and for molecules in the condensed phase (i.e., after the inclusion of $\bar{v}$ with σ_{dp}) then knock-on could be ignored completely in considerations of damage in the medium energy EM. However experimentally measured damage cross sections for the DNA bases (Sec. 1.1) are
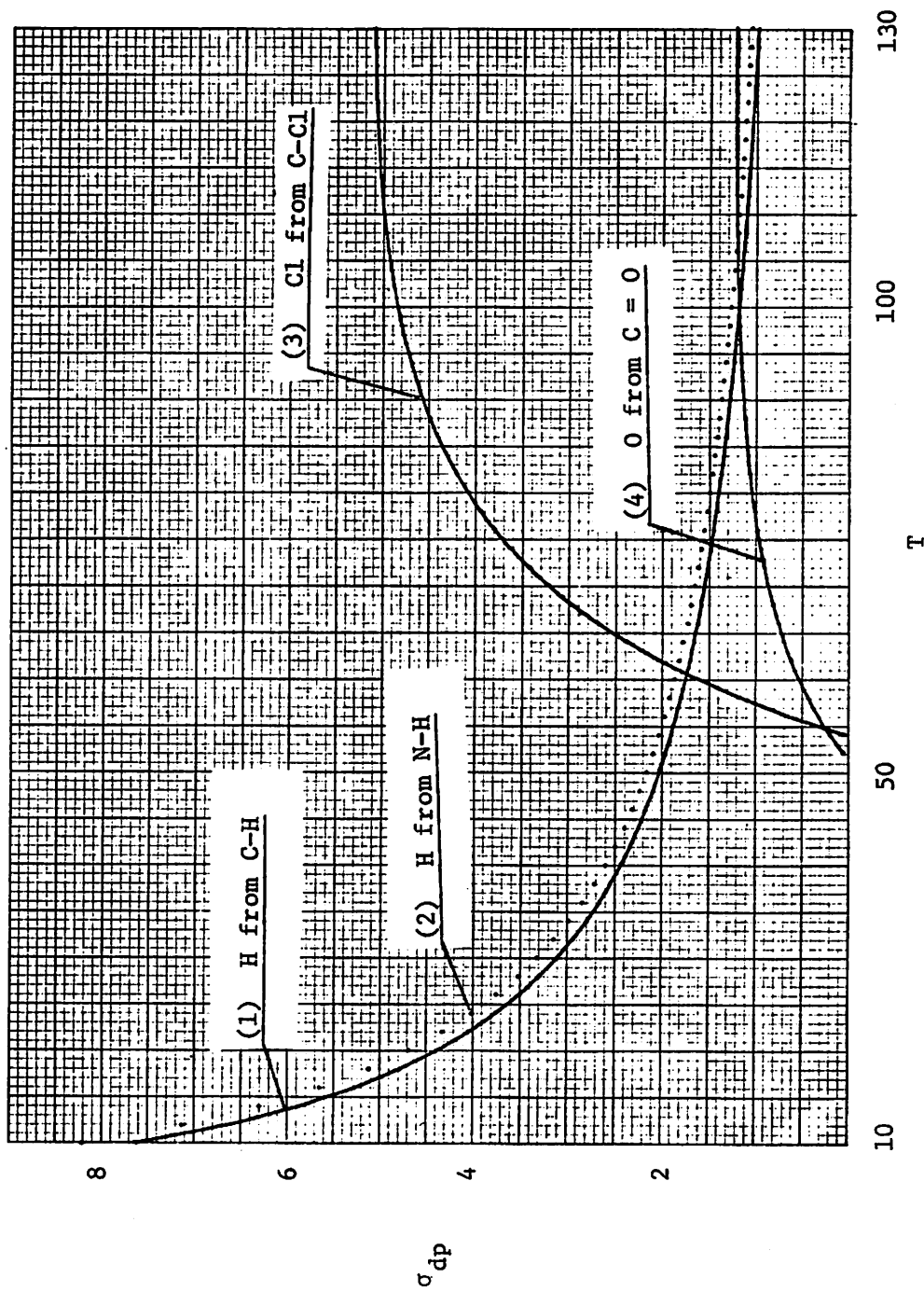
Fig. 5. Displacement cross section σ_{dp} (in $10^{-6}\ \pi a_0^2$) vs. incident electron energy T (in KeV), for the displacement of (1) an H atom from a C-H bond (E_d = 4.28 eV), (2) an H atom from a N-H bond (E_d = 4.05 eV), (3) a Cl atom from C-Cl bond (E_d = 3.51 eV) and (4) an O atom from a C=O bond (E_d = 7.41 eV).

considerably smaller than the values for a saturated molecule like

CH_4; consequently knock-on may not be negligible. The incident

electron, in the medium energy EM, however does not transfer enough

energy [Eqn. (10)] to simultaneously break more than one bond.

Assuming then that only the atoms bound to one atom can be knocked

out, Table 3 lists the atoms that are assumed can be knocked out

of the DNA bases. Using the values of σ_{dp} for the various bonds

from Figure 5, the following values of knock-on cross sections at

T = 25 KeV are obtained:

Adenine: $\sigma_{dp} = 0.189$; $\sigma_D = 0.94 \pm 0.17$
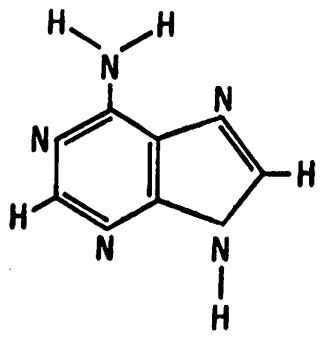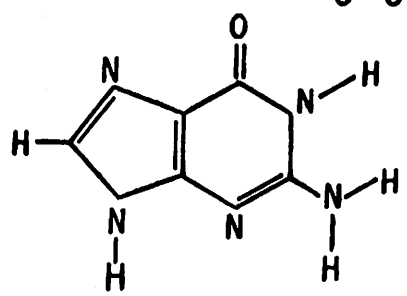
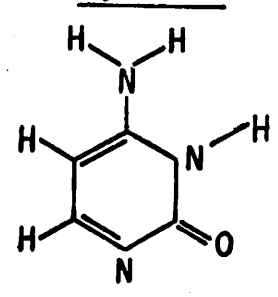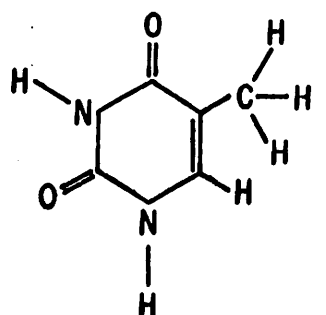Guanine: $\sigma_{dp} = 0.192$; $\sigma_D = 1.13 \pm 0.23$

Cytosine: $\sigma_{dp} = 0.189$; $\sigma_D = 1.25 \pm 0.23$

Thymine: $\sigma_{dp} = 0.224$; $\sigma_D = 3.53 \pm 0.56$

The experimental values for the damage cross sections σ_D are from

the Chicago group[15] and are expressed (along with σ_{dp}) in units of

$10^{-4} \pi a_0^2$. The significant contribution (15-20%) of σ_{dp} to σ_D for

these relatively resistant molecules seems to substantiate the

assertion of Glaeser[16]. Including the possibility of a cascade of

H atom knock-ons, through the factor $\bar{\nu}$, increases σ_{dp} by a factor

of 1.7. Finally consider the highly conjugated molecules copper-

phthalocyanine (CuPTC) and chlorine substituted copper-phtalocyanine

(Cl-CuPTC) shown in Figures 6 (a) and (b). Assuming once again

that just the atoms bound to only one other atom can be knocked

out, one has 16 vulnerable C-H bonds in CuPTC and 16 vulnerable C-Cl

Table 3: Assumed molecular displacement in knock-on from DNA bases.

| Molecule | Presumed removal of nX atoms from n(Y-X) bonds |

Adenine $(C_5 N_5 H_5)$

2 H from 2(C-H)
3 H from 3(N-H)

Guanine $(C_5 H_5 N_5 O)$

1 H from (C-H)
4 H from 4(N-H)
1 O from (C=O)

Cytosine $(C_4 N_3 H_5 O)$

2 H from 2(C-H)
3 H from 3(N-H)
1 O from (C=O)

Thymine $(C_5 N_2 O_2 H_6)$

4 H from 4(C-H)
2 H from 2(N-H)
2 O from (C=O)

bonds in Cl-CuPTC. At 25 KeV incident electron energy, the knock-on cross section for the 16 H atoms from the 16 C-H bonds is $5.85 \times 10^{-5} \pi a_0^2$ and on including the multiplication factor $\bar{\nu}$, σ_{dp}^{eff} is $9.10 \times 10^{-5} \pi a_0^2$. This is in excellent agreement with the experimentally measured[15] damage cross section of $1.02 \pm 0.12 \times 10^{-4} \pi a_0^2$. This seems to indicate that at least in the most resistant biomolecules the knock-on caused damage dominates that caused by other mechanisms (i.e., via ionizations, excitations).

However, experiments by the Japanese group[17] seems to indicate otherwise. These experiments at 100 KeV monitor damage via the decrease in the intensity of the diffraction pattern and do not measure damage cross section; their results do indicate that Cl-CuPTC molecules are 40 times more resistant to damage than CuPTC. This observation cannot be explained by the assumption that the knock-on of H and Cl atoms cause the major fraction of the observed damage. Referring to Figure 5, one sees that at 100 KeV knock-on cross section of Cl from a C-Cl bond is ~ 4.1 times that of H atom and on including hydrogen atom cascade, $\bar{\nu}$ for Cl from C-Cl is ~ 1.86 times σ_{dp}^{eff} for H from C-H. It is emphasized that the Japanese experiments do not measure cross sections for the damage of a molecular structure but only the degradation of the crystalline structure; hence our comparison and expectations of agreement with these experiments may be over ambitious.

b. Relationship between exposure and dissociation cross sections.

In this section, the interaction of an incident electron with molecular electrons is considered. In analogy with the formulations
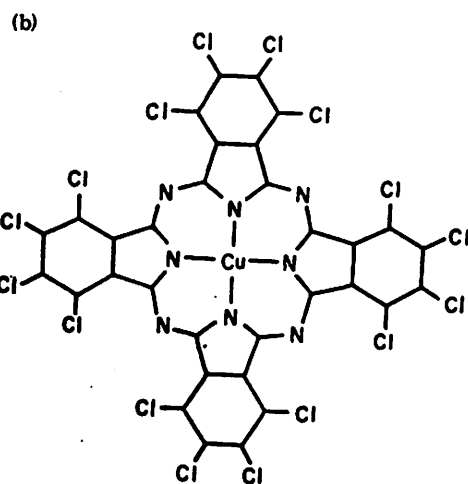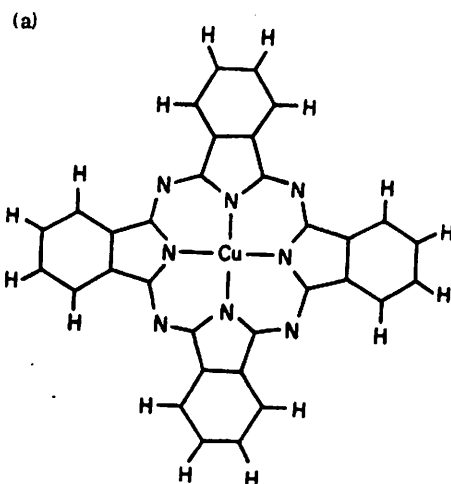
(a)

(b)

Fig. 6. Molecular structure of phthalocyanines.
(a) Cu-phthalocyanine and (b) hexadecachloro-Cu-
phthalocyanine.

2.29

of dissociative attachment a two step process for dissociative excitation and ionization is assumed and relevant quantities are isolated. Dissociative ionization is assumed to be the dominant mechanism for dissociation due to the incident electrons in a medium energy EM.

The interaction of the incident electron with the bound molecular electrons can initiate three possible processes: Ionization, excitation or electron capture (attachment). Each of these processes occur in a time of the order of an electronic orbital period$\sim 10^{-16}$ sec. The subsequent motion of the nuclei, if any, occurs at a relatively later time; about 10^{-13} sec after the initial interaction of the incident electron with the bound electrons. Thus it is physically reasonable to assume that dissociation occurs via a two step process. An intermediate, unstable configuration of the molecule is formed which subsequently can dissociate. And the three processes that lead to dissociation of the molecule AB are: (1) Dissociative ionization (DI), which is represented through the equation

$$e^- + AB \rightarrow (AB^+)^* + e^- + e^- \rightarrow A^+ + B + e^- + e^-. \tag{16}$$
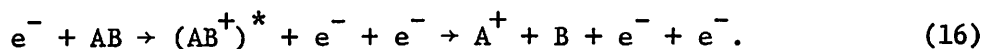
Where $(AB^+)^*$ represents the unstable molecular ion and A^+ and B represent the fragments. (2) Dissociative excitation (DE), which is represented by the equation

$$e^- + AB \rightarrow AB^* + e^- \rightarrow A^* + B + e^-. \tag{17}$$
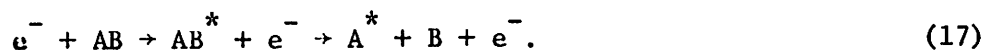
Where AB^* represents the excited molecule, and A^* and B the fragments. (3) Dissociative attachment (DA), which is represented by the equation

$$e^- + AB \rightarrow (AB^-)^* \rightarrow A^- + B. \qquad (18)$$

Where $(AB^-)^*$ represents the negatively charged molecular ion, and A^- and B the fragments.

The third process, DA, has an extremely small probability of occurrence for the fast electrons in the EM. Dissociative attachment is a resonance phenomenon that is determined[18] by the product of the probability of temporary capture of the incident electron by the molecule and the probability of its subsequent dissociation before auto-ionization of the temporary negative ion can occur. As one expects, the initial capture of the incident electron can only occur for incident electron energies comparable to the electron affinity for the molecule – a few electron volts. Experimental data[19] show that for higher incident electron energies the DA cross section is essentially zero, even though for incident electron energies close to the threshold ($\sim$ 0.1-10 eV) large values of DA cross sections ($\sim 10^{-15}$ cm^2 for CCl_4) can occur. Thus DA can be ignored as far as the action of the incident electrons is concerned. However, in the case of secondary dissociations initiated by slow electrons, DA will be seen (Chapter 5) to be an important mechanism.

Unlike dissociative attachment, DE and DI are much more likely to occur in an EM. The two step process, assumed in the writing of Eqns. (16) and (17), is now postulated to be described by the equation:

$$\sigma_D = \sigma_A \cdot P_d \qquad (19)$$

For either DE or DI, the dissociation cross section is written as

σ_D; the molecular cross section to create an 'Activated State' of the molecule [$(AB^+)^*$ in the case of DI and AB^* in the case of DE] is written as σ_A; and the probability that this activated state will lead to dissociation is denoted by P_d. Note that the activated state is not necessarily, indeed rarely, a stationary state of the excited molecule (in the case of DE) or the molecular ion (in the case of DI). A schematic molecular energy vs. inter-fragment separation diagram (Figure 7) elucidates the factors involved in Eqn. (19). Consider the different possible paths that lead to the dissociation of the molecule AB into a particular set of fragments A' + B. The prime on the fragment A in general denotes either an excited fragment A^* or an ionized fragment A^+; while A does not necessarily refer to an atom but to a collection of atoms (e.g., CH_2^+ from CH_4). Then energy conservation requires that transition to the state labeled 0 cannot lead to the fragmentation of AB into A' and B even though it could form the fragments A and B. Thus for this process, some of the possible activated states are labeled a, b, c, d, and e in the figure and $\sigma_A(i)$ are the cross section for making a molecular transition from the ground state X to the activated state i. These transitions are represented schematically by vertical arrows from X to each of the activated states i. The justification for the assumption of these vertical transitions is through the Franck-Condon principle and will be given below. For the fast incident electrons in the EM, the concept of the vertical transition and of the activated state ought to be quite valid. The probability P_d with which each of these activated states dissociates
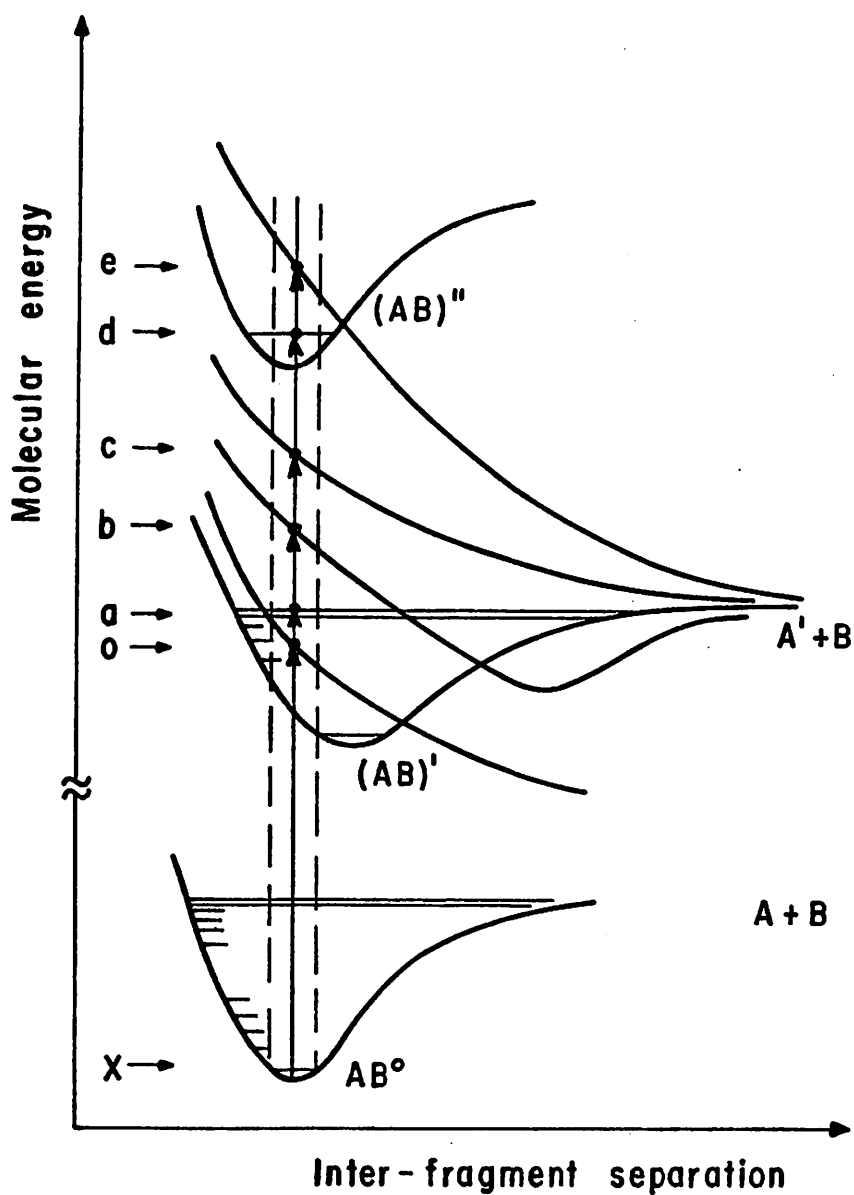
Fig. 7. Schematic molecular energy vs. inter-fragment separation diagram. Electronic transitions occur 'vertically', i.e., in accord with the Franck-Condon principle. The region between the dashed lines is the Franck-Condon region. Ground state is denoted schematically by X, excited states by 0 through e.

depends not only on the particulars of the activated state but also on which intra-molecular and inter-molecular process causes an activated state to decay before dissociation can occur. The mathematical formulation of P_d, the details of these processes and estimation of their magnitudes are postponed until Chapter 5. From now on, until Chapter 5, our attention is focused on the description and the quantification of the activated state cross section $\sigma_A(i)$.

Referring once again to Figure 7, we now very qualitatively describe some of the many possible activated states that can lead to the formation of the fragments A' and B. The activated state denoted by a is a highly excited vibrational state of the bound electronic state of the complex (AB)'. The activated states b and c are actually unbound electronic states of the molecules; however the probability that the particular fragments A' and B are formed is not necessarily unity (especially for the state b). State d represents the formation of a bound state of (AB)", while state e represents an unbound state of the molecule. Once again note that neither of these states (d or e) have a unit probability of leading to the fragments A' and B. This description makes it possible to categorize the activated state of the molecule as one that has involved a transition to either a bound electronic state or to an unbound, resonant electronic state. The mathematical description of scatterings to resonant molecular states (as evolved in the recent theories of DA in diatomic molecules by Bardsley[18] et al., Chen[20] and O'Malley[21]) are beyond the scope of this work. Interest here is primarily in obtaining trends and magnitudes for complex molecules, so that simplistic methods are assumed for these resonant

states.

Consider the inelastic scattering of a sufficiently fast moving (but still non-relativistic) electron with momentum $\hbar\underset{\sim}{k}$ from a stationary molecule with N nuclei and n electrons. Suppose the molecule makes a transition from a ground state with the wave function $\Psi_{00} = \phi_0(\underset{\sim}{r},\underset{\sim}{R})X_{00}(\underset{\sim}{R})$ to an excited state (discrete or continuum) with the wave function $\Psi_{\alpha\beta} = \phi_\alpha(\underset{\sim}{r},\underset{\sim}{R})X_{\alpha\beta}(\underset{\sim}{R})$. Here $\underset{\sim}{r} = \{\underset{\sim}{r}_i\}$ and $\underset{\sim}{R} = \{\underset{\sim}{R}_i\}$ represent the coordinates of all the molecular electrons and the molecular nuclei respectively. Spin coordinates are suppressed. Born-Oppenheimer separation is assumed (Appendix 2a) and the set of quantum numbers labeling the electronic state and the nuclear (vibrational-rotational) state are α and β respectively. In the first Born approximation, the cross section for making this molecular transition and concommittantly scattering the incident electron into a solid angle $d\Omega$ with a final momentum of $\hbar\underset{\sim}{k}'$ is[22],

$$d\sigma_{\alpha\beta} = \frac{1}{(4\pi a_0^2 E_R)^2} \frac{k'}{k} \left| \int e^{i\underset{\sim}{K}\cdot\underset{\sim}{r}'} V_{\alpha\beta,00}(\underset{\sim}{r}')d\underset{\sim}{r}' \right|^2 d\Omega \qquad (20)$$

Here $\underset{\sim}{K}$ is the momentum transfer given by $\underset{\sim}{K} = \underset{\sim}{k} - \underset{\sim}{k}'$ and $V_{\alpha\beta,00}(\underset{\sim}{r}')$ is the matrix element given by,

$$V_{\alpha\beta,00}(\underset{\sim}{r}') = \langle \phi_\alpha(\underset{\sim}{r},\underset{\sim}{R})X_{\alpha\beta}(\underset{\sim}{R}) | V(\underset{\sim}{r},\underset{\sim}{r}') | \phi_0(\underset{\sim}{r},\underset{\sim}{R})X_{00}(\underset{\sim}{R}) \rangle, \qquad (21)$$

where the coulombic coupling between the incident electrons and the molecular electrons is $V(\underset{\sim}{r},\underset{\sim}{r}') = \sum\limits_{i=1}^{n} e^2/|\underset{\sim}{r}' - \underset{\sim}{r}_i|$. Note that since this calculation is restricted to inelastic scattering the coulombic coupling between the incident electron and the nuclei of the molecule

is neglected. Inclusion of this coupling gives rise to elastic

scattering effects (including diffraction) from molecules and also

inelastic scattering by direct energy transfer to the vibrational

modes of the nuclei. The knock-on displacement analysis (in Sec.

2.2.a) has involved then an approximation of this incident electron-

molecular nuclei interaction. Following the treatment of inelastic

scattering from diatomic molecules by Craggs and Massey[23], the

matrix element $V_{\alpha\beta,00}(\underset{\sim}{r}')$ can be approximated as,

$$\langle \phi_\alpha(\underset{\sim}{r},\underset{\sim}{R}^0) | V(\underset{\sim}{r},\underset{\sim}{r}') | \phi_0(\underset{\sim}{r},\underset{\sim}{R}^0) \rangle \ \langle X_{\alpha\beta}(\underset{\sim}{R}) | X_{00}(\underset{\sim}{R}) \rangle . \qquad (22)$$

This is in the spirit of the Franck-Condon principle. Note that

since the electronic matrix element is evaluated for the wave

functions at the initial equilibrium positions of the nuclei $\underset{\sim}{R} =$

$\underset{\sim}{R}^0$, this provides a justification for the vertical transitions

assumed in Figure 7. Also, in general, the matrix element has to

be averaged over all orientations of the molecule with respect to

the incident electrons' direction.

Thus the cross section involves an evaluation of the square

of the overlap integral between the initial (00) and final ($\alpha\beta$)

vibrational states,

$$\langle X_{\alpha\beta}(\underset{\sim}{R}) | X_{00}(\underset{\sim}{R}) \rangle . \qquad (23)$$

This is also called the Franck-Condon (FC) factor. Evaluation of

(23) for the activated states in Figure 7 is straightforward. In

the case of an electronic transition to the unbound activated state

denoted by c and e in Figure 7, the overlap integral involves a

sum over all the possible vibrational states β (i.e., dissociation products with any kinetic energy is of interest). In this case the FC factor, through the use of the completeness relation, is identically equal to one. For an unbound state like b, the FC factor is also very nearly unity since those vibrational states that cannot energetically lead to dissociation lie well outside the FC region. In the case of a bound state such as d all the vibrational states (β) can energetically lead to dissociation. However, in general, the probability that each of these vibrational states will lead to dissociation will be different. Thus the separation of σ_D into σ_A and P_d is no longer useful since σ_A cannot be calculated independently of P_d. Both factors depend on the particular vibrational state of the excited molecule (AB)".

For transitions to particular vibrational states the FC factors are very difficult to evaluate; tabulated values[24] for diatomic molecules are now available. Thus it is only the transition to the highly vibrationally excited state a, that requires an evaluation of the FC factor. Usually such transitions will have very small FC factors, unless the left-hand classical turning point for the nuclear motion falls within the FC region (see Figure 7). Thus the FC factor can be approximated as unity in the calculation of σ_A; any error stems mainly from the neglect of the highly vibrationally excited states of the lowest bound states that can energetically lead to dissociation (such as state a in Figure 7). Recall that it is the P_d factor that determines if the activated state, once formed, will actually lead to the fragmentation of the molecule. Thus the calculation of σ_A should provide

already, a 'worst' case ($P_d = 1$) value for the total dissociation cross section σ_D of the molecule.

An alternate expression for σ_A, more amenable to calculation, is now developed. With the assumption of azimuthal symmetry about the axis of the incident electron, one can use (1) the famous Bethe relation, i.e. $\int e^{i\underset{\sim}{K}\cdot\underset{\sim}{r}'}/|\underset{\sim}{r}'-\underset{\sim}{r}_i|dr' = e^{i\underset{\sim}{K}\cdot\underset{\sim}{r}_i} \, 4\pi/K^2$ and (2) the kinematical relation between the momentum transfer K and the scattering angle θ, i.e. $KdK = \sin\theta d\theta/kk'$. Substitution of these in (20) and (22) gives

$$d\sigma_\alpha = \frac{8\pi a_0^2}{T/E_R} \, |\epsilon_{\alpha 0}(K)|^2 \, \frac{d(Ka_0)}{(Ka_0)^3},\qquad (24)$$

the differential cross section for momentum transfer dK. Here $\epsilon_{\alpha 0}(K)$ is the matrix element,

$$\langle \phi_\alpha(\underset{\sim}{r},\underset{\sim}{R}^0) | \sum_{i=1}^{n} e^{i\underset{\sim}{K}\cdot\underset{\sim}{r}_i} | \phi_0(\underset{\sim}{r},\underset{\sim}{R}^0) \rangle \cdot \qquad (25)$$

Note that the earlier approximation of the Franck-Condon factor allows us here to write the differential cross section $d\sigma_\alpha$ as that which considers transitions between the ground state ϕ_0 and the activated electronic state ϕ_α, both for the initial equilibrium positions of the nuclei.

Finally a general result can be inferred from the form of the matrix element in Eqn. (25). It is seen that at high incident electron energies T, the forward scattering or small momentum transfers (i.e., K $\rightarrow$ 0) dominates the integrated cross section,

$\sigma_A = \int d\sigma_\alpha$. Expanding $e^{i\underset{\sim}{K} \cdot \underset{\sim}{r}_i}$ for small K and using orthogonality one obtains the approximation,

$$\underset{K \to 0}{\ell t} \ |\varepsilon_{\alpha 0}(K)|^2/(Ka_0)^2 \to M_\alpha^2 = |\sum_{i=1}^{n} \underset{\sim}{K} \cdot \langle \phi_\alpha | \underset{\sim}{r}_i | \phi_0 \rangle |^2/(Ka_0)^2, \quad (26)$$

where M_α^2 is recognized to be the square of the dipole moment matrix element. In the case of atomic excitations by fast electrons, M_α^2 gives the optical selection rules, which forbid transitions between states of the same spatial parity. However in the case of scattering from molecules[25], the relative orientation of the direction of the incident electron with that of the molecular symmetry axis has to be considered in the evaluation of the matrix element. Selection rules depend then on this relative orientation and as such are more difficult to obtain. For ionization events, the direction of ejection of the ionized electrons adds a further complication to the determination of the symmetry of the final state. Thus, in general, only after knowing these relative orientations for a particular molecule in a particular experimental arrangement, is it possible to know the selection rules for molecular scattering. For the case of random orientation of molecules in an EM specimen, we shall assume that no selection rules apply.

In summary, the separation of the dissociation cross section σ_D into the σ_A and P_d factors, allows for the conceptual separation of the radiation action into the effect due to the incident electron on the molecule and that due to the subsequent reaction of the molecule to this action. The σ_A depends essentially on the in-

herent properties of the molecule, while P_d depends on both the inter-molecular and intra-molecular interactions. For DE and DI the activated state σ_A involves an evaluation of the nuclear overlap integral which can be approximated by unity. Finally we found that the dipole matrix element leads to the assumption of no selection rules for molecular scattering in the EM.

REFERENCES to Chapter 2.

1. L.V. Spencer and U. Fano, Phys. Rev. 93, 1172 (1954).

2. J.B. Birks, Photophysics of Aromatic Molecules, (Wiley-Interscience, 1970).

3. R. Voltz, Radiation Res. Rev. 1, 301 (1968).

4. D.L. Misell in Scanning Electron Microscopy/1973, ed. O. Johari, p. 225 (1973).

5. E.J. Hart and R.L. Platzman in Mechanisms in Radiobiology, M. Errera and A. Forssberg, Eds. (Academic Press, New York, 1961) , Vol. 1, p. 93.

6. G. Siegel, Z. Naturforsch. 27a, 325 (1972).

7. A.V. Crewe, J. Wall and J.P. Langmore, Science 168, 1338 (1970).

8. F. Seitz and J.S. Koehler in Solid State Physics, F. Seitz and D. Turnbull, Eds. (Academic Press, New York, 1956), Vol. 2, p. 305.

9. T.L. Cottrell, The Strengths of Chemical Bonds (Butterworths, London, 1958), 2nd ed., Table 11.5.1.

10. G.S. Khandelwal and E. Merzbacher, Phys. Rev. 130, 1822 (1963).

11. G.J. Dienes and G.H. Vineyard, Radiation Effects in Solids (Interscience, New York, 1957), Chap. 2.

12. M.J. Makin, Philos. Mag. 18, 637 (1968).

13. L. Pauling, The Nature of the Chemical Bond (Cornell Univ. Press, 1960), 3rd ed.

14. B.L. Schram, et al., J. Chem. Phys. 44, 49 (1966).

15. A.V. Crewe, M. Isaacson and D. Johnson, Rad. Research (to be published).

16. R.M. Glaeser (private communications).

17. N. Uyeda et al., J. Appl. Phys. <u>43</u>, 5181 (1972).

18. J.N. Bardsley, A. Herzenberg and F. Mandl, Proc. Phys. Soc. <u>89</u>, 321 (1966).

19. L.G. Christophorou, <u>Atomic and Molecular Radiation Physics</u> (Wiley-Interscience, 1971), Sec. 6.4.

20. J.C.Y. Chen, J. Chem. Phys. <u>40</u>, 3507 (1964).

21. T.F. O'Malley, Phys. Rev. <u>150</u>, 14 (1966).

22. J.D. Craggs and H.S.W. Massey in <u>Handbuch der Physik</u>, D. Flugge, Ed. (Springer, Berlin, 1959), Vol. 37, Sec. 9.

23. <u>Ibid</u>. p. 334.

24. D.J. Flinn et al., J. Quant. Spectry. Radiative Transfer <u>4</u>, 271 (1964).

25. H.S.W. Massey, <u>Electronic and Ionic Impact Phenomena</u> (Oxford Univ. Press, 1969), 2nd ed., Vol. 2, Sec. 12.4.2.

CHAPTER 3

SCATTERING THEORIES FOR DISSOCIATIVE IONIZATION

In this chapter, a simple theoretical model for the estimation of the activated state cross-section σ_A is developed. Though many-electron theories, which include electron-electron correlation, are more appropriate in fast electron scattering from molecules, an independent-electron approximation is assumed. Fewest possible molecular parameters are introduced so as to keep the model and the mathematics simple. In Sec. 3.1, two different single-electron scattering approximations (the Binary-Encounter and the First Born) are reviewed and extended so as to be useful in our model and to the incident electron energies in the EM. These approximations are applied to a many-electron molecular system in Sec. 3.2. A phenomenologically based scheme is developed to extend the independent electron scattering concept to include scatterings that involve excitation due to interactions amongst the bound electrons. Thus ionizations with concurrent excitation of other bound electrons can be considered. Ionization and DI cross sections for specific atoms and molecules are calculated in the next chapter.

3.1 Scattering from an independent-electron molecule.

a. Description and kinematics.

Before the simple independent-electron (or one-electron) scattering model is described, it is worthwhile to outline briefly the methods necessary for the theoretically more accurate and elaborate calculations concerning scattering from many-electron systems. This will also put our simple model in proper perspective with

respect to these more elaborate calculations.

The cross section for excitation or ionization of a molecule by an incident electron [Eqn. (2-25)] involves the evaluation of the matrix element,

$$< \phi_\alpha(\underline{r},\underline{R}^0) | \sum_i e^{i\underline{K}\cdot\underline{r}_i} | \phi_0(\underline{r},\underline{R}^0) >$$

in the first Born approximation. Recall that $\phi_\alpha(\underline{r},\underline{R}^0)$ and $\phi_0(\underline{r},\underline{R}^0)$ are many-electron (and nuclei) wave functions which have to be obtained in principle from the solution of the Schrodinger equation for a many-inter-acting-particle system. Most calculations of atomic structure (effective potential and wave function) have included electron-electron correlation only approximately. Even then accurate calculated data[1] is available only in numerical form, masking analytical dependences on atomic parameters (such as Z, orbital quantum numbers, occupancy, etc.). Approximate analytical atomic wave functions can be obtained from the modern extension of the quantum defect theory by Seaton[2]. These involve two additional parameters: s and σ , which are respectively the screening constant [giving an effective charge $eZ_{eff} = e(Z-s)$] and the quantum defect [giving an effective principle quantum number of $n^* = (n-\sigma)$]. These parameters are obtained empirically[3] through comparisons with experiment. Excited state wave functions are even more difficult to obtain, while continuum state (ionization) wave functions involve additional complications of normalization. For molecular systems, a first approximation of linear combinations of atomic orbitals can be used. However, more sophisticated

calculations[4] are necessary for reasonably accurate representation of the molecular structure. The sensitivity of the matrix element in Eqn. (1) below, or that in the optical limit given by Eqn. (II-26), on the choice of the wave function is demonstrated by calculations of excitations of the helium atom[5] and of the nitrogen molecule.[6] However, as will be seen, the experimentally measured ionization cross section involves integrations over the two dynamical parameters (K and E, to be defined and discussed below) and consequently the fine details are 'washed out' by the integration process. It may be then that crude approximations for the matrix element may be adequate to give quite accurate integrated cross sections. We will show that this is indeed true.

Since our primary interest here is in an exploratory study in the trends and dependences of σ_A on molecular parameters, we will avoid the more rigorous numerical methods for the simplest possible analytical scattering model. We assume, for now, a molecule composed of non-interacting electrons. Thus the interaction between the incident electron and the whole molecule can be modeled as separate interactions between the incident electrons and individual bound electrons. Extension of this idea to interacting-electron molecular systems is considered in Sec. 3.2 . However the immediate interest is in the interaction between the incident electron and one bound electron. The bound electron should, in principle, be described by its true ground state molecular wave function. We assume hydrogenic wave functions with an effective Z as a variable parameter. It will be shown (Sec. 3.2.a.) that

this parameter, which can be related to the bound electron kinetic energy, is at least approximately obtainable from the experimentally measured ionization potential for that bound electron. Thus this approximation may be considered as the simplest form of the quantum defect theory, i.e., with only one parameter. The evaluation of the one-electron matrix element,

$$< \phi_\alpha(\underset{\sim}{r}) \mid e^{i\underset{\sim}{K}\cdot\underset{\sim}{r}} \mid \phi_0(\underset{\sim}{r}) > \tag{1}$$

and the subsequent calculation of the cross section is the subject of the first half of this chapter. We use two different scattering approximations: (1) The Binary-Encounter (BE) theory and (2) the first Born approximation.

The history of the BE approximation goes back to the classical work of J. J. Thomson who calculated cross sections for ionization of atoms by incident electrons. His assumption of stationary bound electrons gives a very simple expression for the cross section that however did not agree well with experiment. An improvement on this classical approach was made by M. Gryzinski.[7] He allowed for motion of the bound electrons and using classical mechanics was able to obtain analytical closed-form expressions to the ionization and excitation cross sections. Subsequently the Gryzinski theory was simplified,[8] extended[9] and shown to have correspondence to the Born approximation.[10] An excellent review article by Vriens[11] outlines the modern developments.

In the BE theory an incident electron with momentum $\underset{\sim}{k}$ and kinetic energy T is assumed to interact coulombically with one

electron of the target (atom or molecule). This bound electron is assumed to possess momentum $\underset{\sim}{k}_\epsilon$, kinetic energy ϵ , and to have no interaction with other electrons or nuclei in the target. The kinematics of scattering is given by (a) the equation of the conservation of momentum, i.e.,

$$\underset{\sim}{k} + \underset{\sim}{k}_\epsilon = \underset{\sim}{k}_s + \underset{\sim}{k}_{\epsilon s} \tag{2}$$

and (b) the equation of the conservation of energy, i.e.,

$$T + \epsilon = T_s + \epsilon_s \qquad . \tag{3}$$

The quantities on the right hand side of the equality in (2) and (3) are the 'scattered' counterparts of the ones on the left hand side of the equality. In general the indistinguishability of the electrons does not allow such a labeling of these two electrons, as is implied in Eqns. (2) and (3). When the two electrons have comparable energies, the effect due to electron indistinguishability is quite important, as will be seen in Sec. 3.1.c. However, in the case of fast incident electrons $T/\epsilon \gg 1$ the assumption of two distinguishable electrons is quite valid. The momentum transfer $\underset{\sim}{K}$ and the energy transfer E by an incident electron to a bound electron are given by,

$$\underset{\sim}{K} = \underset{\sim}{k} - \underset{\sim}{k}_s = \underset{\sim}{k}_{\epsilon s} - \underset{\sim}{k}_\epsilon \qquad , \tag{4}$$

and

$$E = T - T_s = \epsilon_s - \epsilon \qquad . \tag{5}$$

3.5

for later use, we note that two convenient expressions, derivable from Eqn. (4), for the minimum/maximum momentum transfer $K_{min,max}$ are given by,

$$K_{min,max} = k_{\epsilon s} \mp k_\epsilon \quad , \tag{6}$$

$$(Ka_o)^2_{min,max} = [\sqrt{(E + \epsilon)/E_R} \mp \sqrt{\epsilon/E_R}]^2 \quad . \tag{6'}$$

Recall that a_o and E_R are the bohr radius and the rydberg of energy respectively.

In the Born approximation, unlike in the BE approximation, the kinematics of scattering involves the mutual interaction of the bound electrons with the atomic nuclei. Consider the incident-electron induced transition from a state, with energy $(-U)$, to a discrete or a continuum state, with energy $(-U')$. Conservation of energy requires

$$T + (-U) = T_s + (-U') + T_e + T_N \quad , \tag{7}$$

where T_e is the kinetic energy of an electron ejected in those transitions that involve ionizations; T_N is the kinetic energy imparted to the atomic nuclei, which for inelastic collisions is assumed to be zero. The energy transferred by the incident electron E is

$$E = T - T_s = T_e + (U - U') = T_e + E_t \quad , \tag{8}$$

where $E_t = U - U'$ is the threshold energy for the transition. For the transitions to discrete final states, E takes on discrete values corresponding to the excitation energy for that transition, while for ionizations, E is a continuous variable with a threshold energy corresponding to the ionization potential (i.e., $E_t = I$). The equation for momentum conservation is

$$\underset{\sim}{k} = \underset{\sim}{k}_s + \underset{\sim}{\kappa} + \underset{\sim}{K}_N \quad . \tag{9}$$

In general, $\underset{\sim}{\kappa}$ is the momentum transfer to the bound electron, so that in the case of ionization $\underset{\sim}{\kappa}$ is approximately the momentum of the ejected electron. The momentum transfer to the atomic nuclei $\underset{\sim}{K}_N$ is assumed to be zero, since T_N is set equal to zero. Thus the momentum transfer $\underset{\sim}{K}$ is,

$$\underset{\sim}{K} = \underset{\sim}{k} - \underset{\sim}{k}_s \approx \underset{\sim}{\kappa} \quad . \tag{10}$$

Using Eqns. (8) and (10), one obtains an expression for the magnitude of the momentum transfer K by an incident electron deflected by an angle θ .

$$(Ka_o)^2 = 2(T/E_R) \, [1 - 1/2 \, E/T - \sqrt{1 - E/T} \, \cos \theta]. \tag{11}$$

Note that minimum and maximum values of K are obtained for $\theta = 0$ and π , respectively. For scattering events involving small energy transfers by relatively high incident energy electrons (i.e., in the limit $E/T \ll 1$), one can obtain the minimum momentum transfer from an approximation of Eqn. (11), i.e.,
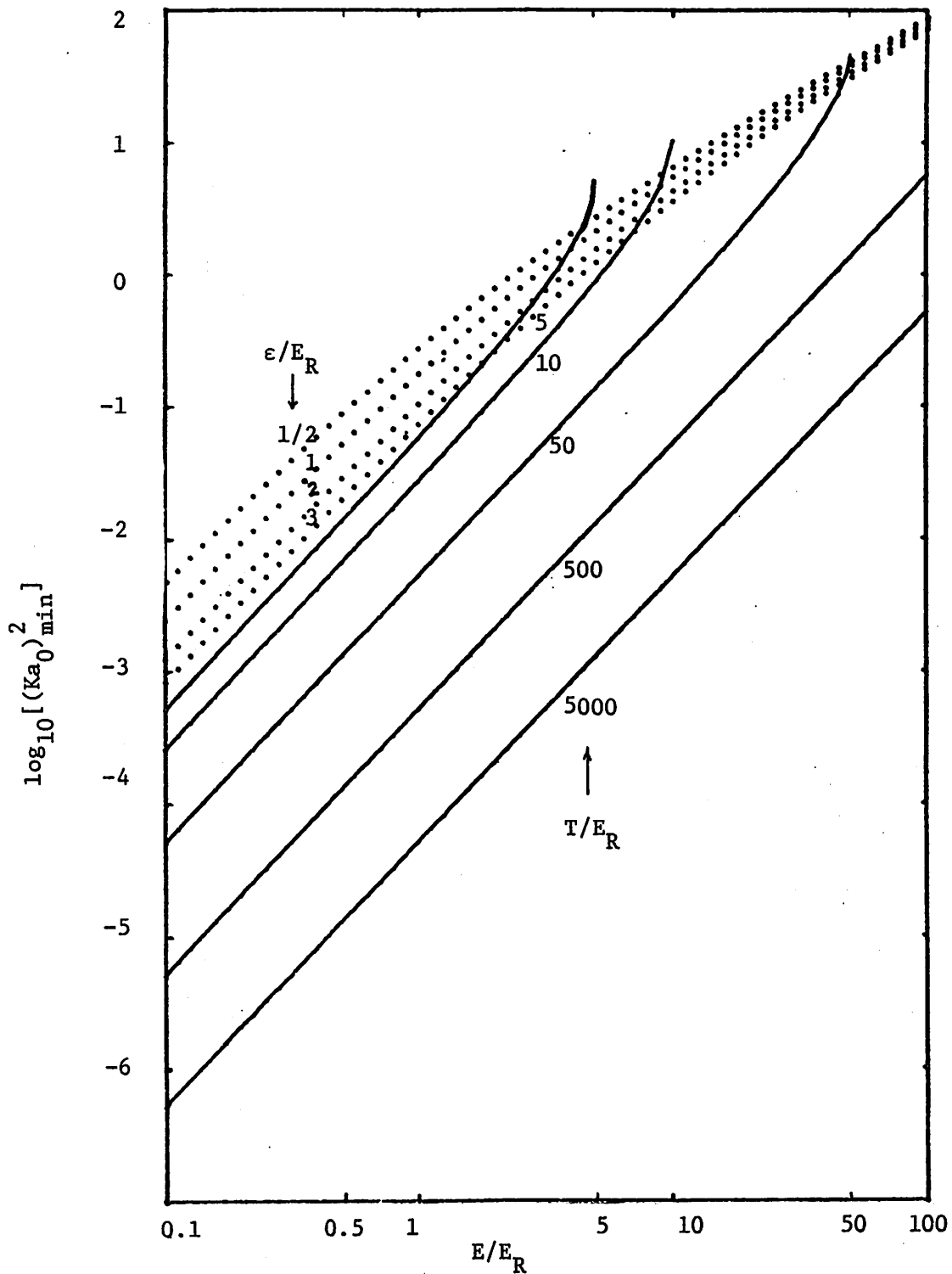
Fig. 1. Comparison of the kinematics of the BE ($\cdot\cdot;\cdot\cdot\cdot\cdot$) and the Born (——) approximations. $\log_{10}[(Ka_0)^2_{min}]$ is plotted versus E/E_R for the two parameters as shown.

$$(Ka_o)^2_{min} \approx \frac{E^2}{4TE_R} \left(1 + \frac{1}{2}\frac{E}{E_R}\right) \qquad (12)$$

The importance of the minimum momentum transfer permitted by the kinematics K_{min} cannot be fully appreciated until the dynamics of scattering is considered in Sec. 3.1.b. Nevertheless an inspection of K_{min} for the two theories reveals several important differences. For the Binary theory, Eqn. (6') shows an explicit dependence of K_{min} on the kinetic energy of the bound electrons ε ; while the Born approximation K_{min} depends on the incident electron energy T. In Fig. 1, the expressions for $(Ka_o)^2_{min}$ in the two theories are plotted against energy transfer E, with values of ε/E_R and T/E_R ($\gtrsim E/E_R$) as parameters. For low incident electron energies ($T/E_R \sim 5,10$) the two expressions for $(Ka_o)^2_{min}$ give comparable answers, especially for values of $E \sim T$. However for larger values of T (and especially for $T/E_R \gtrsim 100$) there is at least an order of magnitude difference between the values of $(Ka_o)^2_{min}$ in the two theories. The difference of course becomes greater with increasing value of T, since the BE expression for $(Ka_o)^2_{min}$ is independent of T. Note that even though $(Ka_o)^2_{min}$ in the BE approximation decreases with increasing ε/E_R , it has an insignificant effect in the comparison. Thus it can already be inferred that since at high incident electron energies, the small momentum transfer events dominate the cross section, the BE approximation results should be significantly different from the Born approximation results in that region.

b. Generalized Oscillator Strength.

The concept of the oscillator strength was born in the classical theories of light scattering from matter. It was thought that

each of the atomic electrons was forced to oscillate by the external electromagnetic radiation at a frequency close to the electrons' characteristic frequency ω_α . The total number of characteristic frequencies ($\sum_\alpha 1$) observed experimentally were far greater than the total number of electrons (Z) in the atom and thus provided a conceptual mire to the classical physicists. The quantum mechanical model of the atom with a statistical distribution of electron positions allows for far more numerous oscillator frequencies (infinite) than the number of electrons. To each frequency ω_α is associated an effective number of oscillators; these are also known as (dipole) oscillator strengths[12] and defined as:

$$f_\alpha = \frac{\omega_\alpha}{\omega_R} |<\phi_\alpha| \sum_i \underset{\sim}{r}_i |\phi_o>|^2 / a_o^2 \quad . \tag{13}$$

The oscillator strengths are essentially a measure of the transition probability, weighted by the characteristic excitation frequency ω_α (Note that $\omega_R \equiv E_R/\hbar$). For transitions to bound states the ω_α values are discrete, while for transitions to states in the continuum, the frequency is a continuous variable. This requires the definition of an oscillator strength density i.e., df/dω . The total oscillator strength for all frequencies is equal to the total number of electrons in the molecule (the sum rule), i.e.,

$$\sum_\alpha f_\alpha + \int \frac{df}{d\omega} = Z \quad . \tag{14}$$

In the scattering of electrons from molecules, an extension of the above concepts leads to the definition of the generalized oscillator strength density, i.e.,

$$\frac{df}{dE}(K,E) = \sum_\alpha \frac{E_\alpha/E_R}{(Ka_o)^2} \left| <\phi_\alpha \right| \sum_i e^{i\underset{\sim}{K}\cdot \underset{\sim}{r}_i} \left| \phi_o> \right|^2 \delta(E - E_\alpha) \quad . \quad (15)$$

The sum (integral) extends over both the discrete and the continuum states ϕ_α of the molecule, so that the effect of $\delta(E - E_\alpha)$ is to 'filter' out those states that lie in the energy interval $(E - \delta E/2, E + \delta E/2)$, the excitation energy E_α is defined such that $E_o = 0$. Notice also that in the limit $K \rightarrow 0$, the above definition reduces to the optical definition of the oscillator strength in Eqn. (13).

The above definition of the generalized oscillator strength density leads to the definition of a new quantity – the double differential cross section[13] $d(\frac{d\sigma}{dE})$ for energy transfer dE and momentum transfer dK, i.e.,

$$d(\frac{d\sigma}{dE}) = \frac{8\pi a_o^2}{T/E_R} \frac{1}{E/E_R} \frac{df}{dE}(K,E) \frac{d(Ka_o)}{(Ka_o)} \quad . \quad (16a)$$

Comparison with $d\sigma_\alpha$ in Eqn. (2-24) gives the total integrated cross section for a transition to a particular state α as

$$\sigma_\alpha = \int_{K_\alpha} d\sigma_\alpha = \int_{E_\alpha} \int_{K_\alpha} d(\frac{d\sigma}{dE}) \, dE \quad . \quad (16b)$$

Here the integration over the momentum transfer K is over the

interval denoted here by K_α , while that over the energy transfer E is over the interval denoted here by E_α . The interval K_α is obtained from the kinematical relations in Eqns. (6) or (11). However the energy transfer interval E_α depends on the particular state α . Details of the integration of $d(d\sigma/dE)$ will be the subject of the next section; here we focus our attention on the evaluation of df/dE.

The BE expression of df/dE is an approximation[14] of the exact definition in Eqn. (1). The dynamics of scattering is governed by a type of an impulse approximation. All forces acting on a bound electron (by other electrons and by the atomic nuclei) are ignored. This makes the approximation valid only for sufficiently large values of energy transfer E, so that the scattering can be considered to be between two essentially free electrons. The expression for df/dE, in the BE approximation, is

$$df/dE = \frac{E/E_R}{(Ka_o)^2} < \phi_o | \ \delta \ (E - \frac{\hbar^2 K^2}{2m} - \frac{\hbar^2 \underset{\sim}{K} \cdot \underset{\sim}{k}}{m}) | \ \phi_o > \ . \qquad (17)$$

This expression is mathematically considerably simpler than the original expression in Eqn. (15); therein lies its main advantage. It requires knowledge of only the ground state wave function and not the final state wave functions. The argument of the delta function merely imposes energy conservation in the scattering of two free particles, i.e.,

$$E - \frac{(\hbar K)^2}{2m} - \frac{\hbar^2 \underset{\sim}{K} \cdot \underset{\sim}{k}}{m} = E - \frac{\hbar (\underset{\sim}{k} + \underset{\sim}{K})^2}{2m} - \frac{\hbar^2 k^2}{2m} \qquad . \qquad (18)$$

Here $\hbar \underline{k}$ is the momentum of the bound electron.

We now evaluate this expression [Eqn. (17)] for two simple distributions of bound electron momenta. The df/dE is most conveniently integrated using momentum-space ground state wave functions $\phi(\underline{k})$, so that Eqn. (17) is rewritten as

$$df/dE = \frac{E/E_R^2}{(Ka_o)^2} \int_o^\infty \int_{-1}^1 \int_o^{2\pi} |\phi(k,\theta,\phi)|^2 \, \delta(E/E_R - (Ka_o)^2 - 2Kka_o^2 \cos \theta)$$

$$\cdot k^2 dk \; d(\cos \theta) \; d\phi \quad . \tag{19}$$

For spherically symmetric $\phi(K)$ the df/dE, after intergration over ϕ and θ , becomes

$$df/dE = \frac{2\pi \; E/E_R^2}{(Ka_o)^2} \int_o^\infty |\phi(k)|^2 \left(\frac{1}{2Kka_o^2}\right)_{\theta = \theta_o} k^2 dk \quad . \tag{20}$$

Here we have used the expression: $\displaystyle\int_a^b \delta[f(x)]dx =$

$\displaystyle\int_a^b \sum_n \delta(x-x_n)/|f'(x_n)|dx$, where x_n are the roots of $f(x)$ that

lie within the interval (a,b). Correspondingly θ_o is the root of the equation

$$E/E_R - (Ka_o)^2 - 2Kka_o^2 \cos \theta_o = 0 \quad . \tag{21}$$

Since $\cos \theta_o$ is bounded by (-1,1), the maximum value of k is unrestricted; however the minimum value of k is restricted by

3.13

$$k_{min} = \frac{1}{2Ka_o^2} \left| E/E_R - (Ka_o)^2 \right| \quad . \tag{22}$$

Substituting in (20), the expression for df/dE for a spherically symmetric $\phi(\underline{k})$ becomes

$$df/dE = \frac{\pi \ E/E_R^2}{(Ka_o)^3} \ \frac{1}{a_o} \int_{K_{min}}^{\infty} |\phi(k)|^2 k \ dk \quad . \tag{23}$$

We choose two simple spherically symmetric distribution for $\phi(k)$: (1) Bound electrons with a fixed speed and (2) Bound electrons with a hydrogenic distribution for $\phi(k)$. The first model describes an s-state hydrogenic system in the old quantum theory of Bohr. The momentum distribution can be written as

$$|\phi(k)|^2 = \frac{\delta(k - k_\epsilon)}{4\pi k^2} \tag{24}$$

where $\hbar k_\epsilon$ is the 'fixed' momentum of the bound electrons. Substitution into Eqn. (23) and integration gives

$$df/dE = \begin{cases} \frac{1}{4} \ \dfrac{E/E_R^2}{(Ka_o)^3} \sqrt{\dfrac{E_R}{\epsilon}} & \text{for } (Ka_o)_{min} \lesssim (Ka_o) \lesssim (Ka_o)_{max} \\ 0 & \text{otherwise} \end{cases} \tag{25}$$

We have used here the relation $\epsilon/E_R = (k_\epsilon a_o)^2$, where ϵ is the kinetic energy of the bound electron. Next we consider the second model. Hydrogenic momentum distribution is obtained in a straight-

forward manner by taking a fourier transform of the hydrogenic wave function. i.e.,

$$\phi_{n,\ell}(k,\theta,\phi) = \frac{1}{k} \, g_{n\ell}(k) \, Y_{\ell m}(\theta,\phi)$$

where   (26)

$$g_{n\ell}(k) = \sqrt{\frac{2}{\pi}} \, i^{-\ell} \int_0^\infty j_\ell(kr) R_{n\ell}(r) \, r \, dr \quad .$$

The $Y_{\ell m}(\theta,\phi)$ and $j_\ell(k_r)$ are respectively spherical harmonics and spherical Bessel functions. The radial part of the solution to the Schrodinger equation is denoted by $R_{n\ell}(r)$, which for a hydrogenic is state is $2(Z/a_o)^{3/2} \exp(-Zr/a_o)$. Thus the momentum distribution for a hydrogenic 1s state is

$$|\phi(k)|^2 = \frac{8}{\pi} \, \frac{(Z/a_o)^5}{[(Z/a_o)^2 + k^2]^4} \quad .$$ (27)

Substitution into Eqn. (23) yields,

$$df/dE = \frac{2^8}{3\pi} \, \frac{(\epsilon/E_R)^{5/2} \, E/E_R^2 \cdot (Ka_o)^3}{[4(Ka_o)^2 \cdot \epsilon/E_R + (E/E_R - (Ka_o)^2)^2]^3} \quad .$$ (28)

Here the parameter Z has been replaced by the parameter ϵ , which is defined through $\epsilon/E_R = Z^2$. Through the identification of $-Z^2 E_R$ as the energy of the one-electron system (excluding a constant energy of the 'core' electrons) and the use of the virial theorem, Z can be considered as the kinetic energy of the bound electrons in the one-electron approximation.

Next we obtain the oscillator strength density in the first
Born approximation. This involves a straightforward determination
of the matrix-element in Eqn. (15). For a hydrogenic system, ana-
lytical expressions are available for all excited state and contin-
uum state wave functions. Fano and Cooper[12] have shown how the
integrated df/dE for the discrete states can be regarded as merely
an extension of the same for the continuum states. We first focus
our attention on the calculation of df/dE for the continuum states.
A method for obtaining the integrated cross sections dσ/dE for the
discrete states will be discussed in the next section. The con-
tinuum state wave functions $|E \ \Omega>$ are specified by E and a set of
all other quantum numbers Ω (ejected electron direction, etc.), so
that the normalization becomes

$$<E' \ \Omega' | \ E \ \Omega> = \delta(E - E') \cdot \delta(\Omega - \Omega') \quad . \tag{29}$$

Then the one-electron matrix element in the case of electron ejec-
tion in all directions is written as

$$\int <E \ \Omega_e | \ e^{i\vec{K} \cdot \vec{r}} | \phi_{n\ell m}> \ d\Omega_e \quad . \tag{30}$$

For the hydrogenic 1s state ϕ_{100} this has been evaluated by Bethe[15].
This expression depends explicitly on the magnitude of the momentum
of the ejected electron $\hbar\kappa$. As such the df/dE derivable from (30)
depends on both E and κ . Rewriting the energy conservation ex-
pression in Eqn. (8), as,

$$T_e/E_R = (a_o K)^2 = (E - E_t)/E_R \tag{31}$$

and, as in (28), substituting $\varepsilon = Z^2 E_R$ we obtain df/dE in terms of the kinetic energy of the bound electron ε and the threshold energy for the ionization process E_t. The expression for df/dE becomes

$$\frac{2^7[(Ka_o)^2 + 1/3 \, (E + \varepsilon - E_t/E_R] \, (\varepsilon/E_R)^3 \, E/E_R^2 \cdot A}{[((Ka_o)^2 - E/E_R)^2 + 2(Ka_o)^2(\varepsilon + E_t)/E_R + (\varepsilon - E_t)(\varepsilon - E_t + 2E)/E_R^2]^3}$$

where   (32)

$$A = \left[1 - \exp(-2\pi\sqrt{\frac{\varepsilon}{E-E_t}})\right]^{-1} \cdot \exp\left\{-2\sqrt{\frac{\varepsilon}{E-E_t}} \tan^{-1}\left(\frac{2\sqrt{\varepsilon}(E-E_t)/E_R}{(Ka_o)^2-(E-E_t-\varepsilon)/E_R}\right)\right\}$$

In (32) the derivation requires that the arctangent lies in the interval $[o,\pi)$.

Next we compare the behavior of the three oscillator strength densities in Eqns. (25), (28) and (32) as a function of momentum transfer K. In order to remove the explicit dependence on E_t in (32), the variables are normalized as follows: $y^2 = E_R/E_t \, (Ka_o)^2$, $E' = E_R/E_t$, $\varepsilon' = \varepsilon/E_t$. The expressions for the normalized oscillator strength densities df/dE' in the BE approximation (for two distributions) and in the Born approximation (for the hydrogenic 1s distribution) are given in Table 1. For the case of the Hydrogen atom (where $E_t = \varepsilon = E_R$) the expressions in Table 1 reduce to those of Vriens and Bonson.[10] In Figures 2, 3 and 5, df/dE' is plotted against $\ell n \, y^2$. It will be seen (next section) that the areas under these df/dE' curves are proportional to the energy transfer cross section $d\sigma/dE$. We now examine the behavior of the df/dE'

Table 1: Normalized generalized oscillator strength densities
df/dE'.

Binary Encounter approximation

(i) Constant speed distribution

$$df/dE' = E'/4\sqrt{\varepsilon'} \cdot 1/y^3 \qquad\qquad \text{(a)}$$

(ii) Hydrogenic 1s distribution

$$df/dE' = \frac{2^8}{3\pi} \frac{(\varepsilon')^{5/2} E' y^3}{[(y^2-E')^2 + 4\varepsilon'y^2]^3} \qquad\qquad \text{(b)}$$

First Born approximation

Hydrogenic 1s distribution

$$df/dE' = \frac{2^7 (\varepsilon')^3 E' [y^2 + 1/3(E'+\varepsilon'-1)] \cdot A}{[(y^2-E')^2 + 2y^2(\varepsilon'+1) + (\varepsilon'-1)\cdot(\varepsilon'-1+2E')]^3} \qquad\qquad \text{(c)}$$

where

$$A = \frac{\exp\left\{- 2\sqrt{\dfrac{\varepsilon'}{E'-1}} \tan^{-1}\left(\dfrac{2\sqrt{\varepsilon'(E'-1)}}{y^2-E'+\varepsilon'+1}\right)\right\}}{\left[1 - \exp\left(-2\pi\sqrt{\dfrac{\varepsilon'}{E'-1}}\right)\right]}$$

curves for small and large values of y^2. Since events occurring with small values of y^2 are those that involve small momentum transfer, they are related to optical absorption transitions (which occur at $K = 0$). Large momentum transfer events (large y^2) are essentially the small impact parameter ('hard') collisions between the incident and the bound electrons.

The two df/dE' obtained in the BE approximation for the two different momentum distributions are shown in Fig. 2, for the case of $E' = 5$ and $\varepsilon' = 1$ and 3. The shapes of the curves for df/dE' vs. $\ell n\ y^2$, as expected, are quite different; the df/dE' in the case of the hydrogenic distribution decreases for values of $(Ka_o)^2$ smaller than $(Ka_p)^2$ – the value at which df/dE' has its maximum. The $(Ka_o)_p^2$ is given by

$$(Ka_o)_p^2 = \frac{E' - 2\varepsilon'}{3} + \frac{2}{3}\sqrt{E'^2 + \varepsilon'^2 - \varepsilon'\ E'} \quad . \qquad (33)$$

While in the case of the fixed speed distribution the rise in df/dE' is monotonic for decreasing $(Ka_o)^2$, until $(Ka_o)_{min}^2$ defined in Eqn. (6'). In both cases we see the 'spreading' of df/dE' with increasing ε' ; in the case of the fixed speed distribution, this 'spreading' can be attributed directly to the increase in the interval $[(Ka_o)_{min}^2$, $(Ka_o)_{max}^2]$. The implications of this behavior will become clear in the calculation of $d\sigma/dE$ in the next section.

It is more interesting to compare the df/dE' for the hydrogenic 1s momentum distribution in the BE and the Born approximations. For large values of E' (Fig. 3a; $E' = 20$) the df/dE' have similar shapes in both approximations. However for $\varepsilon' = 0.5$, the magnitude of the maximum of the Born df/dE' is greater than that

CONSTANT SPEED DISTRIBUTION

$\epsilon' = 3$

$\epsilon' = 1$

HYDROGENIC DISTRIBUTION

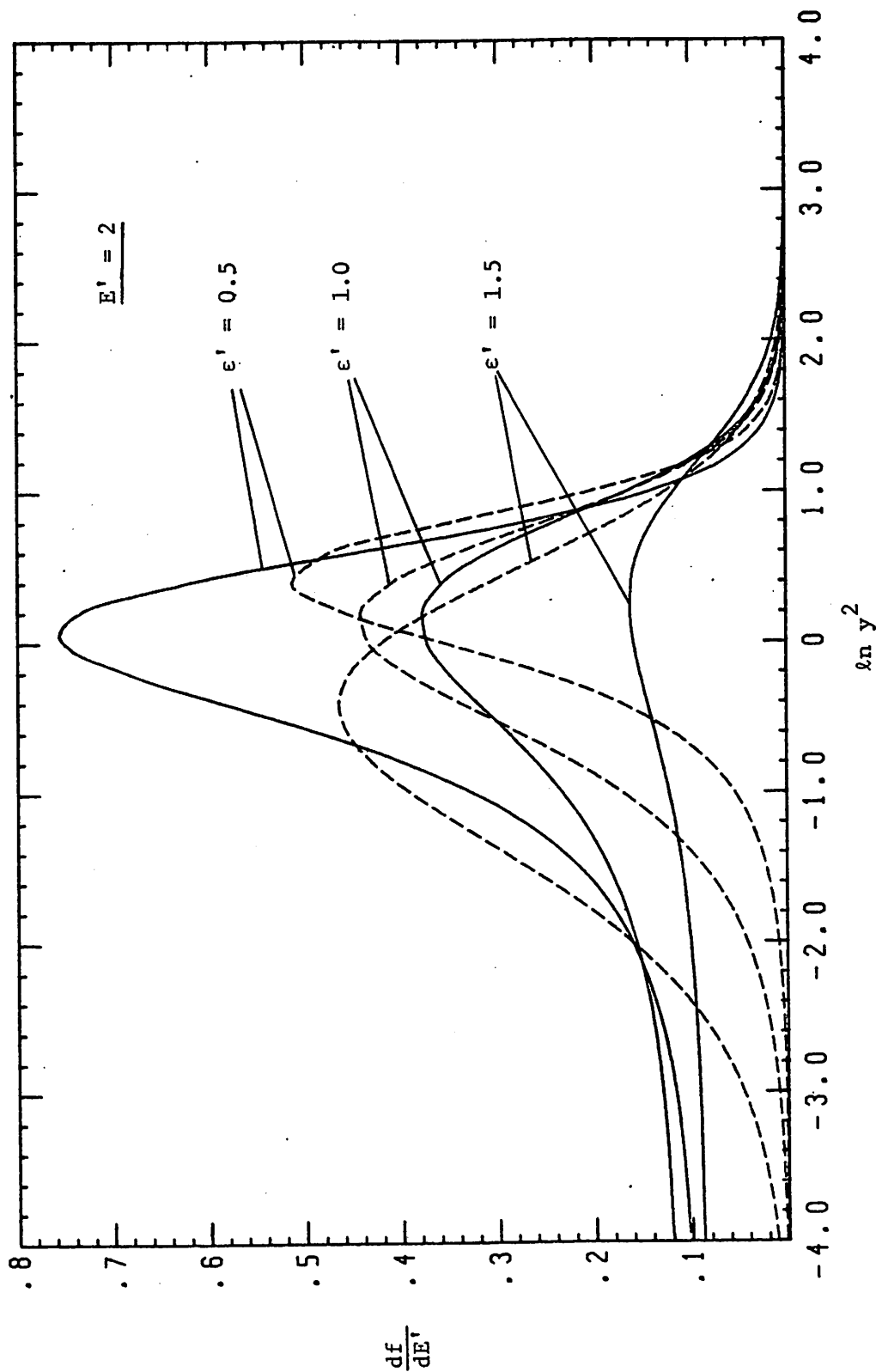$\epsilon' = 1$

$\epsilon' = 3$

$\ell n \, y^2$

$\dfrac{df}{dE'}$
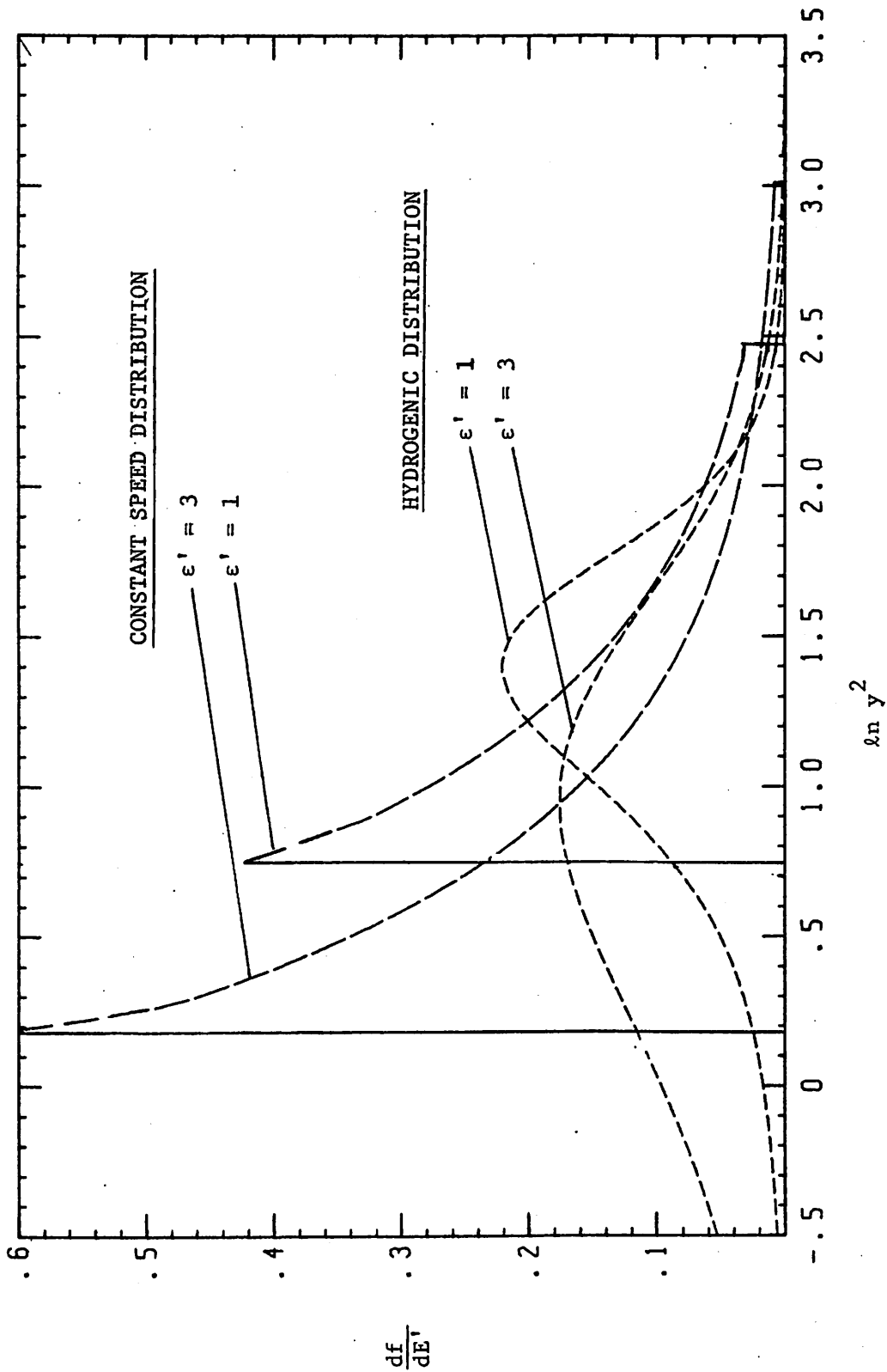
Fig. 2. Comparison of the generalized oscillator strength densities plotted vs. $\ell n \, y^2$, for the two momentum distributions in the BE theory. The solid vertical lines denote cut-offs imposed by Eqns. (6).
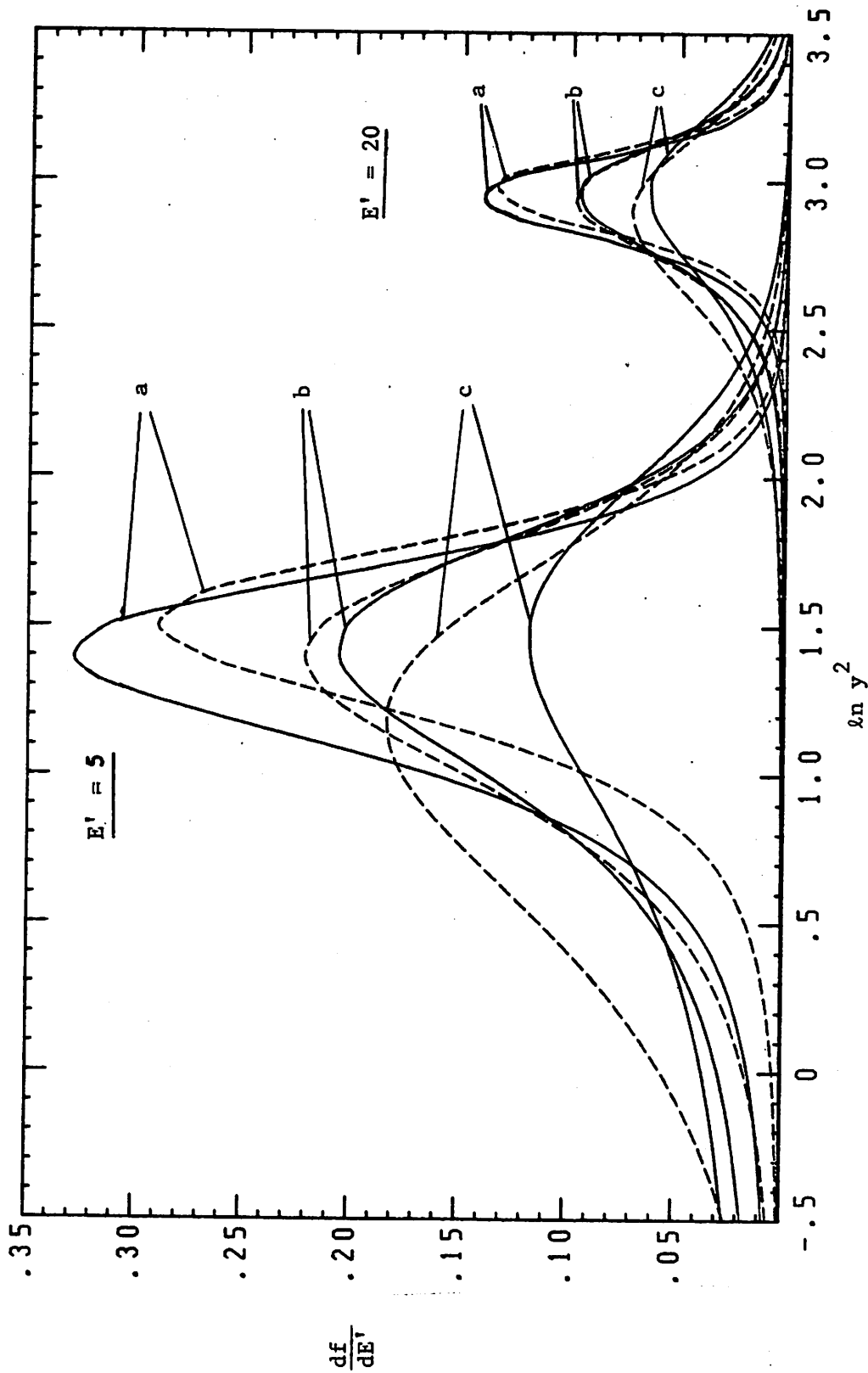
Fig. 3a. Comparison of the generalized oscillator strength densities plotted vs. $\ln y^2$, for the hydrogenic 1s momentum distribution in the BE (dashed curves) and Born (solid curves) approximations for $E' = 5$ and 20 and $\varepsilon' = 0.5$ (curves a), 1.0 (curves b), 2.0 (curves c).

3.21

Fig. 3b. Comparison of the generalized oscillator strength densities plotted vs. $\ln y^2$, for the hydrogenic 1s momentum distribution in the BE (dashed curves) and Born (solid curves) approximations for $E' = 2$ and $\epsilon' = 0.5$, 1.0, and 2.0.

of the BE df/dE'; for $\epsilon' = 2$, the reverse is true. This behavior

is clearly seen in the case of $E' = 5$. Also the positions of the

maxima of the BE approximation df/dE' shift to smaller values of

$(Ka_0)^2$ with increasing ϵ' in accordance with Eqn. (33). For

$E' = 2$ (Fig. 3b) all of the above-mentioned trends are more pro-

nounced. In addition, the low y^2 behavior is now apparent. The

BE approximation df/dE' falls to zero considerably faster than

the Born approximation df/dE'. This is especially significant

since in the Born approximation, the kinematical relation in Eqn.

(11) gives for $(\ell n \, y^2)$ the following values:

For $E' = 5$, $(\ell n \, y^2)_{min} = -5.09$ at $T' = 10^3$

and for $E' = 2$, $(\ell n \, y^2)_{min} = -6.91$ at $T' = 10^3$.

Note that $T' = 10^3$ corresponds to an incident electron energy of

13.6 KeV in the case of an ionization of a hydrogen atom. Thus

at the incident electron energies in an EM, small momentum transfer

events ($K \to 0$ and $\ell n \, y^2 \to$ large negative number) will give a signi-

ficant contribution to the integrated cross sections in the Born

approximation. In the BE approximation, the kinematics (as seen

through Eqn. (6) and Fig. 1) as well as the dynamics inhibit small

momentum transfer events, thereby giving an incorrect value of the

integrated cross section at high incident electron energies. Next

the behavior of the Born approximation df/dE' at y^2_{min} as a function

of ϵ' is investigated. Figure 4 shows the calculated value of

df/dE' (y^2_{min}, ϵ') as function of E' for three values of ϵ' (0.5,

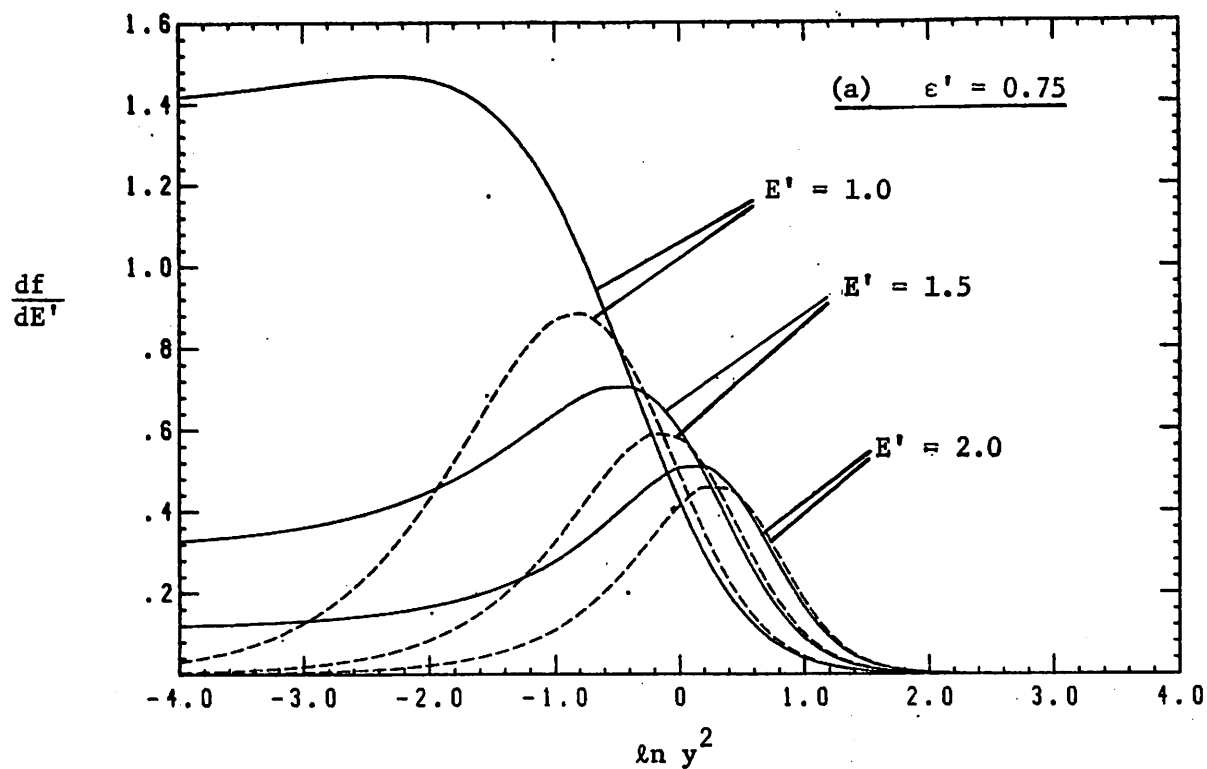1.0 and 1.5). For small E' ($\lesssim 1.5$), the df/dE' decreases with
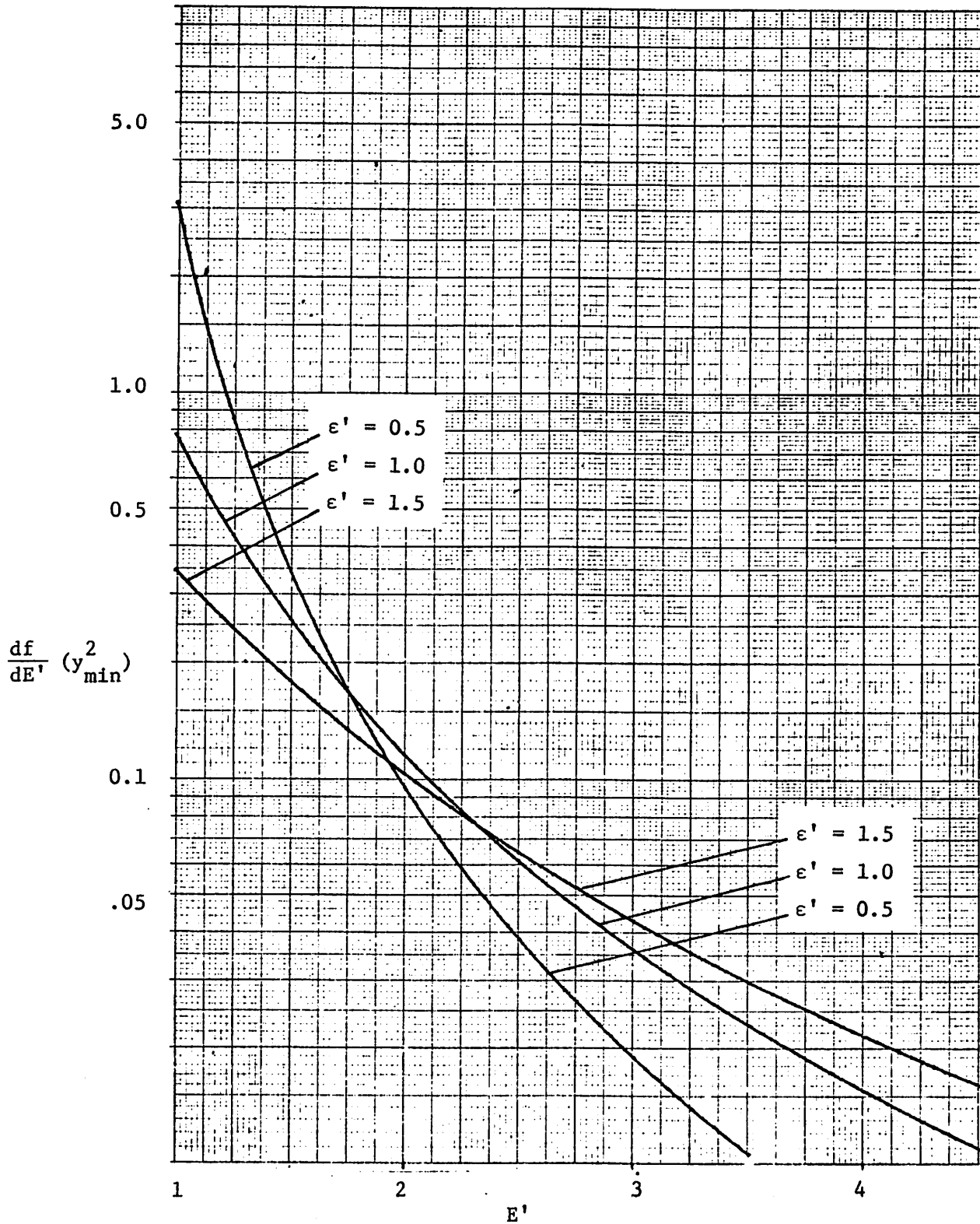
Fig. 4. The generalized oscillator strength density at y^2_{min} plotted vs. E', for the hydrogenic 1s momentum distribution in the Born approximation and for ε' = 0.5, 1.0 and 1.5.
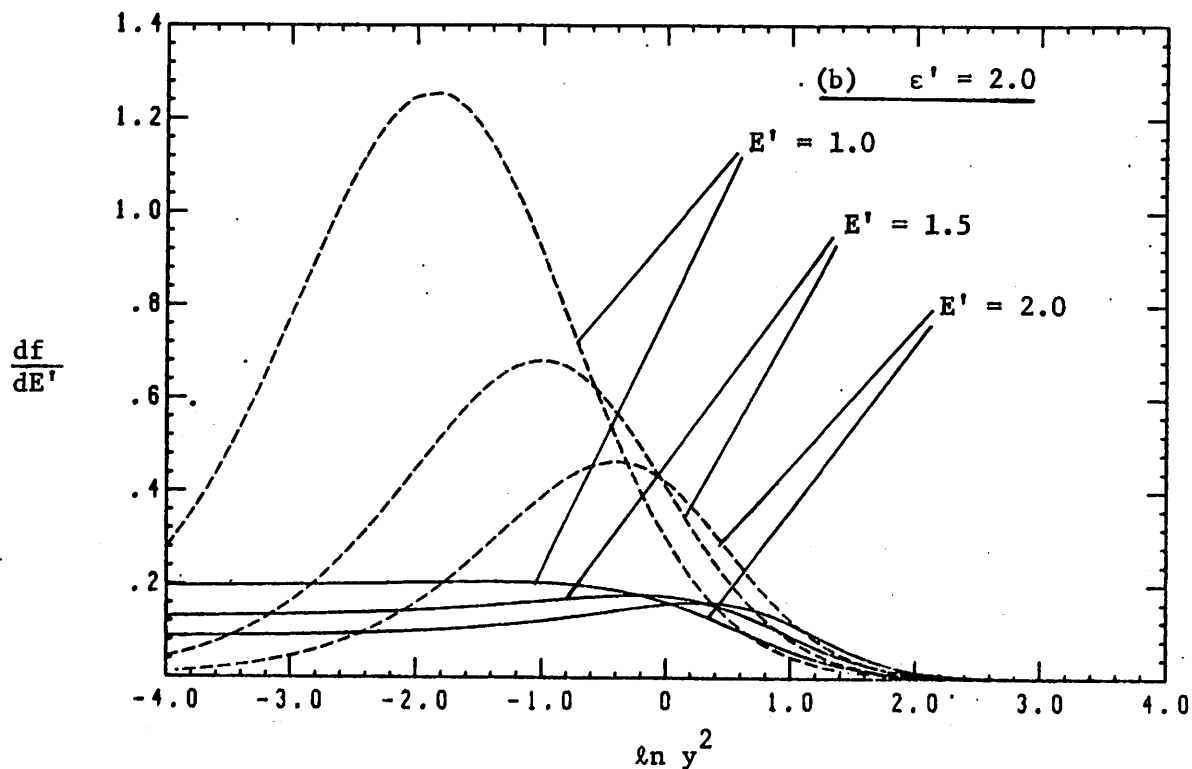
Figs. 5. Comparison of the generalized oscillator strength densities plotted vs. $\ln y^2$, for the hydrogenic 1s momentum distribution in the BE (dashed curves) and Born (solid curves) approximations for (a) $\epsilon' = 0.75$ and (b) $\epsilon' = 2.0$ and $E' = 1.0$, 1.5 and 2.0.

increasing ϵ' while for larger values of E' , this trend is reversed. This shows that even at large values of E', there could be discrepancies in the dependences of the integrated cross sections $d\sigma/dE'$ on ϵ' in the two approximations. Finally Figs. 5a and 5b illustrate the differences at small energy transfers between the df/dE' in the two approximations. For $\epsilon' = 0.75$ (Fig. 5a), the Born df/dE' is substantially greater for $(Ka_o) \gtrless (Ka_o)_p$ than the corresponding df/dE' in the BE approximation. For $\epsilon' = 2$ (Fig. 5b), just the opposite behavior is seen; here the Born df/dE' have essentially no 'humps' that are characteristic of the BE type of 'hard' electron-electron collisions. In conclusion, one already expects that for small energy transfer events $(E' \lesssim 2)$, the integrated cross sections will have opposite dependences on ϵ' and have substantial differences in magnitude in the two approximations. This trend will be seen explicitly by integrations of df/dE' in the following section.

c. Ejected electron and ionization cross section.

In this section the cross section that describes the ejected electron distribution and the total integrated cross section are obtained. The expressions for the df/dE' in the BE and the Born approximation developed in the previous section are used.

The double differential cross section for energy transfer dE and momentum transfer dK, defined in Eqn. (16a), can now be rewritten as,

$$d\left(\frac{d\sigma}{dE'}\right) = \frac{8\pi a_o^2}{T'} \frac{(E_R')^2}{E'} \frac{df}{dE'} (y,E') \frac{dy}{y} . \qquad (33)$$

The energy transfer cross section $d\sigma/dE$ is obtained by an integration over the momentum transfer K. The interval is defined by K_{max} and K_{min} (and thence y_{max} and y_{min}) from Eqns. (6) or (11). Thus,

$$\frac{d\sigma}{dE'} = \int_{y_{min}}^{y_{max}} d\left(\frac{d\sigma}{dE'}\right) \quad . \tag{34}$$

The total cross section for a transition to a state α is obtained by an integration over the variable E'. The limits of integration depend on the type of scattering process involved in the transition. In the case of ionization, the minimum energy transfer E_{min} is equal to the ionization potential while the maximum energy transferred E_{max} by the incident electron is its kinetic energy-T. (Inclusion of exchange and symmetrization will modify E_{max}, as will be seen later). In the case of excitation, the choice of E_{min} and E_{max} is not as unambiguous. The quantum defect theory[16] provides an algorithm for the calculation of excitation cross sections of atoms that have a Rydberg series of bound states. The interval $[E_{min}, E_{max}]$ is defined as $[E_\alpha - \Delta E_\alpha, E_\alpha + \Delta E_\alpha]$, where $\Delta E_\alpha = 1/2(dE_n/dn)_{n = \alpha}$. Here E_α is the energy of the bound state belonging to a Rydberg series with the principal quantum number $n = \alpha$. In the computation of the derivative dE_n/dn, one has to pretend that n is a continuous variable. Thus the interval $[E_{min}, E_{max}] = 2\Delta E_\alpha$ is $(2/\alpha) \cdot E_\alpha$ for a Rydberg series of bound states with $E_n = Z^2/n^2 \cdot E_R$. A different approach was taken by Gryzinski in his work on classical scattering[17]. He assumed that E_{min} was

equal to E_α the energy of the bound state, while E_{max} was the energy of the next higher state. In the case of bound states belonging to a Rydberg series the interval is then equal to $(2\alpha+1)/(\alpha+1)^2 \cdot E_\alpha$; this interval is smaller than the one obtained by the quantum defect theory. The quantum defect expression for E_{max}, E_{min} gives correct values for excitation cross sections for atomic hydrogen, while the Gryzinski approximation does not. The main advantage of the Gryzinski approximation is that it is not limited to only those bound states that belong to a Rydberg series; however knowledge of the 'next higher' energy level is required.

Thus an excitation cross section (to state α) is written as

$$\sigma_\alpha = \int_{E_{min}}^{E_{max}} (d\sigma/dE)dE \quad , \tag{35a}$$

where the limits are to be chosen according to the algorithm of the quantum defect theory or that of the Gryzinski approximation. Ionization cross section σ_I is quite unambiguously given as

$$\sigma_I = \int_{I}^{T} (d\sigma/dE)dE \tag{35b}$$

Using the relation $E = T_e + I$, the ejected electron kinetic energy distribution $d\sigma/dT_e$ can be obtained from the energy transfer cross section $d\sigma/dE$ by a simple change in variable. The distribution of velocities (or speeds) $d\sigma/dv_e$ may be physically and intuitively more satisfying than a distribution in kinetic energies. The $d\sigma/dv_e$ is obtained by another straightforward change of variables.

The ejected electron kinetic energy T_e is $\frac{1}{2} mv_e^2$ and introducing as before the normalization with respect to the threshold energy $E_t = I$, we have $T_e' = T_e/E_t$ and $v_e' = v_e/v_t$ where $v_t^2 \equiv 2I/m$. Thus a convenient expression for the velocity distribution in terms of $d\sigma/dT_e'$ is

$$d\sigma/dv_e' = 2\sqrt{T_e'} \cdot d\sigma/dT_e' \quad . \tag{36}$$

Next expressions for $d\sigma/dE'$ (or equivalently $d\sigma/dT_e'$) are obtained using the expressions for df/dE' in the Born and BE approximations. First we consider the BE theory. The normalized df/dE' for the case of constant speed distribution in the BE approximation [Table 1, Eqn. (a)] after substitution in (33) and (34) leads to,

$$\frac{d\sigma}{dE'} = \frac{8\pi a_o^2}{T'} \cdot \frac{E_R'^2}{E'} \int_{y_{min}}^{y_{max}} \frac{E'}{4\sqrt{\epsilon'}} \cdot \frac{1}{y^3} \cdot \frac{dy}{y} \quad . \tag{37}$$

Where y_{min} and y_{max} are obtained from Eqns. (6). After integration and some algebraic rearrangement one obtains

$$d\sigma/dE' = \frac{4\pi a_o^2 E_R'^2}{T' \cdot E'^2} \cdot (1 + 4/3 \cdot \frac{\epsilon'}{E'}) \tag{38}$$

The hydrogenic 1s distribution of bound electron velocities has a more complicated expression for df/dE' [Table 1, Eqn. (b)] than the one used in (37). The absence of an upper bound on the ϵ in the hydrogenic velocity distribution makes the upper and lower limits of integration in (37) go to infinity and zero respectively.

Attempts to obtain an analytical expression for $d\sigma/dE'$ using this df/dE' have yielded a morass of algebraic expressions. However numerical integration on a desk calculator quickly gives a value for $d\sigma/dE'$ (for the hydrogenic 1s distribution) equal, within numerical accuracy – 5 significant figures – to that given by (38). Thus at least for values of ε' between 0.5 and 2.0 and of E' between 1.0 and 5.0 we can assume that (38) provides an accurate expression for $d\sigma/dE'$ in the BE approximation for both the distributions of bound electron energies. In hindsight this might indeed be expected since the BE approximation considers only the 'hard' electron-electron collisions and thereby is quite insensitive to bound electron velocity distributions.

The modeling of the electron-molecule collision as a pure two electron interaction in the BE theory makes it necessary to explicitly include the indistinguishability of the two electrons in the scattering dynamics. This is quite easy to do as has been shown by Vriens[9]. The BE theory expression can be better understood by first recalling that in the case of elastic scattering of two (indistinguishable) electrons, the cross section[18] for scattering an electron into a solid angle $d\Omega(\theta)$ is

$$\sigma(\theta) = |f(\theta)|^2 + |f(\theta-\pi)|^2 - Re[f^*(\theta)f(\theta-\pi)] \quad . \quad (39)$$

Here $f(\theta)$ is the scattering amplitude for scattering an electron into a solid angle $d\Omega(\theta)$. The first term on the right side of (39) is clearly the contribution to the cross section that would occur even if the particles were distinguishable. The other two terms due to particle indistinguishability and are respectively the exchange and the interference terms. The BE theory expression for $d\sigma/dE$ derived by Vriens, is

$$\frac{d\sigma}{dE} = \frac{4\pi a_o^2 \ E_R^2}{T} \left[\left(\frac{1}{E^2} + \frac{4}{3} \ \frac{\varepsilon}{E^3} \right) + \left(\frac{1}{D^2} + \frac{4}{3} \ \frac{\varepsilon}{D^3} \right) - \left(\frac{\Phi}{E \cdot D} \right) \right] . \quad (40)$$

As in (39), here too the second and third terms [parenthetically enclosed] are the exchange and interference terms respectively. Thus the $D = T-\varepsilon_s$ can be considered to be the 'exchange energy transfer', in analogy with $E = T-\varepsilon$ 'the direct energy transfer'. Using Eqn. (5), one obtains $D = T-E-\varepsilon$. The Φ in the interference term is approximated as

$$\Phi \sim \cos \left\{ \sqrt{\frac{1}{T-\varepsilon}} \cdot \ell n \left(\frac{E}{D} \right) \right\} . \quad (41)$$

Note that the expression for $d\sigma/dE$ in (40) has been derived for the case of a fixed speed distribution for bound electrons, i.e., that given in (24). For the case of a hydrogenic distribution, we assume that the expression for $d\sigma/dE$ should not be different from (40). This is expected since in the case where electron distinguishability is assumed, the same expression for $d\sigma/dE$ [Eqn. (38)] was obtained for both the fixed speed and the hydrogenic momentum distributions.

In spite of the indistinguishability of electrons it is con-
venient to label the electrons that appear after the collision.
The slower electron is labelled the ejected electron, while the
faster is the scattered incident electron. Clearly at high inci-
dent electron energies, this labelling is quite accurate as the
probability of ejecting a high velocity electron is very small.
However at low incident electron energies, the two electrons appear
with comparable velocities and the labelling is reduced to merely
a convenience. Thus the labelling requires that the maximum kine-
tic energy of the ejected electron be equal to the minimum kinetic
energy of the incident scattered electron. Thus $T_e(\max) = T_s(\min)$,
and since $T_e + T_s = T - I$ one gets $T_e(\max) = (T-I)/2$ or

$$E_{\max} = (T + I)/2 \tag{42}$$

Note that in the case of 'distinguishable' electrons, we have
$E_{\max} = T$.

Burgess[19] noticed that the two electrons in the BE theory were
not treated quite symmetrically. When both the incident and the
atomic electrons are at equal distance from the atomic nucleus, the
atomic electron has a potential energy $-Ze^2/r$, while the incident
electron is assumed to have zero potential energy. In order to
'symmetrize' the two electrons, the incident electron is assumed to
gain a certain amount of kinetic energy and lose the same amount of
potential energy. This amount of energy is equal in magnitude to
the potential energy of the bound electron, which, assuming a one-
electron atomic model and using the virial theorem, is equal to

$-E_t - \varepsilon$. Thus the incident electron is assumed to have a new kinetic energy of $T + \varepsilon + E_t$, while its total energy remains equal to T. Thus in this symmetrical BE model $d\sigma/dE'$ can be written in the normalized form.

$$\frac{d\sigma}{dE'} = \frac{4\pi a_0^2 E_R'^2}{(T'+\varepsilon'+1)} \left[\left(\frac{1}{E'^2} + \frac{4/3\ \varepsilon'}{E'^3} \right) + \left(\frac{1}{D_s'^2} + \frac{4/3\ \varepsilon'}{D_s'^3} \right) \right.$$

$$\left. - \Phi_s'/E'\cdot D_s' \right] \quad . \tag{43}$$

Here D_s' is the normalized, symmetrized exchange energy transfer and is equal to $(T'+1-E')$, while Φ_s' , obtained from (41), is

$$\Phi_s' \simeq \cos \left\{ \sqrt{\frac{1}{E'+D_s'}} \cdot \ell n \left(\frac{E'}{D_s'} \right) \right\} \quad . \tag{44}$$

Next, the Born approximation $d\sigma/dE'$ is obtained by substitution of df/dE' in (33) and (34). As was originally pointed out by Miller and Platzman[20], the $d(d\sigma/dE)$ in (38) can be rewritten as

$$d(d\sigma/dE) = \frac{4\pi a_0^2 E_R'^2}{T'E'} \frac{df}{dE'} (y,E')\ d[\ell n\ y^2] \tag{45}$$

This shows that $d\sigma/dE'$ is proportional to the area under the curves of df/dE' plotted in Figs. (2), (3), and (5). Using the df/dE' for the hydrogenic 1s momentum distribution [Table 1, Eqn. (c)] and the expressions for the maximum and minimum $(Ka_0)^2$ [Eqns. (11) and (12)], $d\sigma/dE'$ can be obtained by numerical integration. It
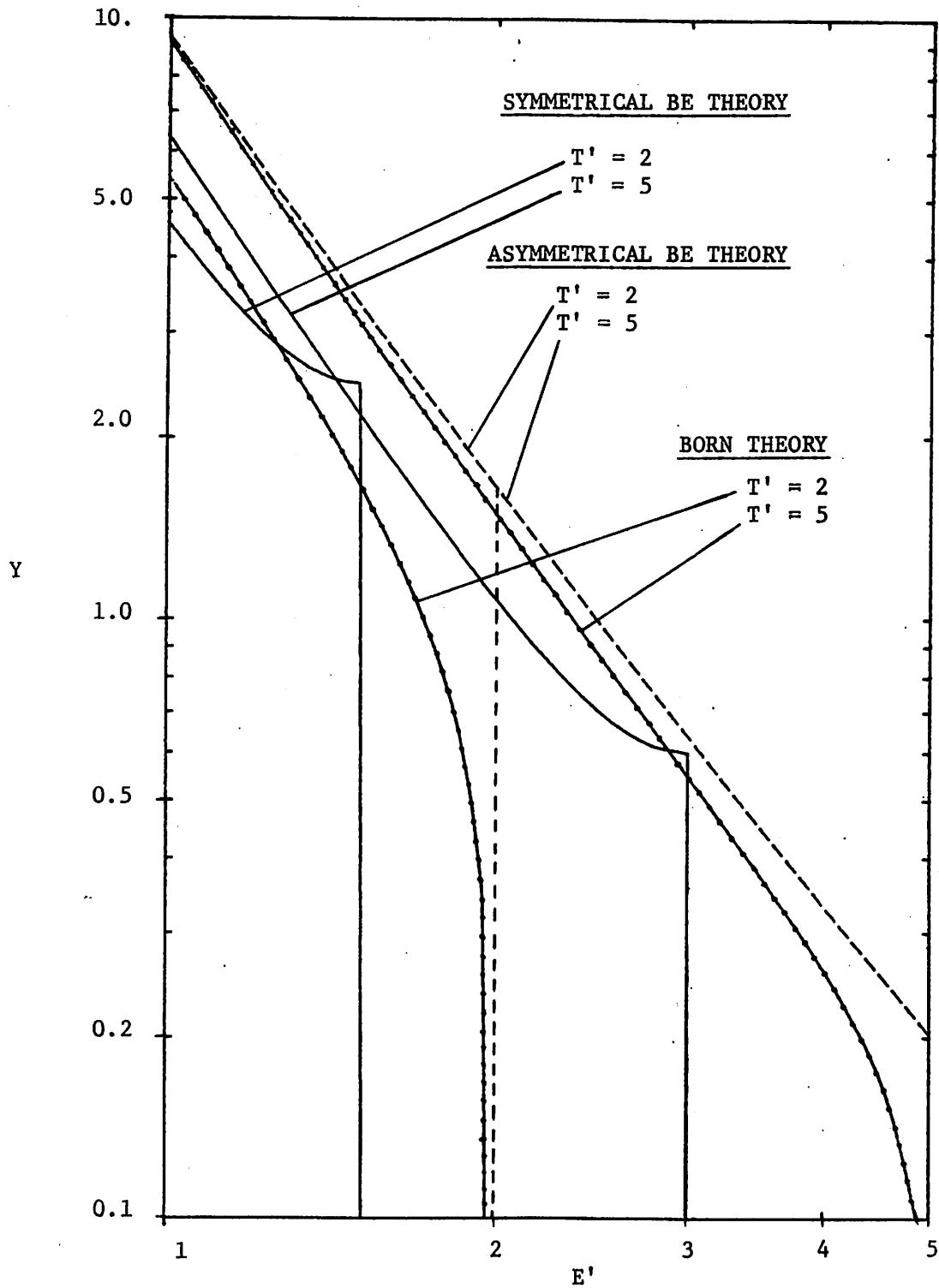
Fig. 6. $Y = T'/(\pi a_0^2 E_R'^2) \cdot d\sigma/dE'$ plotted vs. E', for the two versions of the BE theory and for the Born theory, all for $\epsilon' = 1$.

is estimated that our results for $d\sigma/dE'$ are accurate to within 0.01%.

Comparison of the expressions for $d\sigma/dE'$ in the two versions of the BE theory [the asymmetrical version given by (38) and the symmetrical version given by (43)] and the Born theory will now be presented. We will plot (in Figs. 6-9) the dimensionless quantity $Y \equiv (T'/\pi a_o^2 E_R'^2) \cdot d\sigma/dE'$ versus E'. Thus Y will depend only on T' and ε' as parameters, but will be independent of E_R' . In Fig. 6, the dependence of Y on T' is examined. The magnitude of Y in the symmetrical BE theory depends on T', while that in the asymmetrical BE theory does not. Note also that for all values of E', the Y in the symmetrical BE theory is smaller than that in the asymmetrical BE theory. Both theories exhibit sharp cut-offs in Y at $E = E_{max}$ where E_{max} is given differently in the two theories. It is thus clear that the integrated cross section will be smaller in the symmetrical version than in the asymmetrical version of the BE theory for equal values of ε' and T'. For the sake of comparison the Y in the Born approximation is also plotted in Fig. 6. Its' magnitude also depends on T'; unlike the Y in the two BE approximations, the Y in the Born approximations goes monotonically and smoothly to zero as $E' \to E'_{max} = T'$.

In Fig. 7 and 8 we will examine the dependence of Y on ε'. In Fig. 7a we see that the two versions of the BE theory have approximately similar dependence on ε'; both increase with increasing ε'. Note also that with increasing T', the difference between the two versions of the BE approximation becomes smaller, as expected from a comparison of (38) and (42). In Fig. 7b we compare the dependence
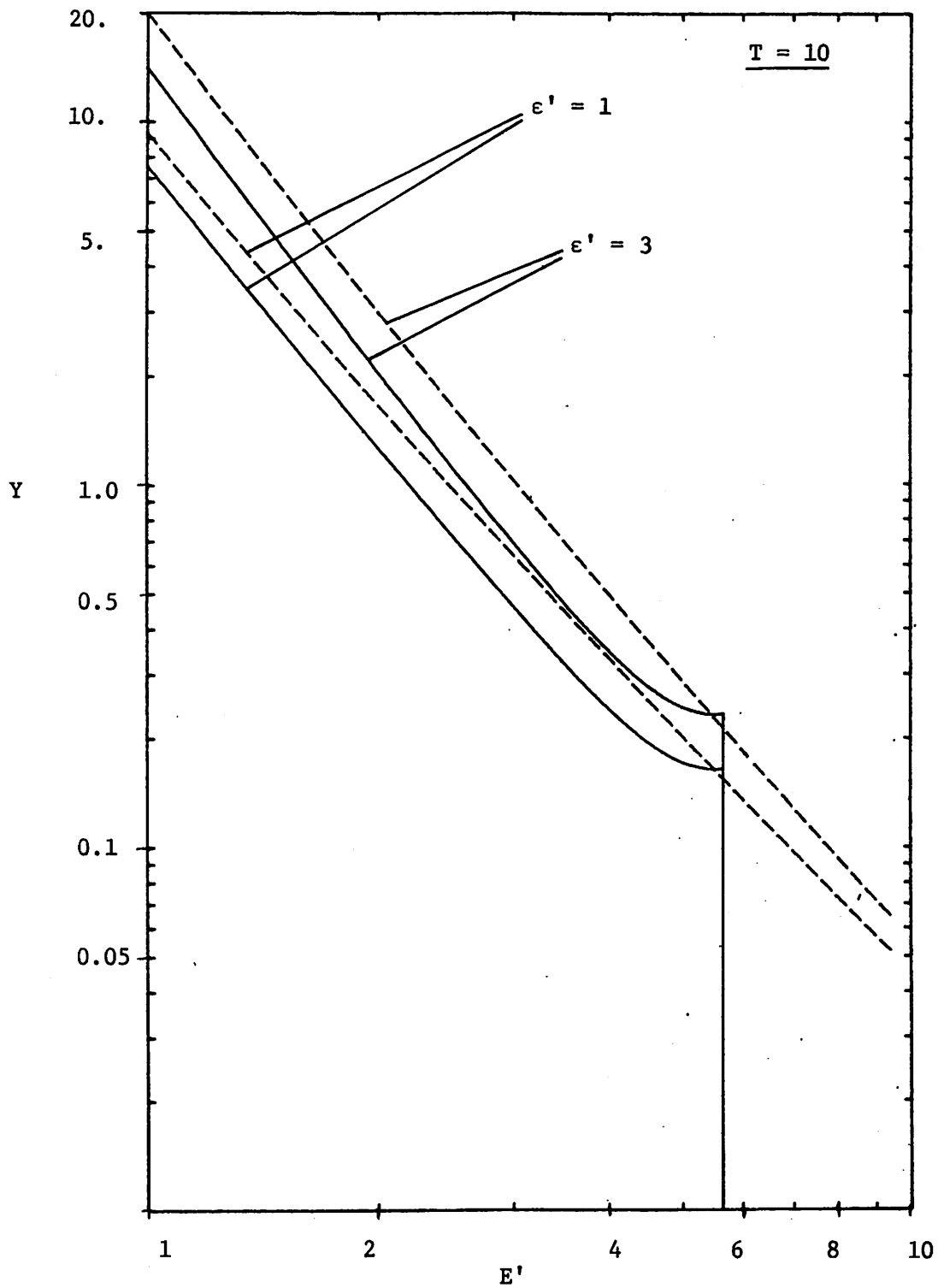
Fig. 7a. $Y = T'/(\pi a_0^2 E_R'^2) \cdot d\sigma/dE'$ plotted vs. E' for the symmetrical (solid line) and the asymmetrical (dashed line) BE theories for $T' = 10$ and $\epsilon' = 1.3$.
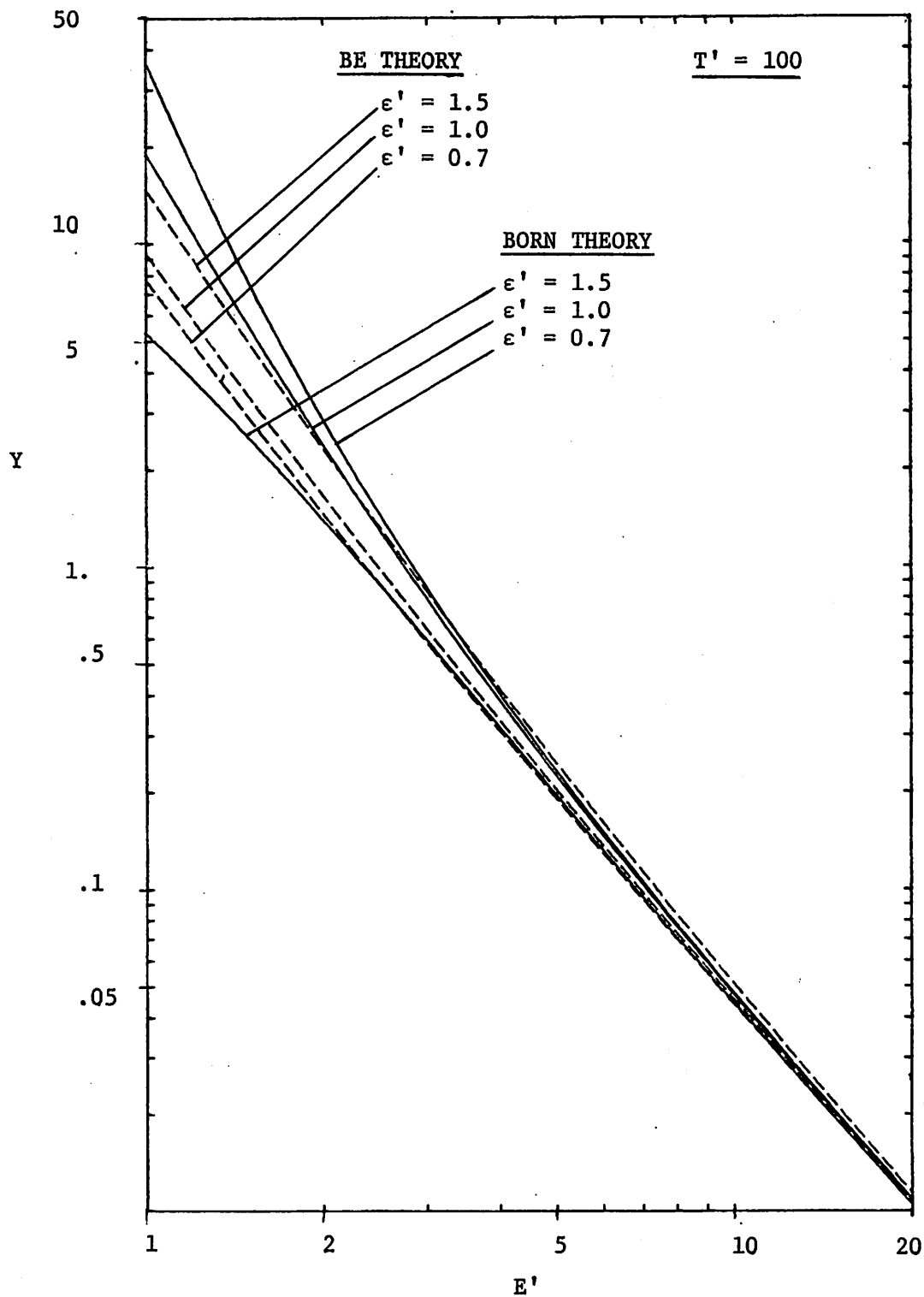
3.36

Fig. 7b. $Y = T'/(\pi a_0^2 E_R'^2) \cdot d\sigma/dE'$ plotted vs. E' for the Born theory (solid line) and the BE theory (dashed line) for T' = 100 and ϵ' as shown.

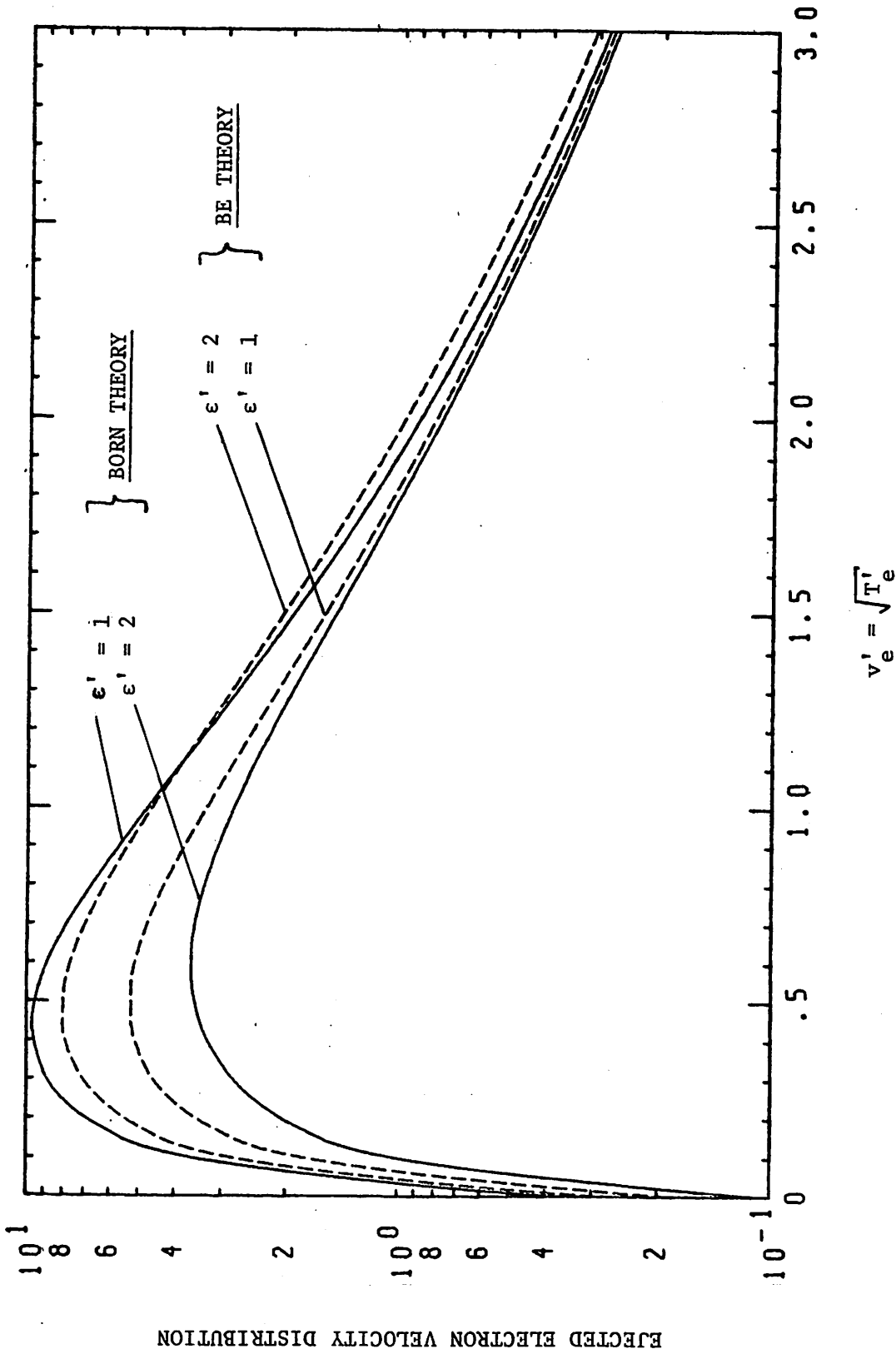Fig. 8. Ejected electron velocity distribution, defined as $T'/(\pi a_0^2 E_R'^2) \cdot d\sigma/dv_e'$ plotted vs. $v_e' = \sqrt{T_e'}$ for the Born theory (solid line) and the BE theory (dashed line) for $T' = 100$ and ϵ' as shown.

3.38

of the Y in the Born approximation and the BE theory (asymmetrical version) on ε'. Here (at $T' = 100$) the symmetrical version is imperceptibly below the asymmetrical version. The Born and the BE theories have clearly opposite dependences on ε'. The Born theory $d\sigma/dE$ (and thus the integrated σ) depends inversely on ε'; this agrees with one's intuition in that the probability for inelastic scattering should decrease with increasing binding of the atomic electron. The differences at $E' \sim 1$ between the two theories is at least a factor of two at $T' = 100$.

It is worth noting that Y (or equivalently $d\sigma/dE'$) is related to the distribution of ejected electron kinetic energies in the case of transitions involving ionization. Since $E' = T'_e + 1$, the abscissae in Figs. 6 and 7 can be equivalently labeled by T'_e. In Fig. 8, the velocity distribution of ejected electrons, in the normalized form $T'/(\pi a_o^2 E_R'^2) \cdot d\sigma/dv'_e$, is plotted versus $v'_e = \sqrt{T'_e}$. [See Eqn. (36)] This distribution, which shows that the probability for ejecting an electron with zero velocity is equal to zero, may be intuitively more satisfying than the distributions (obtainable from Figs. 6 and 7) that show a finite cross section for production of zero kinetic energy ejected electrons.

Finally in Figs. 9, the behavior of the Y in the Born theory is examined. The behavior of Y at large E' can be approximated quite accurately by $1/E'^2$; however Y decreases, only slightly, with increasing ε' - even at the highest possible E'. This is in direct contradiction with the behavior of Y given by the BE theory; at this time we can offer no explanation for this difference.
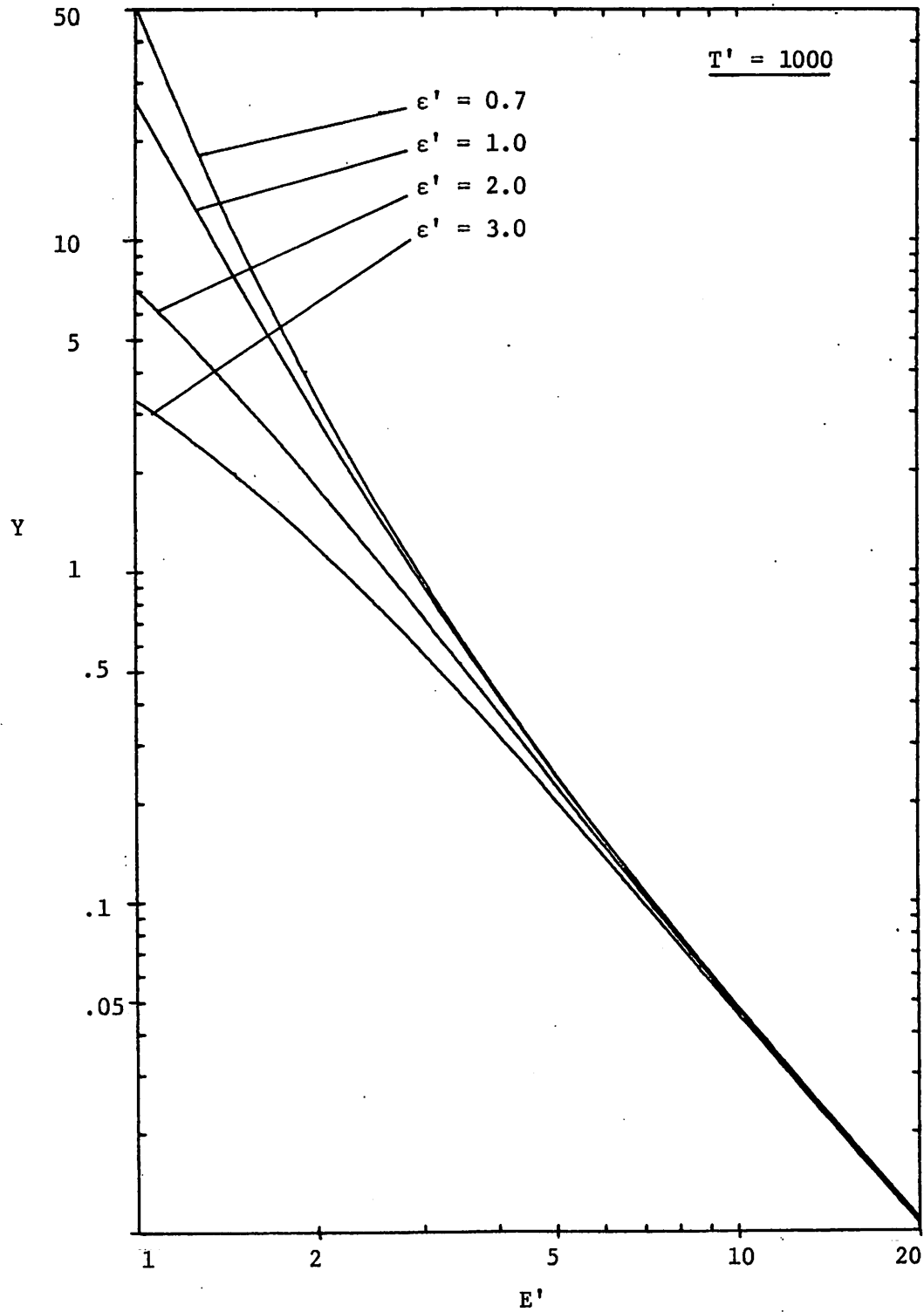
3.39

Fig. 9a. $Y = T'/(\pi a_0^2 E'^2_R) \cdot d\sigma/dE'$ plotted vs. E' in the Born theory for $T' = 1000$ and different values of ϵ'.
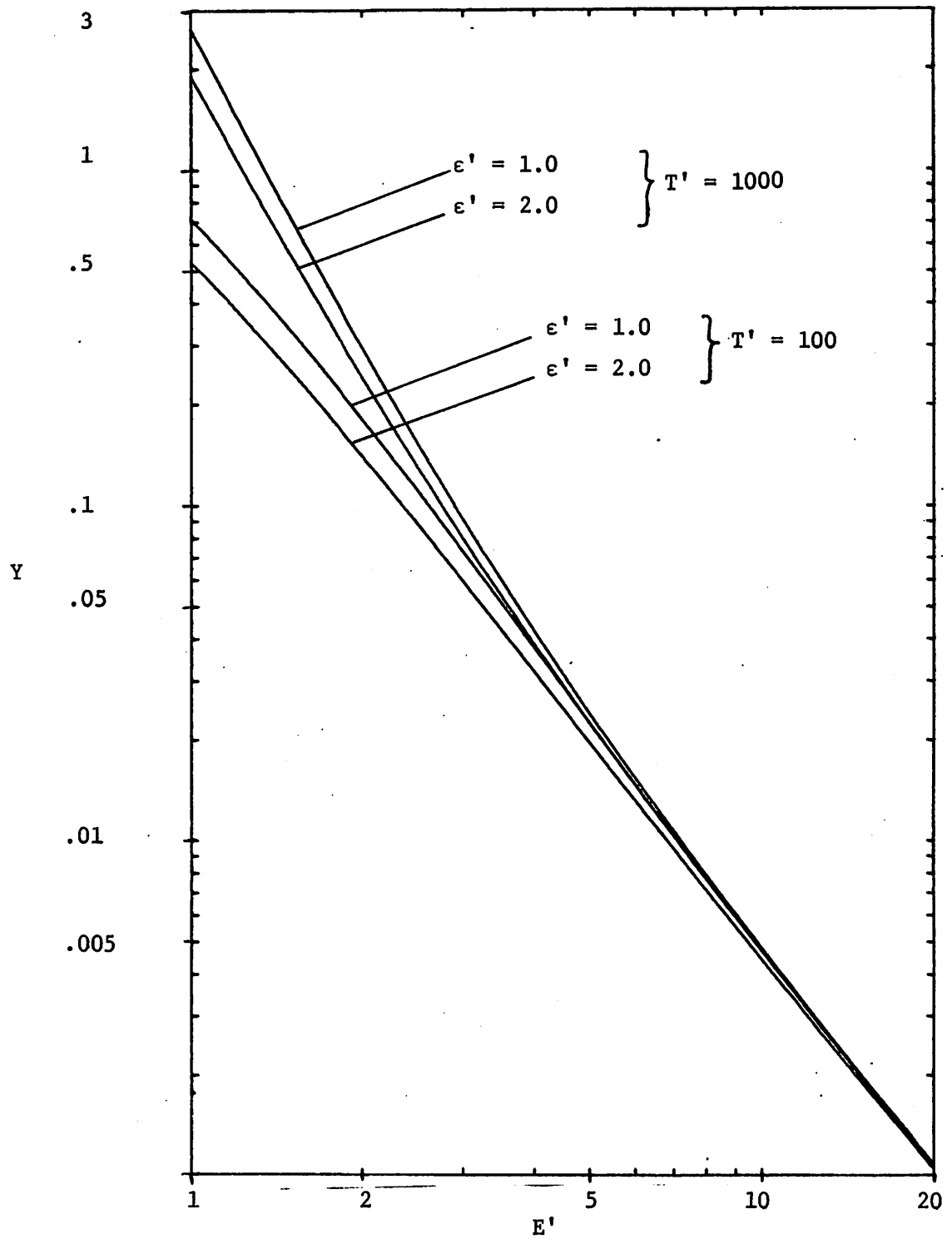
Fig. 9b. $Y = T'/(\pi a_0^2 E_R'^2) \cdot d\sigma/dE'$ plotted vs. E' in the Born theory for $T' = 100$ and 1000 and ϵ' as shown.

Figure 9a displays the sensitivity of Y on ϵ' in the Born approximation. Not only does the magnitude of Y at $E' \sim 1$ decrease by an order of magnitude for a factor of three change in ϵ', but also the curvature of the curves change in the interval $1 \lesssim E' \lesssim 3$. The dependence of Y on T' is illustrated in Fig. 9b. Increasing T', increases $d\sigma/dE'$ (and thus Y'). This is understood entirely by recalling that with increasing T', the minimum momentum transfer K_{min} (and thus y^2_{min}) decreases as given by (11) or (12). Thus the area under the curve of df/dE' versus $\ln y^2$ increases [Eqn. (45) and Figs. 3 and 5]; consequently $d\sigma/dE'$ increases. In other words, at high T' small momentum transfer (large impact parameter) events provide a substantial contribution to $d\sigma/dE'$ in the low E' region.

Next we consider the integrated ionization cross section σ_I. The symmetrized BE theory σ_I is obtained by a straightforward integration of $d\sigma/dE'$ [Eqn. (43)] between the limits [1, E'_{max} = (T'+1)/2]. The result

$$\sigma_I = \frac{4\pi a_o^2 E_R'^2}{(T'+\epsilon'+1)} \left[\left(1 - \frac{1}{T'}\right) + 2/3 \, \epsilon'(1 - 1/T'^2) \right.$$

(46)

$$\left. - \frac{\Phi_s'' \ln T'}{(T'+1)} \right]$$

Where Φ_s'' in the interference term has been approximated by Vriens[9] as,

$$\Phi_s'' \approx \cos \left\{ \frac{\ln T'}{T'+1} \right\} .$$

(47)

The simplicity and the convenience of this expression gets further

magnified when one considers obtaining the integrated ionization

cross section in the Born approximation. The $d\sigma/dE'$, obtained via

numerical integration, have to be integrated numerically over the

interval [1 , T']. We do this on a digital computer in the fol-

lowing way: The integration is performed over the variable T_e

rather than E' and the interval of 0 - 200 eV is selected arbitrar-

ily. This interval is divided into a mesh containing 40 unequal in-

tervals. The interval 0 - 20 eV and 20 - 100 eV each have 16 equal

intervals, while 100 - 200 eV has 8 equal intervals. The contribu-

tion to σ_I from the region beyond 200 eV is obtained in an analyti-

cal form by assuming that beyond T_e = 200 eV, $d\sigma/dE'$ has a $1/E'^2$

behavior. The accuracy of the integrated ionization cross section

obtained using this method is estimated to be within 0.5%. Even

with this modest requirement for accuracy, the double numerical in-

tegration required to obtain the Born theory σ_I costs approximately

400 times as much computer time (and money!) as the corresponding

BE theory σ_I .

In Figs. 10a and 10b, the integrated ionization cross sections

are plotted with ϵ' as a parameter. The symmetrical BE theory σ_I

are compared at low T' (1-50) with the Born theory σ_I in Fig. 10a.

The Born theory σ_I are calculated for only a few values of T' and

is thus labelled by symbols. From now on, unless otherwise stated,

the term BE theory will imply the symmetrical BE theory. We do

not consider the asymmetrical theory because it is conceptually in-

correct within the BE approximation and it gives quite incorrect

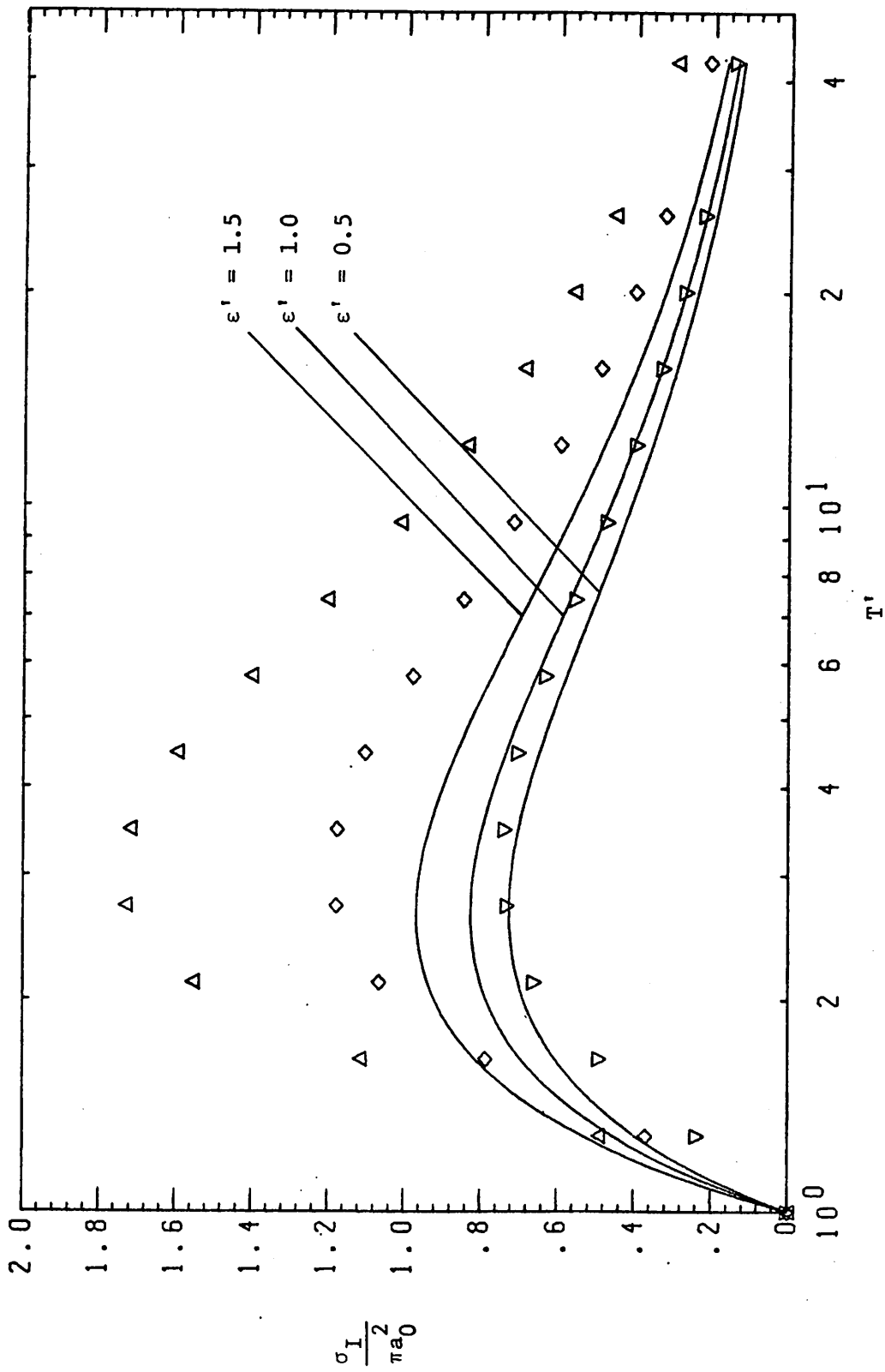(too large) values for σ_I for small T'. At large values of T' the

Fig. 10a. Integrated ionization cross sections $\sigma_I/\pi a_0^2$ for small T' in the Born theory (symbols: $\triangle - \epsilon' = 0.7$, $\diamondsuit - \epsilon' = 1.0$ and $\triangledown - \epsilon' = 1.5$) and the BE theory (solid lines, with ϵ' as shown.
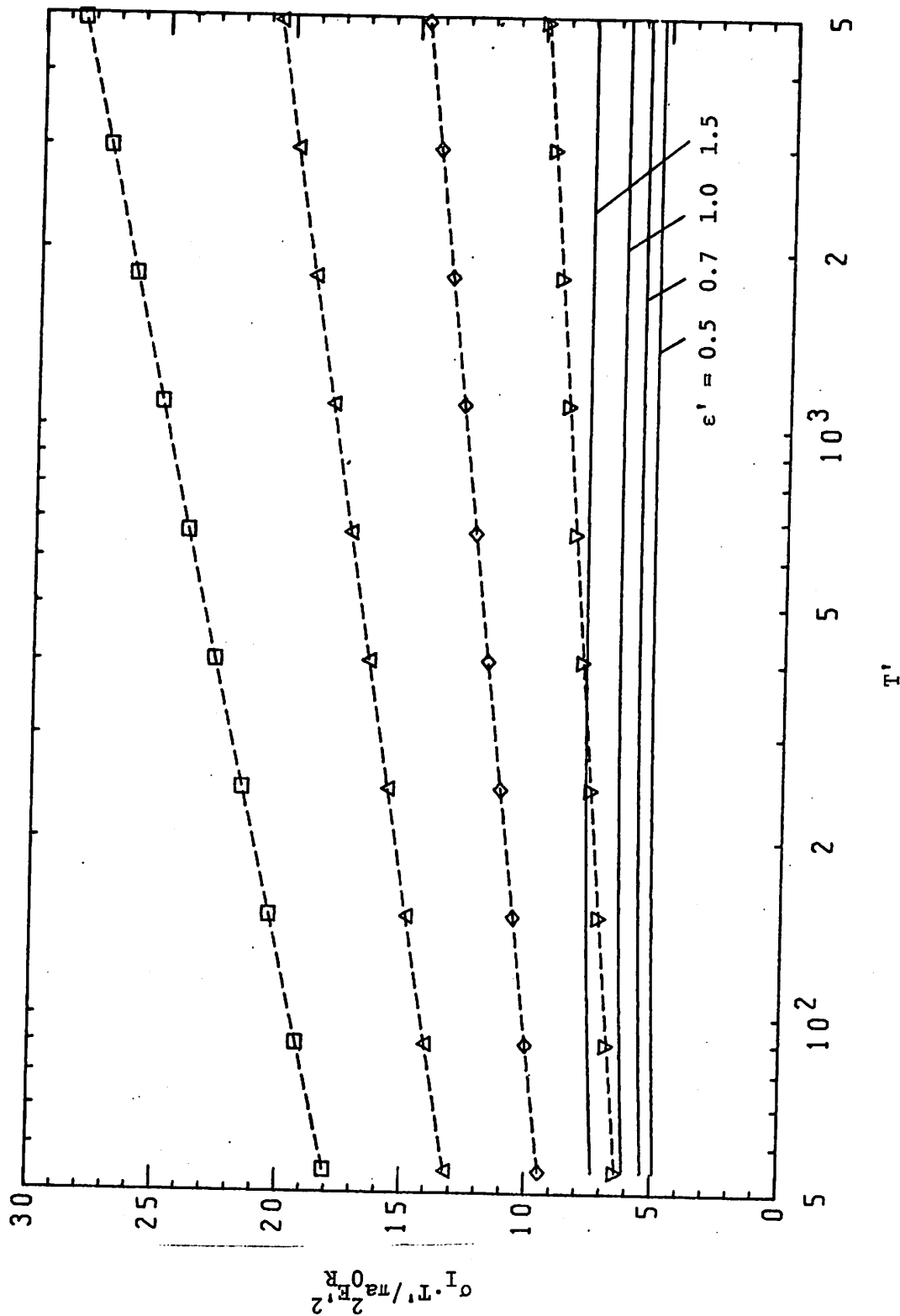
Fig. 10b. Fano plot of the integrated ionization cross sections, i.e., plot of $(\sigma_I \cdot T' / \pi a_0^2 E_R'^2)$ vs. T' (log scale), for the Born theory (symbols: $\square - \epsilon' = 0.5$, $\triangle - \epsilon' = 0.7$, $\diamond - \epsilon' = 1.0$, $\triangledown - \epsilon' = 1.5$) and the BE theory (solid lines, with ϵ' as shown).

two versions of the BE theory have very little difference. As expected the BE theory σ_I are less sensitive to ε' than the Born theory σ_I and for $\varepsilon' \lesssim 1$ are always smaller than the corresponding σ_I in the Born theory. The high T' behavior is plotted in Fig. 10b in a manner suggested by Fano[21] (the Fano plot): $\sigma_I \cdot T'/\pi a_o^2$ is plotted versus $\log_{10} T'$, a straight line with a non-zero slope shows that σ_I depends logarithmically on T'. This is clearly seen to be the case for the Born theory σ_I. However the BE theory σ_I have essentially no logarithmic dependence and for $\varepsilon' \lesssim 1$ at $T' = 5000$ are considerably smaller than the corresponding σ_I in the Born approximation. Increasing ε' increases the BE theory σ_I so that for $\varepsilon' = 1.5$, the σ_I in the two approximations become somewhat comparable.

The Bethe approximation is an approximation of the Born theory for high incident electron energies. The behavior of σ_I displayed in Fig. 10b can be described by an equation:

$$\sigma_I = \frac{4\pi a_o^2 \, E'}{T'} \, M_I^2 \, \ell n \, c_i \, T' \tag{48}$$

where M_I^2 is recognized to be the square of the dipole moment matrix element [Eqn. (2-26)]. Using standard methods for linear and non-linear regression, we fit M_I^2 and c_i to simple expressions that depend only on E_R' and ε'. A compact expression for M_I^2, accurate only to $\pm 3\%$ for $0.5 \lesssim \varepsilon' \lesssim 1.5$, is

$$M_I^2 = E_R' \, [1.011 - 1.11 \cdot \varepsilon' + 0.380 \cdot \varepsilon'^2] \, , \tag{49}$$

3.46

and for c_i , accurate to ± 1.5%, the expression is,

$$c_i = [14.79 + 90.87 \cdot \varepsilon - 27.48 \cdot \varepsilon'^2] \quad . \tag{50}$$

Use of (49) and (50) in (48) should yield σ_I accurate to within 3% of the ones obtained via the double numerical integration described above. It must be emphasized that (48) is a large T' approximation and is not expected to be accurate for T' ≲ 50.

A summary of the differential and integrated cross sections will now be offered. For small T', the (symmetrical) BE approximation gives more accurate (compared to experiment, as will be seen) σ_I than the Born approximation. However at large T', the situation is reversed. The ejected electron distribution in the case of ionizing collisions is probably given more accurately by the Born approximation $d\sigma/dT_e$, at least for large T'. The inverse dependence of the cross sections in the two theories on ε' provides a conceptual enigma; especially at large values of E', where the BE and the Born theory $d\sigma/dE'$ have essentially the same dependence on E', but still have opposite dependence on ε'. Fortunately for computational purposes, the BE theory σ_I and $d\sigma/dE'$ are less sensitive to ε' than the corresponding Born theory cross sections. Thus at low T', additional errors due to an incorrect dependence on ε' are reduced when the BE theory is used.

Finally, some comments on extensions of the theory and methods presented in this section. As stated earlier, the main purpose of this chapter was to obtain ionization cross sections in terms of a few parameters. It has tacitly been assumed that the kinetic energy of the bound electron is one such (and the most important?)

parameter. The hydrogenic 1s wave function provided the simplest

means of testing our ideas and applying them to complex systems

(next section and Chapter 4). However, it is suggested that other

hydrogenic (and non-hydrogenic?) wave functions can be used to ob-

tain the parametric dependence of the effective kinetic energy of

the bound electrons in $d\sigma/dE'$ and σ_I . If these cross sections

dependence on ϵ' are essentially unchanged for different wave func-

tions (or equivalently momentum distributions), then our assumptions

and the results that follow are well justified. Of course the dif-

ferential cross sections $d(d\sigma/dE)$ or $d\sigma/dK$ are expected to be quite

sensitive to the bound electron momentum distribution, but on in-

tegration over K, this sensitivity is expected to be 'washed out'

and the dependence on ϵ' is expected to remain. These assertions

can only be justified by following a program of calculations simi-

lar to the one suggested above.

3.2 Extension to many-electron molecular systems.

In the previous section, the interaction of an incident electron and one bound electron was formulated in the BE and the Born approximations. In this section we extend those one-electron concepts to many-electron molecular systems.

a. Description and bound electron kinetic energy.

One description of the bound state wavefunction can be obtained through the Born-Oppenheimer approximation[22]. Here the many particle (electron and nuclei) wavefunction is written as: $\Psi = \phi_\alpha(\underset{\sim}{r},\underset{\sim}{R}) X_{\alpha\beta}(\underset{\sim}{R})$, where the notation is described in Sec. 2.2.c. At fixed positions of the nuclei $\{\underset{\sim}{R}\}$, the electronic wave functions can be written in terms of n one-electron wavefunctions $\phi_i(\underset{\sim}{r}_i)$, in a determinantal form:

$$\phi_\alpha(\underset{\sim}{r},\underset{\sim}{R}) = \left| \phi_1(\underset{\sim}{r}_1)\phi_2(\underset{\sim}{r}_2) \cdots \phi_n(\underset{\sim}{r}_n) \right|_{\underset{\sim}{R}} \tag{51}$$

The kinetic energy of a bound electron occupying an orbital described by a one-electron wavefunction $\phi_q(\underset{\sim}{r})$ and quantum numbers q, can be written as

$$\epsilon_q = \langle \phi_q(\underset{\sim}{r}) | t | \phi_q(\underset{\sim}{r}) \rangle \tag{52}$$

where $t = p^2/2m = \dfrac{-\hbar^2\nabla^2}{2m}$ is the kinetic energy operator. Since the bound electron kinetic energy ϵ_q, which appears as an important parameter in the BE and the Born scattering approximations, is defined differently by several authors, we will attempt a critical study of the definition and approximation of ϵ_q. We begin with a brief review of the virial theorem.

Classically, the virial theorem states that for a system of particles that interact via forces which are derivable from homogeneous potentials of degree p, the time average of kinetic energies of the particles in the system is equal to p/2 times the time average of the potential. Quantum mechanically an analogous result is obtained; the classical time average being replaced by quantum mechanical expectation values over the stationary states. Thus the theorem for a molecular system which interacts only via coulombic forces, can be written as

$$T_{e\ell} + T_n = - 1/2 \ (I_{ee} + A_{en} + V_{nn}) \qquad (53)$$

Here $T_{e\ell}$ and T_n are the total kinetic energies of all the electrons and all the nuclei in the molecule respectively, while I_{ee}, A_{en} and V_{nn} are respectively the expectation values of the operators representing inter-electronic repulsion, electron-nuclei attraction and nuclei-nuclei repulsion. Thus for the system as a whole, the average contribution to the total potential energy is twice that of the total kinetic energy and opposite in sign. Since the total energy the system (-U) is $T_{e\ell} + T_n + I_{ee} + A_{en} + V_{nn}$, (53) can be rewritten

$$T_{e\ell} + T_n = U \qquad (54)$$

Note that U is a positive number. This shows that the total kinetic energy of the entire system (of electrons and nuclei) is related to the total energy of the system.

In the Born-Oppenheimer approximation, one assumes that the nuclei are held fixed (so that $T_n = 0$) by some external force. This requires modifications[23] in the virial theorem i.e.,

$$T_{e\ell} = -1/2[I_{ee} + A_{ee} + V_{nn} - \underset{\sim}{R} \cdot \nabla U_f(R)], \qquad (54)$$

Where $-U_f(\underset{\sim}{R})$ is the total energy of the system for the nuclei fixed at $\{\underset{\sim}{R}\}$. Thus an alternative expression for the virial theorem is

$$T_{e\ell} = U_f(\underset{\sim}{R}) + \underset{\sim}{R} \cdot \nabla U_f(\underset{\sim}{R}). \qquad (55)$$

This result is exact in the case where the nuclei are assumed to be fixed. Löwdin[24] has shown that, even in this case of fixed nuclei, a necessary criterion for the existence of a stationary state of the Schrödinger equation is the fulfillment of the virial theorem as given in (55). At the equilibrium position of the nuclei the $\nabla U_f(\underset{\sim}{R})$ is, by definition, equal to zero. Thus for molecular systems in equilibrium, the total kinetic energy of the bound electrons is exactly equal to the magnitude of the total energy of the molecule.

The one-electron kinetic energy ε_q can now be related approximately to the ionization potential. If after the removal of an electron from an orbital, labelled by quantum numbers q, the resulting molecular ion does not dissociate, then one can write $U^+ = T_{e\ell}^+(q)$ exactly. Here $-U^+$ is the total energy of the ion, formed after the removal of an electron from the orbital q and $T_{e\ell}^+(q)$ is the total electronic kinetic energy of the ion. Similarly, the neutral molecule has exactly, $U^0 = T_{e\ell}^0$ Thus

$$U^0 - U^+ = T^0 - T_{e\ell}^+(q) \qquad (56)$$

Since the left side of this equation is exactly equal to the experimentally measureable ionization potential $I^+(q)$, we can write (56) as

$$I^+(q) = T_{e\ell}^0 - T_{e\ell}^+(q) \qquad (57)$$

This expression is exact. It shows that the difference between the total electronic kinetic energies of a molecule and its ion is exactly equal to the ionization potential for the formation of that ion. Now we make the first approximation: $[T_{e\ell}^0 - T_{e\ell}^+(q)]$ is equal to ϵ_q, as defined in Eqn. (52). This approximation is certainly justified in the one-electron model. In general however, it is an approximation whose validity is difficult to assess. Thus one can approximate,

$$\epsilon_q \approx I^+(q) \qquad (58)$$

As mentioned earlier, two different definitions of ϵ_q exist in literature. Robinson[25] inexplicably associates ϵ_q with T_e^0, the latter being obtained by Slater's rules, and concludes that ϵ_q should be much greater than the ionization potential. Others[26,27] have obtained an average ϵ_q for n_0 electrons occupying an orbital by the following prescription:

$$\bar{\epsilon} = \sum_{n=1}^{n_0} I^{+n}/n_0 \qquad (59)$$

Where I^{+n} is the nth ionization potential (I^{+1} is abbreviated as I^+). This definition is stated (Ref. 26,27) to be obtained from the virial theorem. Also the nth ionization potential I^{+n} is defined, in this context, to be the energy necessary for removal of an electron from an ion of charge $+(n-1)$. Thus we write $I^{+n} = U^{+(n-1)} - U^{+n} = T_{e\ell}^{+(n-1)} - T_{e\ell}^{+n}$ exactly. Now an approximation has to be made

to relate I^{+n} to the one-electron kinetic energy ε_q of a bound electron the neutral molecule. In Ref. 26, 27, Eqn. (59) is used to approximate $I^{+n} = T^{+(n-1)} - T^{+n} \approx \varepsilon_q$; we believe that this is incorrect. The I^{+n} is a measure of the binding of an electron in the field of an ion and as such $I^{+n} = T_{e\ell}^{+(n-1)} - T_{e\ell}^{+n} \approx \varepsilon_q^{+(n-1)}$ is the one-electron kinetic energy of an electron in an ion, not in a neutral molecule. Physically $\varepsilon_q^{+(n-1)}$ is expected to be greater than ε_q since an ionic electron, compared to an electron in a neutral molecule, suffers stronger binding to the atomic nuclei and weaker electron-electron correlation. Thus we believe Eqn. (59) becomes $\bar{\varepsilon} = \sum_{n=1}^{n_0} \varepsilon_q^{+(n-1)}/n_0$; a quantity that has no direct relation to the average one-electron kinetic energy in a neutral molecule. It is interesting to note that both the Robinson hypothesis of $\varepsilon_q = T_{e\ell}^0$ as well as ε defined in Eqn. (59) give an average bound electron kinetic energy that is significantly greater than I^+ for $n_0 \geq 2$. This behavior is especially significant and fortuitously helpful, when used with the BE theory where an increasing ε_q 'improves' the high incident electron energy behavior of the ionization cross section [Fig. 10b and Ch. 4].

For our purposes we will use only the one-electron approximation in Eqn. (58), i.e., $\varepsilon_q \approx I^+(q)$. It should be noted however that an additional approximation regarding the definition of $I^+(q)$ has to be made. The ionization potential depends not only on the properties of the initial (bound) state, but also on the properties of the final (ionized) state. An ion with a partially filled shell can be created in one of several possible states. These are

separated energetically by the effects of inter-electronic repulsion and spin-orbit coupling and consequently are energetically separated by a few electron volts. Thus we relabel the first ionization potential as $I(s,q)$, where s labels the quantum numbers of the final ionized state. It is now possible to <u>define</u> an average kinetic energy of the electrons in an orbital as $\bar{\varepsilon}(q) \equiv \Sigma_s \frac{I(s,q)}{s_0}$, where s_0 is the total number of final ionized states formed from a given electronic configuration of the ion. Since $I(s,q)$ are generally separated by a few electron volts or less, one expects $\bar{\varepsilon}(q) \sim \varepsilon_q$. For the rest of this study, the kinetic energy of a bound electron in an orbital q is assumed to be exactly equal to the ionization potential $I(s,q)$ for the removal of an electron from that orbital.

b. A model for direct ionization and rearrangement ionization transitions.

The ionized state of an atom or molecule falls into one of two general classes: 1) States that involve the ionizations of one of the bound electrons with no rearrangement in the electronic configuration of the remaining electrons (Henceforth called "direct ionization" states.) And 2) states that involve a rearrangement in the electronic configuration of the un-ionized electrons during an ionization event. (Henceforth called "rearrangement ionization" states). Using Moore's tables[28] of spectroscopic data, we illustrate such states in Fig. 11 for the case of ionizations of a neon atom. Consider first states involving direct ionization only. Removal of one of the six 2p electrons can leave the ion in one of two possible states, $^2P^o_{3/2}$ or $^2P^o_{1/2}$. These states are labeled
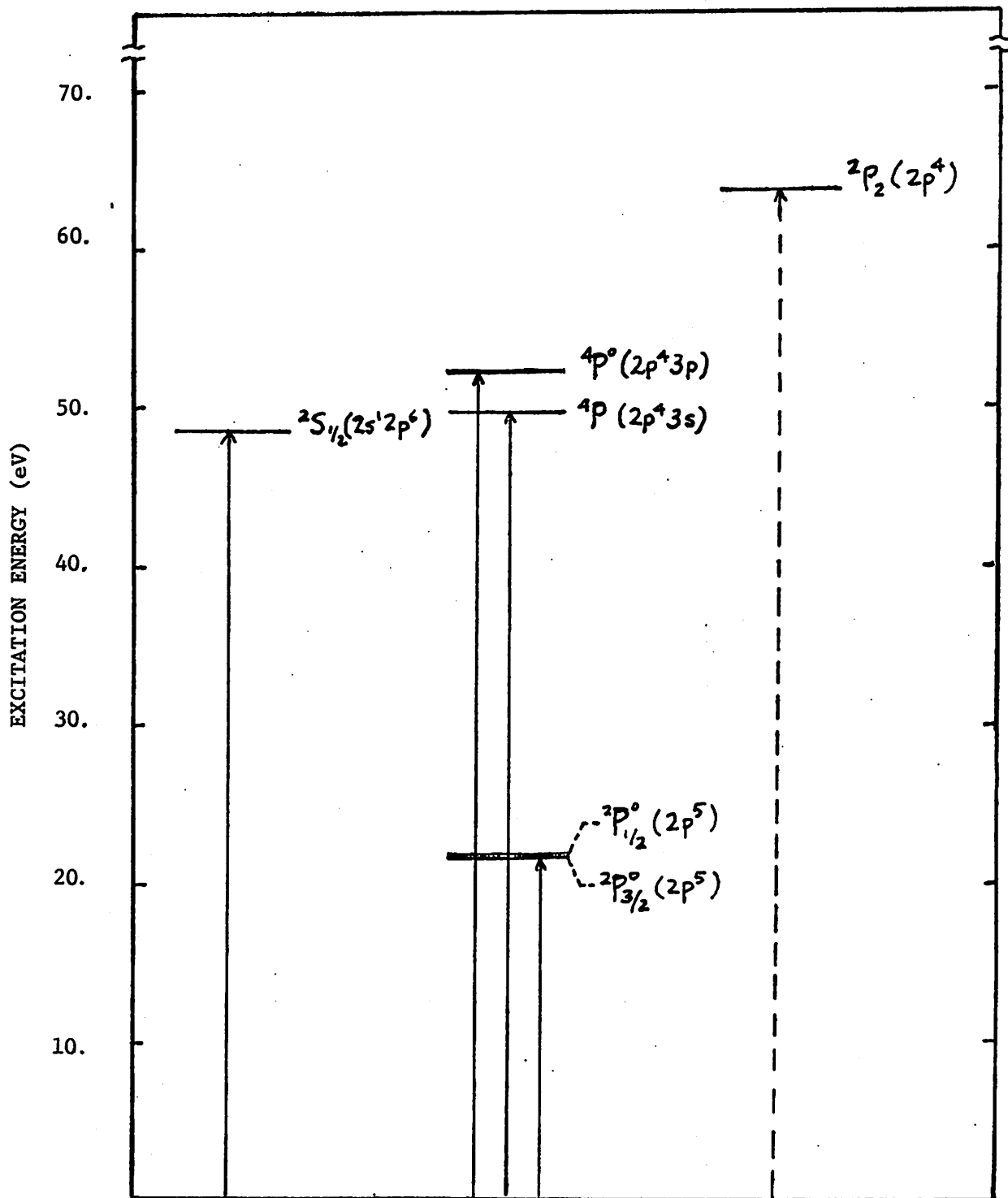
Fig. 11. Energy level diagram for a neon atom using the tables of Moore[28]. Transitions involving single ionization are presented by the solid vertical line; double ionization by a dashed line. Note that the $^2P^o_{1/2}$ – $^2P^o_{3/2}$ splitting is exaggerated on this scale.

according to standard spectroscopic notation[29]; they are identical

except for the magnitude of the total angular momentum quantum

number $J(= |\underset{\sim}{L} + \underset{\sim}{S}|)$. In our notation of the previous section, the

two ionization potentials could be labelled $I(^2P^o_{3/2}, 2p)$ and

$I(^2P^o_{1/2}, 2p)$ respectively. The splitting is due to weak spin-orbit

interaction and is only 0.097 eV. Removal of a 2s electron allows

only one possible state $(^2S_{1/2})$ with an ionization potential

(48.5 eV), which can be labelled $I(^2S_{1/2}, 2s)$. Removal of two

electrons from the 2p orbital can give a doubly ionized Ne atom

(Ne^{++}) with an ionization potential of 63.6 eV. Next we consider

two of the many rearrangement ionization states tabulated by Moore.

Figure 11 shows a term $(^4P$; multiplet structure < 0.1 eV is not

visible on this scale) obtained by an excitation of a 2p electron

into the 3s orbital and another term $(^4P^o)$ obtained by an excitation

of a 2p electron into the 3p orbital. An inspection of the tables

by Moore shows that there are in all 35 identified terms (each with

a fine multiplet structure) that involve rearrangement ionizations,

lying between 49.7 eV and 63.6 eV. All of these are obtained by

excitation of one of the 2p electrons into an unfilled orbital.

Next we propose models for the estimation of direct and re-

arrangement ionization cross sections in a many-electron system.

Recall that the one-electron scattering model considers only a two

body interaction between the incident and the bound electrons; the

two parameters that characterize an ionization cross section are

$I(s,q)$ and ε_q. The orbital or total angular momentum of the initial

state (or the bound electrons) and the final state (or the remaining

electrons) is completely ignored. Thus transitions to direct states,

i.e., those with different quantum numbers but belonging to the same electronic configuration, cannot be estimated in this model per se. We propose an empirical method for the estimation of two such states.

We model the cross section for transition to state s by an ionization of an electron from an orbital with quantum numbers q is given by

$$Q_{s,q} = \gamma_s n_e(q) \sigma_I(I(s,q), \varepsilon_q, T).$$ (60)

Where σ_I is the one-electron ionization cross section given in Sec. 3.1.c. and $n_e(q)$ is the number of electrons in the orbital q. The weight factor γ_s, for a particular direct ionization state, is empirically chosen to be

$$\gamma_s = \frac{\sigma_I(I(s,q), \varepsilon_q, T)}{\displaystyle\sum_{s=1}^{n_s} \sigma_I(I(s,q), \varepsilon_q, T)}.$$ (61)

Where the sum extends over all the n_s possible direct states of the ion. The rationale for this choice of γ_s is seen through consideration of two cases.

First the case where all the direct states s formed out of a given electronic configuration q are energetically degenerate, i.e., $I(s,q) = I_0(q)$ for all s. Then we expect that

$$n_e \sigma_I(I_0(q), \varepsilon_q, T) = \sum_s Q_{s,q}.$$ (62)

This is because $n_e \sigma_I$ is the cross section for the removal of one of

the n_e bound electrons and the remaining electrons arranged in every allowable manner. This is exactly equal to $\Sigma_s \, Q_{s,q}$. In this case of complete degeneracy we expect yet another relationship. The cross sections to each of these degenerate states is expected to be equal. This is because these degenerate states are distinguished only by their magnetic quantum numbers. And as discussed at the end of Chapter 2, the ionization cross section is not subject to any selection rules if the direction of the ejected electron is not specified. Thus cross sections to each of these states are equal to $Q_{s,q} = n_e \sigma_I / n_s$.

The other case we consider is one wherein a given electronic configuration has two states separated by a large difference in ionization potentials. Here we expect the lower state [smaller $I(s,q)$] to have a larger weight factor than the higher state [larger $I(s,q)$]. This is made plausible as follows: (1) the weight factor γ_s is related to the degeneracy [In the L-S coupling scheme, degeneracy is equal to $(2L+1) \cdot (2S+1)$ for the state s with quantum numbers L and S] of the final state s. This is because greater correlation between the initial and final states exists with increasing number of allowed electronic arrangements in the final state. (2) Generally, states with higher degeneracies have lower energies. This is certainly true for the lowest L-S term, as is implied by Hund's rule. It is expected to be approximately true in general. Thus putting together arguments (1) and (2), we arrive at a credible form for γ_s given in Eqn. (61). The main advantage of this simple approximation for γ_s is that it does not require any further information (such as L, S, J etc.) about

the final state. Undoubtedly more accurate description of γ_s can be developed but for our purposes of calculating total ionization cross section it may be unnecessary.

Next we develop a phenomenological model for transitions involving rearrangement ionizations. Our method is inspired by the work of Gryzinski[30] in his quite successful classical theory of double ionizations in atoms. The basic postulate of the method is that the incident electron ejects a bound electron; subsequently the ejected or the scattered electron can interact with other bound electrons causing excitations and rearrangements. In the case of rearrangements induced by the ejected electron motion in the many-electron system, the two step hypothesis is an approximation of the effect of electron-electron correlation amongst the bound electrons. However the rearrangements caused by the motion of the scattered electron, on its 'way out' of the many-electron system, can probably be obtained from the higher-order Born terms in the scattering matrix. Our model may also be considered akin to the description[31] of core relaxation and double excitations in photo-absorption process in atoms.

Consider first the cross section $Q_{s,q}^{R-E}$ for a transition to a rearrangement ionization state s, obtained by the removal of a bound electron from an orbital q by the action of an ejected electron. Note that $Q_{s,q}^{R-S}$ denotes the cross section for an analogous transition, except that it is initiated by a scattered incident electron. The total cross section for this event $Q_{s,q}^{R}$ is ($Q_{s,q}^{R-E}$ + $Q_{s,q}^{R-S}$). We model $Q_{s,q}^{R-E}$ to be dependent on: (1) ϵ_q and ϵ_r; these are respectively, the bound electron kinetic energies of the

orbital q from which the ejected electron emerges and of the orbital r from which the electron involved in the rearrangement is removed. (2) $I_r(s,q)$ the threshold energy transfer for the process of rearrangement ionization. This, it is assumed, can be written as

$$I_r(s,q) = E_r(s,q) + I(s_0,q),\qquad (63)$$

where $E_r(s,q)$ is the excitation energy necessary to cause a rearrangement that results in the formation of a state s, while $I(s_0,q)$ is the ionization potential of the lowest state (s_0) that results from the removal of an electron from an orbital q. From now on we will write I, I_r and E_r without displaying the explicit dependence on s, s_0 and q.

The cross section $Q_{s,q}^{R-E}$ is then written as

$$Q_{s,q}^{R-E} = \sum_t{}' \int_0^{T_e(max)} P_r(t,E_r,T_e)[n_e(q)\,\frac{d\sigma}{dT_e}(I,\varepsilon_q,T)]dT_e \qquad (64)$$

where the terms in the square brackets represent the cross section for the removal of an electron from the orbital q with a kinetic energy between (T_e,T_e+dT_e). While $P_r(t,E_r,T_e)$ represents the probability of causing a rearrangement through an excitation of an electron from the orbital t due to the action of an ejected electron with kinetic energy T_e. Note that the upper limit of the integral is determined by the approximation used in the modelling of $d\sigma/dT_e$. When the symmetrized BE theory expression for $d\sigma/dT_e$ is used, one has $T_e(max) = (T-I)/2$ [see Eqn. (42)]; while when the Born theory is used $T_e(max) = T-I$. Further in Eqn. (64), the sum

over the orbitals r involved in the rearrangement process is restricted. This restriction is generated by the assumption that rearrangements can occur amongst only those electrons that belong to either (a) the orbital from which an ejected electron emerged or (b) an 'adjacent' orbital (in an energetic, rather than spatial, sense) to the one from which the ejected electron emerged. Thus the prime over the summation symbol in (64) denotes a sum over only such orbitals.

The probability of exciting an electron from an orbital t into a state s, with a threshold energy transfer E_r, is modelled as a product of: (1) An integral representing an excitation cross section for a process with a threshold energy of E_r, initiated by an electron with kinetic energy T_e. (2) An approximation to the effective surface density of bound electrons in the orbital r that are involved in the rearrangement process. Thus we write,

$$P_r(t,E_r,T_e) = \frac{(n_e(t) - \delta_{tq})}{A_t} \int_{E_r}^{E_u} \frac{d\sigma}{dE}(\epsilon_t,T_e)dE. \qquad (65)$$

The term outside the integral is the ratio of the number of electrons in the orbital t (Note that σ_{tq} is the symmetric Kronecker δ symbol that equals unity if t = q and is zero otherwise.) to the effective area of that orbital A_t. This latter factor is subject to ambiguity, both in its concept as well as its usage. We will attempt to establish an unambiguous rule in the following chapter. The excitation cross section, represented by the integral, is modelled to be described by the symmetrical BE theory. This description is chosen

3.61

because a major, contribution to $Q_{s,q}^{R-E}$ in Eqn. (64) arises from

small $T_e/E_R (\leq 10)$ and as such the $d\sigma/dE$ in the symmetrical BE

approximation is superior to that in the Born approximation, both

in concept as well as in comparison with experiment. We also

choose the Gryzinski type limits on the integrand (recall discussion

in Sec. 3.1.c) rather than those suggested by the quantum defect

theory for states belonging to a Rydberg series. The upper limit

E_u is obtained from assuming that the rearrangement ionization

process is inhibitated for energy transfers greater than $I_u =$

$(E_u + I)$. Thus Eqn. (65) can be rewritten as

$$P_r(t,E_r,T_e) = \frac{(n_e(t) - \delta_{tq})}{A_t} [\sigma_I(E_r,\varepsilon_t,T_e) - \sigma_I(E_u,\varepsilon_t,T_e)]. \quad (66)$$

Where we have used the BE theory expression for σ_I given in Eqn.

(46).

Consider next the formulation of the cross section $Q_{s,q}^{R-S}$ for

a transition to a rearrangement ionization state s by the action

of the scattered incident electron. In analogy with Eqn. (64) we

write,

$$Q_{s,q}^{R-S} = \sum_t {}' \int_{T_s(min)}^{0} P_r(t,E_r,T_s) [n_e(q) \frac{d\sigma}{dT_s} (I,\varepsilon_q,T)] dT_s. \quad (67)$$

Here $T_s(min)$ is the minimum possible scattered electron kinetic

energy. Since the only difference between Eqn. (64) and (67) is

in the variable of integration and in the limits over the integrand,

one can use $T = T_s + T_e + I$ to rewrite Eqn. (67) as

$$Q_{s,q}^{R-S} = \int_0^{T_e(max)} \sum_t{}' P_r(t,E_r,(T-T_e-I))n_e(q) \frac{d\sigma}{dT_e} (I,\epsilon_q,T)dT_e. \quad (68)$$

Where $T_e(max)$ is, as defined earlier, different for the two scattering approximations.

The form of Eqn. (68) allows for a convenient interpretation of the entire integrand as the differential cross section for the ejection of electrons with kinetic energy T_e. This is the contribution due to the action of the scattered electrons and is therefore written as

$$\frac{dQ^{R-S}}{dT_e} = \sum_t{}' P_r(t,E_r,(T-T_e-I))n_e(q) \frac{d\sigma}{dT_e} (I,\epsilon_q,T). \quad (69)$$

An analogous expression due to the action of the ejected electron is not obtained as directly. The ejected electron, due to its subsequent interaction with the other bound electrons, appears outside the target with a different kinetic energy than that given by $T_e = T - T_s - I$. If one can assume that the ejected electron induced excitation of the bound electrons has a sharp threshold at E_r, then one has $T_e = T_{ex} + E_r$. Here T_{ex} is the kinetic energy of an ionized electron that appears externally. Substituting this in $Q_{s,q}^{R-E}$ [Eqn. (64)], one obtains

$$\frac{dQ^{R-E}}{dT_{ex}} = \sum_t{}' P_r(t,E_r,T_{ex}+E_r)n_e(q) \frac{d\sigma}{dT_{ex}} (I,\epsilon_q,T) \quad (70)$$

due to the action of the ejected electrons. Note that $Q_{s,q}^R = Q_{s,q}^{R-E} + Q_{s,q}^{R-S}$ can thus be written in terms of Eqn. (69) and Eqn. (70). i.e.,

$$Q^R_{s,q} = \int_0^{T_e(max)-E_r} \frac{dQ^{R-E}}{dT_{ex}} \, dT_{ex} + \int_0^{T_e(max)} \frac{dQ^{R-S}}{dT_e} \, dT_e. \qquad (71)$$

We now investigate and compare the behavior of the rearrangement ionization cross sections. We will plot the quantity β^{R-i} [defined as $\beta^{R-i} = A_t Q^{R-i}_{s,q}/(\pi a_0)^4 \cdot (n_e(t)-\delta_{tq})$] for i = E and S, as well as the analogous quantity β^R for the total cross section. Note that β^R and β^{R-i} depend only on various energies ($I_r, I_u, I, \varepsilon_q, \varepsilon_t$ and T) involved in the transition. In Eqns. (69) and (70), the expression for $d\sigma/dT_e$ (or $d\sigma/dT_{ex}$) could either be described in the BE theory (preferable for $T/I \leq 50$) or in the Born theory (for $T/I \geq 50$). The $Q^R_{s,q}$ obtained using the BE approximation $d\sigma/dT_e$ are called the 'BE approximation' rearrangement ionization cross sections. The $Q^R_{s,q}$ obtained using the Born theory $d\sigma/dT_e$ are called the 'Born approximation' rearrangement ionization cross sections. In Fig. 12a, the Born theory β^{R-E}, β^{R-S} and β^R are plotted versus T/E_R. We have also chosen here and in the subsequent examples (Figs. 13-15), $\varepsilon_q = \varepsilon_t = I(s_0,q) = E_R$. This restriction, we believe, still allows for the major trends and dependences (on I_r, I_u, T, etc.) to be visible. Here the contribution due to the scattered incident electrons (i.e., β^{R-S}) is the dominating fraction for $T' \leq 10$; while for $T' \geq 10$ the contribution due to the ejected electrons (i.e., β^{R-E}) dominates the total cross section. This is understood as follows: for small T', the higher order terms (non-first-Born) in the interaction of the incident electron and the bound electrons dominates any corrections that may be due primarily to the many-electron nature of the target.
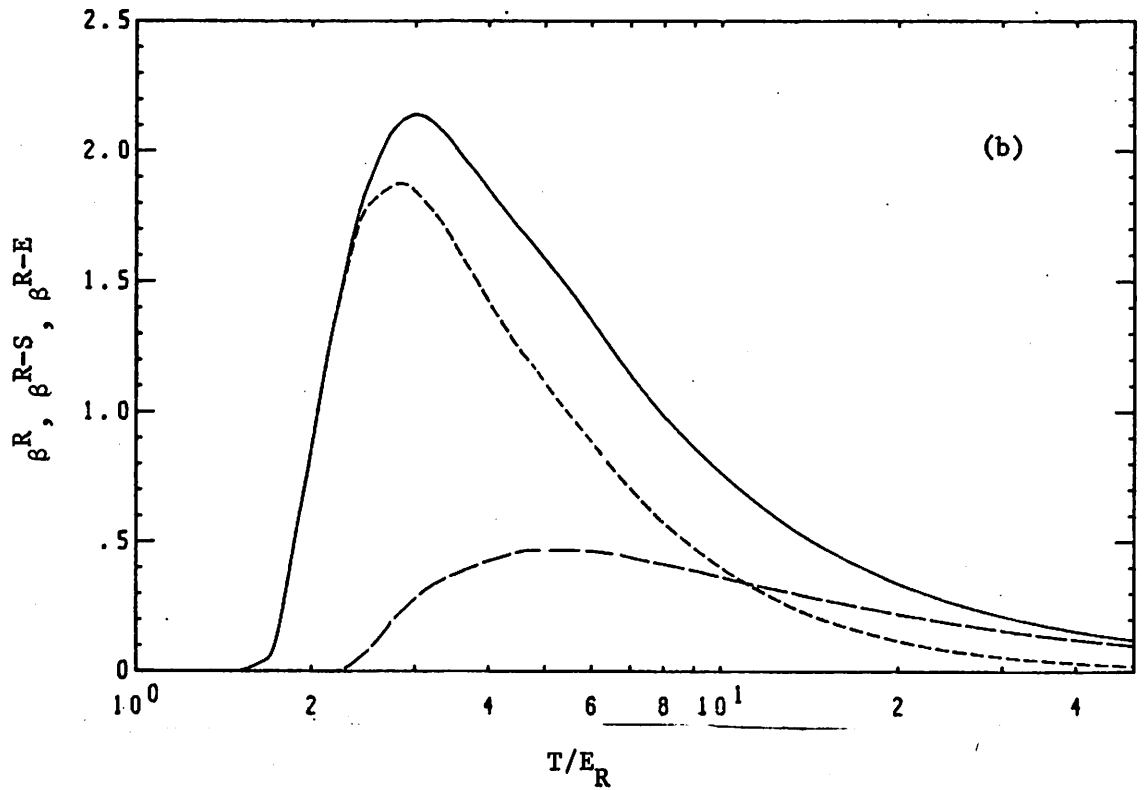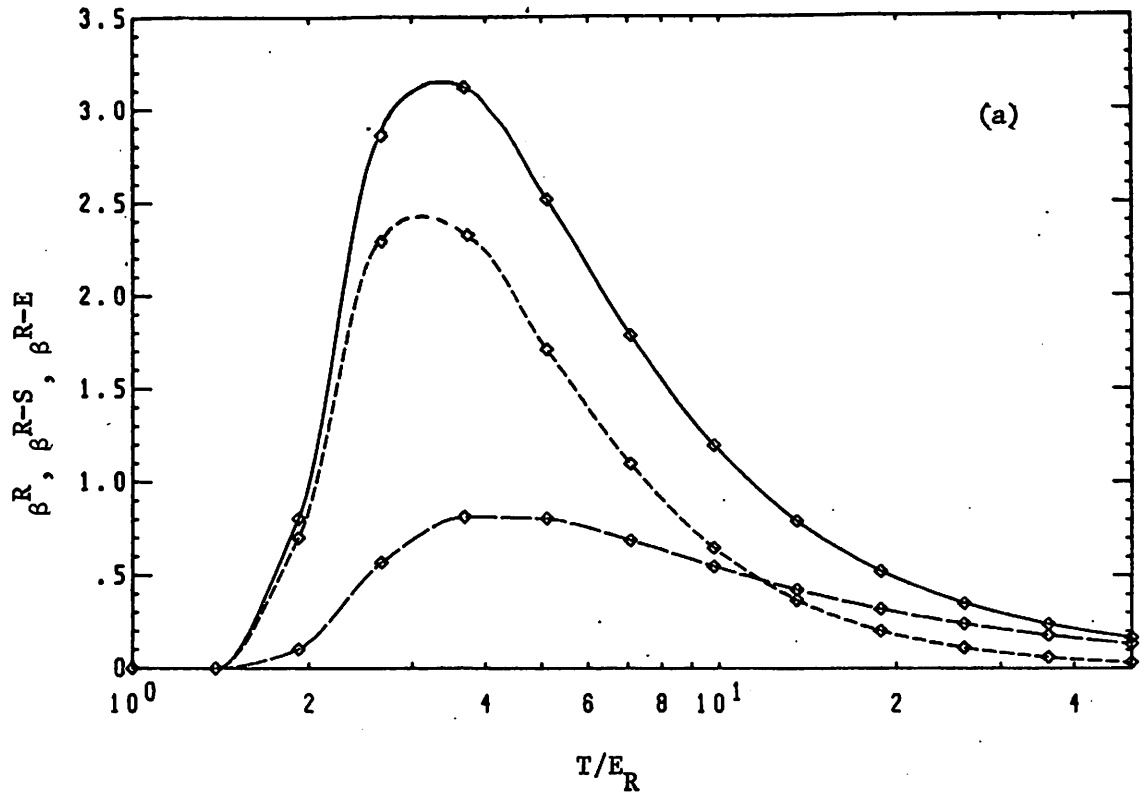
Figs. 12. Plot of β^R (solid curve), β^{R-S} (small dashed curve) and β^{R-E} (large dashed curve) versus T/E_R with $E_r/E_R = 2/3$ and $E_u/E_R = 1.25$. For two cases: (a) the Born approximation in the β's and (b) the BE approximation in the β's.

3.65
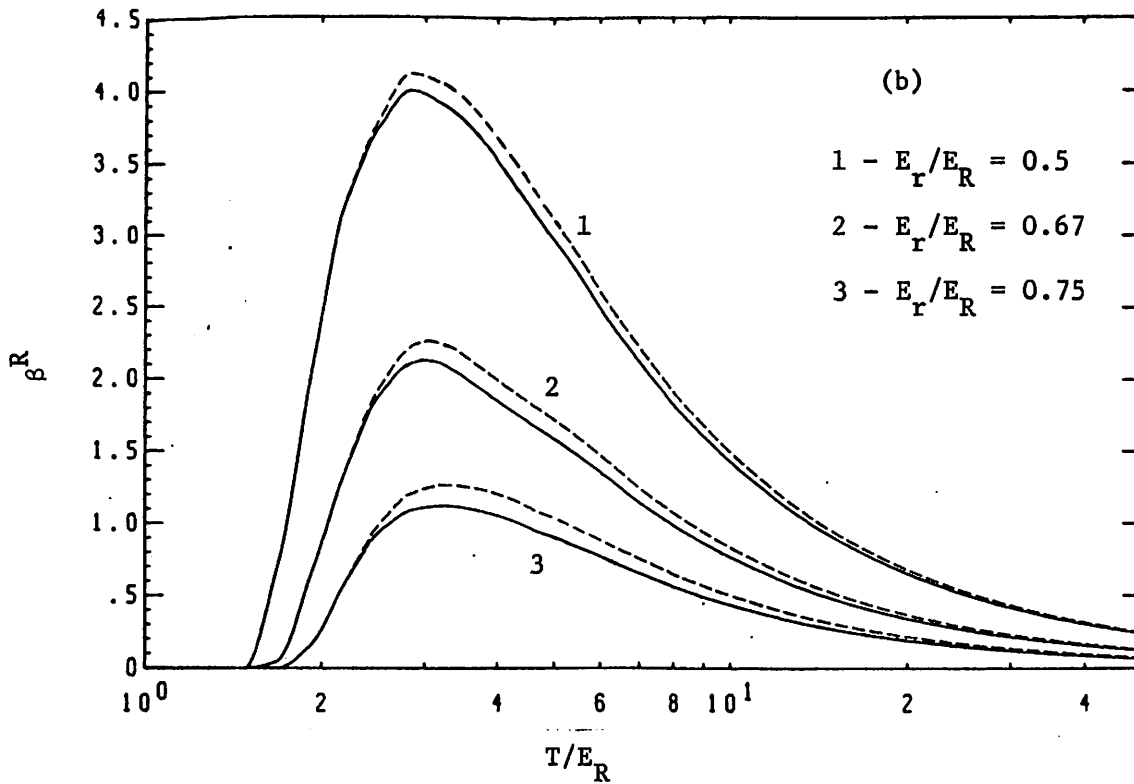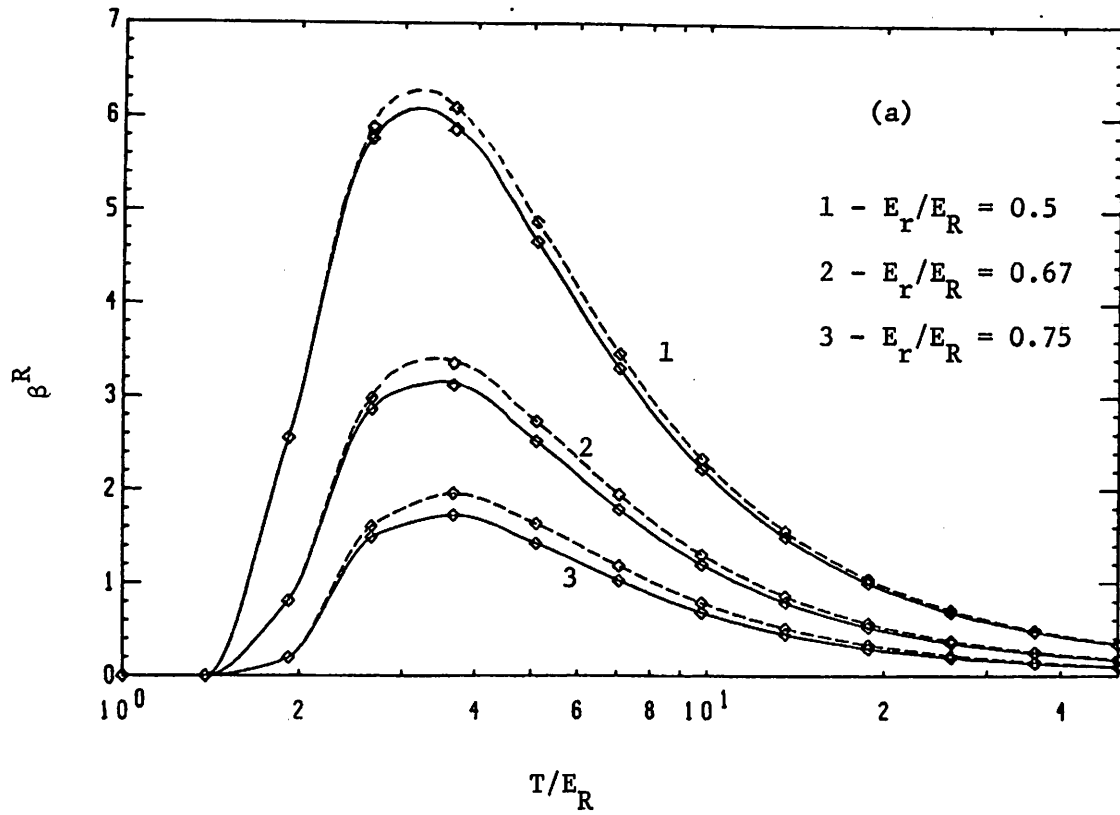
Figs. 13. Plot of β^R versus T/E_R for different values of E_r/E_R (as shown) and $E_u/E_R = 1.25$ (solid curves) and $E_u/E_R = 1.5$ (dashed curves). For two cases: (a) the Born approximation and (b) the BE approximation.

3.66

However at higher T', the Born approximation describes the scattering interaction adequately, but the many-electron aspects of the target yield a significant correction. In Fig. 12b we plot the β^{R-E}, β^{R-S} and β^R in the BE approximation with the same conditions as those in Fig. 12a. Essentially similar behavior is seen as for the case of the Born approximation in Fig. 12a. Note however that the BE theories' β^R are consistently a little smaller than those in the Born approximation. Figs. 13a and 13b show that in both the approximations, β^R is a lot more sensitive to I_r than to I_u.

The large T' behavior of the rearrangement ionization cross sections is displayed in Figs. 14a and 14b. For large T', we will of course only consider the Born approximation rearrangement ionization cross section. A plot of $\beta^R \cdot T'$ versus $\log_{10}T'$ shows that there is only a weak $\ln T'$ behavior in $Q^R_{s,q}$; while β^R/σ_I shows that even at large T', β^R decreases faster (however slightly) than σ_I. Thus at smaller T' the ratio β^R/σ_I must have a maximum. This is seen in Fig. 15. Here, independent of the approximation (Born or BE), one sees a maximum at $T' \approx 3$-4. Note also that the magnitudes of β^R as well as the ratio β^R/σ_I scale with T' in a manner approximately independent of E_r and E_u. The significance of this behavior will become clearer on comparison of our simple model with experimentally observed ionization and dissociative ionization cross sections in the following chapter.
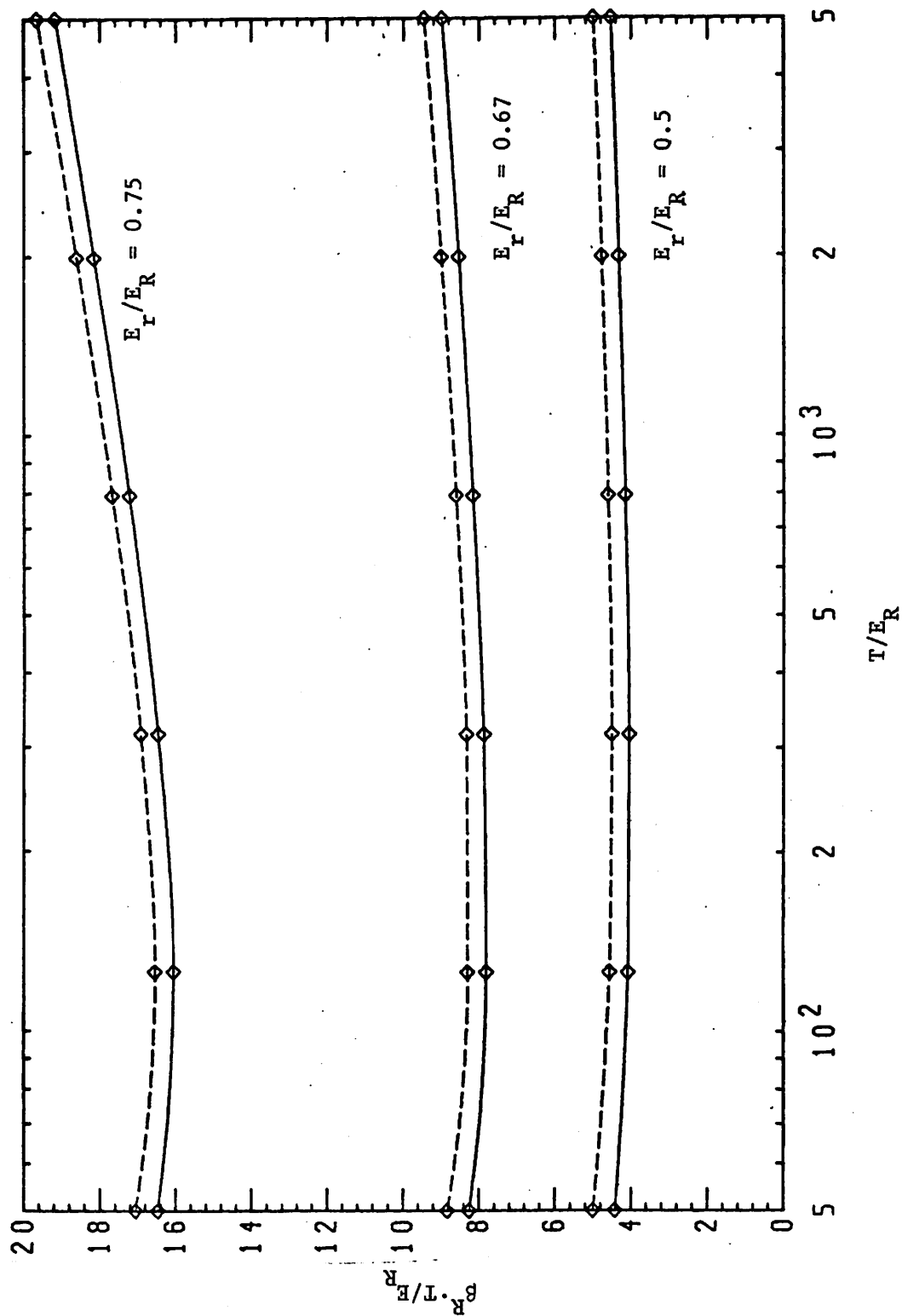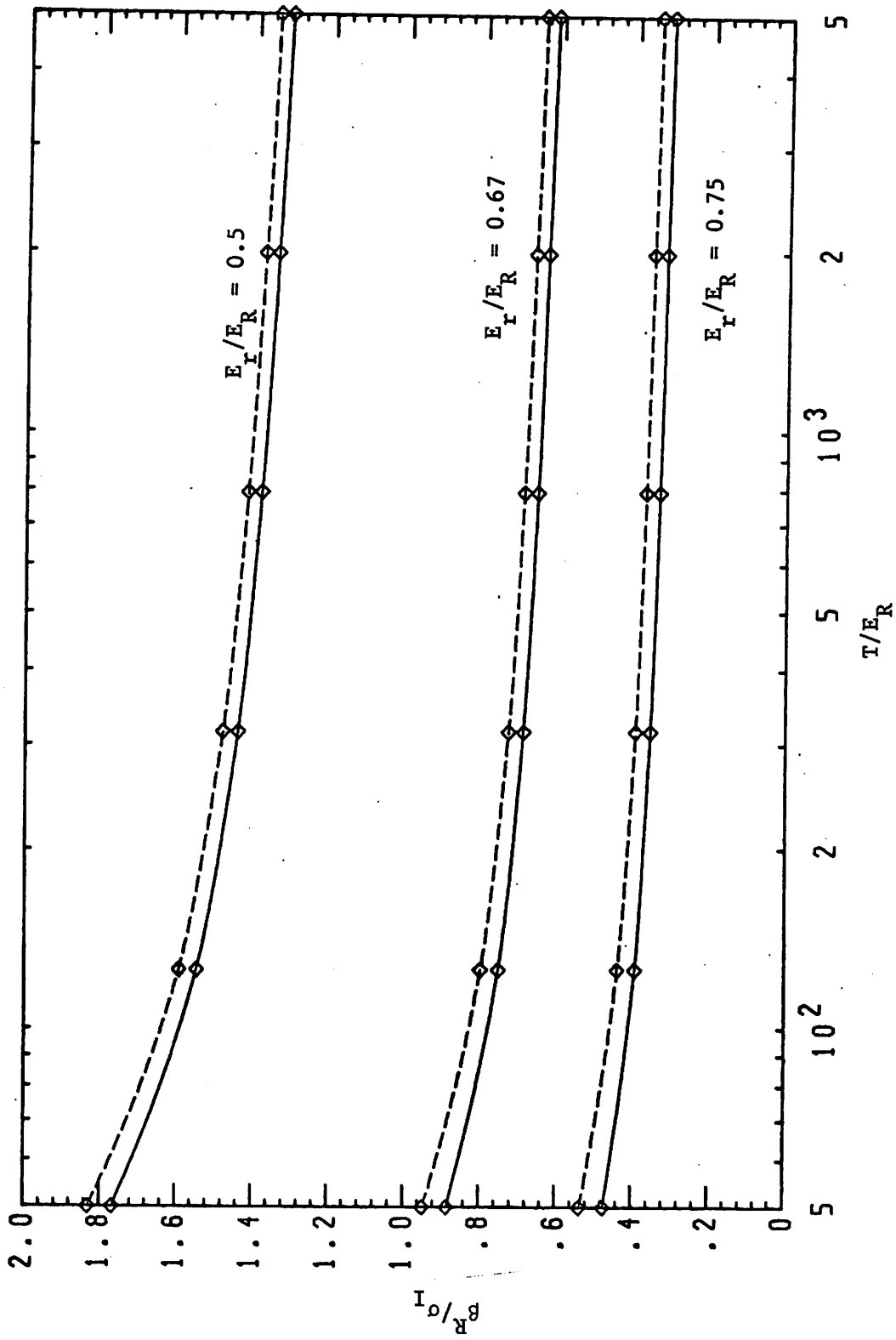
Fig. 14a. Plot of $\beta^R \cdot T/E_r$ versus T/E_R (Note log scale) for different values of E_r/E_R (as shown) and $E_u/E_R = 1.25$ (solid curves) and $E_u/E_R = 1.5$ (dashed curves).

Fig. 14b. Plot of β^R/α_I versus T/E_R for different values of E_r/E_R (as shown) and $E_u/E_R = 1.25$ (solid curves) and $E_u/E_R = 1.5$ (dashed curves).
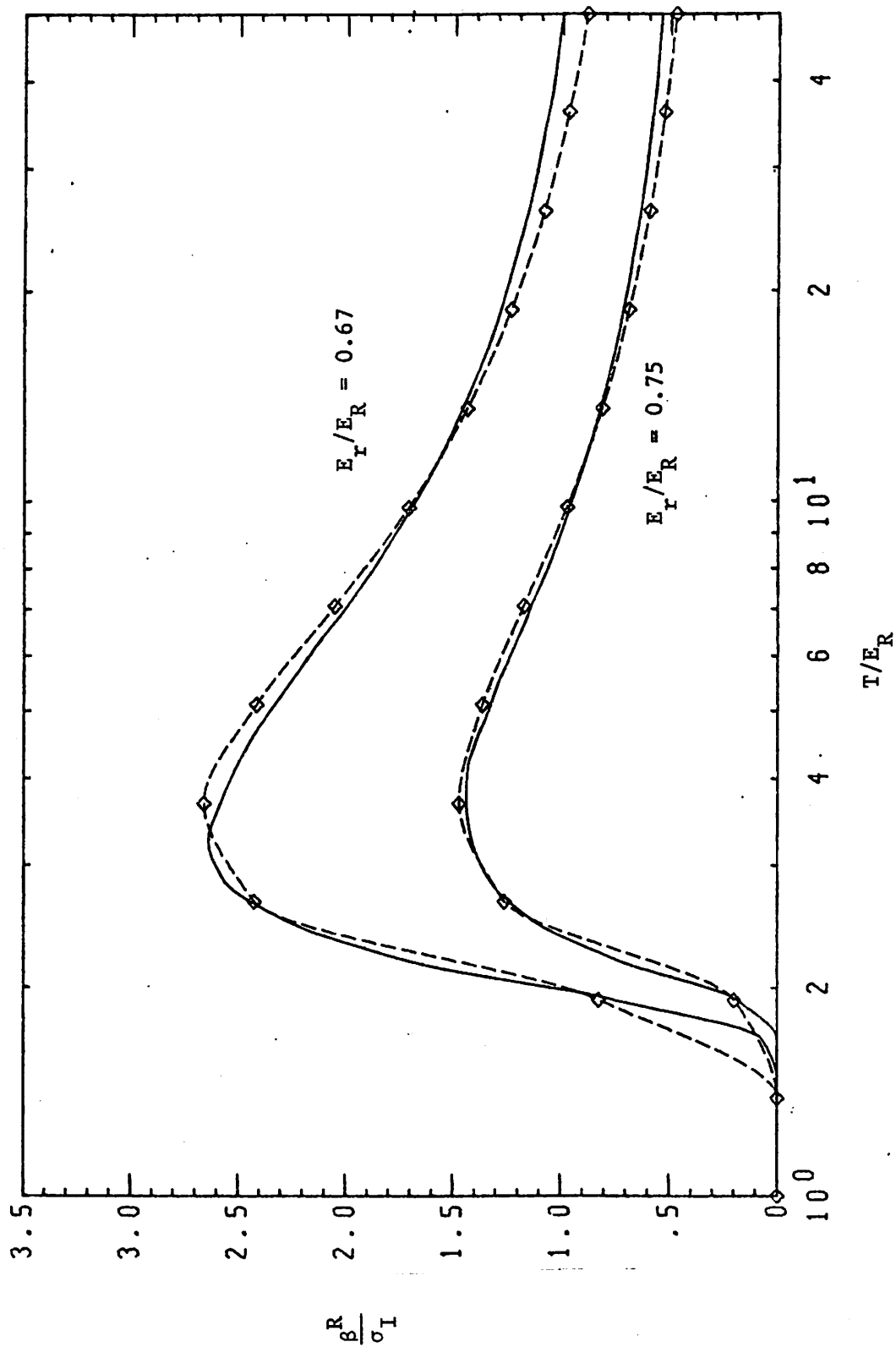
3.69

Fig. 15. Plot of β^R/σ_I for small T/E_R (< 50). Values of E_r/E_R are as shown and $E_u/E_R = 1.25$. For two cases: the Born approximation (---◇---) and the BE approximation (———).

REFERENCES to Chapter 3.

1. F. Herman and S. Skillman, Atomic Structure Calculations
   (Prentice Hall, Inc., Englewood Cliffs, N.J., 1963).

2. M.J. Seaton, Proc. Phys. Soc. (London) 88, 801, 815 (1966).

3. J.C. Slater, Phys. Rev. 36, 57 (1930).

4. H.F. Schaefer, The Electronic Structure of Atoms and Molecules
   (Addison-Wesley Publ. Co., Reading, Mass. 1972).

5. R. Vanderpoorten, Physica 48, 254 (1970).

6. S. Chung and C.C. Lin, Phys. Rev. A6, 988 (1972).

7. M. Gryzinski, Phys. Rev. 115, 374 (1959); Phys. Rev. 138,
   A305, A327, A336 (1965).

8. R.C. Stabler, Phys. Rev. 133, A1268 (1964).

9. L. Vriens, Proc. Phys. Soc. 89, 13 (1966).

10. L. Vriens and T.F.M. Bonson, J. Phys. B 1, 1123 (1968).

11. L. Vriens in Case Studies in Atomic Collision Physics I,
    ed. E.W. MacDaniel and M.R. McDowell (North-Holland, Amsterdam,
    1969), p. 337.

12. U. Fano and J.W. Cooper, Rev. Mod. Phys. 40, 441 (1968).

13. M. Inokuti, Rev. Mod. Phys. 43, 297 (1971).

14. L. Vriens, Op. Cit. (1969), Sec. 6.5-F.

15. H. Bethe, Ann. Physik 5, 325 (1930).

16. L. Vriens, Op. Cit. (1969), Sec. 2.4.

17. M. Gryzinski, Op. Cit., p. A352.

18. L.I. Schiff, Quantum Mechanics (McGraw-Hill Book Co., 1968),
    3rd ed., p. 374.

19. A. Burgess, Proc. 3rd Int. Conf. on Electronic and Atomic Collisions,
    London, 1963 ed., M.R.C. McDowell (North-Holland, Amsterdam, 1964), p. 237.

20. W.F. Miller and R.L. Platzman, Proc. Phys. Soc. 70, 299 (1957).

21. U. Fano, Phys. Rev. 95, 1198 (1954).

22. J.C. Slater, Quantum Theory of Matter (McGraw-Hill, 1968),
     Sec. 12-2.

23. J.C. Slater, J. Chem. Phys. 1, 687 (1933).

24. P.O. Löwdin, J. Mol. Spectry. 3, 46 (1959).

25. B.B. Robinson, Phys. Rev. 140, 764 (1965).

26. T.F.M. Bonsen and L. Vriens, Physica 47, 307 (1970).

27. G.M. Prok et. al., J. Quant. Spect. and Rad. Transfer 9,
     361 (1969).

28. C.E. Moore, Atomic Energy Levels (Circ. 467, Natl. Bur.
     Standards, U.S.A., 1958), vols. 1, 2, and 3.

29. J.C. Slater, Quantum Theory of Atomic Structure (McGraw-
     Hill, 1960), vol. 1, Ch. 10.

30. M. Gryzinski (1965), Op. Cit., p. A349.

31. U. Fano and J.W. Cooper, Op. Cit., Sec. 7.

CHAPTER 4

CALCULATION OF TOTAL AND DISSOCIATIVE IONIZATION CROSS SECTIONS

4.1 Available experimental data.

Using the methods developed in the preceding chapter, we will

here estimate the total ionization and DI cross sections for a few

isolated atoms and small molecules. Recall that the cross sections

$Q_{s,q}$ and $Q_{s,q}^R$ involve an electronic transition to respectively,

either a direct state or a rearrangement state; if these states

can lead to dissociation of the molecules, then the $Q_{s,q}$ or $Q_{s,q}^R$

for such states can be considered to be equal to the activated

state cross sections $\sigma_A(i)$, as defined in Eqn. (2-19). Experimental

data for absolute total (gross) ionization and DI cross sections

are available for a few atoms and molecules in the gas phase.

These experimentally measured DI cross sections [equal to $\sigma_D(i)$, as

defined in (2-19)] can be compared to the theoretically estimated

σ_A, yielding the magnitude and the relative importance of the

dissociation probability of the activated state P_d. Thus if the

calculated σ_A are approximately equal to the measured σ_D then one

can conclude that, at least in the gas phase, the P_d for the pro-

cesses of DI are close to unity. This conclusion will have a

significant influence on the condensed phase estimations of σ_D in

the following chapter.

Next we will briefly review and comment on the accuracy of

available gas phase experimental data on ionization cross sections.

Ionization and DI cross sections are obtained in essentially two

types of experiments:

4.1

(1) Experiments that measure absolute cross sections for a particular

process or a set of processes. (2) Experiments that measure only

relative cross sections of different processes. For experiments

of the first type, a comprehensive review article[1] tabulates gas

phase data for a few atoms and diatomic molecules. In these experi-

ments, an electron beam of calibrated kinetic energy is allowed to

interact with a dilute gas of the target atoms or molecules. The

ion current generated from ionizations is measured and the absolute

ionization cross section deduced from knowledge of gas pressure and

geometrical parameters of the interaction chamber. Thus any errors

in the measurement of the absolute gas pressure, the absolute ion

current and the absolute kinetic energy of the ionizing electrons

could cause substantial errors in the determination of the absolute

cross section. Indeed the two most recent measurements of ionization

cross section (those of the Lockheed group[2,3] and of the Amsterdam

group[4]) have absolute values for the total ionization cross section

differing by as much as 20% for the rare gas atoms and by about 15%

for the diatomic molecules H_2, N_2 and O_2, for incident electrons

with T between 500 and 1000 eV. The Lockheed group's data is taken

at small values of kinetic energy (T $\leq$ 1000 eV); also data for

fragments of molecules formed with kinetic energy (usually greater

than 0.25 eV) is reported. This latter data can be interpreted as

the DI cross section for the generation of a fragment (with a finite

kinetic energy) from a particular molecule and [reported in ref. 2]

is estimated to have an accuracy of only $\pm$ 30%. The Amsterdam

group has obtained data for total ionization only and for large

values of T (i.e., from 600 eV - 20 KeV). Thus we will use these experimental results with the knowledge that the absolute magnitudes may not be very reliable; however the relative cross sections between different species and between different T are expected to be more accurate.

The second type of experiments are usually performed in a mass spectrometer[5], where relative intensities for the production of fragment ions from a molecule are measured. The 'fragmentation pattern' or the collection of relative intensities of different ions produced from a particular molecule is reported to be nearly independent of the incident electron energies greater than 100 eV. However fragmentation patterns depend critically on instrumental parameters and thus large variations in observed patterns for a particular molecule are reported[6]. For a particular instrument and experimental condition, the variation in the fragmentation patterns for a homologous series of molecules is probably quite reliable. Keeping these facts in mind we will compare our theoretically calculated cross sections with the appropriate experimental data in the following section.

4.2 Calculations.

A computer program, in Fortran, has been written to calculate ionization cross sections of atoms and molecules. First it is necessary to identify each of the ionized states of the target as one that has involved either a direct or a rearrangement ionization transition of a bound electron. The cross sections for these events are given by $Q_{s,q}$ [Eqn. (3-60)] and $Q^R_{s,q}$ [Eqn. (3-71)]

respectively. Next the relevant parameters for either case have to be obtained (usually from experiment). With this as the input data, the computer program gives for the particular atom or molecule, at each value of the incident electron energy T, the following output: (a) the ionization cross section to each individual state, (b) sums and ratios of these cross sections and the total ionization cross section, and (c) the ejected electron distribution for T_e between 0 and 200 eV, which corresponds to the total ionization of the atom or molecule. The result of an independent numerical integration over this truncated distribution is usually within a few percent of the total ionization cross section obtained as a sum of the cross sections over the individual states. All calculated cross sections obtained using $Q_{s,q}$ and $Q_{s,q}^R$ are accurate to within 0.5%.

a. Ionization of atoms.

Consider at first the cross sections for ionizations of atoms. This will serve not only to illustrate our method but also to possibly reveal what type of results one can expect from our simple model for complex systems.

The ionization cross sections of a hydrogen atom calculated in the BE and the Born Approximations are shown in Fig. 1. The experimental data is taken from Fig. 3 of Reference 1. As expected the Born approximation is in excellent agreement with experiment for T > 300 eV. In this region, the BE approximation underestimates the ionization cross section significantly. For T < 100 eV, the situation is somewhat reversed; the BE theory cross sections are
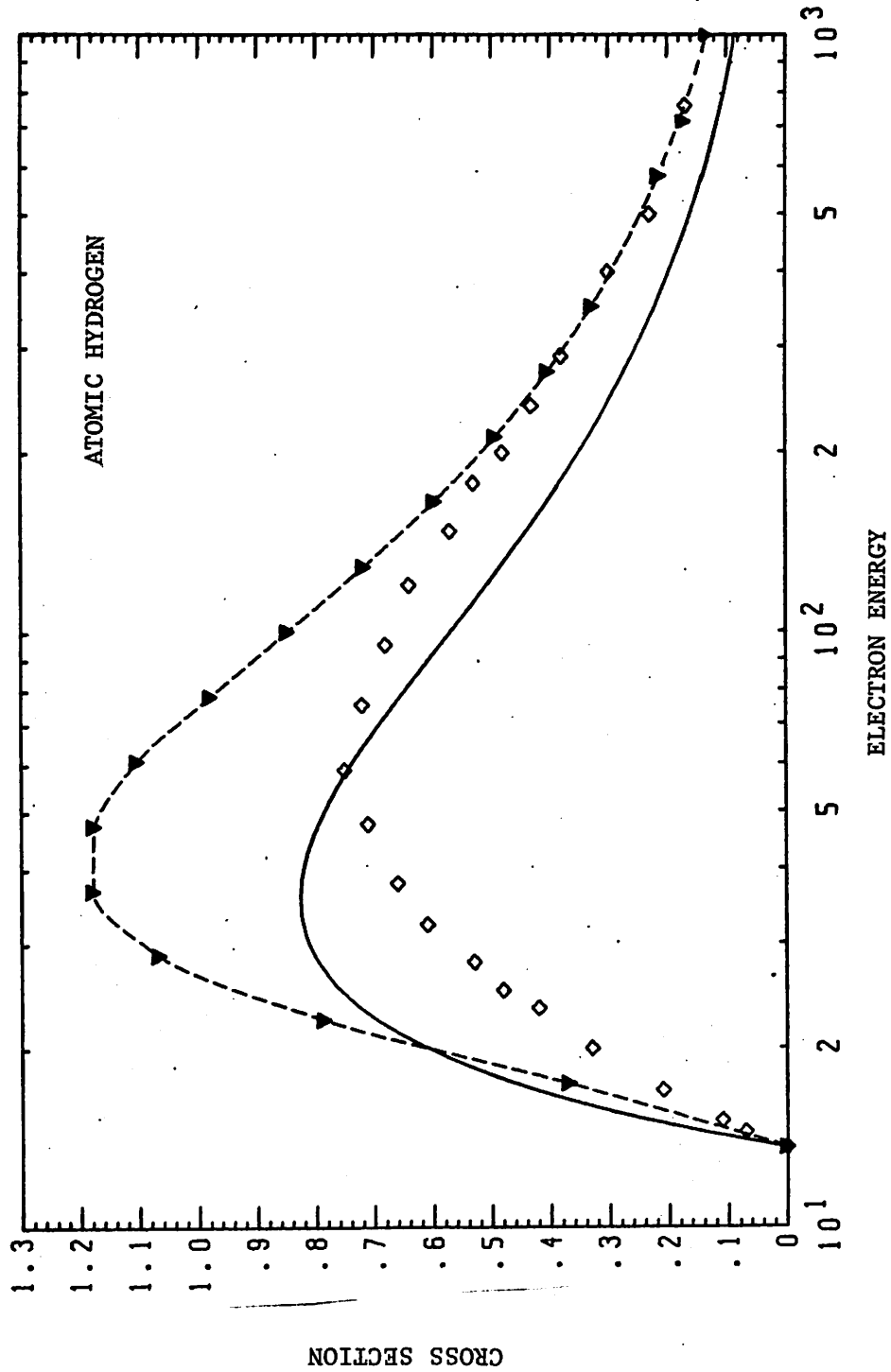
4.4

Fig. 1. Ionization cross sections (in πa_o^2) for a hydrogen atom versus incident electron energy (in eV). Calculated values (▼) in the Born approximation are joined by a dashed curve, while solid curve is obtained using the BE theory. Experimental data (◇) are from Fig. 3 in Reference 1.

in better agreement with experimental data than the Born theory cross sections. Both approximations give a maximum in the cross section at lower value of T than experiment. For this 'exact' one-electron system, the difference between the theoretical and experimental ionizations can only be attributed to the incorrectness in the approximations of the scattering dynamics. Thus the trends seen here may be expected in general.

Next we consider the ionization cross sections of many-electron atoms. For the rare gas atoms, in particular, the experimental data are obtained easily owing to the inertness of the species. However a filled outer shell in these atoms gives rise to strong electron-electron correlation - a quantity not accurately accountable in our (or any that we know) model. In the modelling of the probability P_r of exciting an un-ionized electron [Eqn. (2-65)], we introduced a parameter A_t. This is physically the effective area of the electron cloud (or orbital) involved in the rearrangement process. For atoms we choose A_t to be equal to $4\pi r_m^2$ where r_m is that radius at which the radial probability density [i.e. $P_{n\ell}(r) = rR_{n\ell}(r)$] is a maximum. The values for r_m can be obtained from modern numerical Hartree-Fock calculations of Mann[7]; we will use these exclusively. For the case of helium and neon atoms, Table 1 shows the states, orbital configurations and energetics involved in the processes of ionization as compiled from the tables of spectroscopic data of Moore[8]. These data (without any other parameters) have been used to calculate total ionization cross sections for helium and neon. Note that between the lowest rearrangement state ($^2P^o_{1/2}$ for helium, $^4P_{5/2}$ for neon) and the lowest

Table 1: States and Energies of Helium and Neon Ions

Process	State	Orbital Configuration	Threshold Energy (eV)
(a) Helium atom ($1s^2$), $A_t = 1.295\ \pi_o^2$			
First Ionization	$^2S_{1/2}$	$1s$	24.59
Rearrangement Ionization	$^2P^o_{1/2,3/2}$	$2p$	
	$^2S_{1/2}$	$2s$	65.40
	$\vdots$	$\vdots$	$\vdots$
Second Ionization	–	–	~79.0
(b) Neon atom ($1s^2\ 2s^2\ 2p^6$), $A_t = 1.61\ \pi a_o^2$			
First Ionization	$^2P^o_{3/2}$	$2s^2 2p^5$	21.56
	$^2P^o_{1/2}$	$2s^2 2p^5$	21.66
	$^2S_{1/2}$	$2s^1 2p^6$	48.76
Rearrangement Ionization	$^4P_{5/2..}$	$2s^2 2p^4 3s$	48.73
	$^4P^o$	$2s^2 2p^4 3p$	52.08
	$\vdots$	$\vdots$	$\vdots$
Second Ionization	$^3P_2$	$2s^2 2p^4$	62.63

4.7

state representing a second ionization of the atom, there are only
states that exclusively involve rearrangement ionization (Moore's
Tables[8]). These are not shown in Table 1; their presence is indi-
cated by dots. Thus the total cross section for rearrangement
ionization (i.e., one that is summed over all the rearrangement
states) has the upper limit in Eqn. (3-65) obtained from the second
ionization potential I^{+2} (i.e., $E_u = I^{+2} - I$).

Results of our calculations in the BE and the Born approxi-
mations are compared with the experimental data of the Lockheed
group for $T \leq 1000$ eV [in Fig. 2a] and of the Amsterdam group for
$1000 \leq T \leq 20,000$ eV [in Fig. 2b]. The latter group's data are
consistently smaller than the former's by about 20% for both helium
and neon in the small region where their measurements overlap (i.e.,
600 - 1000 eV); this discrepency is not shown in Figs. 2 but
ought to be borne in mind. In the case of ionization of a helium
atom, the behavior is much like in the case of a hydrogen atom
ionization. In Fig. 2a the BE theory provides a reasonable, but
not as accurate a description as the Born theory for $T > 200$ eV.
This is especially true at high energies (in Fig. 2b: Note Fano
plot) where the discrepancy between the BE theory cross section
and experimental data is more than a factor of two. The difference
between the slopes of the theoretical and experimental curves in
the Fano plot will be discussed below. Two points to be noted in
this comparison (and in all others in the chapter) are: (1) Calcu-
lations using the Born approximation are not performed for $T < 200$
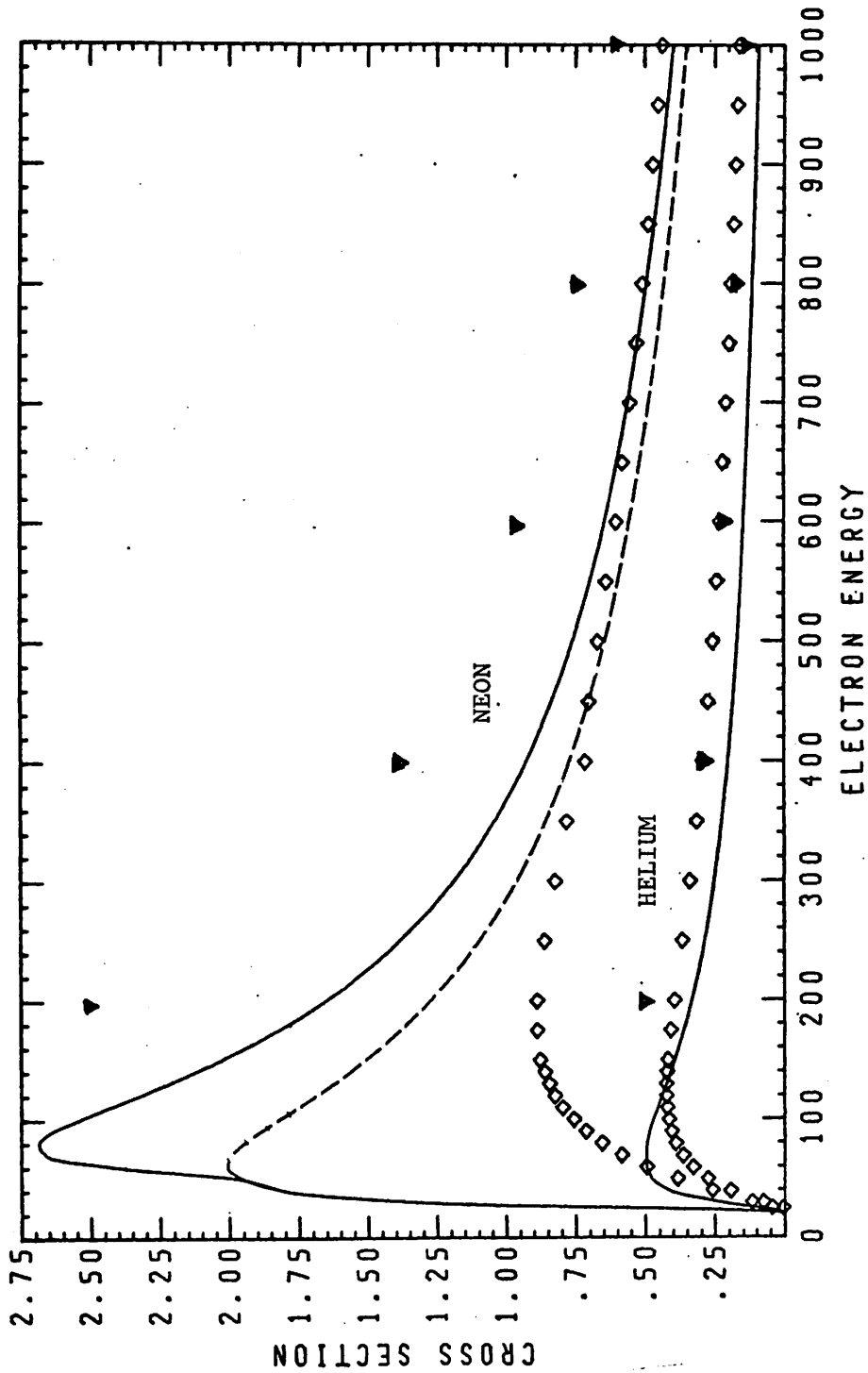eV, because of its conceptual inapplicability. They have essentially

Fig. 2a. Ionization cross sections (in πa_0^2) for helium and neon atoms versus incident electron energy (in eV). Calculated values in the Born approximation are denoted by a symbol (▼), while solid curve is obtained using the BE theory. Experimental data (◇) are from the Lockheed group[2].

the same form as the BE theory cross sections but are substantially larger. (2) Experimental data for total ionization includes contribution from the multiply ionized species (e.g., He^{++}, Ne^{+++} etc.). The contribution from the doubly ionized species is usually at least an order of magnitude smaller than the singly ionized species (Figs. 32-41 in ref. 1). Thus our calculations of singly ionized species should be compared with experimental data with this in mind.

Consider next the ionization of a neon atom; here our one-electron model does not approximate the experimentally observed cross sections as well as it did for helium. In Fig. 2a, the BE approximation provides a better estimate of the total ionization cross section than the Born approximation, which at T = 1000 eV over-estimates by 37 to 71% (depending on the source of the experimental data). The dashed curve in Fig. 2a shows the contribution to the total ionization from purely direct ionization processes; the contributions of rearrangement ionizations to the total ionization at T = 1000 eV, is 10% for neon and only 1% for helium (independent of the two approximations). The rather large discrepancy for T < 200 eV between the BE theory and the experimental cross sections (unlike in the case of H or He) might be due to the inapplicability of the one-electron concept to the strongly many-electron system like neon. Clearly this error is magnified in the calculation of rearrangement ionization which involves essentially a product of two cross sections as we have defined it in Sec. 3.2.b.

At high incident electron energies, the Born theory cross sections may be considered to be in better agreement with the
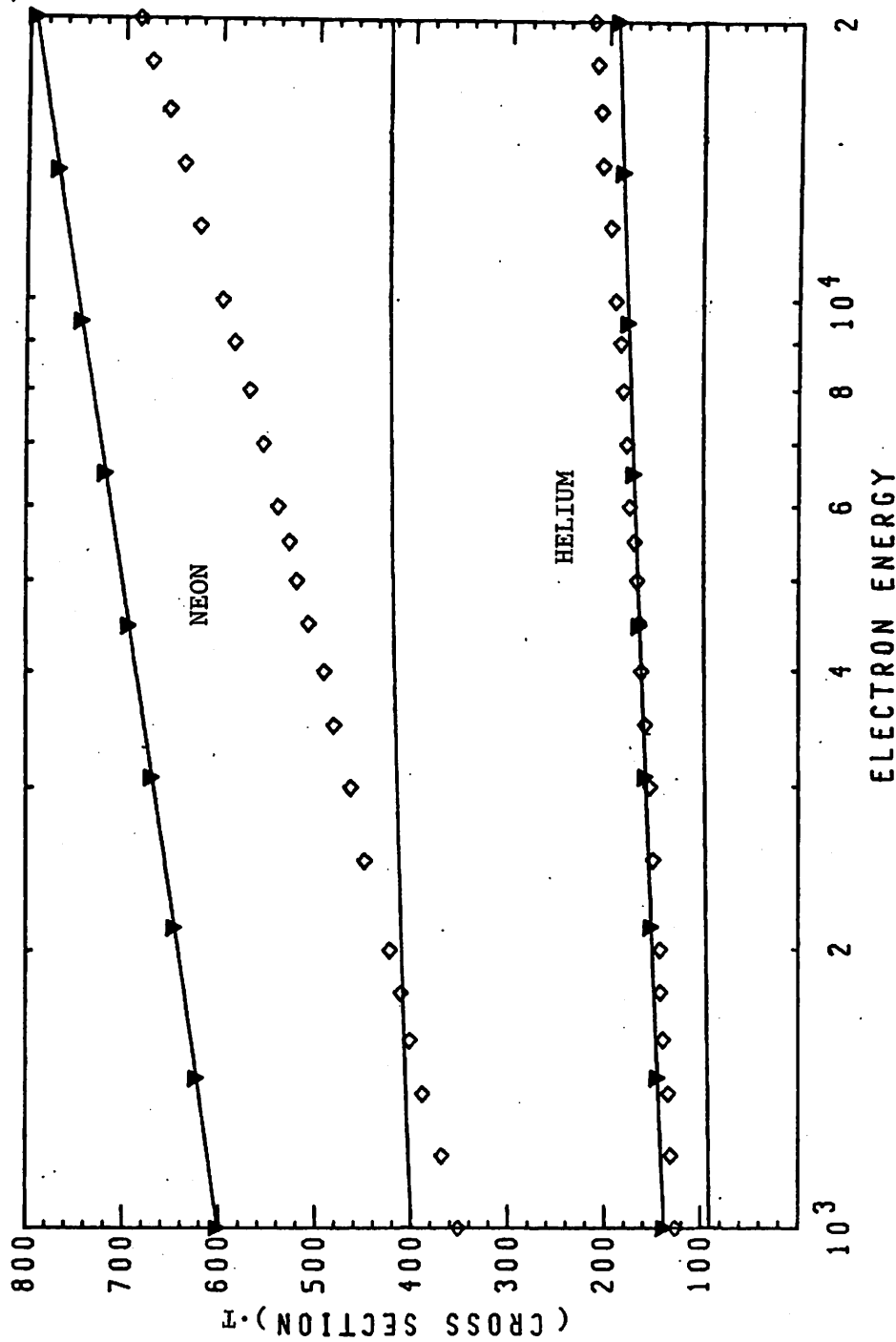
Fig. 2b. Fano plot for the ionization of helium and neon atoms i.e., Plot of (cross section)·T vs. log T. Calculated values (▼) in the Born approximation are joined by a solid line, while the lower curve is obtained using the BE approximation. Experimental data (◇) are from the Amsterdam group[4a].

4.11

Amsterdam group's data than the BE theory cross sections. Recall

that the straight line behavior of the cross section in the Fano

plot (Fig. 2b) provides one with the square of the dipole moment

matrix element M_I^2 and a quantity c_i of no known physical significance.

For helium and neon the calculated M_I^2 are about 35% and 33% smaller

than the experimentally measured value of 0.489 and 1.87 respec-

tively. However the calculated c_i are considerably greater than

those deduced from experiment so that our calculated cross sections

agree reasonably well with experiment.

Rough estimates of ionization cross sections for other rare

gas atoms (Ar, Kr and Xe) reveal that our simple model would under-

estimate cross sections with increasing Z. This could be due both

to the one-electron nature of our approximation as well as to our

use of hydrogenic 1s wave functions. For xenon, the spin-orbit

coupling is strong enough to split the lowest term (^2P) by 1.3 eV.

Clearly the one-electron model is inapplicable here. Thus for

atoms (or molecules) that have electrons occupying (or originating

from) only the K and L atomic shells our one-electron hydrogenic

1s approximation should be quite adequate.

b. Ionization of diatomic molecules.

Consider first ionization and DI of the five diatomic molecules,

H_2, CO, N_2, NO and O_2, for which experimental data are available

The ionization cross sections of these molecules may seem to be of

little interest to the electron microscopist; it is hoped however

that, since C, N and O are the building block atoms for large

molecules, the trends and dependences shown here will prove to be

useful for the study of polyatomic molecules.

(i) Molecular Hydrogen: This simple system should serve as definitive test for our model of rearrangement ionizations. Ionization involves removal of one of the two electrons from the $(1\sigma_g)$ orbital. If the ion is formed in a sufficiently high vibrational state then dissociation of the ion can occur. However the fragments are formed[9] with very little kinetic energy. Formation of H_2^+ in the $^2\Sigma_u^+$ state entails the excitation of a bound electron from the $(1\sigma_g)$ orbital to an antibonding $(1\sigma_u)$ orbital — a clear case of rearrangement ionization. Here the fragments are formed with kinetic energy of at least 5 eV, so that the experimental data of the Lockheed group[2] (cross sections for the production of ions from H_2, with kinetic energy greater than 2.5 eV) can be directly related to our calculated rearrangement ionization cross section. The threshold energies for rearrangement and second ionization (Table 2) are taken from experimental data; they give E_r = 12.4 eV and E_u = 30.4 eV. The effective area of the electron cloud in molecular hydrogen is estimated as follows. The 'radius' [or the maximum of $P_{10}(r)$] of atomic hydrogen is 1 bohr [i.e., a_0] so that the A_t for an H_2 molecule can be considered to be the surface area of two spheres of radius a_0, i.e., $8\pi a_0^2$. However the observed inter-nuclear distance (1.436 a_0) is smaller than the sum of two atomic H radii, so that the electron cloud of H_2 can be pictured like two soap bubbles in contact. Then A_t is given by

$$A_t = 4\pi a_0^2 + 4\pi a_0^2 - 2A_c + 2A_d \qquad (1)$$

# Table 2: States and Energies of Diatomic Molecular Ions

Process[1]	State(s)[2]	Orbital Configuration[3]	Threshold[4] Energy (eV)	N_B[5]	Source[6]
(a) Molecular Hydrogen — $(1\sigma_g)^2$; $A_t = 7.84\,\pi a_o^2$					
1-I	$^2\Sigma_g^+$	$(1\sigma_g)^1$	15.6	1	10
R-I	$^2\Sigma_u^+$	$(1\sigma_u)^1$	[28.0]	-1	2,10
2-I	-	-	46.0	-	10
(b) Carbon Monoxide — $K^2K^2(2\sigma)^2(2\sigma*)^2(1\sigma)^4(3\sigma)^2$; $A_t = 9.12\,\pi a_o^2$					
1-I	$^2\Sigma^+$	$\cdots(2\sigma*)^2(1\pi)^4(3\sigma)^1$	14.1	5	
	$^2\Pi$	$\cdots(2\sigma*)^2(1\pi)^3(3\sigma)^2$	16.5	5	10
	$^2\Sigma^+$	$\cdots(2\sigma*)^1(1\pi)^4(3\sigma)^2$	19.6	7	
R-I	a	$\cdots(2\sigma*)^2(1\pi)^4(3\sigma)^0(A)^1$	[24.5]	3	2
	b	$\cdots(2\sigma*)^2(1\pi)^2(3\sigma)^2(A)^1$		3	
	c	$\cdots(2\sigma*)^2(1\pi)^3(3\sigma)^1(A)^1$		3	
2-I	$^1\Sigma^+$	$\cdots(2\sigma*)^2(1\pi)^4(3\sigma)^0$	36.0	4	10
(c) Molecular Nitrogen — $K^2K^2(2\sigma_g)^2(2\sigma_u)^2(1\pi_u)^4(3\sigma_g)^2$; $A_t = 8.64\,\pi a_o^2$					
1-I	$^2\Sigma_g^+$	$\cdots(2\sigma_u)^2(1\pi_u)^4(3\sigma_g)^1$	15.6	5	
	$^2\Pi_u$	$\cdots(2\sigma_u)^2(1\pi_u)^3(3\sigma_g)^2$	16.7	5	12
	$^2\Sigma_u^+$	$\cdots(2\sigma_u)^1(1\pi_u)^4(3\sigma_g)^2$	18.8	7	
R-I	a	$\cdots(2\sigma_u)^2(1\pi_u)^4(3\sigma_g)^0(A)^1$	[26.0]	3	2
	b	$\cdots(2\sigma_u)^2(1\pi_u)^2(3\sigma_g)^2(A)^1$		3	
	c	$\cdots(2\sigma_u)^2(1\pi_u)^3(3\sigma_g)^1(A)^1$		3	
2-I	$^1\Sigma_g^+$	$\cdots(2\sigma_u)^2(1\pi_u)^4(3\sigma_g)^0$	42.0	4	12

where A_c is the surface area of the cap 'lost' by each H atom on the formation of H_2 and A_d is the area of the disc that exists between the two protons in our soap bubble-like model. Simple arithmetic gives $A_t = 7.841 \, \pi a_0^2$ for H_2 - an almost insignificant difference (2%) from our first estimate.

Calculated and observed ionization cross sections are compared in Figs. 3. As in the case of H and He atoms, the total ionization cross sections in the Born theory are in quite good agreement with experiment; the BE cross sections are considerably smaller. At high incident electron energies, the situation is even more pronounced [Fig. 3d]. The rearrangement ionization cross sections are compared with the corresponding experimental cross sections in Fig. 3b. The rather large over-estimate (even in the case of the BE approximation) for T < 200 eV may be due to incorrectness in the formulation of rearrangement ionization for small T, which essentially magnifies any error in the one-electron scattering approximation. For T > 200 eV, the agreement with experimental data is uncannily good. The ratio of the DI cross section to total cross section is shown in Fig. 3c; the gradual decrease with T in the ratios of experimental cross sections (which are reported to be accurate to only 30%) is duplicated quite well by both the scattering approximations. The low T 'hump' is over-estimated in our theoretical calculations, as expected. The very good overall agreement of our simple model with experiment (except for T < 200 eV) is quite heartening.

(ii) Carbon Monoxide: The molecular-orbital electronic configurations of this 14 electron molecule and some of its ions are
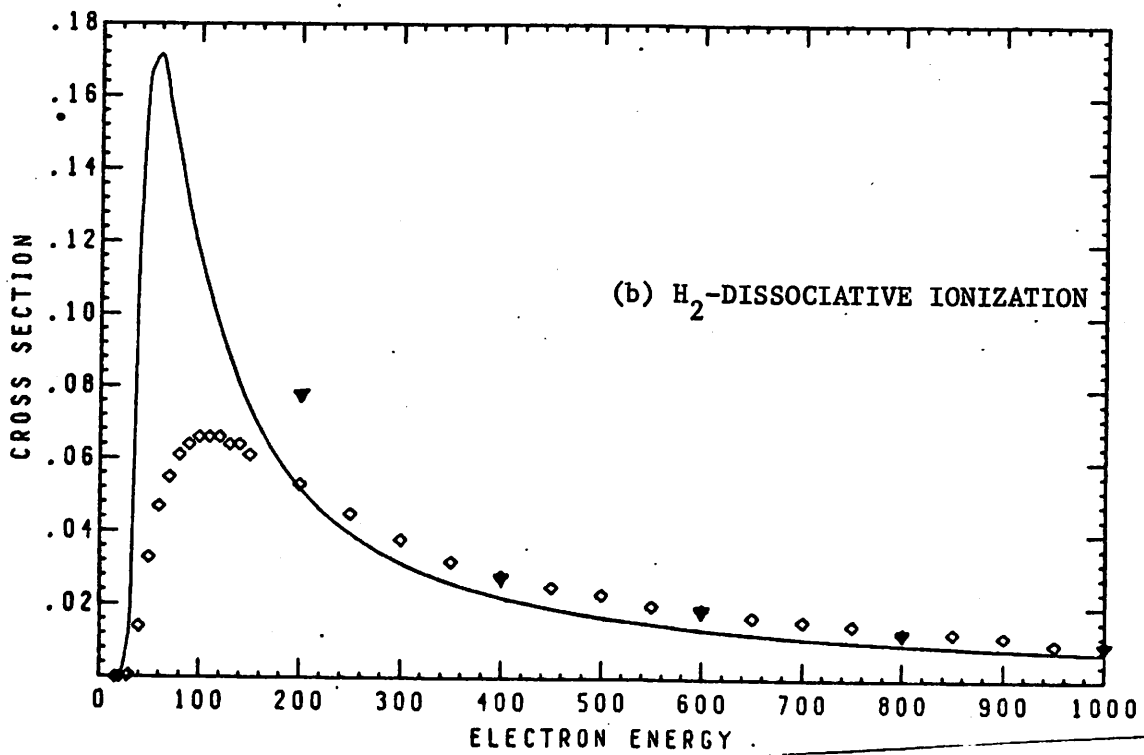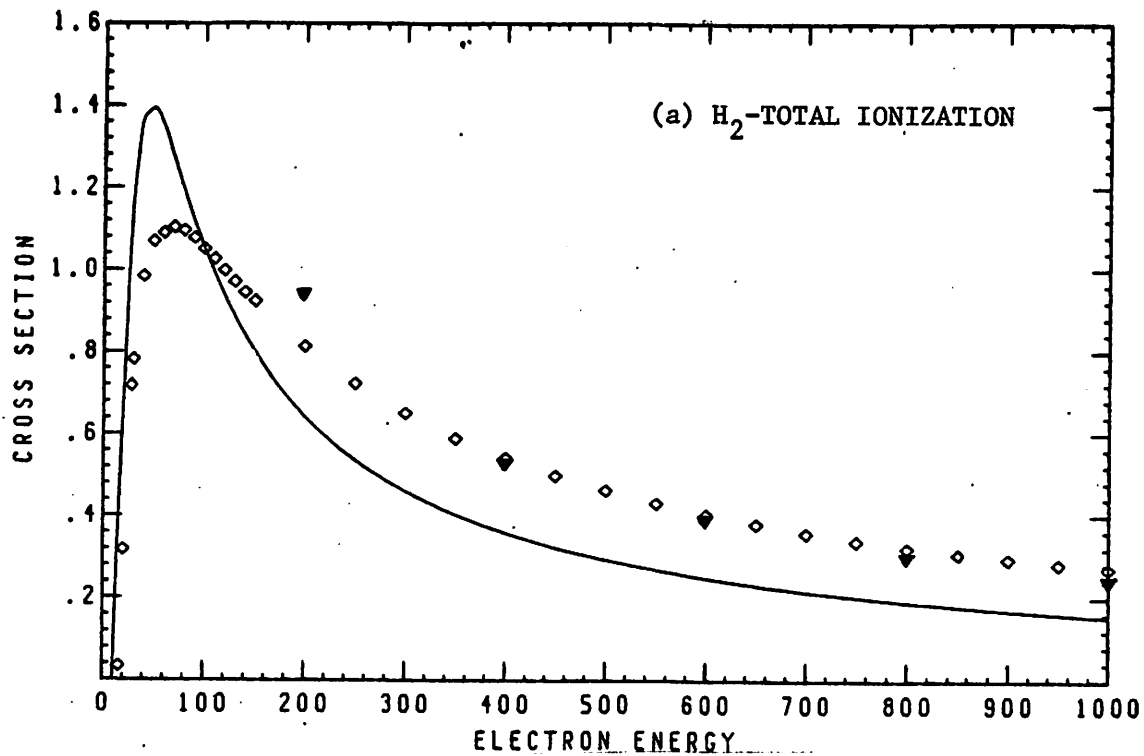
Figs. 3a and 3b. Ionization cross sections (in πa_o^2) for molecular hydrogen for incident electron energies $\leq$ 1000 eV, in the case of (a) total ionization and (b) H^+ production from H_2. Calculated values in the Born approximation are denoted by ($\blacktriangledown$), while solid curve is obtained using the BE theory. Experimental data ($\Diamond$) are from the Lockheed group[2].
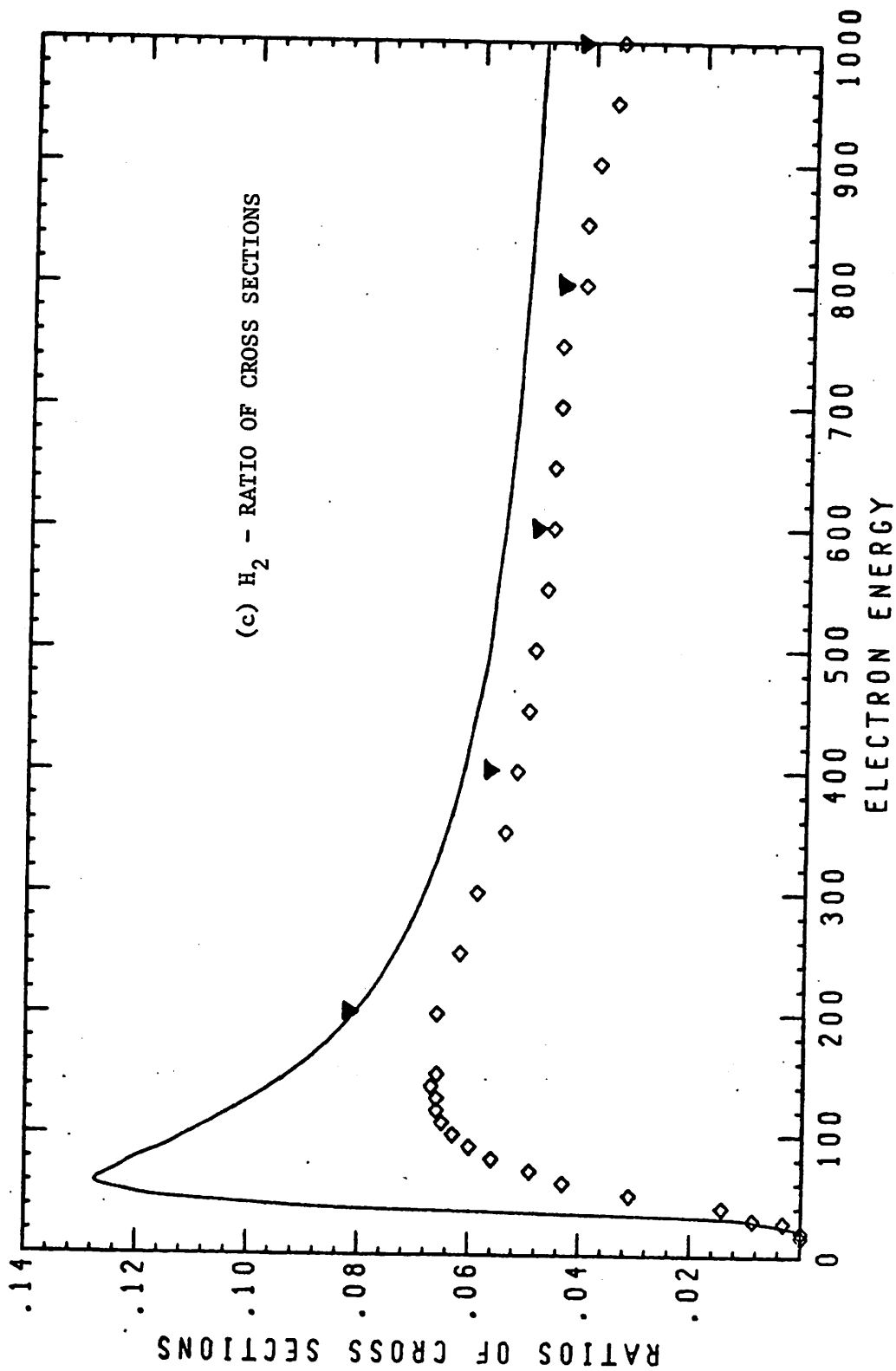
(c) H_2 - RATIO OF CROSS SECTIONS

ELECTRON ENERGY

RATIOS OF CROSS SECTIONS

Fig. 3c. Ratio of DI to total ionization cross sections for H_2 versus incident electron energy (in eV). Calculated values in the Born approximation are denoted by a symbol (▼), while solid curve is obtained using the BE approximation. Experimental data (◇) are from the Lockheed group[2].
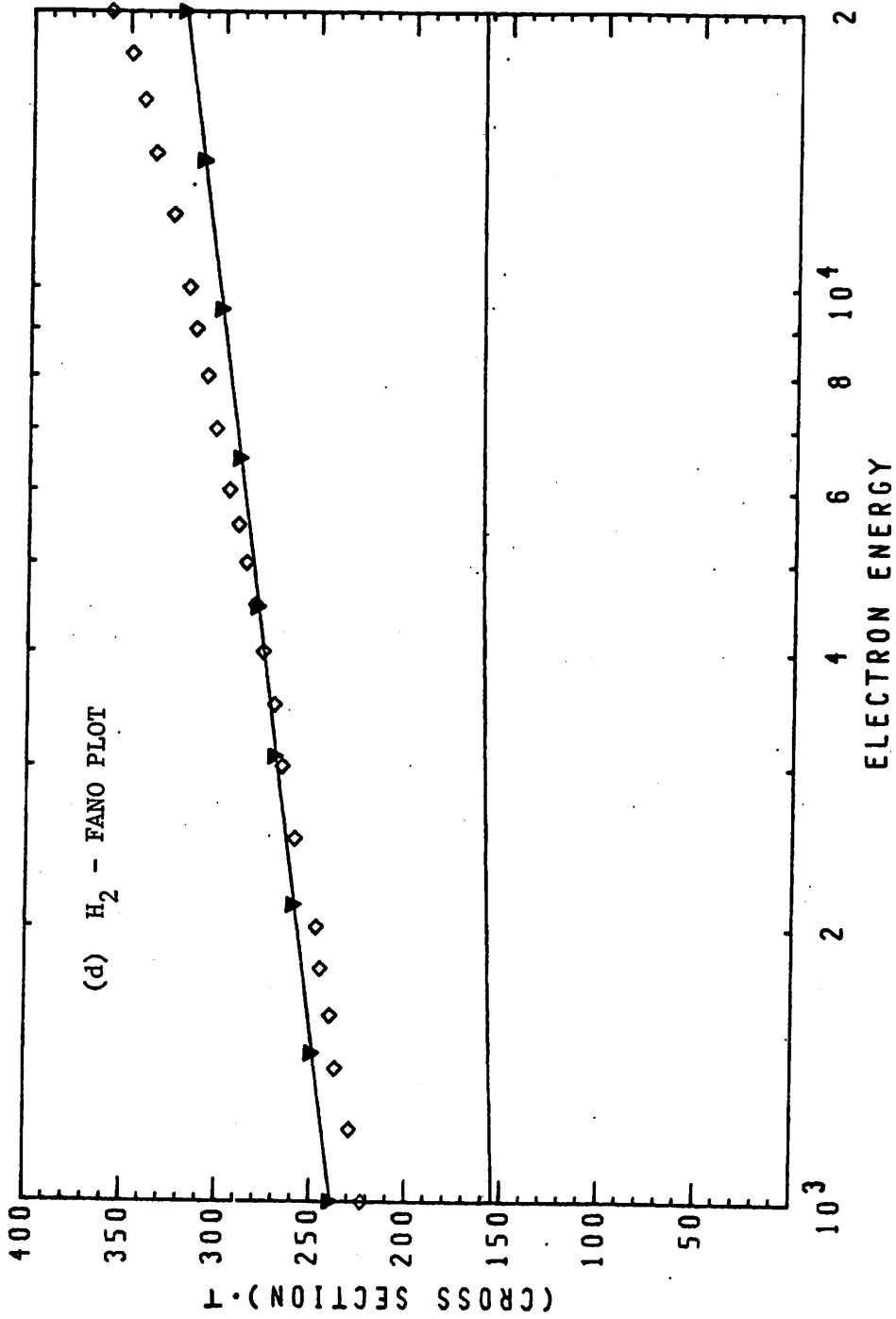
Fig. 3d. Fano plot of the total ionization for H_2 i.e., Plot of (cross section)·T vs. log T. Calculated values (▼) in the Born approximation are joined by a curve, while the lower curve is obtained using the BE approximation. Experimental data (◇) are from the Amsterdam group[4a].

shown in Table 2. Since (1π) and (3σ) are bonding orbitals, removal of an electron from these orbitals reduces the number of bonding electrons to 5, while removal of an electron from the anti-bonding orbital increases the binding of the ion. Thus we hypothesize that a process of rearrangement ionization that excites an electron from the (1π) or the (3σ) orbitals into an anti-bonding orbital leads to the dissociation of the molecular ion. The anti-bonding orbital could be the (1π*) orbital; for generality, it is denoted by (A) in Table 2. As shown in Table 2, the three possible final configurations can arise from an ionization and an excitation of two bound electrons from (1) the same orbital (states a and b in Table 2) or (2) different orbitals (states c in Table 2). Thus the experimentally observed threshold energy (34.5 eV) for the production of fragments from CO is related to the threshold energy for state a. Using (3-63), we have the excitation energy E_r to cause a rearrangement of an electron from the orbital (3σ) equal to (24.5-14.1) = 10.4 eV. Similarly the energy E_r for the excitation of a (1π) electron into an anti-bonding (A) orbital can be obtained if the experimental threshold energies were available. Lacking this we approximate E_r for the (1π) orbital to be the same as that for the (3σ) orbital. Intuitively, one expects this number to be a lower bound, since an electron in the (1π) orbital, being more tightly bound than one in the (3σ) orbital, will have a larger E_r than that for the (3σ) orbital. Also note that since, state c is obtained by an excitation of an electron from an orbital adjacent to the one from which an electron was ionized, it gives the $t \neq q$ contribution to $Q_{s,q}^R$ in Eqn. (3-64).

4.21

Table 3: Effective area of diatomic molecules

Molecule (a-b)	$r_a^{(1)}$, $r_b^{(1)}$	$\ell_b^{(2)}$	$A_t^{(3)}$
CO	1.216, 0.833	2.1354	9.120
N_2	0.988, 0.988	2.0787	8.642
NO	0.988, 0.833	2.1732	9.446
O_2	0.833, 0.833	2.2866	10.457

Notes:

(1) Theoretical atomic radius (in a_o) at maximum radial probability density for the outer-most electrons in the atoms a and b that form molecule a-b. Data is from Ref. 7.

(2) Experimentally measured bond lengths (in a_o) from Ref. 11.

(3) Effective area of the electron orbital (in πa_o^2).
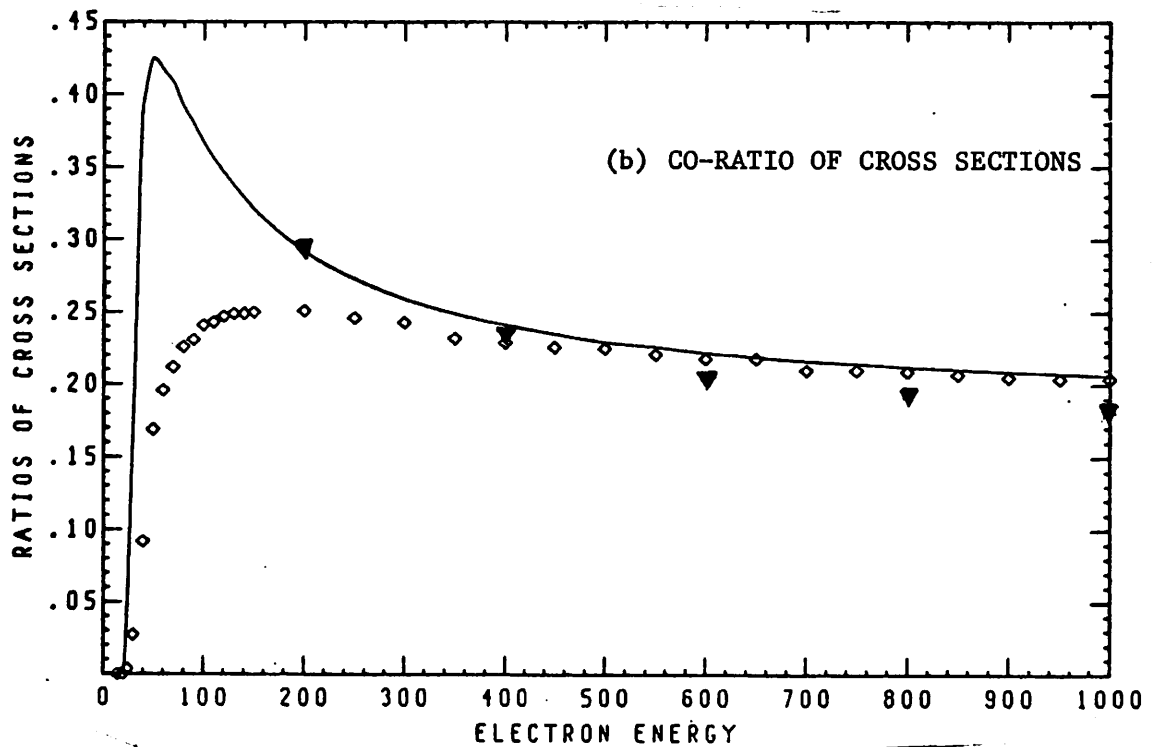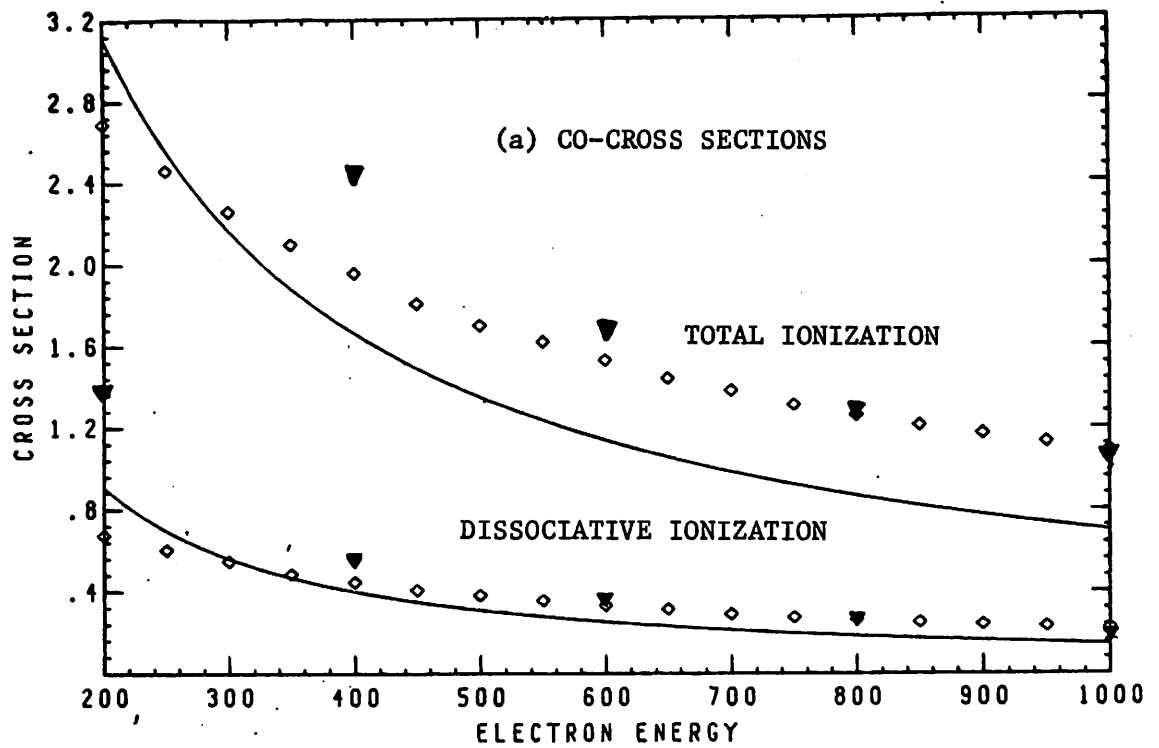
Figs. 4. Ionization cross sections (in πa_0^2) for CO versus incident electron energy (in eV), plotted in (a) for the cases of total and DI cross sections and in (b) for the ratios of the two cross sections. Calculated values in the Born approximation are denoted by a symbol (▼), while solid curve is obtained using the BE approximation. Experimental data (◊) are from the Lockheed group[2].

The effective surface area of the orbitals A_t is estimated from the experimentally measured bond lengths ℓ_b. When the sum of the theoretical atomic radii $r_a + r_b$ (see Table 3) for the constituent atoms is smaller than ℓ_b, we assume that A_t is the surface area of two spheres of radius $\ell_b/2$ i.e.,

$$A_t \sim 4\pi \, [(\frac{\ell_b}{2})^2 + (\frac{\ell_b}{2})^2] = 2\pi\ell_b^2 . \tag{2}$$

If the unequal radii of constituent atoms is considered in the model, than A_t increases slightly [for CO, 3.4% from that given by (2)]. Thus for the four molecules (CO, N_2, NO and O_2) we obtain A_t exclusively from (2) using experimental values for ℓ_b as given in Table 3.

Figures 4 show the calculated cross sections for CO which were obtained using the data presented in Table 2. In Fig. 4a (as well as in Figs. 5a, 6a, 7a, 9a and 10a), the cross sections are not plotted for T < 200 eV, where as one expects, both the approximations are 2-4 times larger than experiment. With in-creasing T, the Born theory total ionization and DI cross sections are in better agreement with experimental data than the corres-ponding BE theory cross sections. The ratios of the two cross sections are reproduced for T > 300 eV quite well in magnitude and behavior by both the approximations.

(iii) Molecular Nitrogen: Since CO and N_2 are isoelectronic, they have many similar properties. Table 2 shows identical molecular-orbital electron configurations for the two molecules (except that in the case of N_2 an additional symmetry is displayed). The
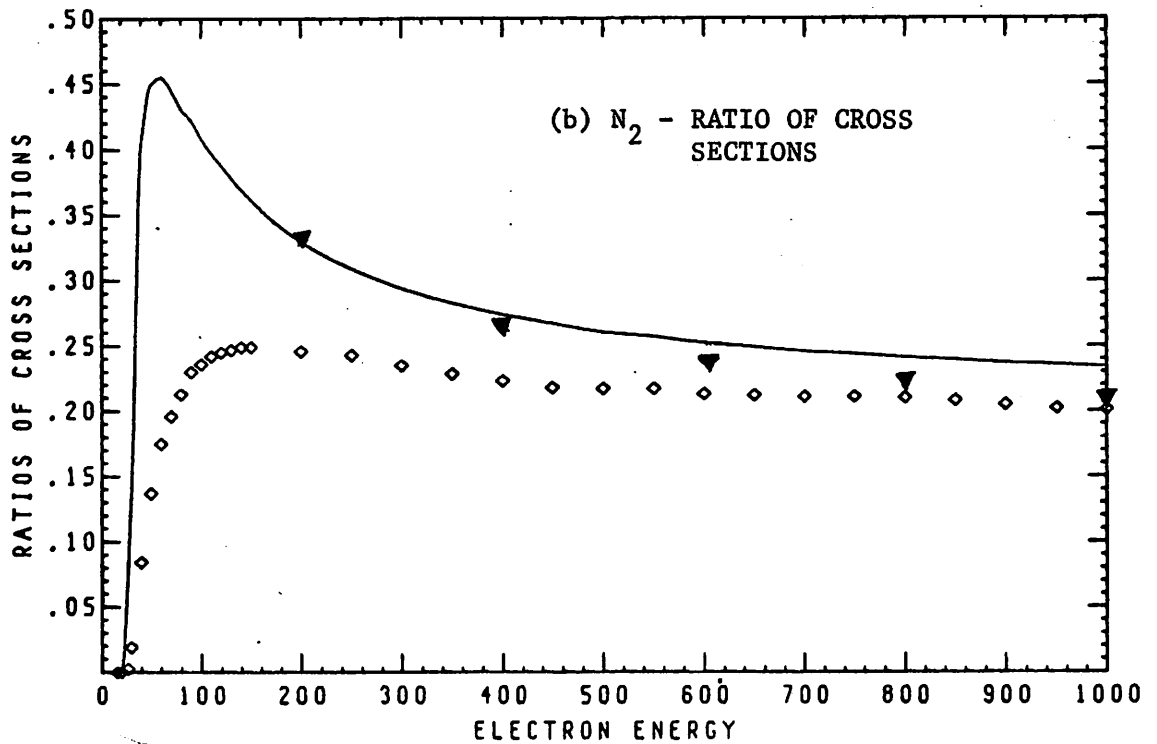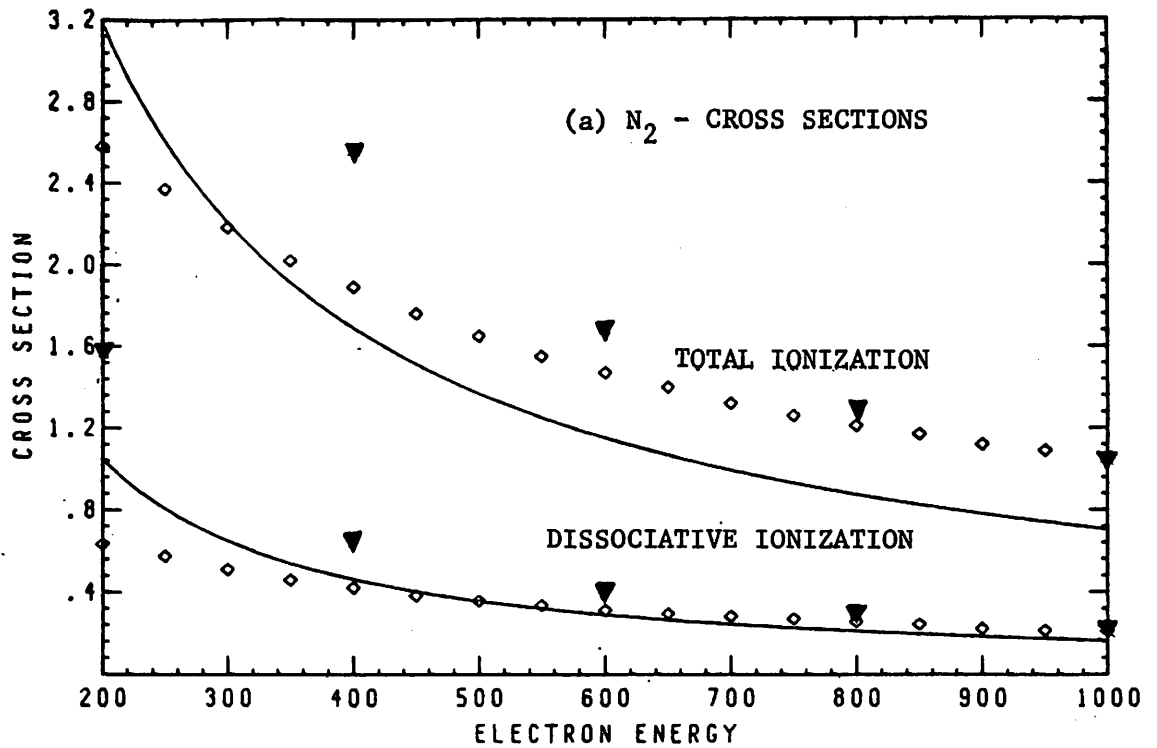
Figs. 5a and 5b. Ionization cross sections (in πa_o^2) for N_2 versus incident electron energy (in eV), plotted in (a) for the cases of total and DI cross sections and in (b) for the ratios of the two cross sections. Calculated values in the Born approximation are denoted by a symbol (▼), while solid curve is obtained using the BE approximation. Experimental data (◊) are from the Lockheed group[2].
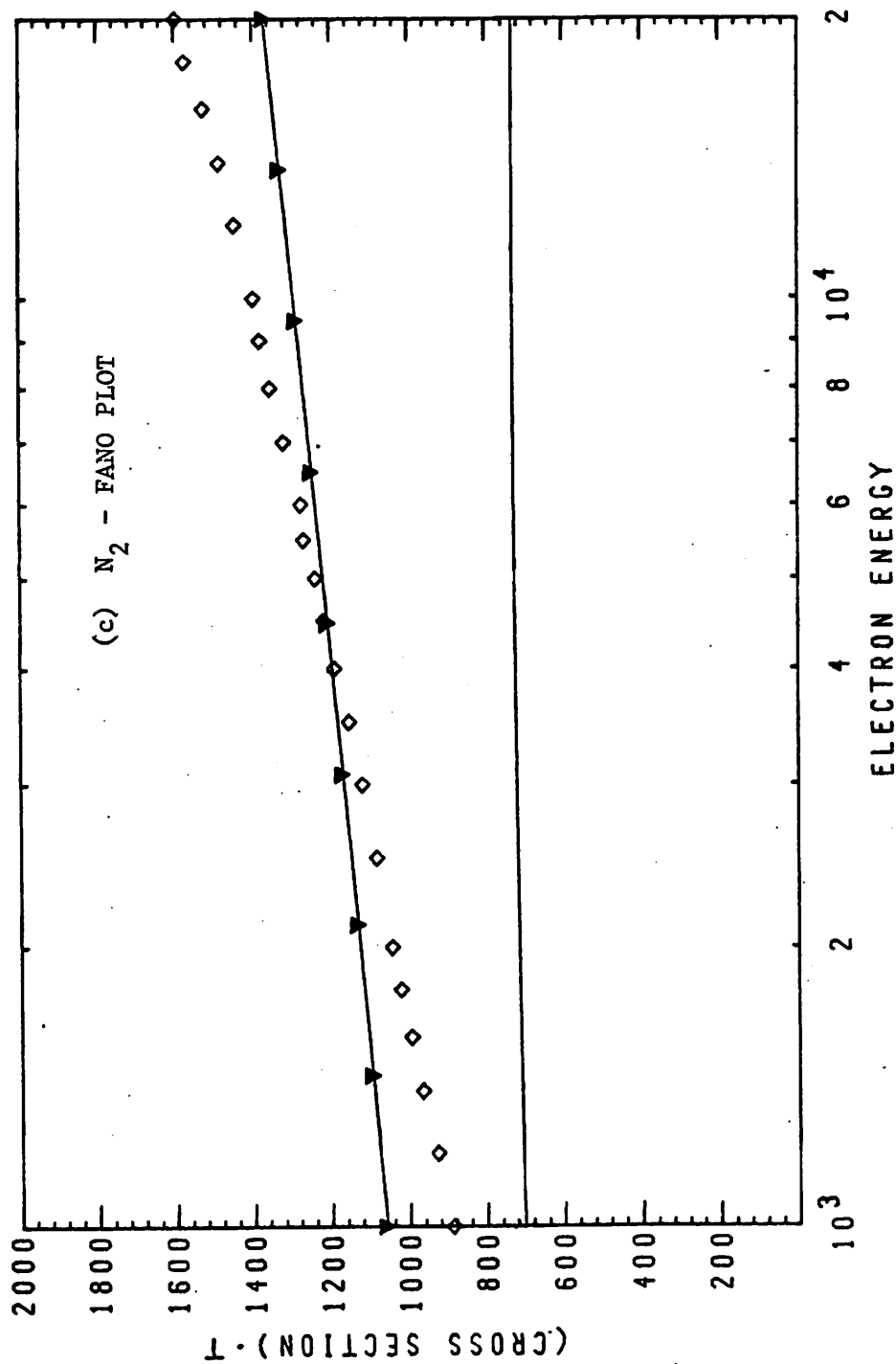
Fig. 5c. Fano plot of the total ionization for N_2 i.e., Plot of (cross section)·T vs. log T. Calculated values (▼) in the Born approximation are joined by a curve, while the lower curve is obtained using the BE approximation. Experimental data (◇) are from the Amsterdam group[4a].

threshold energies for ionization are obtained from the compilation of Gilmore[12]. Using exactly the same algorithm as for CO, we obtain results shown in Figs. 5. The calculated total ionization and DI cross sections have approximately the same trends and magnitudes as the experimental cross sections, in much the same manner as they did for CO. For N_2, the Amsterdam group's experimental data[4] for large T are compared with our calculated cross sections. The superiority of the Born theory over the BE theory is clearly evident.

(iv) Nitric Oxide: Here the outermost electron occupies an anti-bonding orbital - $(1\pi^*)$; its removal increases the binding between N and O. Thus a naive conclusion might be that the relative DI cross section of NO might be smaller than for, say CO or N_2. However experimental data show just the opposite behavior; our calculations reproduce this trend.

Ionization from the bonding (1π) or (3σ) orbitals can leave the ion in one of several possible states [i.e., $^3\Sigma^+$, $^3\Delta$, $^3\Sigma^-$ etc., for the $\cdots\cdots$ $(3\sigma)^2$ $(1\pi)^3$ $(1\pi^*)^1$ electronic configuration]. Cross sections to each of these states are obtained from $Q_{s,q}$ [Eqn. (3-60)]. As can be seen from the compilation of spectroscopic data by Gilmore[12], the threshold energies of some of the higher lying states have not yet been reliably identified. Fortunately our formulation of $\gamma_{s,q}$ makes $Q_{s,q}$ quite insensitive to this error, especially if only the sum over the direct ionization cross sections ($\sum\limits_{s} Q_{s,q}$) is of interest. Thus Table 2, shows the data (states, configurations and energies) used in our direct ionization calculations. As for CO and N_2, it is assumed here
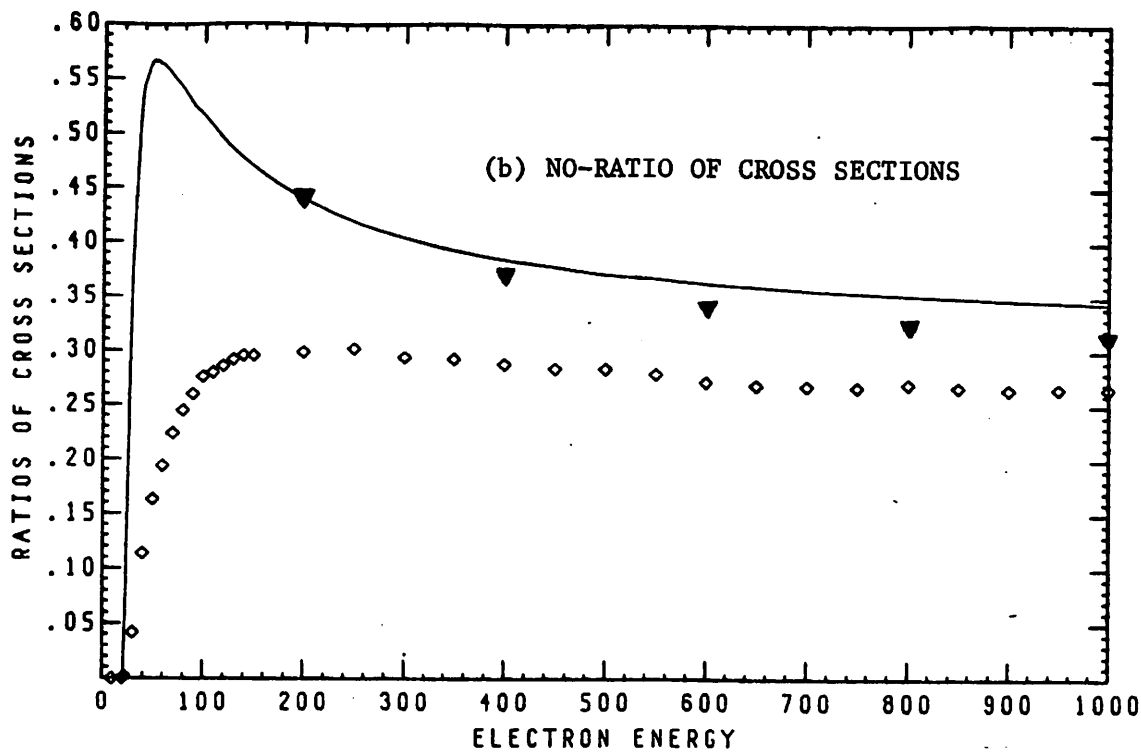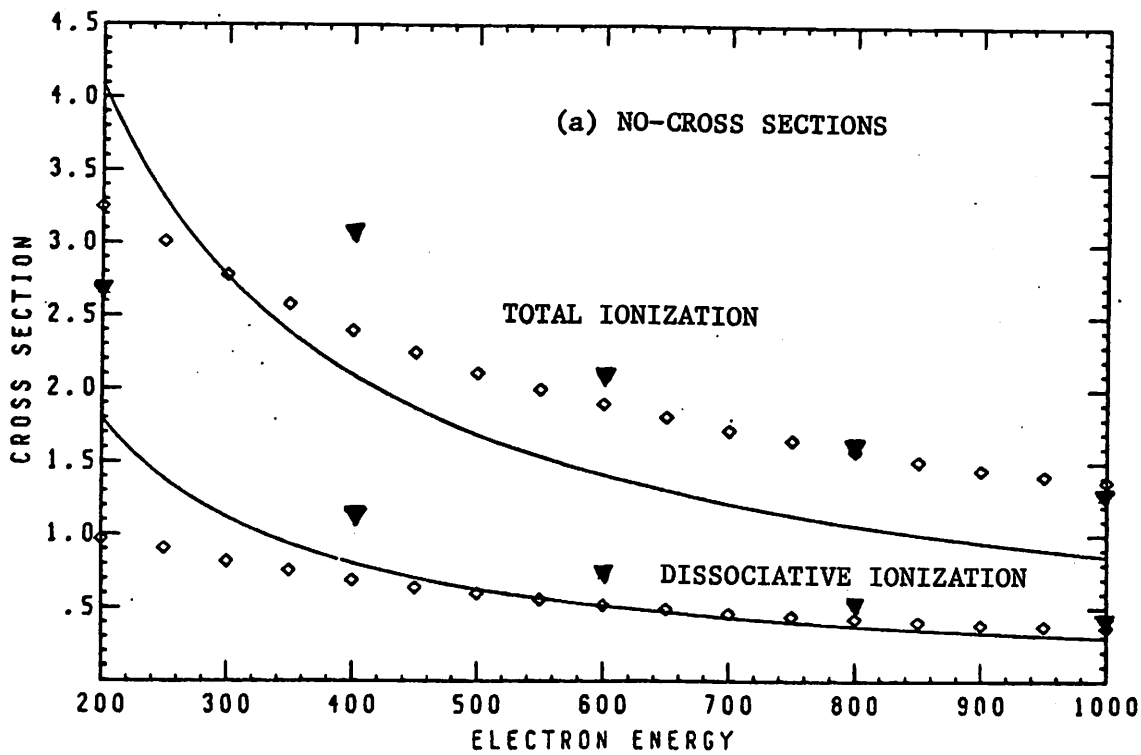
Figs. 6. Ionization cross sections (in πa_o^2) for NO versus incident electron energy (in eV), plotted in (a) for the cases of total and DI cross sections and in (b) for the ratios of the two cross sections. Calculated values in the Born approximation are denoted by a symbol (▼), while solid curve is obtained using the BE approximation. Experimental data (◇) are from the Lockheed group[2].

Process [1]	State(s) [2]	Orbital Configuration [3]	Threshold Energy (eV) [4]	N_B [5]	Source [6]
(d) Nitric Oxide — K K$(2\sigma)^2(2\sigma*)^2(3\sigma)^2(1\pi)^4(1\pi*)^1$; $A_t = 9.45\ \pi a_o^2$					
1-I	$^1\Sigma^+$	$\cdots(3\sigma)^2(1\pi)^4(1\pi*)^0$	9.25	6	
	$^3\Sigma^+$		14.2	4	
	$^3\Delta$	-	16.6	4	
	$^3\Sigma^-$	$\cdots(3\sigma)^2(1\pi)^3(1\pi*)^1$	18.3	4	
	$^1\Sigma^-$		18.8 + 1.	4	12
	$^1\Delta$		19.5 $\pm$ 1.	4	
	$^1\Sigma^+$		?	4	
	$^3\Pi$	$\cdots(3\sigma)^1(1\pi)^4(1\pi*)^1$	17.0	4	
	$^1\Pi$		18.3	4	
R-I	a	$\cdots(3\sigma)^2(1\pi)^2(1\pi*)^1(A)^1$	[22.5]	2	2
	b	$\cdots(3\sigma)^0(1\pi)^4(1\pi*)^1(A)^1$		2	
	c	$\cdots(3\sigma)^1(1\pi)^3(1\pi*)^1(A)^1$		2	
2-I		$\cdots(3\sigma)^2(1\pi)^3(1\pi*)^0$	40.0	5	12
(e) Molecular Oxygen — K^{2}K$^2(2\sigma_g)^2(2\sigma_u)^2(3\sigma_g)^2(1\pi_u)^4(1\pi_g)^2$; $A_t = 10.46\ \pi a_o^2$					
1-I	$^2\Pi_g$	$\cdots(3\sigma_g)^2(1\pi_u)^4(1\pi_g)^1$	12.05	5	
	$^4\Pi_u$		16.1	3	
	$^2\Pi_u$	$\cdots(3\sigma_g)^2(1\pi_u)^3(1\pi_g)^2$	16.8	3	
	$^2\Phi_u$		?	3	
	?		?	3	12
	$^4\Sigma_g^-$		18.2	3	
	$^2\Sigma_g^+$	$\cdots(3\sigma_g)^1(1\pi_u)^4(1\pi_g)^2$	?	3	
	$^2\Delta_g$		20.0 $\pm$ 1.	3	
	$^2\Sigma_g^-$		20.3	3	

Table 2: (contd.)

Process[1]	State(s)[2]	Orbital Configurations[3]	Threshold[4] Energy (eV)	N_B[5]	Source[6]
		(e) Molecular Oxygen (contd.)			
R-I	a	$\cdots(3\sigma_g)^2(1\pi_u)^2(1\pi_g)^2(A)^1$	[20.5]	1	2
	b	$\cdots(3\sigma_g)^0(1\pi_u)^4(1\pi_g)^2(A)^1$		1	
	c	$\cdots(3\sigma_g)^1(1\pi_u)^3(1\pi_g)^2(A)^1$		1	
2-I		$\cdots(3\sigma_g)^2(1\pi_u)^4(1\pi_g)^0$	36.0	6	12

Notes:

(1) "1-I" denotes first ionization: "R-I" denotes rearrangement ionization: "2-I" denotes second ionization.
(2) Symmetry of unknown states denoted by "?". The "a", "b" and "c" denote symmetry of all possible rearrangement ionization states with electron configurations as shown.
(3) An unspecified anti-bonding orbital is denoted by "(A)", in the case of rearrangement ionization events.
(4) Threshold energies in square brackets are for production of positive ions with kinetic energies 0.25 eV (2.5 eV, in the case of H_2).
(5) N_B is the net number of bonding electrons in the ion.
(6) Sources of data are given in terms of reference numbers.

that rearrangement ionization involves the excitation of electrons

from the (1π) or (3σ) bonding orbitals to an anti-bonding orbital

(A), with an excitation energy of $(22.5-14.2) = 8.3$ eV. Note

that here the net number of bonding electrons is reduced from 5

in NO to only 2, so that dissociation is highly probable. As in

the case of CO and N_2, three possible arrangements (a, b, and c)

are possible. Results of our calculations are presented in

Figs. 6. The trends are essentially similar to those for CO and

N_2; however the calculated ratio of the DI to the total ionization

cross sections are somewhat larger than the corresponding experi-

mental values.

(v) Molecular Oxygen: This 16 electron molecule has two

electrons in its outermost $(1\pi_g)$ anti-bonding orbital (Table 2).

Removal of one of these increases the bond strength of the system.

However removal of an electron from either the $(1\pi_u)$ or the $(3\sigma_g)$

anti-bonding orbitals reduces the number of bonding electrons to

three. An ion with the configuration $\{ \cdots (3\sigma_g)^2 (1\pi_u)^3 (1\pi_g)^2 \}$

is known to have two stable states $^4\Pi_u$ and $^2\Pi_u$; other states,

with total multiplicity of 12 have not been identified and could

be unstable states of the ion. Ions with the configuration

$\{ \cdots (3\sigma_g)^2 (1\pi_u)^4 (1\pi_g)^2 \}$ are known to have four possible states.

While $^2\Sigma_g^+$ may be repulsive, $^2\Delta_g$ and $^2\Sigma_g^-$ are known to give stable

ions, with threshold energies above the lowest dissociation limit

of O_2 (~ 18.5 eV). Hence these states can, at least energetically,

lead to dissociation. The rearrangement ionization states of O_2^+

(a, b, and c in Table 2) have N_B, the net number of binding electrons,

equal to one, so that it seems they will lead to dissociation with
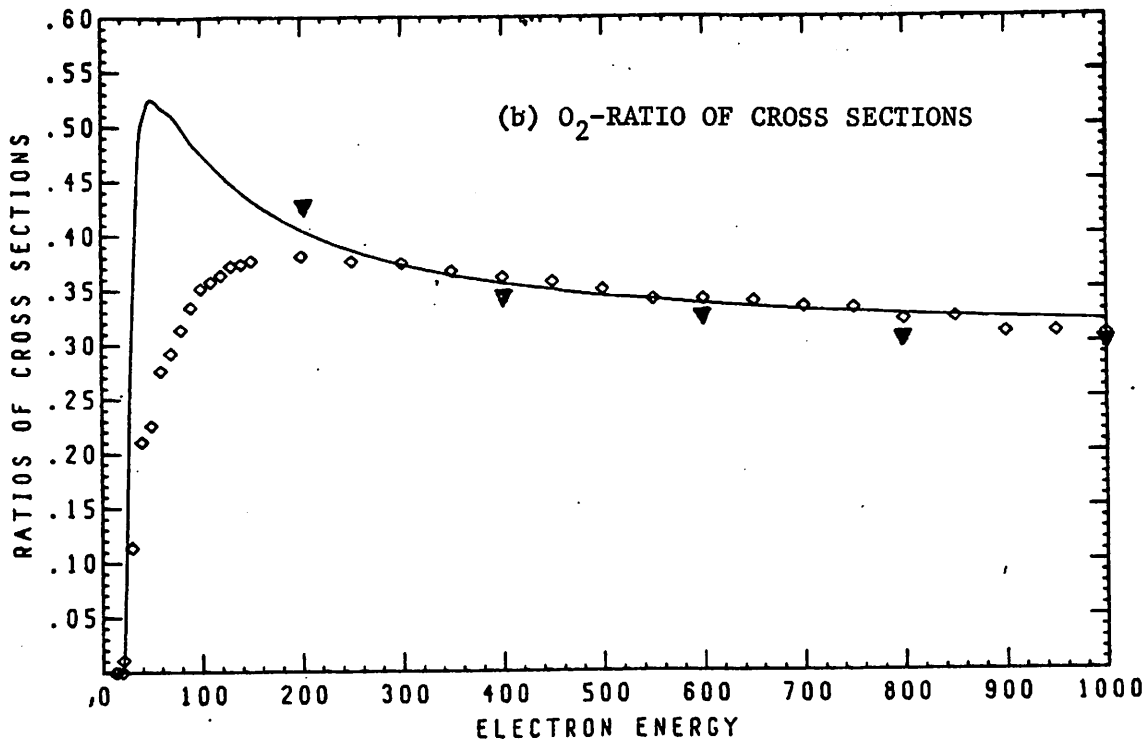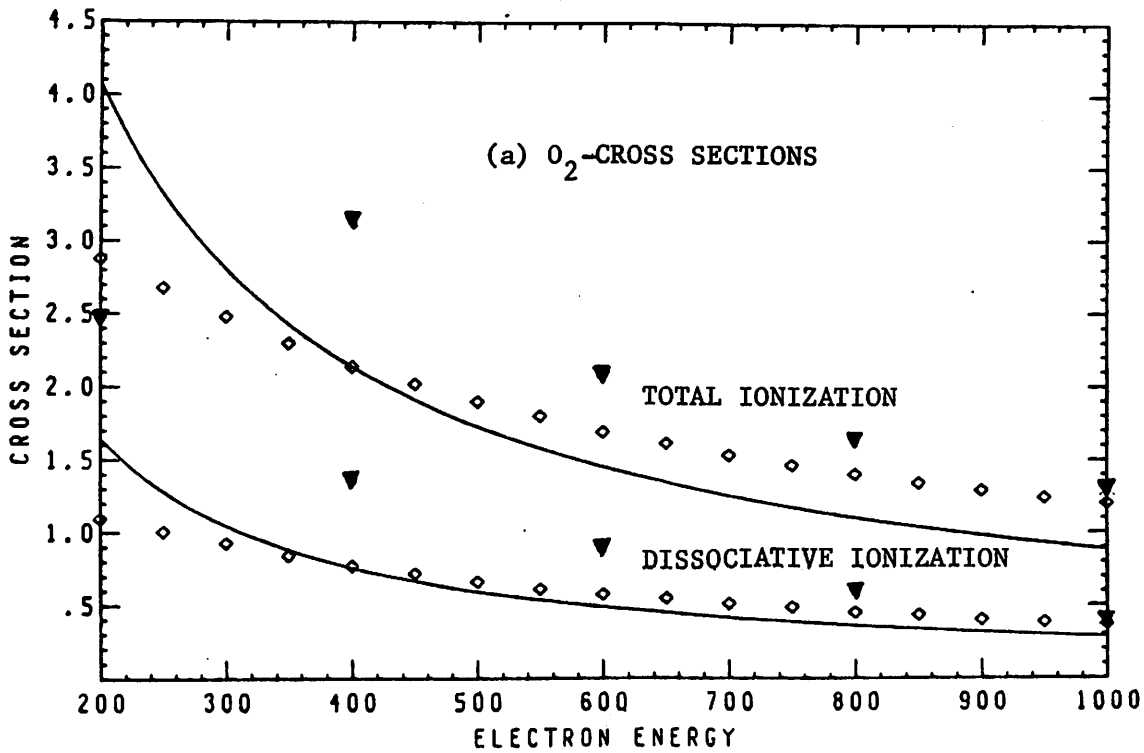
Figs. 7a and 7b. Ionization cross sections (in πa_o^2) for O_2 versus incident electron energy (in eV), plotted in (a) for the cases of total and DI cross sections and in (b) for the ratios of the two cross sections. Calculated values in the Born approximation are denoted by a symbol (▼), while solid curve is obtained using the BE approximation. Experimental data (◇) are from the Lockheed group[2].
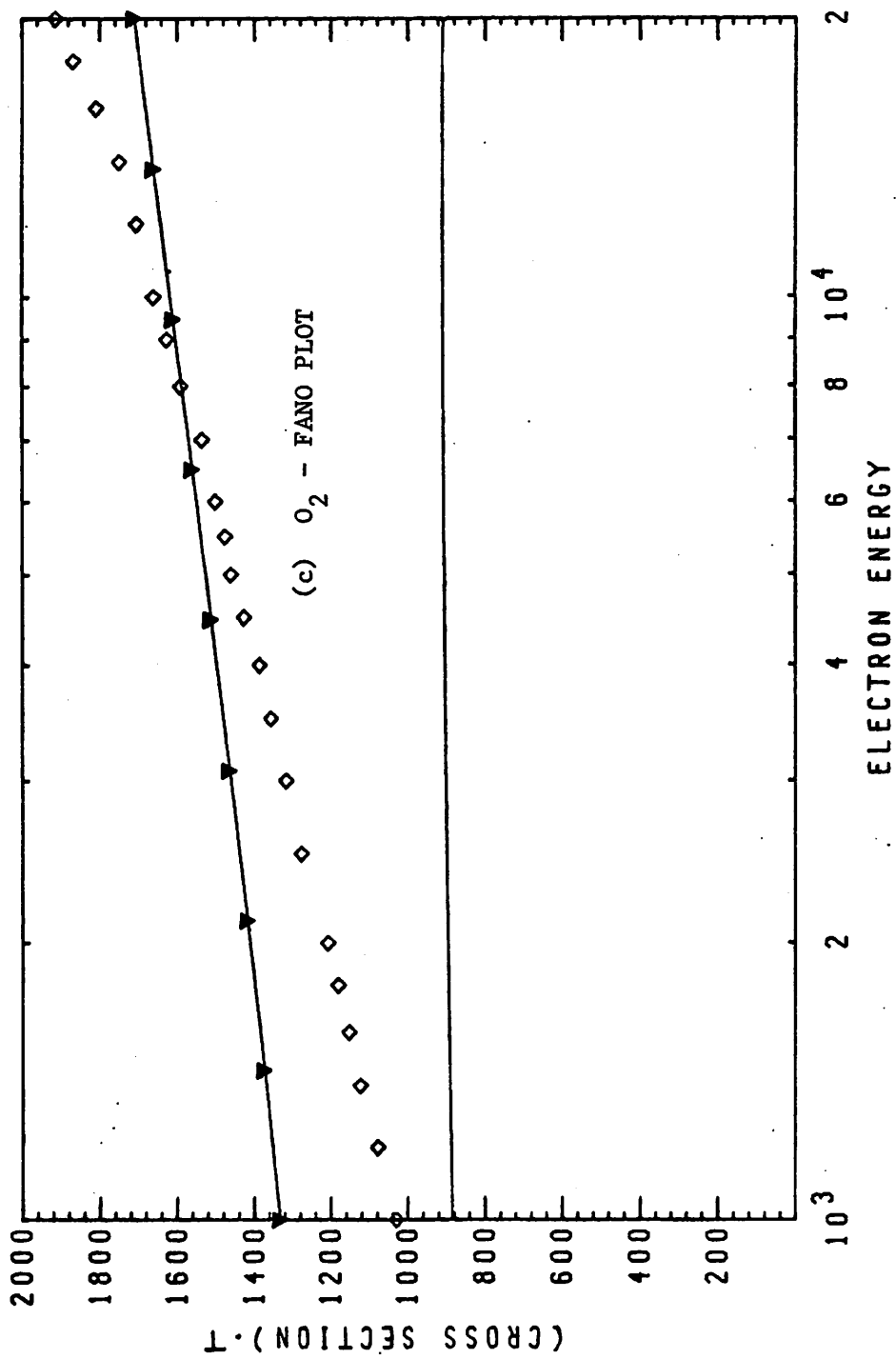
Fig. 7c. Fano plot of the total ionization for O_2 i.e., Plot of (cross section)·T vs. log T. Calculated values (▼) in the Born approximation are joined by a curve, while the lower curve is obtained using the BE approximation. Experimental data (◇) are from the Amsterdam group[4a].

certainty. Thus for O_2 one does not have a clearcut specification of the type (and the energetics) of state that will lead to dissociation.

Calculations performed with the hypothesis that direct ionization of electrons from the $(1\pi_u)$ and $(3\sigma_g)$ orbitals causes dissociation (with a threshold energy of 20.5 eV) give DI cross sections at T = 1000 eV that are 40% smaller than experimental cross sections. While if rearrangement ionization of the $(1\pi_u)$ and $(3\sigma_g)$ electrons (with a threshold energy E_r = 20.5-16.1 = 4.4 eV) is assumed, one obtains DI cross sections at T = 1000 eV that are 316% larger than the experimental value! This behavior may be expected, since the former case has three binding electrons in the final state of the ion, while the latter case has only one. Also the comparison of the E_r for DI of O_2 with those for CO, N_2 and NO shows that the value of 4.4 eV for O_2 is usually small. If E_r = 7.9 eV is used, quite good agreement with both the DI and the total ionization cross sections is obtained (Figs. 7). The total ionization cross section for large T (Fig. 7c) has essentially the same type of behavior as that for H_2 and N_2.

In Fig. 8, the calculated total and DI cross sections (in the Born approximation) at T = 1000 eV for the five diatomic molecules (H_2, CO, N_2, NO, and O_2) are compared. One sees the inherent 'correctness' in the predictability of our simple model, in spite of the need to choose an empirical E_r for O_2. In going from CO to N_2, the bond strength of the diatomic molecules decrease monotomically and our calculated DI cross sections increase. Intuitively this is expected. Our calculated DI cross sections depend, on the
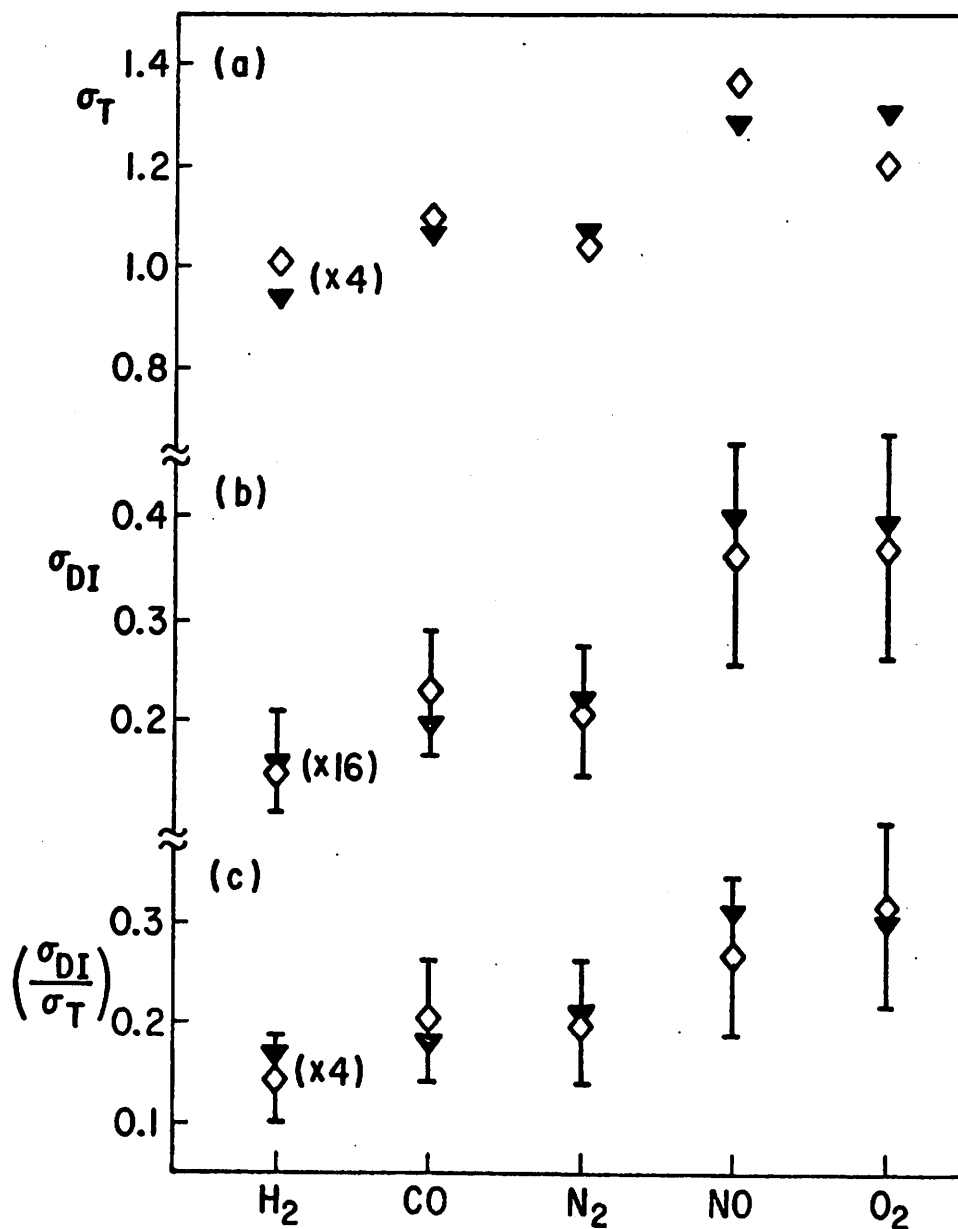
Fig. 8. Comparison at T = 1000 eV of the (a) total ionization
cross sections $(\pi a_0^2)\ \sigma_T$, (b) dissociative ionization cross sec-
tions $(\pi a_0^2)\ \sigma_{DI}$ and (c) ratio of the two cross sections for H_2,
CO, NO and O_2. For H_2 they are shown multiplied by a factor
(n) as shown. Experimental data ($\diamond$) from the Lockheed group[2]
have errors as shown by the error bars.

rearrangement excitation energy E_r. The monotonic decrease of

this quantity as defined in our model (if somewhat precipitously

for O_2) is probably the primary factor that governs the trends of

the calculated DI cross sections.

One last point to note is that the dissociation probability

of the activated state P_d seems to be close to unity, at least

for isolated diatomic molecules. Thus we approach the investiga-

tion of more complex molecules with confidence.

c. Ionization of polyatomic molecules.

Here we will calculate, for a few polyatomic molecules (CO_2,

CH_4 and CH_3X; where X = Halide), the total ionization cross sections.

Also we will venture to estimate the cross sections for the

production of fragments.

(i) Carbon Dioxide: This linear molecule has an electron

configuration as shown in Table 4. The $(4\sigma_g)$, $(3\sigma_u)$ and $(1\pi_u)$ are

ascribed by Herzberg[13] to be the bonding orbitals between the C

and the two O atoms, while the remaining orbitals are non-bonding.

As for the diatomic molecules, we assume here that rearrangement

ionization of an electron from these bonding orbitals will lead to

dissociation of CO_2. These states are represented by "a" - "e" in

Table 4. The excitation energy E_r for the $(1\pi_u)$, $(3\sigma_u)$ and $(4\sigma_g)$

orbitals is, as for the diatomic molecules, taken to be (24.0-17.23)

= 6.77 eV. The effective surface area of the electron cloud A_t is

obtained from the surface area of three spheres with radii equal

to $\ell_b/2$ (where ℓ_b, the experimentally measured bond length in CO_2,

is 2.192 a_0). Note that the separate cross sections for the forma-

# Table 4: States and Energies of the CO_2 Ion

Carbon Dioxide: $K_o^2 K_c^2 K_c^2 (3\sigma_g)^2 (2\sigma_u)^2 (4\sigma_g)^2 (3\sigma_u)^2 (1\pi_u)^4 (1\pi_g)^4$
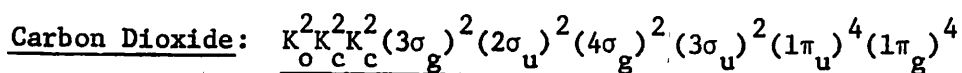
$$(A_t = 14.42 \ \pi a_o^2)$$

Process[1]	State(s)[2]	Orbital Configuration[3]	Threshold[4] Energy (eV)	N_B[5]	Source[6]
1-I	$^2\Pi_g$	$\cdots (4\sigma_g)^2 (3\sigma_u)^2 (1\pi_u)^4 (1\pi_g)^3$	13.85	4	14
	$^2\Pi_u$	$\cdots (4\sigma_g)^2 (3\sigma_u)^2 (1\pi_u)^3 (1\pi_g)^4$	17.23	3 1/2	14
	$^2\Sigma_u^+$	$\cdots (4\sigma_g)^2 (3\sigma_u)^1 (1\pi_u)^4 (1\pi_g)^4$	18.08	3 1/2	15
	$^2\Sigma_g^+$	$\cdots (4\sigma_g)^1 (3\sigma_u)^2 (1\pi_u)^4 (1\pi_g)^4$	19.25	3 1/2	14
R-I	"a"	$\cdots (4\sigma_g)^2 (3\sigma_u)^2 (1\pi_u)^2 (1\pi_g)^4 (A)^1$	[24.0]	2 1/2	2
	"b"	$\cdots (4\sigma_g)^2 (3\sigma_u)^0 (1\pi_u)^4 (1\pi_g)^4 (A)^1$		2 1/2	
	"c"	$\cdots (4\sigma_g)^0 (3\sigma_u)^2 (1\pi_u)^4 (1\pi_g)^4 (A)^1$		2 1/2	
	"d"	$\cdots (4\sigma_g)^2 (3\sigma_u)^1 (1\pi_u)^3 (1\pi_g)^4 (A)^1$		2 1/2	
	"e"	$\cdots (4\sigma_g)^1 (3\sigma_u)^2 (1\pi_u)^4 (1\pi_g)^4 (A)^1$		2 1/2	
2-I		$\cdots (4\sigma_g)^2 (3\sigma_u)^2 (1\pi_u)^4 (1\pi_g)^2$	36.4		16

Notes:

(1) See Note (1) of Table 2.
(2) See Note (2) of Table 2.
(3) See Note (3) of Table 2.
(4) N_B is the average net number of bonding electrons per bond.
(5) See Note (5) of Table 2.
(6) See Note (6) of Table 2.
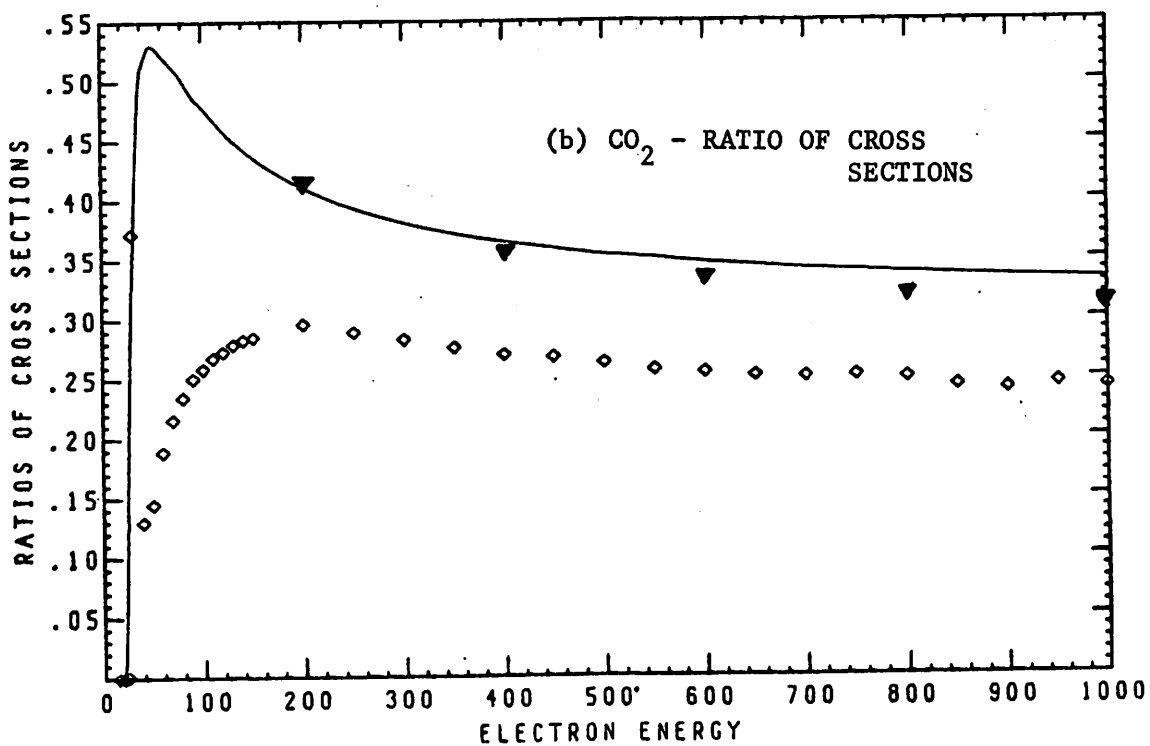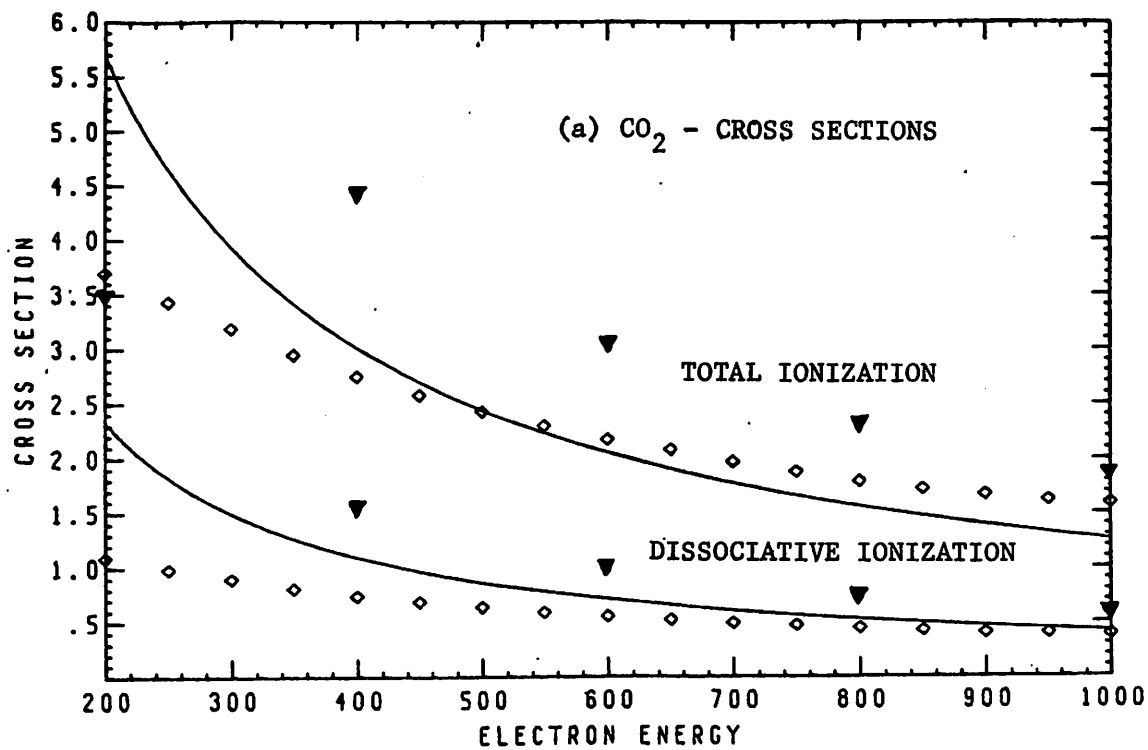
Figs. 9. Ionization cross sections (in πa_0^2) for CO_2 versus incident electron energy (in eV), plotted in (a) for the cases of total and DI cross sections and in (b) for the ratios of the two cross sections. Calculated values in the Born approximation are denoted by a symbol (▼), while solid curve is obtained using the BE approximation. Experimental data (◊) are from the Lockheed group[2].

tion of the fragments $(CO + O^+)$ and $(CO^+ + O)$, cannot be obtained from our theory. The results of our calculation (using the data shown in Table 4) are shown in Figs. 9. The total cross sections have essentially the same type of behavior as for the diatomic molecules. The experimental data[2] for dissociative ionizations is restricted to measurement of those ions with kinetic energy < 0.25 eV. It is quite possible that CO^+ ions, which receive only 36% of the net energy released during dissociation, are not detected. Thus our calculated rearrangement ionization cross sections (and the ratios in Fig. 9b) may be expected to be consistently larger than those experimentally measured; indeed they are.

(ii) Methane: This ten electron molecule, with tetrahedral symmetry (T_d), has six electrons in the $[1t_2]$ orbital. Removal of an electron from this orbital can not only ionize the molecule but as will be seen, form a variety of fragments. Table 5 lists the electronic configurations of the ion and the fragments (CH_3^+, CH_2^+, CH^+, H^+ and C^+) in their lowest electronic states. The orbitals are denoted by standard spectroscopic, group theoretical notation[21]. For example, the wave function of an electron in the $[1t_2]$ orbital, transforms according to the T_2 irreducible representation of the T_d symmetry group. This information is necessary here because we need to identify the type of transition (i.e., direct or rearrangement) that leads to the formation of a particular fragment. Thus if the state (or equivalently, the irreducible representation) of the fragments correlates with the state of the parent ion, then one can assume a direct ionization event may have caused the fragmenta-

4.37

Table 5: Fragmentation of Methane

Electron Configuration of the Fragments	Threshold Energy (eV)	Ref. No.
$CH_4^+\{(1a_1)^2(2a_1)^2[1t_2]^5\} + e^-$	13.1	17
$CH_4^+\{(1a_1)^2(2a_1)^1[1t_2]^6\} + e^-$	19.5	17
$CH_3^+\{(1a_1')^2(2a_1')^2(1e')^4\} + H\{(1s)\} + e^-$	14.3	18
$CH_2^+\{(1\sigma_g)^2(2\sigma_g)^2(1\sigma_u)^2(1\pi_u)^1\} + H_2\{(1\sigma_g)^2\}$ $+ e^-$	15.6	19
$CH^+\{(1s\sigma)^2(2s\sigma)^2(2p\sigma)^2\} + H_2\{(1\sigma_g)^2\}$ $+ H\{(1s)^1\} + e^-$	22.4	20
$H^+ + CH_3\{(1a_1')^2(2a_1')^2(1e')^4(1a_2'')^1\} + e^-$	24.0	2
$C^+\{(1s)^2(2s)^2(2p)^1\} + 2H_2\{(1\sigma_g)^2\} + e^-$	26.2	20

tion. The analysis by McDowell[22] of CH_3^+ production from CH_4 supports our view.

As shown in Table 5, the ionization of methane can occur via removal of an electron from either the $[1t_2]$ or the $(2a_1)$ orbitals. The threshold energies for the production of CH_3^+ and CH_2^+ are only 1.2 and 2.5 electron volts above the first ionization potential. Also the E' representation of the symmetry group of CH_3^+ (D_{3h}) correlates (via the intermediate C_{3v} symmetry group) with the T_2 representation of the symmetry group of CH_4 (T_d); thus one can assume that CH_3^+ is formed via a direct ionization event. By a similar type of correlation, one can conclude that CH_2^+ is also formed via a direct ionization transition. The fragments CH^+, H^+ and C^+ are formed at substantially higher threshold energies. Intuitively we expect that ejection of three or all four of the hydrogen atoms from CH_4, must be a violent process involving excitation (and rearrangement?) of the bound electrons in CH_4. The minimum energy transfer necessary to eject a proton from methane also requires that a methyl (CH_3) radical be formed. The outermost electron in CH_3 occupies a <u>non</u>-bonding ($1a_2''$) orbital. One can therefore hypothesize that a bound electron from the orbital of CH_4 must have been sufficiently excited (by the incident electron) to resist the strong electron affinity of the proton but to yield to the non-bonding ($1a_2''$) orbital of CH_3. Thus we assume that CH^+, H^+ and C^+ are produced via rearrangement ionization transitions of electrons from the $[1t_2]$ orbital of CH_4 with E_r given by the respective threshold energies in Table 5. Also the effective area of the electron cloud

A_t is assumed to be equal to the surface area of a sphere of radius $\bar{r}$, the calculated radii of the 2p electrons in carbon. Thus $A_t = 5.915 \; \pi a_0^2$.

Calculations, using the threshold energies listed in Table 5, are compared with experimental ionization cross sections in Figs. 10. The total ionization cross sections have essentially the same trend as for the other molecules investigated. The Lockheed group[2] has obtained data for production of energetic ions (assumed to be H^+) from CH_4. Our calculated estimates for H^+ production, compare quite well in magnitude as well as behavior. The large incident electron energy behavior (Fig. 10c) of the total ionization cross section in the Born theory compares reasonably with the sparse experimental data from the Amsterdam group[4b].

Next we will attempt to compare our calculated cross sections to the observed relative cross sections for fragment production. Note that our calculated $Q_{s,q}$ and $Q^R_{s,q}$ give the cross section to form a molecule in a particular activated state. In the case of diatomic molecules, the probability to dissociate P_d, gives the probability $(1-P_d)$ that no dissociation can occur. However in the case of polyatomic molecules, the higher lying activated states (that can lead to a particular fragmentation of the molecule) can decay into lower lying activated states (that can lead to a different fragmentation of the molecule). This complication forbids, in general, a direct comparison of the activated state cross section with measured dissociation cross sections. It requires that our calculated activated state cross sections satisfy a set
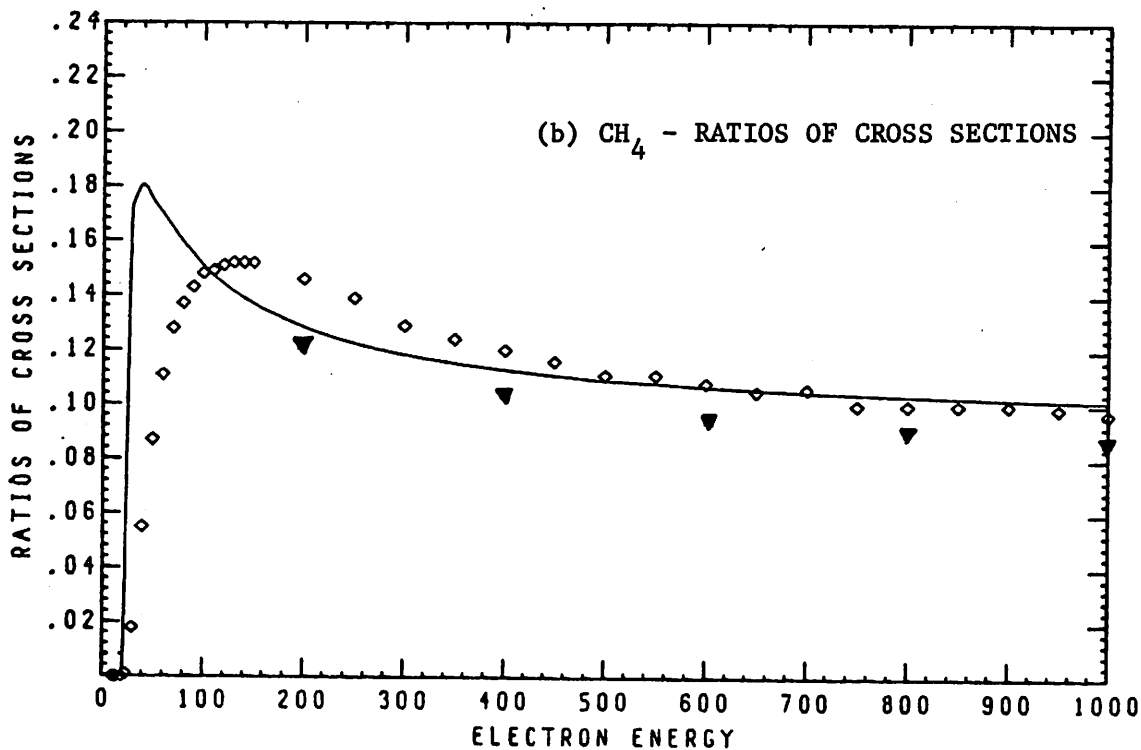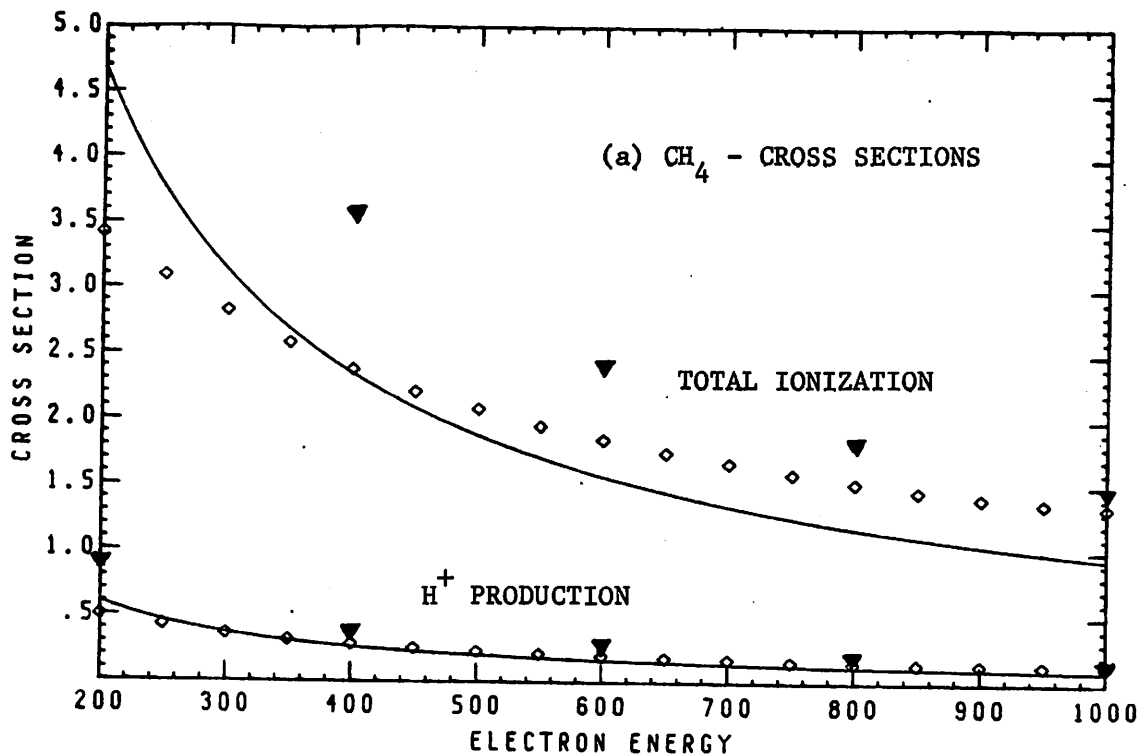
Figs. 10a and 10b. Ionization cross sections (in πa_o^2) for CH_4 versus incident electron energy (in eV), plotted in (a) for the cases of total ionization and H^+ production cross sections and in (b) for the ratios of the two cross sections. Calculated values in the Born approximation are denoted by a symbol (▼), while solid curve is obtained using the BE theory. Experimental data (◊) are from the Lockheed group[2].
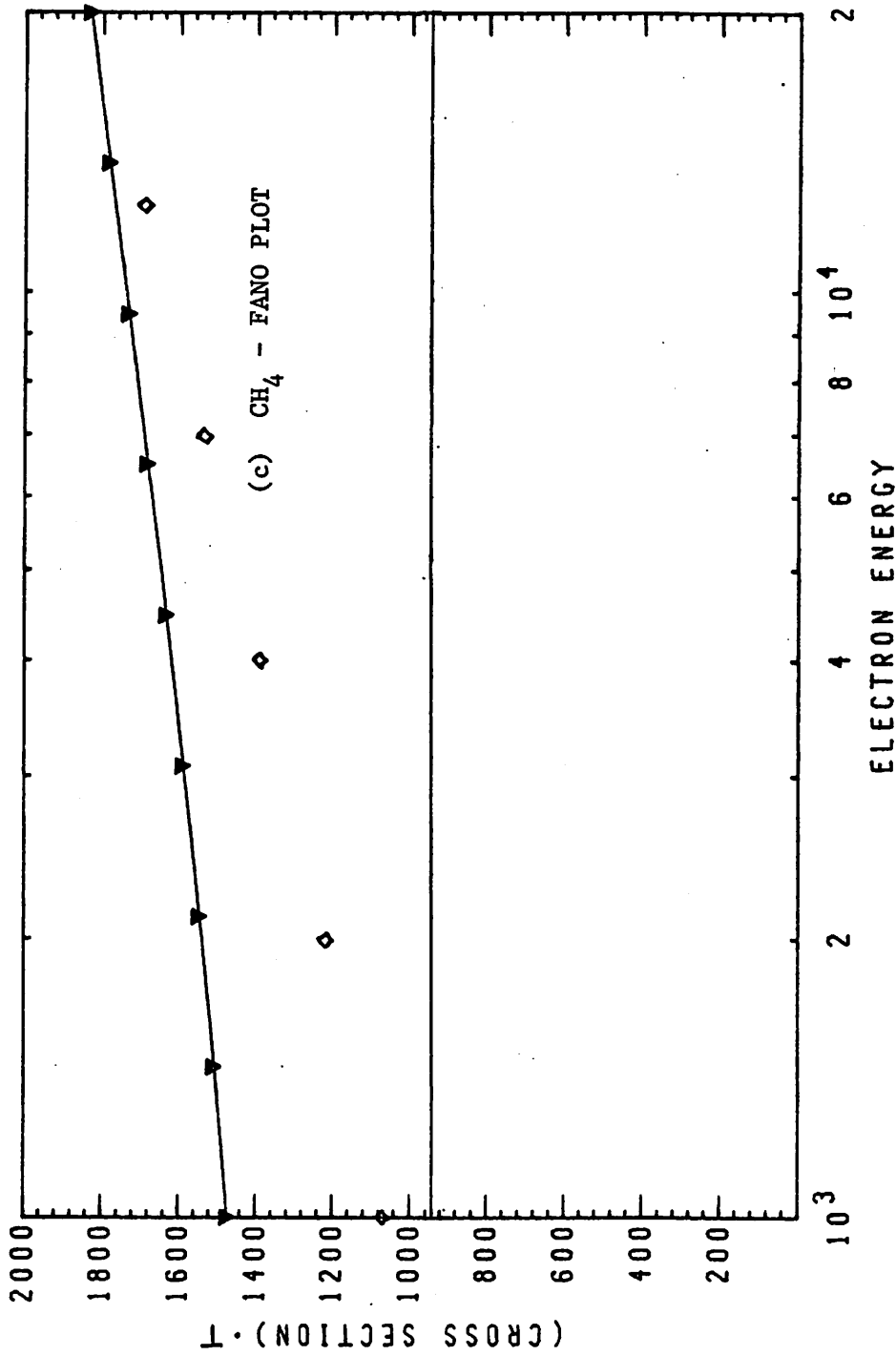
Fig. 10c. Fano plot of the total ionization for CH_4 i.e., Plot of (cross section)·T vs. log T. Calculated values ($\blacktriangledown$) in the Born approximation are joined by a curve, while the lower curve is obtained using the BE approximation. Experimental data ($\diamond$) are from the Amsterdam group 4b.

of general conditions that ensure internal self consistency between our calculations and our model. We derive these next.

Consider the simple case of a closed three level system (Fig. 11). The calculated activated state cross section $\sigma_A(3)$, for example, is related to the observed dissociation cross section $\sigma_D(3)$ via

$$\sigma_D(3) = \sigma_A(3) \left[1 - d_{32} - d_{31}\right] \tag{3a}$$

where d_{32} and d_{31} are the probability for decay of the activated state 3 into the states 2 and 1 respectively. Consequently the $\sigma_D(2)$ and $\sigma_D(1)$ can be written as

$$\sigma_D(2) = \sigma_A(2) \left[1 - d_{21}\right] + \sigma_A(3) d_{32} \tag{3b}$$

and

$$\sigma_D(1) = \sigma_A(1) + \sigma_A(2) d_{21} + \sigma_A(3) d_{31}. \tag{3c}$$

Here the contribution of the decay of the upper states into the lower states is apparent. Since the decay probabilities (d_{ij}) are positive definite quantities it is clear that

$$\sigma_D(3)/\sigma_A(3) \leq 1 \tag{4a}$$

and

$$\sigma_D(1)/\sigma_A(1) \geq 1 . \tag{4b}$$

Further if one defines $\alpha_D(i) = \sigma_D(i)/\sigma_A(i)$, then one obtains using Eqns. (3),
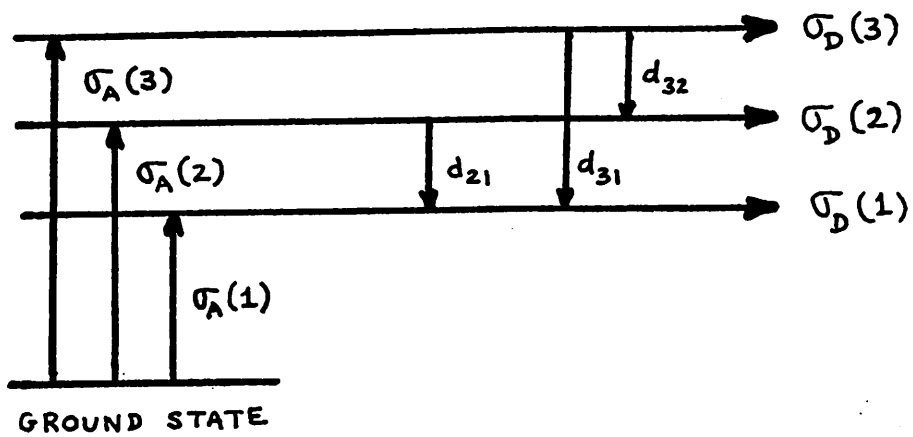
Fig. 11. Schematic three level system displaying the decay
of activated states into lower states.

$$\sum_{i=1}^{3} \alpha_D(i) = 3 - d_{32}[1 - \sigma_A(3)/\sigma_A(2)] - d_{31}[1 - \sigma_A(3)/\sigma_A(1)]$$

$$- d_{21}[1 - \sigma_A(2)/\sigma_A(1)]. \qquad (5)$$

It is easy to convince oneself that Eqns. (4) agree with one's intuition. They with Eqn. (5), when used with experimentally measured $\sigma_D(i)$ and calculated $\sigma_A(i)$, provide an independent consistency check between our calculations and model. The d_{ij} are rarely available; thus if $\sigma_A(3) \leq \sigma_A(2) \leq \sigma_A(1)$, one has at least $\sum_{i=1}^{3} \alpha_D(i) \leq 3$. Note that here we have ignored two-step decay probability products (i.e., $d_{32}d_{21}$); inclusion leaves Eqns. (4) unchanged but Eqn. (5) would be modified somewhat. Generalization to an n-level system is straightforward and therefore not presented here.

The fragmentation pattern of methane is obtained at incident electron kinetic energies of 50-75 eV. At those energies our calculations are highly inaccurate. However the mass spectroscopists claim that the fragmentation pattern is virtually unchanged at higher T. Since our calculated relative cross sections depend weakly on T for T > 200 eV, we will compare our results at T = 200 eV with the available mass-spectral data. In Table 6 we use the reported[20] fragmentation pattern for methane (ratio of intensities of CH_3^+/CH_4^+ = 0.764; of CH_2^+/CH_4^+ = 0.158; of CH^+/CH_4^+ = 0.06; of C^+/CH_4^+ = 0.02) and the Lockheed group data [$\sigma(H^+)/\sigma$ (total ionization) = 0.09] in a comparison with our calculated $\sigma_A(i)$ (in the Born approximation). Both the measured total ionization cross sections and the calculated total activated state cross sections

Table 6: Calculated and Observed Fragmentation of Methane

FRAGMENT	EXPERIMENTAL	CALCULATED	
(i)	$\sigma_D(i)$	$\sigma_A(i)$	$\alpha_D(i)$
CH_4^+	0.458	0.265	1.724
CH_3^+	0.349	0.136	2.566
CH_2^+	0.072	0.112	0.643
CH^+	0.027	0.165	0.163
H^+	0.085	0.126	0.675
C^+	0.009	0.194	0.046

are normalized to unity. Use of the BE theory gives $\sigma_A(i)$ and $\alpha_D(i)$ within 1% of those given in Table 6. For CH_4^+ and CH_3^+, the calculated $\sigma_A(i)$ are smaller than the measured $\sigma_D(i)$ by a factor of 2-3. Thus, as expected, the decay of the higher lying activated states (for CH_2^+, CH^+, H^+ and C^+ production) gives $\alpha_D > 1$ for CH_4^+ and CH_3^+ and $\alpha_D < 1$ for CH_2^+, CH^+, H^+ and C^+. The results for CH_4^+ and C^+ are consistent with the generalized version of (4). Finally it is interesting to note that $\sum\limits_{i=1}^{6} \alpha_D(i)$ is equal to 5.82. While a generalization of the expression in (5) for a six-level system gives $\sum\limits_{i=1}^{6} \alpha_D(i) = 6 - q$, where q is probably a small number that depends on the 15 unknown d_{ij} in this six-level system.

Thus it seems that for methane while our one-electron model was adequate to predict with reasonable accuracy the total ionization and proton production cross sections, the cross sections for CH_2^+, CH^+ and C^+ production was rather largely overestimated So far one does not know whether this is due to inaccuracies in the model and the methods of calculation or due to the inherently large decay probabilities of the activated state of CH_2^+, CH^+ and C^+.

(iii) Methyl Halides: The observed fragmentation patterns of these molecules show a dependence on the specific halide atom that is attached to the methyl radical. In order to see whether our model can also show these trends, we calculate here the activated state cross sections for the formation of CH_3^+, X^+, CH_2X^+ and CH_2^+ (where X represents a Halide atom) from CH_3X. Only three halogens, chlorine, bromine and iodine are considered; since the available experimental data for flourine are sparse and somewhat

contradictory. The molecular-orbital electron configuration for
the methyl halides has been obtained by Mulliken[23]. Seven valence
electrons from the halide atom (ns^2, np^2) combine with nine electrons
from the CH_3 radical to give a 16 (valence) electron configuration
of:

$$(1s_c)^2(ns_x a_1)^2[sa_1]^2[\pi e]^4[\sigma a_1]^2(np_x \pi e)^4. \tag{6}$$

The molecular orbitals are localized on various parts of the molecule.
The $(ns_x a_1)$ and the $(np_x \pi e)$ are localized orbitals on the halogen,
formed from the ns and np electrons of the free atom. The $[\sigma a_1]$
is the primary carbon-halogen bonding orbital, while $[\pi e]$ is a
doubly degenerate orbital localized primarily on the methyl radical.
The $[sa_1]$ is believed to be delocalized over the methyl group as
well as the halogen atom. Using this information, one can associate
with the observed threshold energies for the ionized fragment produc-
tion, the removal of an electron from an appropriate localized
orbital. As in the case of CH_3^+ and CH_2^+ formation from CH_4, we
assume here that direct ionization is sufficient to cause dis-
ruption of the weak bonds in the methyl halides. The experimental
data for the threshold energies for CH_3X^+, CH_3^+, X^+, CH_2X^+ and CH_2^+
formation have been obtained by Hamill's group[24]. Table 7 lists
the particular orbitals and the threshold energies involved in
specific fragmentations.

Before our calculated results can be compared with mass
spectral fragmentation patterns, we have to consider an additional
process that occurs at the low incident electron energies in a
mass spectrometer: polar dissociation. This process is especially

Table 7: Energies in the Fragmentation of Methyl Halides

Electronic Configuration of $(CH_3X)^+$	Fragment Produced	Threshold Energies for X =		
		Cℓ	Br	I
$[sa_1]^2[\pi e]^4[\sigma a_1]^2(\pi_x e)^3$	CH_3X^+	11.3	10.5	9.5
	X^+	16.6	14.7	12.9
$[sa_1]^2[\pi e]^4[\sigma a_1]^1(\pi_x e)^4$	CH_3X^+	11.9	11.5	11.2
	CH_3^+	13.6	13.0	12.2
	X^+	16.6	14.7	12.9
	CH_2^+	14.6	14.9	14.6
$[sa_1]^2[\pi e]^3[\sigma a_1]^2(\pi_x e)^4$	CH_3X^+	13.2	12.9	13.1
	CH_3^+	13.6	13.0	13.1
	CH_2X^+	13.6	13.6	13.7
	CH_2^+	14.6	14.9	14.6
$[sa_1]^1[\pi e]^4[\sigma a_1]^2(\pi_x e)^4$	CH_3X^+	18.7	19.1	19.8

likely when the high electron-affinity halogen atoms are present. While our calculations can provide the cross section for the DI process

$$e^- + CH_3X \rightarrow CH_3^+ + X + 2e^- \tag{7}$$

the analogous polar dissociation process,

$$e^- + CH_3X \rightarrow CH_3^+ + X^- + e^- \tag{8}$$

cannot be incorporated in our scattering calculations. Fortunately there exist estimations[26] of the experimentally obtained relative cross sections for $CH_3^+ - X$ and $CH_3^+ - X^-$ processes from CH_3X. Using these we determine that our calculated cross section for the process given in (7) has to be multiplied by a factor n, so that both the processes are taken into account. The factor n is 13/4, 13/5 and 38/30 for Cl, Br and I halogen atoms in CH_3X respectively.

In Fig. 12 our calculated activated state cross sections [with the approximate inclusion of the process in (8)] are plotted against available experimental data[6,26]. The experimental data by Cox (denoted by triangles in Fig. 12)are obtained on one instrument for all the methyl halides and probably represent · the trends accurately. It is clear that our calculated σ_A reproduce the observed trends. Note that the increase in X^+ production with increasing Z of the halogen atom can be related to the decreasing C-X bond strength. However the opposite trend for CH_3^+ production can be only attributed to the process of polar dissociation.
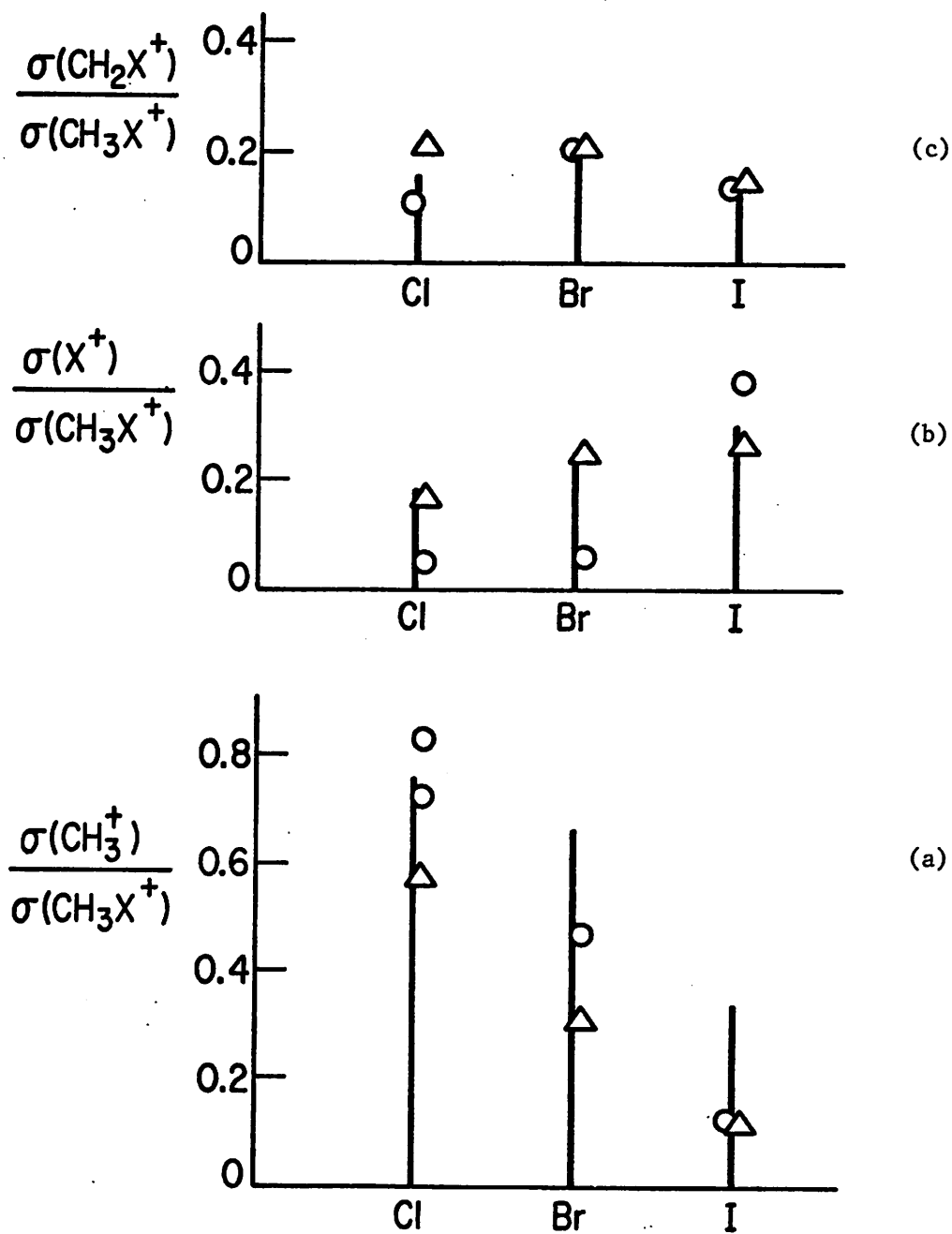
Fig. 12. Fragmentation of Methyl halides (CH_3X, where X = Cl, Br, I). Experimental data for the production of (a) CH_3^+ (b) X^+ and (c) CH_2X^+ from CH_3X are obtained from Ref. 6 (o) and Ref. 26 (Δ). Calculated activated state cross sections are represented by the height of the solid bars.

The virtual independence of CH_2X^+ production on the Z of the halogen atom is also predicted by our theory. The calculated cross sections for CH_2^+ production (not shown in Fig. 12!) are about a factor of 2-3 greater than the corresponding measured cross sections; however both are essentially independent of the halogen atom. Thus, it is important to note that the inclusion of the processes for CHX^+, HX^+ etc. production (which have small probability of occurrence) could alter the absolute magnitude of our calculated cross sections for the formation of CH_3^+, X^+ etc., but would not alter the trends in Fig. 12 on the halide atom.

In summary, our calculations provide a reasonable first estimate for total ionization cross sections, at least for the molecules investigated. For diatomic molecules, the calculated cross section for dissociation agree quite well with the corresponding measured quantities. Note especially that the gradual decrease with T of the ratios of the experimentally observed cross sections are duplicated quite well by our model calculations for all the molecules investigated (see Figs. 3c, 4b, 5b, 6b, 7b, 9b, and 10b). For polyatomic molecules, it seems that the most probable fragments are best estimated by our model. Errors in our model stem from two main areas: (1) Approximation of the many-electron scattering interaction via the factor $\gamma_{s,q}$ in the case of direct ionization events and via the phenomenological modelling of rearrangement ionization events. (2) Approximation in the two-particle scattering dynamics. Use of more accurate one-electron wave functions could improve the large T behavior of the cross

sections. This would also probably complicate the calculation, especially if the matrix elements $\langle \phi_\alpha | e^{i\underline{K} \cdot \underline{r}} | \phi_0 \rangle$ were not available in an analytical form.

REFERENCES to Chapter 4.

1. L.J. Kieffer and G.H. Dunn, Rev. Mod. Phys. 38, 1 (1966).

2. P. Englander-Golden and D. Rapp, "Total Cross Sections for Ionizations of Atoms and Molecules", No. LMSC-6-74-64-12 (Lockheed Missiles and Space Company, Palo Alto, California 94304, 1964).

3. D. Rapp, et al., J. Chem. Phys. 42, 4081 (1965) and 43, 1464 (1965).

4a. B.L. Schram et al., Physica 32, 94 (1965).

4b. B.L. Schram et al., J. Chem. Phys. 44, 49 (1966).

5. J.D. Craggs and H.S.W. Massey in Handbuch der Physik ed. S. Flugge (Springer-Verlag, Berlin, 1959), Vol. 37, Part 1, Sec. 24-36.

6. American Petroleum Institute Research Project 44, Catalog of Mass Spectral Data, Carnegie Inst. of Tech., Pittsburg, 1953.

7. J.B. Mann, "Atomic Structure Calculations. II. Hartree-Fock Wave Functions and Radial Expectation Values: Hydrogen to Lawrencium", Report no. LA-3691 (1968) Los Alamos Scientific Laboratory, Los Alamos, New Mexico.

8. C.E. Moore, Atomic Energy Levels (circ. 467, Nat'l. Bur. Standards, U.S.A., 1958) vol. 1.

9. H.S.W. Massey, Electronic and Ionic Impact Phenomena (Oxford Univ. Press, 1969), v. 2, p. 916.

10. G. Herzberg, Molecular Spectra and Molecular Structure I. Diatomic Molecules (D. Van Nostrand Co. Inc., 1950).

11. G.C. Pimentel and R.D. Spratley, Chemical Bonding Clarified through quantum mechanics (Holden-Day, Inc., San Francisco, 1969), Appendix d.

12. F.R. Gilmore, J. Quant. Spectry. Rad. Transfer 5, 369, (1965).

13. G. Herzberg, Molecular Spectra and Molecular Structure III. Electronic Spectra and Electronic Structure of Polyatomic Molecules (D. Van Nostrand Co. Inc., 1966), p. 315 and 393.

14. J. Collin, J. Chim., Phys. 57, 424 (1960).

15. M.I. Al-Joboury, D.P. May, D.W. Turner, J. Chem. Soc., 6350 (1965).

16. F.H. Dorman and J.D. Morrison, J. Chem. Phys. 35, 575 (1961).

17. D.C. Frost and C.A. McDowell, Proc. Roy. Soc. (London) A241, 194 (1957).

18. S. Tsuda, C.E. Melton and W.H. Hamill, J. Chem. Phys. 41, 689 (1964).

19. S. Tsuda and W.H. Hamill, J. Chem. Phys. 41, 2713 (1964).

20. C.A. McDowell and J.W. Warren, Faraday Soc. Disc. 10, 53 (1951).

21. G. Herzberg, Op. Cit. (1966), Chapter III.2.

22. C.A. McDowell, Trans. Faraday Soc. 50, 423 (1954).

23. R.S. Mulliken, Phys. Rev. 47, 413 (1935).

24. S. Tsuda, C.E. Melton and W.H. Hamill, Op. Cit. and S. Tsuda, W.H. Hamill, Op. Cit.

25. S. Tsuda, C.E. Melton and W.H. Hamill, Op. Cit., Table II.

26. J.D. Craggs and H.S.W. Massey, Op. Cit., Fig. 61.

CHAPTER 5

FATE OF THE ACTIVATED STATE

In this chapter, we consider the dissociation probability
(P_d) of the activated state. The P_d is formulated to depend on
two competing processes: the separation of the fragments and the
decay of the activated state. Dependences of P_d on molecular para-
meters are obtained. Next we examine the lifetime of the activated
state of an isolated molecule and of one in the condensed phase.
Finally we discuss a formulation and possible calculation of secon-
dary dissociation caused by ejected electrons.

5.1. Dissociation probability of the activated state.

   a. Formulation

The formulation of the dissociation probability P_d of the
activated state, which we will develop here, is conceptually moti-
vated by the rigorous derivation of an analogous quantity in the
theory[1] of dissociative attachment (DA) of slow electrons in a gas
of molecular hydrogen. Recall (Sec. 2.2.b) that P_d is defined to
be the probability that an activated state i (for the formation of
a particular type of fragments i) will not decay into any state
that cannot lead to the generation of the fragments i. Alternatively,
P_d is the probability that the activated state i will remain 'active'
and thereby lead to the dissociation of the molecule.

We model P_d to depend on two competing processes. The acti-
vated molecule, once formed, can do one of two possible things. 1)
It can decay into an energetically lower, vibrational or electronic,

state (j) that cannot lead to the formation of the fragments i.
Or 2) it can remain in the activated state i. The molecular nuclei,
of the activated molecule, feel a repulsive potential. This leads
to separation of the nuclei from their equilibrium positions.
If the activated state does not decay into a stable, non-fragmenting
state before the nuclei separate to some critical distance, then
one can assume that fragmentation of the molecule has occured.
The decrease in the probability dP_d in the existence of the acti-
vated state due to decay (with characteristic lifetime τ_{dj}) into
state j can be written,

$$dP_d = - P_d \sum_j \frac{dt}{\tau_{dj}(t)} . \tag{1}$$

Note that the lifetime of the decay of the activated state depends
both on the characteristics of the final state j as well as on the
relative location of the nuclei at the time t. For convenience,
we define

$$1/\tau_d(t) = \sum_j 1/\tau_{dj}(t). \tag{2}$$

The $\tau_d(t)$ is the total decay lifetime of the activated state.
Integrating (1), one obtains the probability $P_d(\tau_s)$, for the exis-
tence of the activated state at the time τ_s after the formation of
the activated state by the incident electron action, to be

$$P_d(\tau_s) = \exp[-\int_0^{\tau_s} dt/\tau_d(t)]. \tag{3}$$

We have assumed of course that $P_d(0) = 1$. This equation shows

explicitly the very sensitive dependence of the probability of fragmentation on the decay lifetime τ_{ds}. In the next section we will discuss mechanisms and magnitudes of the individual τ_{di}, here we concentrate on elucidating Eqn. (3) and determining its dependences on the parameters of the molecule.

Next an alternative expression to (3) for $P_d(\tau_s)$ is obtained. For a diatomic molecule, the relative average velocity of the fragments during separation is given by

$$\langle v(R) \rangle = \frac{dR}{dt} = \sqrt{\frac{2T_\mu(R)}{\mu}}, \tag{4}$$

where R is the interfragment separation distance and $T_\mu(R)$ is the total kinetic energy of the fragments. The μ in (4) is the reduced mass [$\mu = m_1 m_2/(m_1 + m_2)$] of the two fragments of mass m_1 and m_2. For polyatomic molecules R can be considered to be an interfragment distance in a hypothetical plane in the potential energy surface of the molecule. Thus the dependences (on molecular parameters) that we will obtain below will be less applicable to polyatomic molecules than to diatomic molecules. The kinetic energy $T_\mu(R)$ of the fragments is determined by the repulsive potential as 'seen' by the nuclei and therefore depends on the potential energy surface of the molecule. Next, we discuss and parameterize τ_d and T_μ.

The decay lifetime τ_d can be equivalently written in terms of the energy width Γ of the resonant unbound state, i.e.,

$$1/\tau_d = \Gamma/\hbar. \tag{5}$$

The energy width Γ provides an explicit indication of the decaying

nature of the unbound activated state, whose total energy is complex, i.e., $E - 1/2\, i\Gamma$, where E and Γ are real. Calculation of an explicit dependence of Γ on R has been obtained[2] for DA in H_2. We model $\Gamma(R)$ to be given by

$$\Gamma(R) = \Gamma_m[1 - (R/R_c)^n],$$

where (6)

$$\Gamma_m = \Gamma_0/[1 - (R_0/R_c)^n].$$

Here $\Gamma_0 = \Gamma(R_0)$ is the energy width at the equilibrium positions R_0 of the nuclei. R_c is the critical distance at which the molecule can be considered to be dissociated; thus R_c corresponds to the inter-fragment separation at time τ_s. The exponent n provides a 'shape' parameter. Figure 1 shows shapes of our modelled $\Gamma(R)$ compared with a typical calculated shape from a theoretical study[1a] of DA in H_2.

The kinetic energy $T_\mu(R)$ can be similarly modelled by a simple analytical expression. Conservation of energy gives $E(R_0) = E_0 = T_\mu(R) + V(R)$, where $V(R)$ is the interaction (potential) energy of the fragments. Here the zero of energy is chosen such that as $R \to \infty$ and $V(R) \to 0$, the maximum possible total kinetic energy of the fragments becomes equal to E_0. Modelling $V(R) = S/R^m$, where m is the shape parameter of the potential energy curve, we obtain

$$T_\mu(R) = E_0 - S/R^m$$
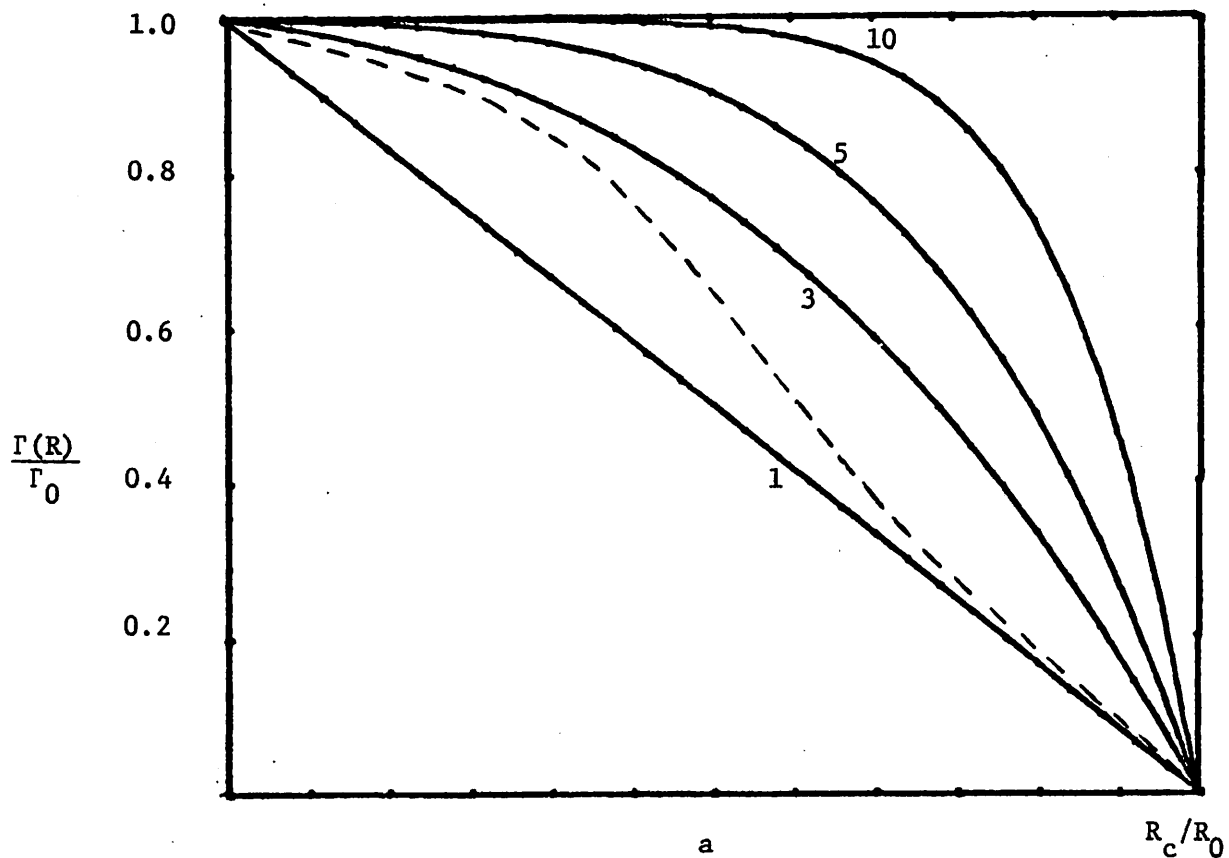
or (7)

$$T_\mu(R) = E_0[1 - (R_0/R)^m].$$

5.4

Fig. 1. Normalized energy width $\Gamma(R)/\Gamma_0$ of the activated state versus the normalized interfragment separation $a = R/R_0$. Modelled $\Gamma(R)$, as given by Eqn. (6), is shown by solid lines with the parameter m as indicated. A typical calculated $\Gamma(R)$ from Ref. 1a is shown by the dashed curve.

The expression for P_d can now be rewritten as

$$P_d(R_c) = \exp\left\{-\sqrt{\frac{\mu}{2}\frac{1}{\hbar}} \int_{R_0}^{R_c} \frac{\Gamma(R)\,dR}{\sqrt{T_\mu(R)}}\right\} . \tag{8}$$

This form displays the explicit dependence on the reduced mass and the energies involved in the fragmentation process. Substitution of (6) and (7) in (8) yields,

$$P_d(R_c) = \exp\left\{-\sqrt{\frac{\mu}{2E_0}} \cdot \frac{\Gamma_0}{\hbar} \cdot R_c \cdot S(R_c/R_0)\right\} \tag{9}$$

where $S(R_c/R_0)$ is a 'shape' factor that depends primarily on the exponents (n and m) chosen for the shapes of $T_\mu(R)$ and $\Gamma(R)$. The $S(R_c/R_0)$ is obtained from:

$$S(a) = \frac{1}{a(1 - 1/a^n)} \int_1^a \frac{[1 - (y/a)^n]}{\sqrt{1 - 1/y^m}} \, dy. \tag{10}$$

We consider now the magnitude of S(a) and its dependence on n, m and a. The integral in (10) can be evaluated analytically for only a few integral values of n and m. As it stands in (10), the integrand has a singularity at $y = 1$ and therefore is not amenable to numerical integration. Defining $g^2 = y^m - 1$, we can rewrite the integral in (10) in a form amenable to numerical integration, i.e.,

$$\int_0^{g_0} \frac{2}{m} (1 + g^2)^\alpha [1 - k(1 + g^2)^{n/m}]\,dg, \tag{11}$$

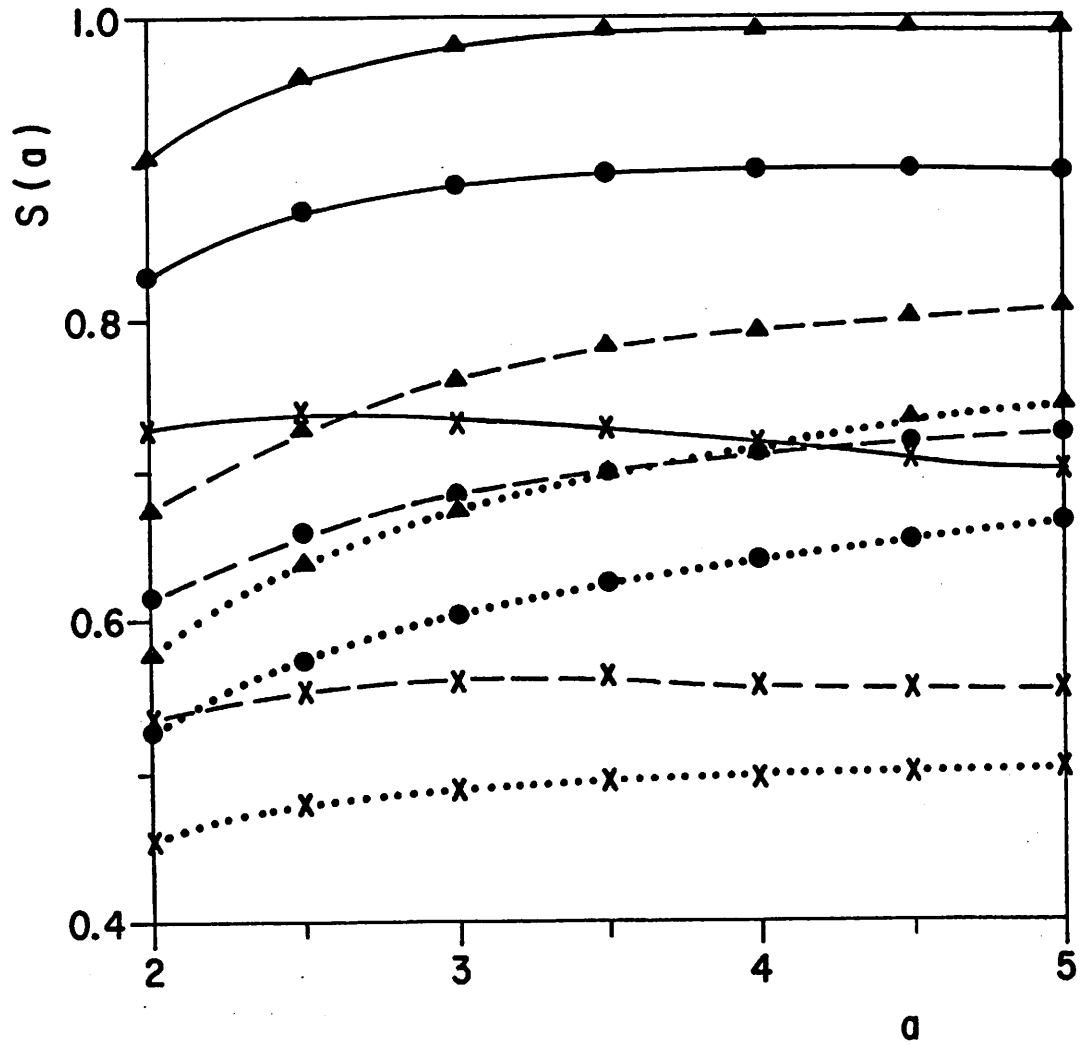where $k = 1/a^n$ and $\alpha = (2-m)/2m$. Figure 2 shows the numerically

5.6

Fig. 2. Shape parameter S(a) versus a = R_c/R_0 for various values of n and m. The values of the parameters in each case can be obtained by noting the symbols (X: n = 1, ●: n = 3, ▲: n = 5) and by noting if the curve is a solid line (m = 1), dashed line (m = 2) or a dotted line (m = 3).

computed $S(a)$ for different values of m and n. The magnitude of $S(a)$ lies between ~ 0.5 and 1.0 for all likely values of n and m (or likely shapes of $V(R)$ and $\Gamma(R)$). The dependence of $S(a)$ on a becomes progressively weaker with increasing a; the dependence on n and m is relatively stronger. Increasing m (or the concavity in the shape of the potential in a potential energy diagram), for fixed value of n, decreases $S(a)$. However increasing n (Fig. 1), at a fixed value of m, increases $S(a)$, as expected intuitively.

Consider next the dependence and the magnitude of P_d [Eqn. (9)] on the four parameters (μ, E_0, Γ and R_c). Figure 3 shows P_d versus the lifetime of the activated state τ_d. The critical distance R_c is assumed to be 4 Å and $S(a)$ is chosen to be 0.6, corresponding to typical shapes of $V(R)$ and $\Gamma(R)$. Also we choose three values of the reduced mass μ as parameters: (a) $\mu = 1$, corresponding to the ejection of an H atom/ion from a large molecule. (b) $\mu = 8$, corresponding to the fragmentation of O_2. And (c) $\mu = 13.4$, corresponding to the fragmentation of CH_3I into CH_3 and I. For the case where the fragments are formed with small kinetic energies ($E_0 = 0.1$ eV), the probability P_d is greater than 0.1 for all $\tau_d > 10^{-13}$ sec, even for $\mu = 13.4$. In the case where the fragments are formed with greater kinetic energy ($E_0 = 1.0$ eV), as in the case of diatomic molecules, the P_d is greater than 0.5 at $\tau_d = 10^{-13}$ sec for all three cases of μ. For $\tau_d < 10^{-13}$ sec, the probability decreases precipitously. Thus the importance of estimations of τ_d is now evident.

b. Lifetime of the activated state

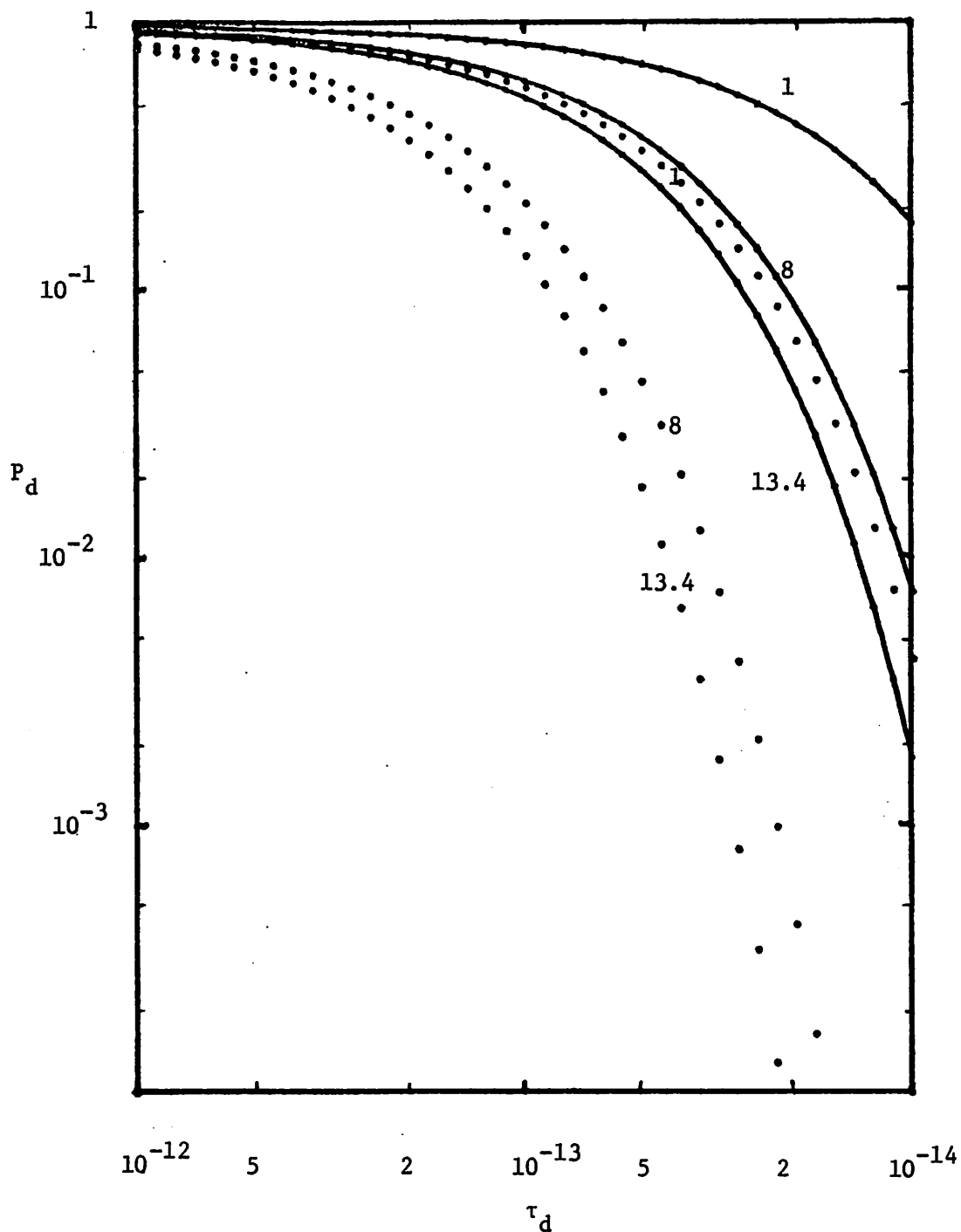In this section, we will briefly survey some intra-molecular

Fig. 3. The probability to dissociate P_d versus the lifetime of the activated state τ_d, for values of the reduced mass (μ) as shown. The solid curves are for $E_0 = 1.0$ eV, while the dotted curves are for $E_0 = 0.1$ eV.

and inter-molecular energy transfer processes that cause the activated
state to decay. A comprehensive study is beyond the scope of this
work; our primary interest is in understanding the types of mechanisms
involved in the decay process and in their magnitudes.

Consider first an isolated molecule. The activated state of a
(neutral or ionized) molecule can decay[3] into a lower stable state
by (a) giving up its excess energy via an emission of a photon or
(b) by partitioning the excess energy amongst other vibrational
modes. The former process (a) involves a luminescence transition.
Depending on whether this radiative transition is between states
of the same multiplicity or not, it is by convention called
fluorescence or phosphoresence respectively. Fluorescence usually
occurs in a transition from the first excited singlet to the lowest
singlet state; it has a typical lifetime of $10^{-9} - 10^{-6}$ sec.
Phosphorescence is considerably slower (with typical lifetimes
greater than 10^{-3} sec) since it involves a spin-forbidden transition.
The second process (b): vibrational energy redistribution within the
molecule usually occurs only in large molecules. This is because
vibrational energy can be transferred efficiently between the many
vibrational modes of a large molecule. Thus a molecule formed in
a given vibrational state of a particular vibrational mode can
spontaneously make a transition to a vibrational state of a different
mode. In addition to vibrational redistribution, radiationless
transitions can occur between isoenergetic vibrational levels of
different electronic states. Such transitions are described as
internal conversions. In general, vibrational transitions (if
allowed by symmetry) occur very rapidly with typical rates of the

order of $10^{13} - 10^{12} \, \text{sec}^{-1}$.

Unlike polyatomic molecules, isolated diatomic molecules cannot redistribute vibrational energy (since they have only one vibrational mode) and are known to have a small probability for internal conversion or fluorescence. Thus an activated state of an isolated diatomic molecules has a decay lifetime τ_d of 10^{-13} sec or greater. This gives P_d of the order of 1.0 and thereby provides further credability to the agreement (Sec. 4.2.b) of our calculated σ_A and the measured σ_D. In the case of isolated polyatomic molecules, vibrational redistribution and internal conversion probably cause the decay of a 'higher' activated state (e.g., the state for CH^+ production from CH_4) into a 'lower' state (e.g., the state for CH_3^+ production), thereby making the prediction of a fragmentation pattern difficult. The quasi-equilibrium theory[4] of mass spectra attempts to predict fragmentation patterns of large molecules by developing a statistical description of the activated state and vibrational energy equipartition in the molecule. Consideration of such a theory is beyond the scope of this work.

The activated state of a molecule in a condensed phase (solid or liquid) can decay by the energy transfer processes considered above (i.e., those for the isolated molecule) as well as by those processes that are due to inter-molecular interactions. These latter process are considerably more difficult to analyse. They can be classed in three general categories: (a) interactions that involve a transfer of electronic energy, (b) interactions that involve a transfer of vibrational energy and (c) charge transfer. As

can be expected from considerations of oscillation times of electrons and nuclei, the first mechanism (a) involves times of the order of 10^{-15} sec or longer, while the process (b) is slower, with time constants of the order of 10^{-13} sec. The third mechanism can involve a transfer of an electron or an ion (usually a proton); consequently transfer times range from 10^{-15} to 10^{-13} sec. Below, we provide a brief description of these three mechanisms.

The electronic energy transfer in molecular solids is the subject of an extensive study in physical and radiation chemistry. A detailed study[5] has been made of the excitation propogation along an idealized chain of coupled diatomic molecules that are in the process of dissociating; its application to experimental systems has yet to be demonstrated. More modern treatments[6] of electronic energy transfer in aromatic materials have been developed via the concept of molecular excitons. However they do not, as yet, provide an understanding of the role of excitation transfer amongst electronically coupled aromatic molecules that are in the process of dissociation (due to the action of an incident electron beam). Such a study would be of interest to the microscopist; unfortunately it is beyond our scope. The role of vibrational energy transfer in solid specimens is even more difficult to ascertain than the uncertain role of electronic energy transfer. Vibrational relaxation is a common occurence in liquid systems; in solid systems, they are expected to be as likely, even though they may be difficult to isolate and identify.

Charge transfer processes can cause deactivation of excited molecules. Excited neutral molecules can spontaneously eject electrons (i.e., auto-ionize) and thereby reach a lower state.

Neutral molecules with large electron affinities can capture low energy electrons and either become stable traps for these electrons or spontaneously dissociate (i.e., dissociative attachment). Ionized molecules can, via an electron capture, be neutralized and subsequently deactivated. Attachment or capture of slow electrons by molecules is being studied[7], however extension of this extensive gas phase experimental data to the solid or liquid phase is quite unreliable. Charge transfer in ion-molecule reactions in the gas phase has yielded extensive data[8], which also cannot be reliably extended into the condensed phase. Radiation chemistry of solids and liquids has provided macroscopic quantities like the 'g factor', but it cannot give information on the mechanisms on the microscopic scale.

In summary, our calculation of P_d when coupled with the estimation of τ_d lead to the conclusion that gas phase diatomic molecules in the activated state will have a large probability to dissociate. Isolated polyatomic molecules due to energy redistribution, internal conversion etc., may not dissociate as readily. The fate of the activated state in the condensed phase is, at present, open to speculation as well as to further investigation.

5.2. Comments on secondary dissociation.

Finally a brief comment on the possibility of secondary dissociations. In distinction to the discussion in the previous section on the decay of the activated state due to inter-molecular effects, we consider here the activation and subsequent dissociation of a molecule due to the action of a different molecule that has been

excited or ionized by an incident electron. Recall in Sec. 2.1.c., we considered the relationship between the exposure and the direct dissociation and the secondary dissociation cross sections. Here we will formulate the secondary dissociation cross section σ_{SD}.

Phenomenologically, the σ_{SD} can be understood to be made up of two parts: (1) The generation of the excitation energy by the incident electron and (2) the probability that this excitation energy will cause dissociation of a (neighboring) molecule. Consider the case where the excitation energy is in the form of an ejected electron of kinetic energy T_e. Also consider (Fig. 4), a thin molecular film (thickness L, molecular density n_0) of the type investigated in modern EMs. The ejected electron has a probability of interacting with one or more molecules in the film; these interactions may lead to dissociation of a molecule. An electron 'formed' (from an ionizing event by the incident electron) close to the surface of the film can escape with few or no interactions. Hence we formulate σ_{SD} as:

$$\sigma_{SD} = \frac{2\pi}{L} \int_0^L \int_0^\pi \int_0^{(T-I)} \frac{\sigma_D(T_e)}{\sigma_T(T_e)} \cdot [1 - \exp(-n_0 \sigma_T(T_e)\ell)] \cdot \frac{d^2\sigma}{dT_e d\theta} (T_e, T)$$

$$dT_e \sin\theta d\theta dx \qquad (12)$$

The second differential cross section $d^2\sigma/dT_e d\theta$ for the ejection of an electron with kinetic energy T_e and in the direction θ, represents the generation of the excitation energy. Here it is assumed that an incident electron ionizes a molecule at most once in the film and the site of ionization can be anywhere along x. The term in the
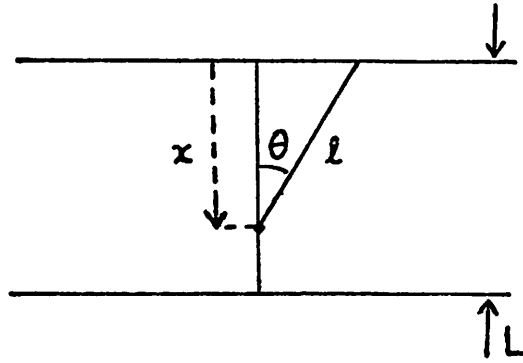
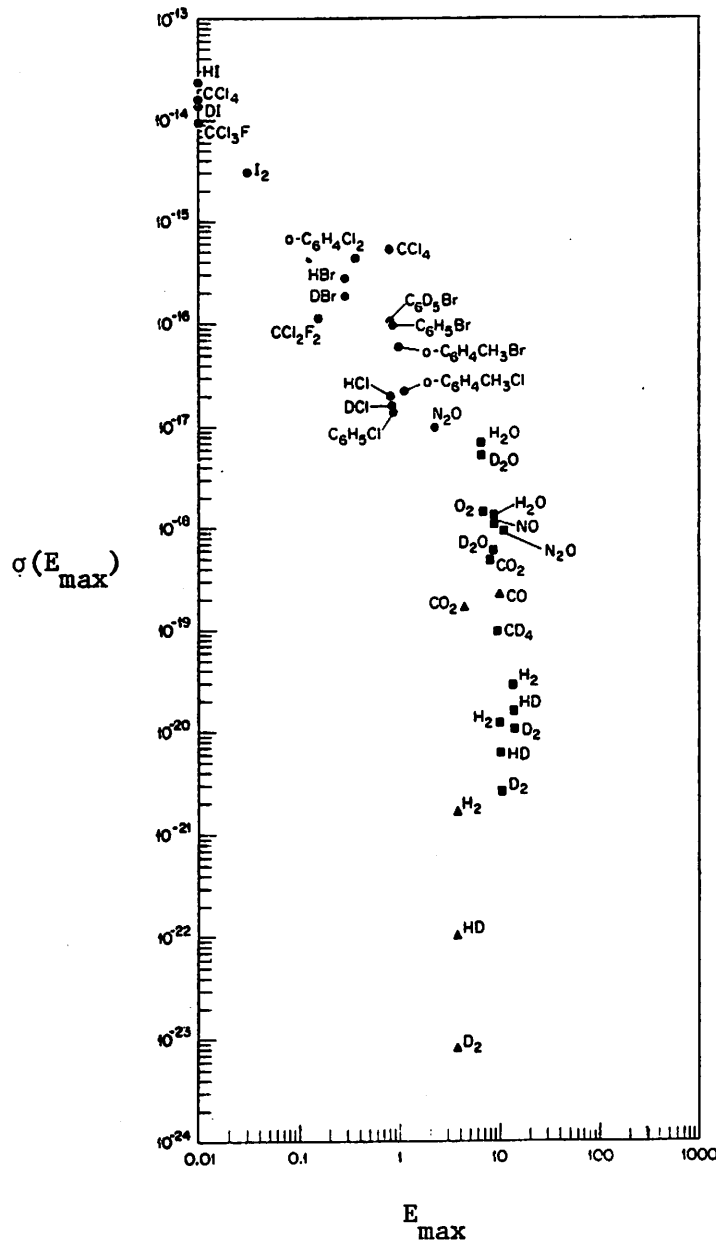Fig. 4. Geometry in the molecular film of thickness L.

Fig. 5. Maximum value of the dissociative attachment cross section $\sigma(E_{max})$ as a function of the energy E_{max} at the peak of the cross section. From Ref. 7.

square bracket represents the probability that the ejected electron
will interact with a molecule in the film, with a total interaction
cross section given by $\sigma_T(T_e)$. The probability that this interaction
will lead to dissociation is assumed to be given by $\sigma_D(T_e)/\sigma_T(T_e)$,
where $\sigma_D(T_e)$ is the cross section for molecular dissociation,
initiated by an ejected electron.

Even though this formulation involves many simplifications
of a very complex problem, the problem remains computationally
intractable. This is because of the absence of a reliable expression
(or estimate) for $d^2\sigma/dT_e d\theta$ and $\sigma_T(T_e)$. The former factor requires
an accurate calculation of $d^2\sigma/dEdK$ for small values of E and K;
as seen in Ch. 3, this is quite difficult to obtain at the present
time. The latter factor is even more difficult to obtain, because
of the lack of a fundamental understanding of all the processes
(and their magnitudes) that occur in the total interaction of a
slow electron with a molecule. Simplification of (12) arises in
the case of an infinite medium, so that:

$$\sigma_{SD} = \int_0^{(T-I)} \sigma_D(T_e)/\sigma_T(T_e) \cdot \frac{d\sigma}{dT_e} (T_e,T)dT_e \cdot \qquad (13)$$

Here too, the presence of $\sigma_T(T_e)$ makes the equation insolvable.

At this stage, we reconcile ourselves to a brief summary of
some of the possible contributions[9] to $\sigma_T(T_e)$. The slow electron,
depending on its energy, interacts with both the electrons and
the ions in the molecular solid. It can loose energy via attach-
ment to an ion, excitation or ionization of an electron configuration,

production of low energy phonons, etc.; eventually it becomes 'thermalized' or is captured by an electron trap. In general, interaction cross sections of slow electrons in molecular solids are quite large ($\sim 10^{16} - 10^{-17}$ cm^2); consequently mean free paths are short and the infinite medium approximation of (12) may be adequate even for 100 Å thick films.

The dissociation cross sections $\sigma_D(T_e)$ can be estimated from the measured data[7] for dissociative ionization (DI) and dissociative attachment processes (DA) in dilute gases. The DA cross sections, in particular, are large for molecules with large electron affinities. The threshold for DA is usually below 10 eV. The trend in the measured data (Fig. 5) shows that the larger maxima in the DA cross sections occur at smaller thresholds (and energies at the peak of the threshold). This is significant since $d\sigma/dT_e$ has a maximum at $T_e = 0$ (Figs. 3-9), so that contribution from processes with the smaller thresholds and larger cross section maxima will give large contribution to σ_{SD}. Halogenated hydrocarbons fall into this category. The influence of DI on σ_{SD} will be small since molecular ionization thresholds are usually above 10 eV, where $d\sigma/dT_e$ is small. The process of dissociative excitation (DE) may be more important than DI, since DE has lower thresholds. However magnitude of DE cross sections are unavailable due to the absence of experimental data. Thus we realize that, even though the magnitude for σ_{SD} cannot be obtained at present, the contribution of DA to σ_{SD} could be greater than that of DE or DI, especially in halogenated compounds.

REFERENCES to Chapter 5

1a) J.N. Bardsley, A. Herzenberg and F. Mandl, Proc. Phys. Soc. 89, 321 (1966).

b) T.F. O'Malley, Phys. Rev. 150, 14 (1966).

2. J.N. Bardsley, A. Herzenberg and F. Mandl, Proc. Phys. Soc. 89, 305 (1966).

3. J.B. Birks, Photophysics of Aromatic Molecules (Wiley-Interscience, 1970), Chap. 3, 4 and 5.

4a) H.M. Rosenstock, H.B. Wallenstein, A.L. Wahraftig and H. Eyring, Proc. Natl. Acad. Sci. U.S. 38, 667 (1952).

b) M. Vestal in Fundamental Processes in Radiation Chemistry, P. Ausloos ed. (Interscience, 1968), p. 59.

5. J.L. Magee and K. Funabashi, J. Chem. Phys 34, 1715 (1961).

6. R. Voltz, Rad. Res. Rev. 1, 301 (1968).

7. L.G. Christophorou, Atomic and Molecular Radiation Physics (Wiley-Interscience,1971), Ch. 6.

8. J.H. Futtrell and T.O. Tiernan in Fundamental Process in Radiation Chemistry, P. Ausloos ed. (Interscience, 1968), p. 171.

9. H.S.W. Massey and E.H.S. Burhop, Electronic and Ionic Impact Phenomena (Clarendon, Oxford, 1969), vol. 2.

Appendix 1: Approximate solutions to coupled equations (2-9).

Here solutions to the coupled equations (2-9) are obtained for selected values of coupling constants and cross sections for the case of (1) one-species model and (2) two-species model. It is hoped that, in spite of the simplistic approximations that will have to be made, at least the trends of survival concentrations and inter-molecular coupling parameters will approximate reality.

The one-species model: Here there is only one equation to solve,

$$dn/dE_c = - \sigma n - \lambda n^2 \qquad (1)$$

where n is the concentration of the molecules, E_c is the exposure, σ is the dissociation cross section and λ is the inter-molecular coupling parameter. For an initial concentration of n_o, the concentration of the surviving molecules is

$$n(E_c) = \frac{n_o \, \sigma \, \exp(- \sigma E_c)}{[\sigma + \lambda n_o (1 - \exp(- \sigma E_c))]} \, . \qquad (2)$$

It is clear that in the limit of $\lambda \to 0$, the $n(E_c) \to n_o \exp(- \sigma E_c)$ as one expects. However for a non-zero coupling constant, the simple exponential behavior is modified. The solution given in Eqn. (2) does not scale linearly with n_o (or $n(E_c)/n_o$ is not independent of n_o); thus the initial concentration of molecules plays a significant role. Even at large values of σE_c, one has $n(E_c)/n_o \to \sigma e^{-\sigma E_c}/(\sigma + \lambda n_o)$; for small values of σE_c, the behavior of $n(E_c)$ is not exponential. For the case where $\sigma \to 0$ Eqn. (1)

can be integrated to yield the solution

$$n(E_c) = \frac{n_o}{n_o \lambda E_c + 1} \qquad (3)$$

Both the dependence of $n(E_c)/n_o$ on n_o as well as the non-exponential behavior are evident here and can clearly be attributed to the presence of the inter-molecular coupling constant. A plot of fractional survival, $n(E_c)/n_o$, on the log scale versus exposure, E_c, (Figure 1) for different values of σ and λ, shows the above mentioned behaviors. Note that the deviation from a straight line represents a non-exponential behavior; also all the quantities used in the figure and hereafter are chosen suitably to be dimensionless, as the primary interest is in determining trends and behaviors on relative magnitudes of σ and λ.

With these preliminaries in mind, consider next, the behavior of molecular concentrations in a two-molecular species model. Here there are only two coupled equations to solve:

$$da/dE_c = - \sigma_a a - \lambda_{aa} a^2 - \lambda_{ab} ab \ ,$$
$$\qquad (4)$$
$$db/dE_c = - \sigma_b b - \lambda_{bb} b^2 - \lambda_{ba} ba \ .$$

The molecular concentrations are denoted by a and b; the σ_a and σ_b are molecular cross sections, while inter-molecular coupling constant arising from excitation of a molecule of species i and dissociation of a molecule of species j, is denoted by λ_{ji}. Note that, as seen through Eqn. (5) below, in general $\lambda_{ij} \neq \lambda_{ji}$ for $j \neq i$. Since these coupled equations are to be solved for a given
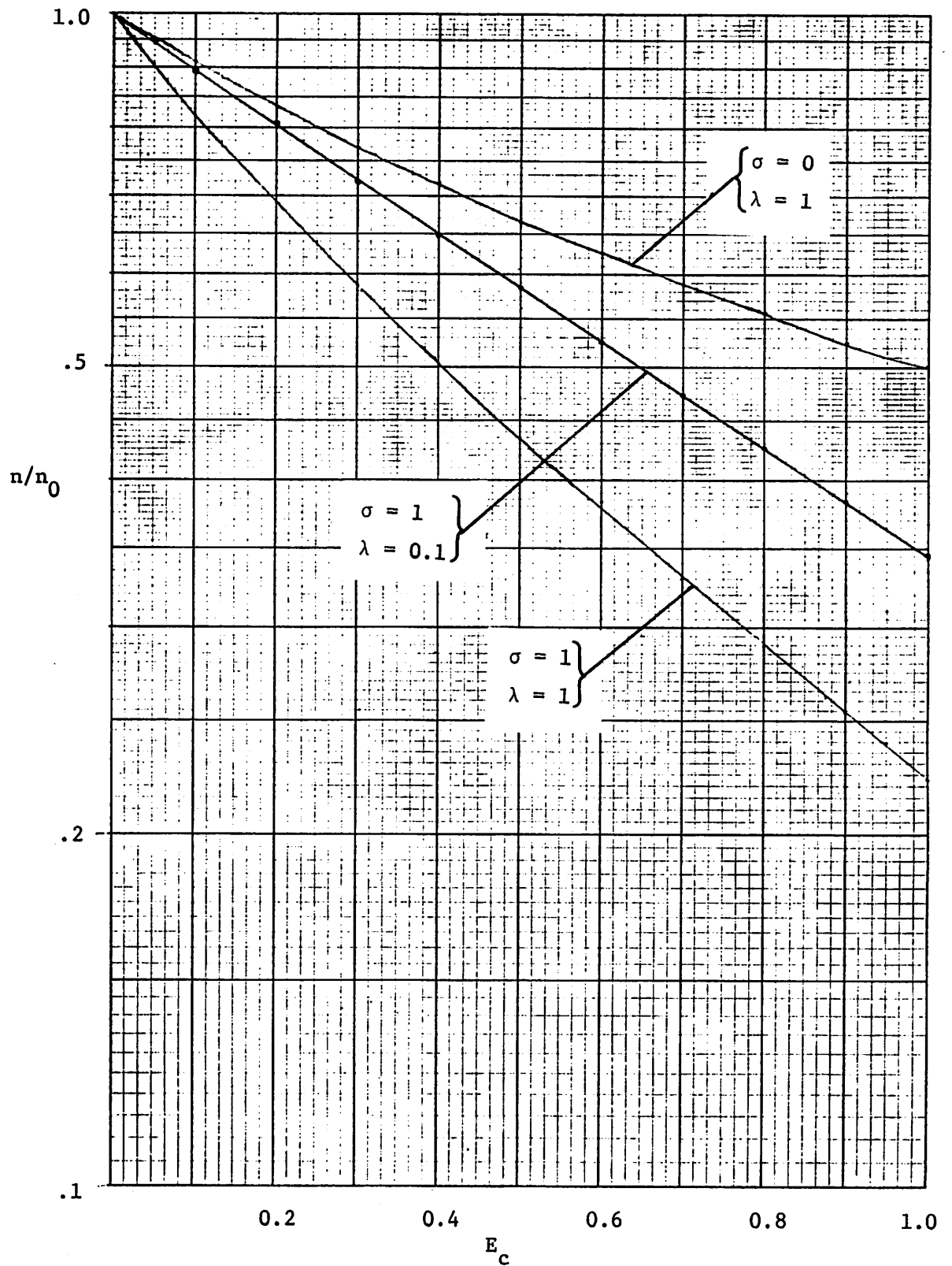
Fig. 1. Molecular survival (n/n_0) vs. incident electron exposure E_c. Initial concentration was chosen to be $n_0 = 1$. Curves have parameters (σ and λ) as shown.

set of initial conditions, $a(0) = a_o$ and $b(0) = b_o$, one has in all

eight 'parameters' $(a_o, b_o, \sigma_a, \sigma_b, \lambda_{ab}, \lambda_{ba}, \lambda_{aa}$ and $\lambda_{bb})$ that

determine the $a(E_c)$ and $b(E_c)$. In order to observe trends in the

behavior of a and b for different values of these parameters, the

following approximation is made. Recall (Sec. 2.1.c) that the

inter-molecular coupling constants are written as

$$\lambda_{ij} \propto \int c(E) \sigma_D^i(E) \frac{d\sigma^j}{dE} (E,T) dE. \tag{5}$$

If the incident electron-initiated energy transfer cross section

for molecule j is assumed to be proportional to dissociation cross

section of molecule j, due to the incident electron, then we can

write:

$$\lambda_{ij} = C_{IS}^i \sigma_j ,$$

$$\tag{6}$$

$$\lambda_{ii} = C_{SS}^i \sigma_i .$$

where C_{SS}^i and C_{IS}^i are the similar-species, and inter-species

interaction constants respectively. If the dependence of these

constants on molecular species is neglected then:

$$\lambda_{aa} = C_{SS} \sigma_a , \qquad \lambda_{bb} = C_{SS} \sigma_b ,$$

$$\tag{7}$$

$$\lambda_{ba} = C_{IS} \sigma_a , \qquad \lambda_{ab} = C_{IS} \sigma_b .$$

Thus, it is assumed that the inter-molecular coupling constant

depends primarily on the molecule generating the excitation (and

hence, somewhat proportional to the dissociation cross section of

that molecule), rather than on the molecule receiving the dissociation. Admittedly, this assumption is crude and inaccurate, yet in the context of determining magnitudes and trends of the two species concentrations it is quite useful in that it reduces the number of parameters to six. The two coupled equations can then be rewritten:

$$da/dE_c = - \sigma_a a - C_{SS} \sigma_a a^2 - C_{IS} \sigma_b ab,$$

$$db/dE_c = - \sigma_a b - C_{SS} \sigma_b b^2 - C_{IS} \sigma_a ba. \tag{8}$$

Numerical solutions to the coupled quations can be obtained easily on a computer using standard differential equation solving programs. Solutions are obtained for different values of cross sections and coupling constants for a particular choice of initial concentration of the molecules. As in the one species case, the solutions depend on the initial concentrations chosen. We choose in the two cases: (1) Equal initial concentration, $a_o = b_o = 0.5$ and (2) unequal initial concentration with $a_o = 0.9$ and $b_o = 0.1$.

Consider first the case of <u>equal initial concentration</u> of molecules, the choice of the dissociation cross section falls into two classes:

(i) Equal dissociation cross section (we choose $\sigma_a = \sigma_b = 0.1$), and

(ii) dissociation cross section of either one of the two species greater than the other (we choose $\sigma_a = 1.0$ and $\sigma_b = 0.1$). Table 1 shows the results obtained from numerical solutions to

Table 1

Molecular survival concentrations after an exposure $E_c = 1$

Initial concentration: $a_0 = b_0 = 0.5$

		(i) $\sigma_a = \sigma_b = 0.1$		(ii) $\sigma_a = 1.0$, $\sigma_b = 0.1$	
c_{SS}	c_{IS}	$a(1)$	$b(1)$	$a(1)$	$b(1)$
0.	0.1	.450	.450	.183	.438
0.	0.5	.442	.442	.180	.386
0.	1.0	.432	.432	.177	.332
1.	0.1	.430	.430	.139	.420
1.	0.5	.422	.422	.137	.378
1.	1.0	.413	.413	.135	.332

Eqns. (8) for the choices of parameters indicated in the Table.
The magnitudes of C_{SS} and C_{IS} are chosen arbitrarily; though
they are expected to approximate actual values within at least
an order of magnitude. The trends that are most evident from the
data in Table 1 are: (1) For case (i) with equal magnitudes of
the cross section, the survival concentrations at $E_c = 1$ for both
molecular species are the same i.e., $a(1) = b(1)$. They decrease
by about 4% for an order of magnitude change in either one of
C_{SS} or C_{IS} and a fixed value of the other. (2) For the unequal
magnitude cross sections of case (ii), the a-species molecules
survive considerably less than in case (i), due primarily to an
increase in a factor of 10 in the dissociation cross section σ_a.
Note however that the b-species molecules also have lower concen-
trations than in case (i), even though their cross sections are
left unchanged. The effect is clearly due to coupling between
molecules of the two species, since $b(1)$ changes by about 24% for
an order of magnitude change in the inter-species constant, C_{IS},
(with C_{SS} constant) but by less than 4% for a similar change in
similar-species constant, C_{SS} (fixed C_{IS}). Similarily the a-
species molecules are less resistant by about 24% for an order of
magnitude increase in coupling between molecules of similar species,
i.e., C_{SS} (fixed C_{IS}).

Next consider molecular survival in a mixture containing
<u>unequal initial concentration</u> of two molecular species. Table 2
shows the results obtained for a variety of arbitrarily chosen
magnitudes of cross sections. The choice of cross sections falls

A.7

Table 2

Molecular survival concentrations after an exposure $E_c = 1$

Initial concentration: $a_0 = 0.9$, $b_0 = 0.1$

c_{SS}	c_{IS}	(i) $\sigma_a = 2.0,\ \sigma_b = 0.1$		(ii) $\sigma_a = 1.0,\ \sigma_b = 0.1$		(iii) $\sigma_a = 0.1,\ \sigma_b = 0.1$		(iv) $\sigma_a = 0,\ \sigma_b = 0.1$		(v) $\sigma_a = 0.1,\ \sigma_b = 1.0$	
		$a(1)$	$b(1)$	$a(1)$	$b(1)$	$a(1)$	$b(1)$	$a(1)$	$b(1)$	$a(1)$	$b(1)$
0.	0.1	.121	.0837	.331	.0855	.813	.0897	.899	.0905	.809	.0365
0.	0.5	.121	.0613	.330	.0681	.810	.0867	.896	.0905	.789	.0353
0.	1.0	.121	.0416	.329	.0513	.806	.0831	.891	.0905	.766	.0339
1.	0.1	.0684	.0846	.211	.0857	.749	.0889	.899	.0896	.746	.0343
1.	0.5	.0683	.0673	.210	.0717	.747	.0860	.896	.0896	.729	.0333
1.	1.0	.0681	.0506	.209	.0573	.743	.0826	.891	.0896	.708	.0320

into one of the following three categories:

(1) The majority species have a cross section greater than that of the minority [cases (i) and (ii) in the Table].

(2) The majority and the minority species have exactly the same cross sections [case (iii) in the Table] and

(3) The majority species have a cross section smaller than that of the minority [cases (iv) and (v) in the Table]. Now the behavior of the survival concentrations for changes in the cross sections and coupling constants can be elucidated.

The general trend that is noticed, from a glance at cases (i) - (iv) in the Table, is that for fixed σ_b = 0.1 and increasing σ_a, from 0.1 to 2.0, the majority species' concentration decreases considerably faster than the concentration of the minority species, just as one expects. This trend is, of course, reversed on keeping σ_a fixed and increasing σ_b [cases (iii) and (v)]. However there are significant effects on the concentrations due to the similar-species and inter-species coupling constants (C_{SS} and C_{IS}, respectively). Consider cases (i) through (iv), where σ_b = 0.1 and σ_a lies between 0 and 2. For a fixed value of the similar-species constant C_{SS}, the variation of the inter-species constant C_{IS}, causes virtually no change (less than 1%) in the survival of the majority species (a). However under the same conditions, the minority species molecules (b) are quite sensitive and their survival decreases drastically (up to 50%) especially for large values of σ_a. This behavior indicates that, as one expects, the inter-species coupling is quite important for minority species, especially when the majority species have large dissociation cross

sections (and consequently, within our earlier assumption, large energy transfer $d\sigma/dE$).

Now, consider changes in molecular survival for a change in the similar-species constant C_{SS} from 0 to 1, while the inter-species constant C_{IS} is kept fixed. The majority species (a) survival is almost independent of the change in C_{SS} for $\sigma_a = \sigma_b$, but decreases quite rapidly (as much as 44% for $\sigma_a = 2$, $\sigma_b = 0.1$) with an increasing ratio of σ_a to σ_b. The minority species (b) is also almost independent of the change in C_{SS} (fixed C_{IS}) for $\sigma_a = \sigma_b$; however increasing σ_a increases the survival of the b species at a faster rate when $C_{SS} = 1$ than when $C_{SS} = 0$. The consequence of this behavior is that, for large values of σ_a/σ_b, the minority species have <u>greater</u> survival for a large similar-species constant, $C_{SS} = 1$, than for $C_{SS} = 0$ [In case (i) of Table 2, for a change in C_{SS} from 0 to 1, there is 21.6% increase in survival for $C_{IS} = 1$ and 9.7% increase for $C_{IS} = 0.5$.]. Note, however, that this increased minority survival is still smaller than the survival of these molecules were they by themselves under the beams (essentially as in Case (iv), Table 2).

The results of the calculations in Table 2 are for an idealized set of parameters, nevertheless it may be that the trends observed above may be true in general. In summary, one sees that in the above model, neither the inter-species constant C_{IS}, nor the similar-species constant C_{SS}, strongly influence either the majority or the minority species when both species have comparable direct dissociation cross sections. However at large values of
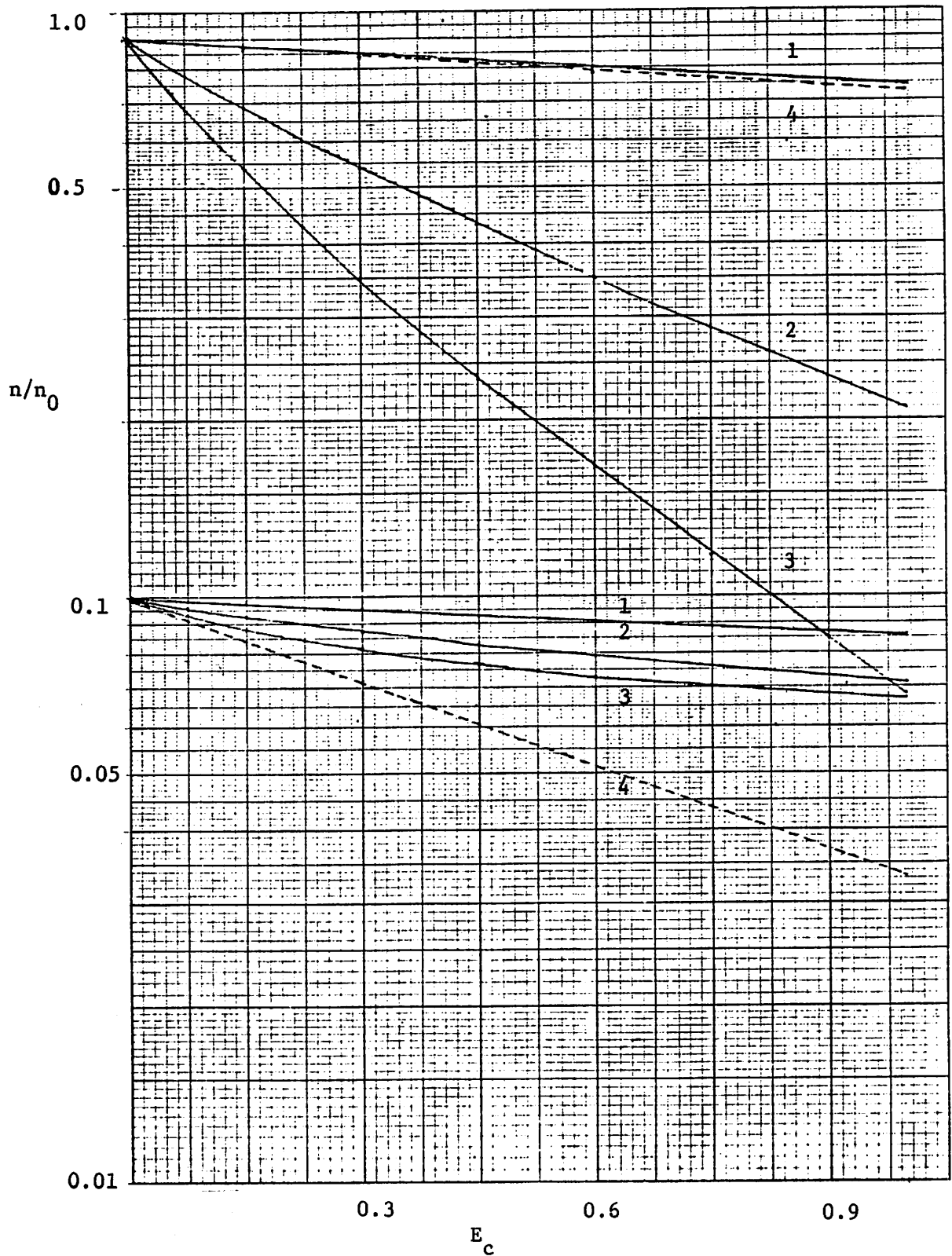
A. 10

Fig. 2. Molecular survival of species with unequal initial concentrations ($a_0 = 0.9$, $b_0 = 0.1$) vs. incident electron exposure. The four sets of curves have the following parameters. Curves 1: $\sigma_a = 0.1$, $\sigma_b = 0.1$, curves 2: $\sigma_a = 1$, $\sigma_b = 0.1$, curves 3: $\sigma_a = 2.0$, $\sigma_b = 0.1$ and curves 4: $\sigma_a = 0.1$, $\sigma_b = 1$.

σ_a/σ_b, increasing C_{IS} decreases the survival of the minority species (b); but increasing C_{SS}, not only decreases the survival of majority species (a), but also increases minority species (b) survival! It is hoped that more detailed and accurate analysis of this type will give results to substantiate this trend and provide useful, accurate data to the microscopist so that he can, via appropriate specimen preparation, use the coupling constants to his advantage in reducing damage.

Finally, Figure 2 shows the behavior of molecular concentrations for some of the parameters considered above [Cases (i), (ii), (iii) and (v) in Table 2]. An approximate straight line for $E_c >$ 4.5, implies an independent molecular type of an exponential behavior, with an appropriate "effective dissociation cross section" σ_D^{eff}.